

NRL Report 6133

Systematic Errors in Ultrasonic Propagation Parameter Measurements

Part 2 - Effects of Guided Cylindrical Modes

V. A. DEL GROSSO

*Propagation Branch
Sound Division*

January 29, 1965



APPROVED FOR PUBLIC
RELEASE - DISTRIBUTION
UNLIMITED

U.S. NAVAL RESEARCH LABORATORY
Washington, D.C.

PREVIOUS REPORT IN SERIES

"SYSTEMATIC ERRORS IN ULTRASONIC PROPAGATION PARAMETER MEASUREMENTS—Part 1 - Effect of Free-Field Diffraction," V. A. Del Grosso, NRL Report 6026, Jan. 1964.

CONTENTS

Abstract	ii
Problem Status	ii
Authorization	ii
INTRODUCTION	1
GUIDED MODE FORMULATION IN A RIGHT-CIRCULAR CYLINDRICAL CAVITY.....	2
CHARACTERISTIC FUNCTION EXPANSIONS—ORTHOGONAL AND NONORTHOGONAL	4
CHARACTERISTIC EQUATIONS	
Absolutely Rigid Boundary	8
Infinitely Flexible Boundary.....	9
Thin Elastic Wall	9
Liquid Boundary	10
Elastic Solid Boundary	12
ORTHOGONALITY CHECKS AND NONORTHOGONAL SIMPLIFICATION	15
INTRODUCTION OF ABSORPTION	20
ADDITIONAL PARAMETERS	24
DISCUSSION AND APPLICATION	25
CONCLUSIONS	33
FUTURE WORK.....	34
ACKNOWLEDGMENTS	34
REFERENCES	34
APPENDIX A – Time Convention for an Outgoing Wave	36
APPENDIX B – Redefinition of Vector Displacement Potential Ψ	41
APPENDIX C – Selection of Appropriate Bessel Function Solutions	50

Systematic Errors in Ultrasonic Propagation Parameter Measurements

V. A. DEL GROSSO

Propagation Branch

Sound Division

It was shown in Part I of this series of reports that appreciable errors in sound speed and sound absorption determinations may be attributed to a neglect in applying appropriate corrections to those situations closely approximating free-field conditions (finite size, plane-parallel source). In the present report it is shown that appreciable errors in the measurement of sound speed and sound absorption for guided mode propagation may be attributed to neglect in applying corrections that may be required because of the selection of geometric parameters or the method of measurement.

This report contains graphs of pressure and phase, relative to plane-wave values and averaged over a plane-parallel receiver of size equal to the source size, for acoustic energy propagation down a right-circular liquid cylinder with lateral boundary condition appropriate to one of the following: absolutely rigid walls, infinitely flexible walls, liquid walls, or elastic solid walls. The latter boundary condition, which is considered to be that most appropriate to the situation of a liquid contained within a thick-walled metal tube, is shown to result in maximum anomalies in sound speed determinations when the transducer completely closes one end of the tube.

INTRODUCTION

Because the apparently incompatible results obtained by different experimenters using both similar and different techniques (1-3) indicate the presence of unresolved systematic errors, an investigation into the anomalies of ultrasonic propagation parameter measurements has been undertaken. These systematic errors do not lend themselves to statistical manipulation, so the present attempt is to predict the theoretical behavior for specific geometric configurations of acoustic test setups and to correlate this behavior with experimental observations. The intent is to gain a sufficient grasp of the behavior of laboratory acoustic instrumentation in order to ascertain the need for, and, if necessary, to apply, appropriate corrections. Of course, if the proper corrections are known and made, there is then no error due to the particular effect in question. Ideally, experimental methods requiring no corrections could then be selected.

Part I of this series of reports (4) considered some predictable, and observed, effects of free-

field diffraction and indicated that appreciable errors in both sound speed and sound absorption could be attributed to these effects. An earlier report (5), primarily concerned with the measurement of sound speed by interferometry, dealt also with the relatively simple problem of axial waveguide propagation in a right-circular cylinder with absolutely rigid walls; the results indicated that a deliberate attempt to destroy cylindrical symmetry could in fact closely approximate the conditions of free-field propagation even for continuous waves in a terminated enclosure.

The present report is concerned with guided mode propagation of acoustic energy and the anomalies caused by geometric constraints. For simplicity of calculation the medium considered is assumed to fill a right-circular cylindrical cavity of finite radius and semi-infinite length—that is, terminated only at one end by a driving source. This cavity in turn is assumed to be located in another medium of otherwise infinite extent in order to avoid ring resonances, outer reflections, and other phenomena associated with the finite wall thickness of a container. The lateral boundary conditions considered are those relevant to (a) an absolutely rigid boundary, (b) an infinitely flexible boundary, (c) a liquid

NRL Problem S01-02; Project RF 001-03-45-5251. This is an interim report on the problem; work is continuing. Manuscript submitted June 15, 1964.

boundary, or (d) an elastic solid boundary. Part 3 of this series of reports will remove the above restriction and consider liquid cylinders contained in shells; Part 4 will add viscosity to more adequately specify the appropriate boundary conditions; Part 5 will deal with iterative reflection for continuous waves resulting from the addition of an elastic termination to the open end of this cylindrical cavity, and Part 6 will correlate these predictions with recent experimental results. It should not be necessary to state here that small confined samples are nearly prerequisites for adequate specification of homogeneity and external physical conditions of a test liquid.

Many reports pertinent to this investigation may be found in the available literature. Possibly the earliest report, dealing with gases, dates from 1877 and is due to Lord Rayleigh (6). Krasnooshkin (7-9), though principally developing an interferometer theory, followed the 1868 results of Kirchhoff (10) in assuming the near-trivial case of absolutely rigid walls with no losses, no thermal conductivity, and perfect smoothness to allow free slipping. Experimental confirmation of some of the predictions of Krasnooshkin were made for absorption results by Van Itterbeek in 1951 (11) and for sound speed results by Bell in 1950 (12). Morse (13) discussed the theoretical treatment given by Rayleigh. Hartig and Swanson (14) gave an excellent account of these modes for low frequencies in 1938, and Jacobi (15) in 1949 continues not only for high frequencies but also for the interesting case of liquid walls, besides the other near-trivial case of infinitely flexible walls. Biot (16) discusses a cylindrical bore through an elastic solid and Lin and Morgan (17) consider thin elastic walls.

It should be noted that a complete theoretical treatment of the case of propagation in infinitely long solid cylinders was also done by Pochhammer (18) and Chree (19) in the previous century. The liquid cylinder with infinitely flexible walls is a degenerate case of this, although in some recent work it has been offered as a representation of the rigid wall situation.

Many other investigators (20-48) have considered aspects of this problem. Among the latest are Redwood (42) and Carome and Witting (44) at John Carroll University. The latter group

pose the interesting thesis that the example of a liquid confined in a metal-walled cylinder is described more accurately by the theoretical formulation pertinent to infinitely flexible walls rather than to absolutely rigid walls or some combination of the two. Needless to say, this statement, for which experimental evidence is proffered, merits very careful analysis. Reference must also be made to the recent work of Elco and Hughes (48) who point out the obviously inadequate approximation of an elastic lossy boundary by an absolutely rigid one and who rightly question the validity of the common, but unsatisfactory, assumption of free slipping along perfectly smooth walls.

The formulation of this report will be derived in a rather elementary fashion. It is hoped that this will facilitate interpretation and permit more easy reconciliation with the intuitive feelings of experienced investigators which are too often quickly dismissed.

GUIDED MODE FORMULATION IN A RIGHT-CIRCULAR CYLINDRICAL CAVITY

As stated in the Introduction, for simplicity of calculation this report will assume a liquid medium contained in a right-circular cylindrical cavity of finite radius b and infinite extent along the positive z axis. The cavity, which is terminated at one end by a baffle containing a driving source, is located in another medium of infinite extent (see Fig. 1).

As usual we assume a velocity potential $\phi(r, \theta, z, t)$ throughout the cylinder which satisfies the wave equation

$$\nabla^2 \phi = \frac{1}{c^2} \frac{\partial^2 \phi}{\partial t^2}. \quad (1)$$

Separating out the time-dependent variable so that

$$\phi \equiv \phi(r, \theta, z) T(t),$$

the separation constant k^2 is introduced as

$$\frac{\nabla^2 \phi}{\phi} = \frac{1}{c^2 T} \frac{\partial^2 T}{\partial t^2} \equiv -k^2$$

and the homogeneous time-independent wave equation, or Helmholtz equation, is

$$\nabla^2 \phi + k^2 \phi = 0.$$

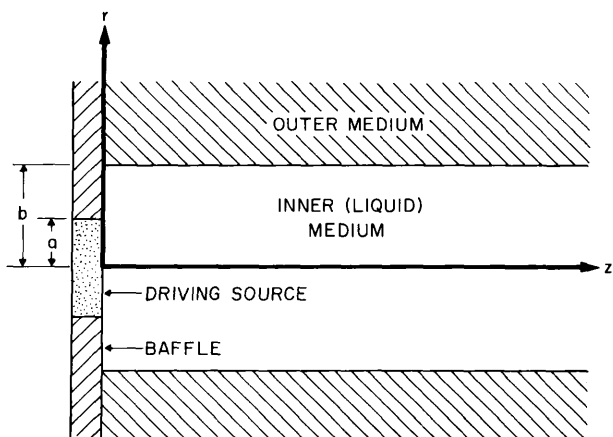


Fig. 1 - A right-circular, liquid, cylindrical cavity of radius b is assumed as the geometry for this discussion of guided mode propagation. The cavity is capped at one end by a driving source of radius a and a baffle. The cavity is assumed to be infinitely long in the $+z$ direction. The outer medium is infinite in extent.

For simple harmonic time variation, the time-dependent equation

$$\frac{\partial^2 T}{\partial t^2} + k^2 c^2 T = 0$$

yields

$$T = Ae^{i\omega t} + Be^{-i\omega t}$$

where

$$k = \frac{\omega}{c} = \frac{2\pi}{\lambda}.$$

In cylindrical coordinates the Helmholtz equation is expressed as

$$\frac{\partial^2 \phi}{\partial r^2} + \frac{1}{r} \frac{\partial \phi}{\partial r} + \frac{1}{r^2} \frac{\partial^2 \phi}{\partial \theta^2} + \frac{\partial^2 \phi}{\partial z^2} + k^2 \phi = 0.$$

Separating the variables so that

$$\phi = R(r) \Theta(\theta) Z(z),$$

the solutions of the equation are of the form

$$\Theta = C \cos n\theta + D \sin n\theta$$

$$Z = Ee^{iqz} + Fe^{-iqz}$$

and

$$R = G \mathcal{J}_n \left(\frac{r\sqrt{k^2 - q^2}}{n \geq 0} \right)$$

where $q = \beta + i\alpha$, $\beta = 2\pi/\lambda$ ($\equiv k$), n is an integer, and \mathcal{J}_n is the n th-order Bessel function of

the first kind. So the general solution of the time-independent part of the wave equation is

$$\begin{aligned} \phi_{nm} &= (K_{nm} \cos n\theta + L_{nm} \sin n\theta) \\ &\mathcal{J}_n(r\sqrt{k^2 - q_{nm}^2}) e^{\pm iq_{nm}z}. \end{aligned} \quad (2a)$$

To limit consideration only to those solutions with circular symmetry, n is restricted to zero and the function ϕ is independent of θ ; thus

$$\begin{aligned} \phi_{0m} &= \phi(r, z) \\ &= K_{0m} \mathcal{J}_0(r\sqrt{k^2 - q_{0m}^2}) e^{\pm iq_{0m}z} \end{aligned} \quad (2b)$$

If only outward going waves are considered, then

$$\phi_{0m} = K_{0m} \mathcal{J}_0(r\sqrt{k^2 - q_{0m}^2}) e^{\pm iq_{0m}z} \quad (2c)$$

is appropriate for a time dependence $e^{-i\omega t}$. If $\gamma_{0m} \equiv iq_{0m}$ ($= i\beta - \alpha$) is imaginary, Eq. (2c) represents a wave propagating along the positive z axis with a complex phase velocity

$$C_{0m} = \frac{\omega}{\beta_{0m} + i\alpha_{0m}}.$$

If γ_{0m} is real, there is no propagation. If absorption is neglected, then of course $\alpha_{0m} = 0$ and $C_{0m} = \omega/\beta_{0m}$. In the immediately previous report (4), it was shown that phase velocity C_{0m} , group velocity V_{0m} , and free-field plane-wave phase velocity C are related as

$$C^2 = C_{0m} V_{0m} \quad (3)$$

where V_{0m} is the group velocity of a particular "mode" (corresponding to a specific value of m).

Without here specifying the particular characteristic equations whose solutions or characteristic values are the particular modes referred to (the calculation of the appropriate characteristic functions is detailed in later sections of this report), we may express the characteristic value X_{0m} as

$$X_{0m} \equiv b \sqrt{k^2 - q_{0m}^2} \quad (4)$$

where b is the cylindrical cavity radius. So the argument of the zero-order Bessel function may be expressed as

$$\mathcal{J}_0(r\sqrt{k^2 - q_{0m}^2}) = \mathcal{J}_0\left(r \frac{x_{0m}}{b}\right). \quad (5)$$

For now, since the specification of the characteristic values involves boundary conditions equivalent to equating impedances, we calculate the impedance in the radial direction on the liquid cylinder side of the radial boundary. Restoring the time dependence temporarily,

$$\phi_{0m} = M_{0m} \mathcal{J}_0\left(r\sqrt{k^2 - q_{0m}^2}\right) e^{i(q_{0m}z - \omega t)}.$$

The excess pressure is given by

$$P = -\rho \frac{\partial \phi}{\partial t},$$

whereby

$$P = M_{0m} \mathcal{J}_0\left(r\sqrt{k^2 - q_{0m}^2}\right) i\omega\rho e^{i(q_{0m}z - \omega t)}$$

or

$$P(r) = P_0 \mathcal{J}_0\left(r\sqrt{k^2 - q_{0m}^2}\right) \quad (6)$$

where

$$P_0 \equiv i\omega\rho M_{0m} e^{i(q_{0m}z - \omega t)}.$$

The particle velocity in the radial direction is given by

$$U(r) = \frac{\partial \phi}{\partial r},$$

whereby

$$U(r) = M_{0m} e^{i(q_{0m}z - \omega t)} \frac{\partial}{\partial r} \left[\mathcal{J}_0\left(r\sqrt{k^2 - q_{0m}^2}\right) \right] \quad (7)$$

$$= \frac{iP_0}{\omega\rho} \sqrt{k^2 - q_{0m}^2} \mathcal{J}_1\left(r\sqrt{k^2 - q_{0m}^2}\right).$$

The impedance is given by the excess pressure divided by the particle velocity, so

$$\text{Impedance} = \frac{P}{U} = \frac{-i\omega\rho \mathcal{J}_0\left(r\sqrt{k^2 - q_{0m}^2}\right)}{\sqrt{k^2 - q_{0m}^2} \mathcal{J}_1\left(r\sqrt{k^2 - q_{0m}^2}\right)} \quad (8)$$

in the radial direction. The particle velocity and displacement ξ are related by

$$U = \xi i\omega$$

so that $P/\xi = Pi\omega/U$, or

$$\frac{P}{\xi} = \frac{\rho\omega^2 \mathcal{J}_0\left(r\sqrt{k^2 - q_{0m}^2}\right)}{\sqrt{k^2 - q_{0m}^2} \mathcal{J}_1\left(r\sqrt{k^2 - q_{0m}^2}\right)}. \quad (9)$$

CHARACTERISTIC FUNCTION EXPANSIONS—ORTHOGONAL AND NONORTHOGONAL

We will assume that the time-independent velocity field inside the cylinder may be expanded in terms of the natural modes ϕ_{0m} as

$$\phi(r, z) = \sum_{m=0} K_{0m} \mathcal{J}_0\left(r\frac{X_{0m}}{b}\right) e^{iq_{0m}z} \quad (10)$$

where we have assumed radial symmetry. The sequence of characteristic functions must be a complete set in order for this representation by a series to be possible. To easily calculate the expansion coefficients K_{0m} we would like the sequence of characteristic functions to be mutually orthogonal.

To determine the amplitude of the various modes we write the velocity potential at $z = 0$ as

$$\phi(r, 0) = \sum_m K_{0m} \mathcal{J}_0\left(r\frac{X_{0m}}{b}\right). \quad (11)$$

Multiplying both sides by

$$r \mathcal{J}_0\left(r\frac{X_{0l}}{b}\right)$$

and integrating with respect to r over the limits 0 to b we obtain

$$\int_0^b \phi(r, 0) \mathcal{J}_0\left(r\frac{X_{0l}}{b}\right) r dr = \int_0^b \sum_m K_{0m} \mathcal{J}_0\left(r\frac{X_{0m}}{b}\right) \mathcal{J}_0\left(r\frac{X_{0l}}{b}\right) r dr. \quad (12)$$

Assuming a transmitter of radius a ($a \leq b$) undergoing harmonic vibration as a plane circular piston, then

$$\phi(r, 0) \rightarrow \phi_0 \text{ (a constant)}$$

and the left-hand side of Eq. (12) becomes

$$\int_0^a \phi_0 \mathcal{J}_0\left(r \frac{X_{0l}}{b}\right) r dr = \phi_0 \frac{ab}{X_{0l}} \mathcal{J}_1\left(X_{0l} \frac{a}{b}\right). \quad (13)$$

Further, assuming (a) a receiving transducer of the same radius as the transmitter (i.e., $r = a$) with response proportional to the vectorial average of the excess pressure over the area of the crystal and (b) weak interaction of the transducers with the acoustic field, we obtain for the average potential

$$\begin{aligned} \langle \phi \rangle &= \frac{1}{\pi a^2} \int_0^a \phi(r, z) 2\pi r dr \\ &= \frac{1}{\pi a^2} \sum_m 2\pi \int_0^a K_{0m} \mathcal{J}_0\left(r \frac{X_{0m}}{b}\right) e^{iq_{0m}z} r dr. \end{aligned} \quad (14)$$

Now if the orthogonality relation could be invoked, the only term remaining on the right-hand side of Eq. (12) would be that for $l = m$, viz.,

$$\begin{aligned} \int_0^b K_{0m} \mathcal{J}_0\left(r \frac{X_{0m}}{b}\right) r dr &= \\ K_{0m} \frac{b^2}{2} \left[\mathcal{J}_0^2(X_{0m}) + \mathcal{J}_1^2(X_{0m}) \right]. \end{aligned} \quad (15)$$

Using Eqs. (12), (13), and (15), the expansion coefficients are given by

$$K_{0m} = \phi_0 \frac{2a \mathcal{J}_1\left(X_{0m} \frac{a}{b}\right)}{b X_{0m} \left[\mathcal{J}_0^2(X_{0m}) + \mathcal{J}_1^2(X_{0m}) \right]} \quad (16)$$

for orthogonal characteristic functions, and Eq. (14) would then become

$$\langle \phi \rangle = \sum_m \frac{2\pi \phi_0}{\pi a^2} \int_0^a \frac{2a \mathcal{J}_1\left(X_{0m} \frac{a}{b}\right) \mathcal{J}_0\left(r \frac{X_{0m}}{b}\right) e^{iq_{0m}z} r dr}{b X_{0m} \left[\mathcal{J}_0^2(X_{0m}) + \mathcal{J}_1^2(X_{0m}) \right]}, \quad (17)$$

and, finally,

$$\langle \phi \rangle = \sum_m \frac{4\phi_0 \mathcal{J}_1^2\left(X_{0m} \frac{a}{b}\right) e^{iq_{0m}z}}{X_{0m}^2 \left[\mathcal{J}_0^2(X_{0m}) + \mathcal{J}_1^2(X_{0m}) \right]} \quad (18)$$

Relative to the plane-wave value, the time-independent velocity potential is given by

$$\langle \phi \rangle_{\text{rel}} = \sum_m \frac{4\mathcal{J}_1^2\left(X_{0m} \frac{a}{b}\right) e^{-i(k - q_{0m})z}}{X_{0m}^2 \left[\mathcal{J}_0^2(X_{0m}) + \mathcal{J}_1^2(X_{0m}) \right]} \quad (19)$$

As in the immediately previous report dealing with free-field diffraction (4), we calculate the magnitude of the rms pressure (averaged vectorially, relative to the plane-wave value) over the receiving transducer as

$$\langle p \rangle_{\text{rel}} = \sqrt{\text{Re}^2 \langle \phi \rangle_{\text{rel}} + \text{Im}^2 \langle \phi \rangle_{\text{rel}}}. \quad (20)$$

The phase difference $\langle \theta \rangle_{\text{rel}}$ from plane-wave phase is given by

$$\begin{aligned} \langle \theta \rangle_{\text{rel}} &\equiv \langle \theta \rangle_{\text{diffracted}} - \langle \theta \rangle_{\text{plane}} \\ &= \tan^{-1} \frac{\text{Im} \langle \phi \rangle_{\text{rel}}}{\text{Re} \langle \phi \rangle_{\text{rel}}}. \end{aligned} \quad (21)$$

If we are not able to invoke orthogonality so that Eq. (15) is not the only term remaining on the right-hand side of Eq. (12), or, in other words, if

$$\int_0^b \mathcal{J}_0\left(r \frac{X_{0m}}{b}\right) \mathcal{J}_0\left(r \frac{X_{0l}}{b}\right) r dr \neq 0 \quad \text{for } m \neq l, \quad (22)$$

the determination of the expansion coefficients is somewhat more difficult. In this case Eq. (14) becomes

$$\langle \phi \rangle = \frac{2b}{a} \sum_m K_{0m} \frac{1}{X_{0m}} \mathcal{J}_1\left(X_{0m} \frac{a}{b}\right) e^{iq_{0m}z}, \quad (23)$$

with

$$\begin{aligned} \langle \phi \rangle_{\text{rel}} &= \frac{2b}{a\phi_0} \sum_m K_{0m} \\ &\frac{1}{X_{0m}} \mathcal{J}_1\left(X_{0m} \frac{a}{b}\right) e^{-i(k - q_{0m})z}, \end{aligned} \quad (24)$$

and K_{0m} is not given by Eq. (16). To determine K_{0m} in this case, first we simplify the notation and write the characteristic functions as

$$R_{nm} \equiv \mathcal{J}_n\left(r \frac{X_{0m}}{b}\right) \quad (25)$$

so that the previous orthogonality condition may be written as

$$\int_0^b R_{0m} R_{0\ell} r dr = 0. \quad (26)$$

The criterion for this condition is derived as follows.

Bessel's equation, with the parameter $k^2 - q^2$, may be written as

$$r \frac{d^2 R}{dr^2} + \frac{dR}{dr} + \left((k^2 - q^2)r - \frac{n^2}{r} \right) R = 0 \quad (27)$$

and cast in the form of the Liouville equation as

$$\frac{d}{dr}(rR') + \left((k^2 - q^2)r - \frac{n^2}{r} \right) R = 0 \quad (28)$$

where the parameter represents the separation constants, and $R' = dR/dr$. To check orthogonality we consider solutions for different values of the parameter for which

$$R_{0m} = \mathcal{J}_0\left(r\sqrt{k^2 - q_{0m}^2}\right) = \mathcal{J}_0\left(r \frac{X_{0m}}{b}\right). \quad (29)$$

Because the Liouville equation is self-adjoint we may simply write it down twice with different subscripts, multiply the first equation by the characteristic function of the second, multiply the second equation by the characteristic function of the first, subtract the two, and integrate over our limits of r from 0 to b (the tube radius). The result of this procedure, after a slight rearrangement, is

$$\frac{X_{0m}^2 - X_{0\ell}^2}{b^2} \int_0^b r R_{0m} R_{0\ell} dr = \int_0^b R_{0m} \frac{d}{dr}(rR'_{0\ell}) dr - \int_0^b R_{0\ell} \frac{d}{dr}(rR'_{0m}) dr \quad (30)$$

$$\int_0^b R_{0m} \frac{d}{dr}(rR'_{0\ell}) dr - \int_0^b R_{0\ell} \frac{d}{dr}(rR'_{0m}) dr$$

Considering the first integral on the right-hand side, integration by parts, with

$$u = R_{0m}, \quad du = R'_{0m} dr,$$

$$dv = \frac{d}{dr}(rR'_{0\ell}) dr, \quad \text{and } v = rR'_{0\ell},$$

transforms the integral to

$$R_{0m} rR'_{0\ell} \Big|_0^b - \int_0^b rR'_{0\ell} R'_{0m} dr.$$

Similarly, the second integral on the right-hand side of Eq. (30) becomes

$$R_{0\ell} rR'_{0m} \Big|_0^b - \int_0^b rR'_{0m} R'_{0\ell} dr,$$

and the difference between the two, or the complete right-hand side, is

$$R_{0m} rR'_{0\ell} \Big|_0^b - R_{0\ell} rR'_{0m} \Big|_0^b,$$

which may be written

$$\begin{aligned} \text{right-hand side} &= - \left[\mathcal{J}_0\left(r \frac{X_{0m}}{b}\right) r \frac{X_{0\ell}}{b} \mathcal{J}_1\left(r \frac{X_{0\ell}}{b}\right) \right] \Big|_0^b \\ &\quad + \left[\mathcal{J}_0\left(r \frac{X_{0\ell}}{b}\right) r \frac{X_{0m}}{b} \mathcal{J}_1\left(r \frac{X_{0m}}{b}\right) \right] \Big|_0^b \end{aligned} \quad (31)$$

Finally,

$$\begin{aligned} \text{right-hand side} &= X_{0m} \mathcal{J}_0(X_{0\ell}) \mathcal{J}_1(X_{0m}) \\ &\quad - X_{0\ell} \mathcal{J}_0(X_{0m}) \mathcal{J}_1(X_{0\ell}) \end{aligned} \quad (32)$$

so that

$$\begin{aligned} \int_0^b R_{0m} R_{0\ell} r dr &= \frac{b^2}{X_{0m}^2 - X_{0\ell}^2} \\ &\quad \left[X_{0m} \mathcal{J}_0(X_{0\ell}) \mathcal{J}_1(X_{0m}) \right. \\ &\quad \left. - X_{0\ell} \mathcal{J}_0(X_{0m}) \mathcal{J}_1(X_{0\ell}) \right] \end{aligned} \quad (33)$$

and the orthogonality criterion is

$$X_{0m} \mathcal{J}_0(X_{0\ell}) \mathcal{J}_1(X_{0m}) - X_{0\ell} \mathcal{J}_0(X_{0m}) \mathcal{J}_1(X_{0\ell}) = 0 \quad \text{for } \ell \neq m. \quad (34)$$

But whether or not the characteristic functions are orthogonal, Eq. (33) remains valid. We also find straightforwardly that

$$\int_0^b R_{0m}^2 r dr = \frac{b^2}{2} [\mathcal{J}_0^2(X_{0m}) + \mathcal{J}_1^2(X_{0m})]. \quad (35)$$

Returning to Eq. (12) and using (13) we have

$$\phi_0 \frac{ab}{X_{0\ell}} \mathcal{J}_1\left(X_{0\ell} \frac{a}{b}\right) = \int_0^b \sum_m K_{0m} \mathcal{J}_0\left(r \frac{X_{0m}}{b}\right) \mathcal{J}_0\left(r \frac{X_{0\ell}}{b}\right) r dr, \quad (36)$$

or, using the definition

$$R_{nm} \equiv \mathcal{J}_n\left(r \frac{X_{0m}}{b}\right)$$

we obtain

$$\phi_0 \frac{ab}{X_{0\ell}} \mathcal{J}_1\left(X_{0\ell} \frac{a}{b}\right) = \int_0^b \sum_m K_{0m} R_{0m} R_{0\ell} r dr, \quad (37)$$

Which may be expanded as a set of simultaneous equations as follows:

$$\begin{aligned} \ell = 0: \quad \phi_0 \frac{ab}{X_{00}} \mathcal{J}_1\left(X_{00} \frac{a}{b}\right) &= \int_0^b K_{00} R_{00}^2 r dr + \int_0^b K_{01} R_{00} R_{01} r dr \\ &+ \int_0^b K_{02} R_{00} R_{02} r dr + \int_0^b K_{03} R_{00} R_{03} r dr + \dots \\ \ell = 1: \quad \phi_0 \frac{ab}{X_{01}} \mathcal{J}_1\left(X_{01} \frac{a}{b}\right) &= \int_0^b K_{00} R_{01} R_{00} r dr + \int_0^b K_{01} R_{01}^2 r dr \\ &+ \int_0^b K_{02} R_{01} R_{02} r dr + \int_0^b K_{03} R_{01} R_{03} r dr + \dots \\ \ell = 2: \quad \phi_0 \frac{ab}{X_{02}} \mathcal{J}_1\left(X_{02} \frac{a}{b}\right) &= \int_0^b K_{00} R_{02} R_{00} r dr + \int_0^b K_{01} R_{02} R_{01} r dr \\ &+ \int_0^b K_{02} R_{02}^2 r dr + \int_0^b K_{03} R_{02} R_{03} r dr + \dots, \text{ etc.} \end{aligned} \quad (38)$$

If the above series in ℓ is terminated after a finite number of terms, that is, if the characteristic function expansion contains a finite number of modes, then the set of simultaneous equations above may be solved directly for the expansion coefficients K_{0m} , which may then be used in Eq. (24). Obviously, the simpler method of determining the coefficients by Eq. (16), which is valid for an orthogonal set of characteristic functions, is much to be preferred.

After we determine the characteristic functions from the characteristic equations for the several boundary value conditions to follow, we will check their orthogonality and investigate possible simplification of the determination of the expansion coefficients if any characteristic functions prove to be nonorthogonal.

CHARACTERISTIC EQUATIONS

Absolutely Rigid Boundary

Though the absolutely rigid boundary condition cannot be obtained in reality, it does present an interesting limiting case. If we consider that the hypothetical cylinder of liquid down which our signal is propagating is enclosed radially with an absolutely rigid wall in the standard sense; we must have the radial component of particle velocity $U(r)$ going to zero at the boundary $r = b$, i.e.,

$$U(r) \Big|_{r=b} = 0. \quad (39)$$

From Eq. (7) we find that this is equivalent to letting

$$\mathcal{J}'_0 = (-\mathcal{J}'_1) = 0, \quad \text{for } r = b, \quad (40)$$

or

$$\mathcal{J}_1 \left(b \sqrt{k^2 - q_{0m}^2} \right) = 0,$$

which may also be written

$$\mathcal{J}_1(X_{0m}) = 0.$$

This condition is tantamount to letting the displacement ξ go to zero or the impedance go to infinity, which is readily seen from Eqs. (8) and (9).

To indicate that the above characteristic equation applies to rigid boundary conditions we write

$$\mathcal{J}_1(X_{Rm}) = 0 \quad (41)$$

where the R stands for rigid. We number the modes m from zero since $X_{Rm} = 0$ is a characteristic value in this case. Thus

$$m = 0, 1, 2, 3, \dots$$

and

$$X_{Rm} \equiv b \sqrt{k^2 - q_{Rm}^2}$$

or

$$q_{Rm} \equiv \sqrt{k^2 - \left(\frac{X_{Rm}}{b} \right)^2}, \quad (42)$$

where $k = \omega/c = 2\pi/\lambda$ and $q_{Rm} = \omega/C_{Rm} = 2\pi/\lambda_{Rm}$.

From these we find that the real modes are limited by

$$\frac{C^2 X_{Rm}^2}{b^2} \leq \omega^2$$

which is equivalent to

$$X_{Rm} \leq kb.$$

For a value of m which makes the characteristic value greater than this value, the wavelength becomes imaginary and we have a nonpropagating or evanescent mode; so we shall use this limiting value for m . Finally, from

$$\left(\text{Re} \langle \phi \rangle_{\text{rel}} \right)_R = \sum_{m=0}^{X_{Rm} \leq kb} \left\{ \frac{4 \mathcal{J}_1^2 \left(X_{Rm} \frac{a}{b} \right) \cos \left[(q_{Rm} - k) z \right]}{X_{Rm}^2 \mathcal{J}_0^2 \left(X_{Rm} \right)} \right\} \quad (43)$$

and

$$\left(\text{Im} \langle \phi \rangle_{\text{rel}} \right)_R = \sum_{m=0}^{X_{Rm} \leq kb} \left\{ \frac{4 \mathcal{J}_1^2 \left(X_{Rm} \frac{a}{b} \right) \sin \left[(q_{Rm} - k) z \right]}{X_{Rm}^2 \mathcal{J}_0^2 \left(X_{Rm} \right)} \right\}, \quad (44)$$

which are obtained from Eq. (19) using $\mathcal{J}_1(X_{Rm}) = 0$, we find that $a = b$ is a special case which, by the application of L'Hospital's rule, yields only $m = 0$; this value of m is found to be the plane-wave mode $C_{R0} = C$ and is sometimes written $C = C_{00}$, and $\lambda_{R0} = \lambda \equiv \lambda_{00}$.

We recall that Eq. (19) is a result of invoking orthogonality. If this does not hold, then we have Eq. (24) with different values for K_{Rm} or

$$\left(\text{Re} \langle \phi \rangle_{\text{rel}} \right)_R = \sum_{m=0}^{X_{Rm} \leq kb} \left\{ \frac{2bK_{Rm}}{a\phi_0 X_{Rm}} \mathcal{J}_1 \left(X_{Rm} \frac{a}{b} \right) \cos \left[(q_{Rm} - k)z \right] \right\} \quad (45)$$

and

$$\left(\text{Im} \langle \phi \rangle_{\text{rel}} \right)_R = \sum_{m=0}^{X_{Rm} \leq kb} \left\{ \frac{2bK_{Rm}}{a\phi_0 X_{Rm}} \mathcal{J}_1 \left(X_{Rm} \frac{a}{b} \right) \sin \left[(q_{Rm} - k)z \right] \right\}. \quad (46)$$

Infinitely Flexible Boundary

The infinitely flexible boundary condition is another trivial case which could be reproduced only if a cylinder of liquid could support itself in a vacuum. However, this case is a limiting situation and we will therefore calculate it. The statement invoking a pressure release boundary means just that; the pressure goes to zero on the radial boundary, or

$$P(r) \Big|_{r=b} = 0. \quad (47)$$

From Eq. (6) we note that this is tantamount to the condition

$$\mathcal{J}_0 \left(b \sqrt{k^2 - q_{0m}^2} \right) = 0, \quad (48)$$

which will be written

$$\mathcal{J}_0(X_{Fm}) = 0 \quad (49)$$

where the F stands for flexible. In this situation $X_{Fm} = 0$ is not a characteristic value, so m takes on the values

$$m = 1, 2, 3, \dots$$

Again, as in the case for an absolutely rigid boundary, we find that m is summed to

$$\frac{C^2 X_{Fm}^2}{b^2} \leq \omega^2 \quad \text{or} \quad X_{Fm} \leq kb,$$

but here C_{F0} does not exist.

Finally,

$$\left(\text{Re} \langle \phi \rangle_{\text{rel}} \right)_F = \sum_{m=1}^{X_{Fm} \leq kb} \left\{ \frac{4\mathcal{J}_1^2 \left(X_{Fm} \frac{a}{b} \right) \cos \left[(q_{Fm} - k)z \right]}{X_{Fm}^2 \mathcal{J}_1^2 \left(X_{Fm} \right)} \right\} \quad (50)$$

and

$$\left(\text{Im} \langle \phi \rangle_{\text{rel}} \right)_F = \sum_{m=1}^{X_{Fm} \leq kb} \left\{ \frac{4\mathcal{J}_1^2 \left(X_{Fm} \frac{a}{b} \right) \sin \left[(q_{Fm} - k)z \right]}{X_{Fm}^2 \mathcal{J}_1^2 \left(X_{Fm} \right)} \right\} \quad (51)$$

where we have used $\mathcal{J}_0(X_{Fm}) = 0$ and have again invoked orthogonality of the characteristic functions R_{Fm} . If this latter does not hold, the modification previously discussed for absolutely rigid boundary conditions must be made.

Thin Elastic Walls

Although the thin elastic wall situation is not calculated in this report, it is included here mainly because of the interesting observation of Jacobi (15) that a 2-1/4-in. (outside) diameter steel tube with a 1/64-in.-thick wall was found

to be flexible enough so that the observed mode (the first real one) experimentally followed that for a pressure release tube.

If we use the equations of motion for a tube, given by Lin and Morgan (17), which neglect rotatory inertia we find that the X_{0m} (here designated X_{Tm}) are the zeroes of

$$\frac{\rho_b}{\rho_t h} \frac{\mathcal{J}_0(X_{Tm})}{X_{Tm} \mathcal{J}_1(X_{Tm})} = 1 - \left(\frac{C_p}{b\omega}\right)^2 + \nu^2 \left(\frac{C_p}{b\omega}\right)^2 \left(\frac{1}{1 - \left(\frac{C}{C_p}\right)^2}\right) - \frac{h^2}{12b^2} \left(\frac{b\omega}{C_p}\right)^2 \left(\frac{C_p}{C}\right)^2 \frac{1}{\left(\frac{C}{C_p}\right)^2 + \left(\frac{h^2}{12b^2}\right) \left(\frac{2}{(1-\nu)K}\right) \left(\frac{b\omega}{C_p}\right)^2} \quad (52)$$

where ρ is the contained liquid density, ρ_T is the tube metal density, ν is the Poisson's ratio, C_p is the compressional velocity in the wall material, h is the wall thickness, K is a somewhat arbitrary constant slightly less than unity, and the subscript T refers to the tube.

We further find that there exists one imaginary root so that

$$C_{T0}^2 < C^2,$$

but for all the other modes

$$C_{Tm}^2 > C^2.$$

Another observation is the existence of C_{T0} and C_{T1} at all frequencies, but the other modes have cutoff frequencies given by

$$\frac{\mathcal{J}_0\left(\frac{b\omega}{C_p} \frac{C_p}{C}\right)}{\mathcal{J}_1\left(\frac{b\omega}{C_p} \frac{C_p}{C}\right)} = \frac{\left(\frac{b\omega}{C_p}\right)^2 - 1}{\frac{\rho_b}{\rho_t h} \frac{C}{C_p} \frac{b\omega}{C_p}}. \quad (53)$$

For $m \neq 0$ we have the relation

$$\frac{\mathcal{J}_0(X_{Tm})}{X_{Tm} \mathcal{J}_1(X_{Tm})} = \frac{\mathcal{J}_0\left(b\sqrt{k^2 - q_{Tm}^2}\right)}{b\sqrt{k^2 - q_{Tm}^2} \mathcal{J}_1\left(b\sqrt{k^2 - q_{Tm}^2}\right)}, \quad (54)$$

while for $m = 0$ this becomes

$$\frac{-\mathcal{J}_0\left(b\sqrt{q_{T0}^2 - k^2}\right)}{b\sqrt{q_{T0}^2 - k^2} \mathcal{J}_1\left(b\sqrt{q_{T0}^2 - k^2}\right)} \quad (55)$$

using $\mathcal{J}_0(iX) \equiv \mathcal{J}_0(X)$ and $\mathcal{J}_1(iX) \equiv i\mathcal{J}_1(X)$.

Liquid Boundary

The liquid boundary condition is the first really interesting situation and requires that we distinguish between the two media involved (see Fig. 2). Medium I is assumed to have an impedance $\rho_1 C_1$ and medium II an impedance $\rho_2 C_2$.

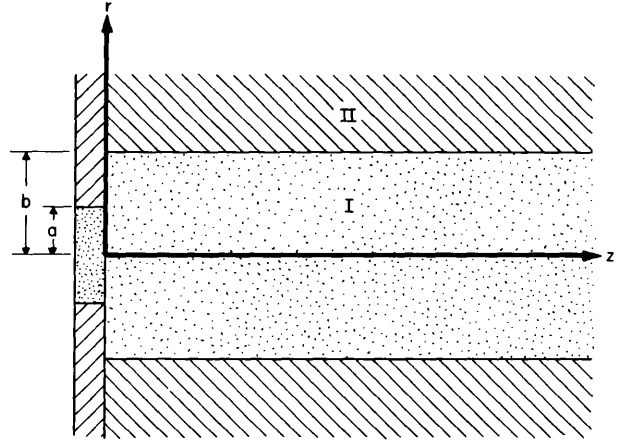


Fig. 2 - Cylindrical cavity containing (liquid) medium I having an impedance $\rho_1 C_1$, surrounded by medium II with impedance $\rho_2 C_2$. (See Fig. 1 and caption.)

The previous relation for the time-independent velocity potential given by Eq. (2c) is then rewritten as

$$\phi_{0m}^I = K_{0m}^I \mathcal{J}_0\left(r\sqrt{k_1^2 - q_{0m}^2}\right) e^{iq_{0m}z} \quad (56)$$

and

$$\phi_{0m}^{II} = K_{0m}^{II} \mathcal{H}_0^{(1)}\left(r\sqrt{k_2^2 - q_{0m}^2}\right) e^{iq_{0m}z} \quad (57)$$

where, in the notation of Jahnke and Emde,

$$\mathcal{H}_0^{(1)} = \mathcal{J}_0 + i\mathcal{N}_0. *$$

*See discussion concerning this function in Appendices A and C.

Imposing the boundary conditions at $r = b$ of continuity of pressure and continuity of the normal component of velocity amounts to requiring continuity of impedance, or

$$\frac{i\omega\rho_1(\phi^I)}{\left(\frac{\partial\phi^I}{\partial r}\right)}\bigg|_{r=b} = \frac{i\omega\rho_2(\phi^{II})}{\left(\frac{\partial\phi^{II}}{\partial r}\right)}\bigg|_{r=b}, \quad (58)$$

which becomes

$$\frac{\rho_1 \mathcal{J}_0\left(b\sqrt{k_1^2 - q_{0m}^2}\right)}{\sqrt{k_1^2 - q_{0m}^2} \mathcal{J}_1\left(b\sqrt{k_1^2 - q_{0m}^2}\right)} = \frac{\rho_2 \mathcal{H}_0^{(1)}\left(b\sqrt{k_2^2 - q_{0m}^2}\right)}{\sqrt{k_2^2 - q_{0m}^2} \mathcal{H}_1^{(1)}\left(b\sqrt{k_2^2 - q_{0m}^2}\right)}. \quad (59)$$

$$\sqrt{k_1^2 - q_{Rm}^2} \mathcal{J}_1\left(b\sqrt{k_1^2 - q_{Rm}^2}\right) \equiv q_{Rm} \sqrt{\left(\frac{C_{Rm}}{C}\right)^2 - 1} \mathcal{J}_1\left(q_{Rm} b \sqrt{\left(\frac{C_{Rm}}{C}\right)^2 - 1}\right) = 0, \quad (65)$$

Defining

$$X \equiv b\sqrt{k_1^2 - q_{0m}^2}$$

so that

$$X^2 = b^2 \left(\frac{\omega^2}{C_1^2} - \frac{\omega^2}{C_{0m}^2} \right), \quad (60)$$

and

$$Y \equiv b\sqrt{k_1^2 - k_2^2}$$

so that

$$Y^2 = b^2 \left(\frac{\omega^2}{C_1^2} - \frac{\omega^2}{C_2^2} \right), \quad (61)$$

by rearranging we obtain

$$\frac{\mathcal{J}_0(X)}{X\mathcal{J}_1(X)} = \frac{\rho_2}{\rho_1} \frac{\mathcal{H}_0^{(1)}(\sqrt{X^2 - Y^2})}{\sqrt{X^2 - Y^2} \mathcal{H}_1^{(1)}(\sqrt{X^2 - Y^2})} \quad (62)$$

Now for truly guided waves, ϕ^{II} must vanish as $r \rightarrow \infty$. The function $\mathcal{H}_0^{(1)}$ vanishes for an infinite complex argument with the imaginary part positive, so we require

$$q_{0m}^2 > k_2^2$$

or

$$Y^2 > X^2. \quad (63)$$

For Y to be real we require $C_2 > C_1$ and may write

$$\frac{\mathcal{J}_0(X)}{X\mathcal{J}_1(X)} = \frac{\rho_2}{\rho_1} \frac{\mathcal{H}_0^{(1)}(i\sqrt{Y^2 - X^2})}{i\sqrt{Y^2 - X^2} \mathcal{H}_1^{(1)}(i\sqrt{Y^2 - X^2})}, \quad (64)$$

and m is summed to $X_{0m} \leq Y$. We may note that for an absolutely rigid wall the particle velocity U goes to 0 at the boundary; so from Eq. (7)

which implies that either $C_{Rm} = C$, the "plane-wave" mode, or

$$\mathcal{J}_1\left(q_{Rm} b \sqrt{\left(\frac{C_{Rm}}{C}\right)^2 - 1}\right) = 0, \quad (66)$$

the "reflected conical wave" modes. Just as the characteristic function for the rigid wall limiting case is derivable as above from this liquid wall case, so may we obtain the infinitely flexible wall limit (where $p \rightarrow 0$) as

$$\mathcal{J}_0\left(q_{Fm} b \sqrt{\left(\frac{C_{Fm}}{C}\right)^2 - 1}\right) = 0. \quad (67)$$

In both these limiting cases the argument of the Bessel functions is just X_{0m} .

Returning to the liquid wall case, we note that for $\rho_1 = \rho_2$ and $k_1 = k_2$ we obtain (from Eq. (62))

$$\frac{\mathcal{J}_1}{\mathcal{J}_0} = \frac{\mathcal{H}_1^{(1)}}{\mathcal{H}_0^{(1)}} = \frac{\mathcal{J}_0\mathcal{J}_1 + \mathcal{N}_0\mathcal{N}_1 - i(\mathcal{J}_1\mathcal{N}_0 - \mathcal{J}_0\mathcal{N}_1)}{\mathcal{J}_0^2 + \mathcal{N}_0^2}. \quad (68)$$

By equating the imaginary parts we find

$$0 = \mathcal{J}_1 \mathcal{N}_0 - \mathcal{J}_0 \mathcal{N}_1;$$

but $\mathcal{J}_1 \mathcal{N}_0 - \mathcal{J}_0 \mathcal{N}_1 = 2/\pi X \neq 0$ for any X (except $X = \infty$), so we find that the above limit is not valid in this equation. That is, we may not, following the development of Eq. (62), let $\rho_2 \rightarrow \rho_1$ and $k_2 \rightarrow k_1$.

The values of X satisfying the characteristic equation (64) are the characteristic values for liquid boundary conditions and will be denoted by X_{Lm} for future use.

Elastic Solid Boundary

As in the previous liquid boundary case, we must also consider two media for an elastic solid boundary. But here, as usual for elastic media, we will use a displacement vector \mathbf{s} given by

$$\mathbf{s} = \nabla\Phi + \nabla_{\mathbf{x}}\Psi \quad (69)$$

where Φ is the scalar displacement potential and Ψ the vector displacement potential satisfying respectively, the "wave" equations*

$$\begin{aligned} \nabla^2\Phi - \frac{1}{C_c^2} \frac{\partial^2\Phi}{\partial t^2} &= 0 \\ \nabla^2\Psi - \frac{\Psi}{r^2} - \frac{1}{C_s^2} \frac{\partial^2\Psi}{\partial t^2} &= 0 \end{aligned} \quad (70)$$

with the compressional velocity

$$C_c = \sqrt{\frac{\lambda + 2\mu}{\rho}}$$

and the shear wave velocity

$$C_s = \sqrt{\frac{\mu}{\rho}}$$

being related to Poisson's ratio ν by

$$\left(\frac{C_c}{C_s}\right)^2 = \frac{2(1-\nu)}{1-2\nu}.$$

Because of our axial symmetry we will retain only the single component θ of Ψ and indicate this by the scalar Ψ .

*The word *wave* is written with quotation marks because of the extraneous term in the second half of Eq. (70). See Appendix B for more details.

For guided waves in the liquid cylinder, we write

$$\Phi_1 = \Phi_0 \mathcal{J}_0\left(r\sqrt{k^2 - q_{0m}^2}\right) e^{i(q_{0m}z - \omega t)} \quad (71)$$

for $k^2 > q_{0m}^2$. For $q_{0m}^2 > k^2$ we would have Stonely waves and would write

$$\Phi_1 = \Phi_0 \mathcal{J}_0\left(r\sqrt{k^2 - q_{0m}^2}\right) e^{i(q_{0m}z - \omega t)} \quad (72)$$

where $\mathcal{J}_0(ix) = \mathcal{J}_0(x)$. Since Φ_1 is a scalar displacement potential, we have the pressure

$$p = -\rho_1 \ddot{\Phi}_1$$

and the particle velocity

$$U_r^\ell = \frac{d}{dr} \dot{\Phi}_1,$$

but the particle displacement is

$$\mathbf{s}_r^\ell = \frac{\partial}{\partial r} \Phi_1$$

where the subscript r refers to the r component and the superscript ℓ refers to the liquid media. For $C_{0m} > C$, the above relations become

$$p = \Phi_0 \rho_1 \omega^2 \mathcal{J}_0\left(r\sqrt{k^2 - q_{0m}^2}\right) e^{i(q_{0m}z - \omega t)} \quad (73)$$

and

$$\begin{aligned} \mathbf{s}_r^\ell &= -\Phi_0 \sqrt{k^2 - q_{0m}^2} \\ &\mathcal{J}_1\left(r\sqrt{k^2 - q_{0m}^2}\right) e^{i(q_{0m}z - \omega t)} \end{aligned} \quad (74)$$

where we have used

$$\mathcal{J}_1(x) = -\mathcal{J}_0'(x)$$

so that

$$\left.\frac{p}{\mathbf{s}_r^\ell}\right|_{r=b} = \frac{-\rho_1 \omega^2 \mathcal{J}_0\left(b\sqrt{k^2 - q_{0m}^2}\right)}{\sqrt{k^2 - q_{0m}^2} \mathcal{J}_1\left(b\sqrt{k^2 - q_{0m}^2}\right)}. \quad (75)$$

Using the previous definition

$$X_{0m} \equiv b\sqrt{k^2 - q_{0m}^2},$$

this ratio becomes

$$\left. \frac{p}{s_r} \right|_{r=b} = -\rho_1 \omega^2 b \frac{J_0(X_{0m})}{X_{0m} J_1(X_{0m})}. \quad (76)$$

Returning to the elastic wall, in analogy with the previous solutions to the wave equation, we write*

$$\Phi = \Phi_0 K_0\left(r\sqrt{q_{0m}^2 - k_c^2}\right) e^{-i(\omega t - q_{0m}z)} \quad (77)$$

$$\Psi = \Psi_0 K_1\left(r\sqrt{q_{0m}^2 - k_s^2}\right) e^{-i(\omega t - q_{0m}z)}$$

where the subscripts c and s refer to compressional and shear waves, respectively, and K_0 and K_1 are modified Bessel functions of the second kind.

The displacement components for the elastic medium are

$$s_r = \frac{\partial \Phi}{\partial r} - \frac{\partial \Psi}{\partial z} \quad (78)$$

and

$$s_z = \frac{\partial \Phi}{\partial z} + \frac{1}{r} \frac{\partial}{\partial r}(r\Psi),$$

and the stress components are given by

$$\begin{aligned} \sigma_{rr} = & 2\rho_2 C_s^2 \frac{\partial s_r}{\partial r} \\ & + 2\rho_2 C_s^2 \left(\frac{\nu}{1-2\nu}\right) \left(\frac{\partial s_r}{\partial r} + \frac{s_r}{r} + \frac{\partial s_z}{\partial z}\right) \end{aligned} \quad (79)$$

and

$$\sigma_{rz} = \rho_2 C_s^2 \left(\frac{\partial s_r}{\partial z} + \frac{\partial s_z}{\partial r}\right)$$

where $\rho_2 C_s^2$ is equal to the shear modulus μ and $2\rho_2 C_s^2 \left(\frac{\nu}{1-2\nu}\right)$ is equal to the other Lamé constant usually denoted by λ .

For axially symmetric cylindrical coordinates, the elastic wave equations become

$$\frac{\partial^2 \Phi}{\partial r^2} + \frac{1}{r} \frac{\partial \Phi}{\partial r} + \frac{\partial^2 \Phi}{\partial z^2} = \frac{1}{C_c^2} \frac{\partial^2 \Phi}{\partial t^2} \quad (80)$$

and

$$\frac{\partial^2 \Psi}{\partial r^2} + \frac{1}{r} \frac{\partial \Psi}{\partial r} - \frac{\Psi}{r^2} + \frac{\partial^2 \Psi}{\partial z^2} = \frac{1}{C_s^2} \frac{\partial^2 \Psi}{\partial t^2}$$

so that, using these results with the equations for σ and s and the relationship between C_s and C_c , we obtain

$$\sigma_{rr} = 2\rho_2 C_s^2 \left(\frac{\partial^2 \Phi}{\partial r^2} - \frac{\partial^2 \Psi}{\partial r \partial z}\right) + \rho_2 \left(\frac{\nu}{1-\nu}\right) \frac{\partial^2 \Phi}{\partial t^2} \quad (81)$$

and

$$\sigma_{rz} = 2\rho_2 C_s^2 \left(\frac{\partial^2 \Phi}{\partial r \partial z} - \frac{\partial^2 \Psi}{\partial z^2}\right) + \rho_2 \frac{\partial^2 \Psi}{\partial t^2}.$$

The two appropriate boundary conditions are the vanishing of tangential stress at the boundary, or

$$\left. \sigma_{rz} \right|_{r=b} = 0,$$

and the equality

$$\left. \frac{p}{s_r} \right|_{r=b} = \left. \frac{-\sigma_{rr}}{s_r} \right|_{r=b}.$$

From the vanishing of tangential stress we obtain

$$\frac{\Phi_0}{\Psi_0} = \frac{i(2q_{0m}^2 - k_s^2) K_1\left(b\sqrt{q_{0m}^2 - k_s^2}\right)}{2q_{0m} \sqrt{q_{0m}^2 - k_c^2} K_0'\left(b\sqrt{q_{0m}^2 - k_c^2}\right)} \quad (82)$$

where the prime refers, as usual, to differentiation with respect to the entire argument. Now, solving for $\sigma_{rr}|_{r=b}$ we find

$$\begin{aligned} \left. \sigma_{rr} \right|_{r=b} e^{i(\omega t - q_{0m}z)} = & 2\rho_2 C_s^2 (q_{0m}^2 - k_c^2) \Phi_0 K_0''\left(b\sqrt{q_{0m}^2 - k_c^2}\right) \\ & - i2\rho_2 C_s^2 q_{0m} \sqrt{q_{0m}^2 - k_s^2} \Psi_0 K_1'\left(b\sqrt{q_{0m}^2 - k_s^2}\right) - \rho_2 \omega^2 \left(\frac{\nu}{1-\nu}\right) \Phi_0 K_0\left(b\sqrt{q_{0m}^2 - k_c^2}\right). \end{aligned} \quad (83)$$

Solving for $s_r|_{r=b}$ we find, eliminating Φ_0 by using Eq. (82),

*See Appendix C for discussion of appropriate Bessel Function solutions.

$$s_r \Big|_{r=b} e^{i(\omega t - q_{0m} z)} = - \frac{ik_s^2}{2q_{0m}} \Psi_0 \mathcal{K}_1 \left(b \sqrt{q_{0m}^2 - k_s^2} \right) \quad (84)$$

so that

$$\begin{aligned} \frac{\sigma_{rr}}{s_r} \Big|_{r=b} &= \left(\frac{i4\rho_2 C_s^2}{k_s^2} \right) q_{0m} (q_{0m}^2 - k_c^2) \frac{\Phi_0 \mathcal{K}_0'' \left(b \sqrt{q_{0m}^2 - k_c^2} \right)}{\Psi_0 \mathcal{K}_1 \left(b \sqrt{q_{0m}^2 - k_s^2} \right)} \\ &+ \left(\frac{4\rho_2 C_s^2}{k_s^2} \right) q_{0m}^2 \sqrt{q_{0m}^2 - k_s^2} \frac{\mathcal{K}_1' \left(b \sqrt{q_{0m}^2 - k_s^2} \right)}{\mathcal{K}_1 \left(b \sqrt{q_{0m}^2 - k_s^2} \right)} - i2\rho_2 C_s^2 q_{0m} \left(\frac{\nu}{1-\nu} \right) \frac{\Phi_0 \mathcal{K}_0 \left(b \sqrt{q_{0m}^2 - k_c^2} \right)}{\Psi_0 \mathcal{K}_1 \left(b \sqrt{q_{0m}^2 - k_s^2} \right)}. \end{aligned} \quad (85)$$

Replacing the ratio Φ_0/Ψ_0 in Eq. (85) by Eq. (82), Eq. (85) becomes

$$\begin{aligned} \frac{\sigma_{rr}}{s_r} \Big|_{r=b} &= - \left(\frac{2\rho_2 C_s^2}{k_s^2} \right) \sqrt{q_{0m}^2 - k_c^2} (2q_{0m}^2 - k_s^2) \frac{\mathcal{K}_0'' \left(b \sqrt{q_{0m}^2 - k_c^2} \right)}{\mathcal{K}_0' \left(b \sqrt{q_{0m}^2 - k_c^2} \right)} \\ &+ \left(\frac{4\rho_2 C_s^2}{k_s^2} \right) q_{0m}^2 \sqrt{q_{0m}^2 - k_s^2} \frac{\mathcal{K}_1' \left(b \sqrt{q_{0m}^2 - k_s^2} \right)}{\mathcal{K}_1 \left(b \sqrt{q_{0m}^2 - k_s^2} \right)} \\ &+ \rho_2 C_s^2 (2q_{0m}^2 - k_s^2) \left(\frac{\nu}{1-\nu} \right) \frac{\mathcal{K}_0 \left(b \sqrt{q_{0m}^2 - k_c^2} \right)}{\sqrt{q_{0m}^2 - k_c^2} \mathcal{K}_0' \left(b \sqrt{q_{0m}^2 - k_c^2} \right)}. \end{aligned} \quad (86)$$

Using the identities

$$\mathcal{K}_0'(x) = -\mathcal{K}_1(x) \quad \mathcal{K}_1'(x) = -\mathcal{K}_0(x) - \frac{\mathcal{K}_1(x)}{x} \quad \mathcal{K}_0''(x) = -\mathcal{K}_1'(x) = \mathcal{K}_0(x) + \frac{\mathcal{K}_1(x)}{x}$$

and the relationship

$$\frac{\nu}{1-\nu} = 1 - 2 \frac{k_c^2}{k_s^2},$$

we obtain

$$\begin{aligned} \frac{\sigma_{rr}}{s_r} \Big|_{r=b} &= - \frac{2\rho_2 \omega^2}{bk_s^2} - \left(\frac{4\rho_2 \omega^2 q_{0m}^2}{k_s^4} \right) \sqrt{q_{0m}^2 - k_s^2} \frac{\mathcal{K}_0 \left(b \sqrt{q_{0m}^2 - k_s^2} \right)}{\mathcal{K}_1 \left(b \sqrt{q_{0m}^2 - k_s^2} \right)} \\ &+ \frac{\rho_2 \omega^2}{k_s^4} \frac{(2q_{0m}^2 - k_s^2)^2 \mathcal{K}_0 \left(b \sqrt{q_{0m}^2 - k_c^2} \right)}{\sqrt{q_{0m}^2 - k_c^2} \mathcal{K}_1 \left(b \sqrt{q_{0m}^2 - k_c^2} \right)}. \end{aligned} \quad (87)$$

Finally, using the second boundary condition in conjunction with Eq. (76), we have

$$\begin{aligned} \frac{\mathcal{J}_0(X_{0m})}{X_{0m} \mathcal{J}_1(X_{0m})} \frac{\rho_1}{\rho_2} &= - \frac{2}{b^2 k_s^2} - \left(\frac{4q_{0m}^2}{bk_s^4} \right) \sqrt{q_{0m}^2 - k_s^2} \frac{\mathcal{K}_0 \left(b \sqrt{q_{0m}^2 - k_s^2} \right)}{\mathcal{K}_1 \left(b \sqrt{q_{0m}^2 - k_s^2} \right)} \\ &+ \frac{(2q_{0m}^2 - k_s^2)^2 \mathcal{K}_0 \left(b \sqrt{q_{0m}^2 - k_c^2} \right)}{bk_s^4 \sqrt{q_{0m}^2 - k_c^2} \mathcal{K}_1 \left(b \sqrt{q_{0m}^2 - k_c^2} \right)}. \end{aligned} \quad (88)$$

Defining

$$Y_s \equiv b\sqrt{k^2 - k_s^2}$$

and

$$Y_c \equiv b\sqrt{k^2 - k_c^2},$$

and using the previous $X_{0m} = b\sqrt{k^2 - q_{0m}^2}$, we obtain

$$\frac{\mathcal{J}_0(X_{0m})}{X_{0m} \mathcal{J}_1(X_{0m})} \frac{\rho_1}{\rho_2} = - \frac{2}{b^2 k_s^2} -$$

$$\left(\frac{4q_{0m}^2}{b^2 k_s^4} \right) \sqrt{Y_s^2 - X_{0m}^2} \frac{K_0(\sqrt{Y_s^2 - X_{0m}^2})}{K_1(\sqrt{Y_s^2 - X_{0m}^2})} \quad (89)$$

$$+ \frac{(2q_{0m}^2 - k_s^2)^2}{k_s^4 \sqrt{Y_c^2 - X_{0m}^2}} \frac{K_0(\sqrt{Y_c^2 - X_{0m}^2})}{K_1(\sqrt{Y_c^2 - X_{0m}^2})}.$$

which applies to the reflected waves or $C_{0m} > C$. There is also one imaginary root or Stonely wave for $C > C_{0m}$. The subscripts 1 and 2 on the density ρ refer to the liquid and wall, respectively. The applicable values of k_s/k_c are between $\sqrt{2}$ and ∞ , which correspond to values of Poisson's ratio ν between 0 and 0.5. For guided waves $q_{0m} \leq k$, or m is summed to $X_{0m} \leq kb$ since $X_{0m} \geq 0$. Now $C_c > C_s$, or $k_s > k_c$, which implies that $Y_s < Y_c$. Again, for truly guided waves, $\Phi^{II} \rightarrow 0$ as $r \rightarrow \infty$ implies that $q_{0m}^2 > k_s^2$ and $q_{0m}^2 > k_c^2$, so $q_{0m}^2 > k_s^2 > k_c^2$ or, finally,

$$0 \leq X_{0m} < Y_s < Y_c.$$

Again we will denote the roots of the characteristic equation (89) as the characteristic values X_{Em} where the E stands for elastic wall.

It should be noted that Eq. (89) differs from any previous work. A particularly pleasing circumstance is that the liquid boundary case can readily be shown to be a degenerate case of (89). For if there is no shear, then $C_s = 0$, $k_s = \infty$, and Eq. (89) becomes directly

$$\frac{\mathcal{J}_0(X_{0m})}{X_{0m} \mathcal{J}_1(X_{0m})} = \frac{\rho_2}{\rho_1} \frac{K_0(\sqrt{Y_c^2 - X_{0m}^2})}{\sqrt{Y_c^2 - X_{0m}^2} K_1(\sqrt{Y_c^2 - X_{0m}^2})}$$

which, by virtue of the definitions

$$\mathcal{H}_0^{(1)}(iX) = \frac{2}{\pi i} K_0(X)$$

$$\mathcal{H}_1^{(1)}(iX) = -\frac{2}{\pi} K_1(X),$$

may be written

$$\frac{\mathcal{J}_0(X_{0m})}{X_{0m} \mathcal{J}_1(X_{0m})} = \frac{\rho_2}{\rho_1} \frac{\mathcal{H}_0^{(1)}(i\sqrt{Y_c^2 - X_{0m}^2})}{i\sqrt{Y_c^2 - X_{0m}^2} \mathcal{H}_1^{(1)}(i\sqrt{Y_c^2 - X_{0m}^2})}$$

which, with $Y_c \equiv Y$, is identically Eq. (64) for liquid boundaries.

We note that for an absolutely rigid wall, the impedance going to infinity at the boundary amounts to the denominator of Eq. (75) going to zero, or $\mathcal{J}_1(X_{Rm}) = 0$. For an infinitely flexible wall, again, we have the impedance going to zero or, directly from the numerator of Eq. (75), $\mathcal{J}_0(X_{Fm}) = 0$; these are the limiting cases previously employed.

ORTHOGONALITY CHECKS AND NONORTHOGONAL SIMPLIFICATION

We will now turn our attention to the determination of the appropriate characteristic functions and the calculation of the expansion coefficients in Eq. (24) by using Eq. (38) or, if the functions prove orthogonal, by using Eq. (16). Equation (33) is

$$\int_0^b R_{0m} R_{0\ell} r dr = \frac{b^2}{X_{0m}^2 - X_{0\ell}^2}$$

$$[X_{0m} \mathcal{J}_0(X_{0\ell}) \mathcal{J}_1(X_{0m}) - X_{0\ell} \mathcal{J}_0(X_{0m}) \mathcal{J}_1(X_{0\ell})]$$

where $R_{nm} \equiv \mathcal{J}_n\left(r \frac{X_{0m}}{b}\right)$ and the orthogonality criterion is that Eq. (33) be equal to zero for $m \neq l$.

In this section only we shall, for simplicity, standardize the parameters as shown in Table 1.* (These parameters are all varied later).

TABLE 1

Standard Reference Parameters Used in Calculating Characteristic Functions and Expansion Coefficients in Eq. (24)

$\lambda = 0.15$ cm (acoustic source operating wavelength)
$a = 10\lambda = 1.5$ cm (acoustic source radius)
$b = 2a = 20\lambda = 3.0$ cm (propagation-cylinder radius; radius ratio $b/a = 2$)
$k = 2\pi/\lambda$ (wave number associated with wavelength λ)
$k_1 a = 20\pi$
$k_1 b = 40\pi$
$\rho_2/\rho_1 = 7$ (ρ_1 is density of medium inside cylinder; ρ_2 is density outside)
$k_1/k_2 = 4$ (wave number ratio for the two media)
$(k_1/k_2 = \lambda_2/\lambda_1 = C_2/C_1; C$ is the velocity in the indicated medium)
$\nu = 0.325$ (Poisson's ratio)
$\alpha = 0$ (absorption coefficient)

For rigid wall boundary conditions, Eq. (41) shows that the appropriate characteristic values are the zeros of \mathcal{J}_1 , including zero, up to kb where k is the wave number and b is the tube radius. For the standardized parameters in Table 1 we find that $kb = 125.66370616$ and the appropriate list of characteristic values is given in Table 2.

However, for this rigid wall boundary condition case we find that we do not need the actual

*All the calculations in this report use $ka = 20\pi$, which implies that $a = 10\lambda$. In the previous report (4), we recall that graphs of $\langle p \rangle_{rel}$ and $\langle \theta \rangle_{rel}$ plotted vs. $z\lambda/a^2$ superimpose for all $ka \geq 20\pi$. Thus all the graphs in the present report are valid for $a \geq 10\lambda$. The b/a parameter variations used herein are obtained by changing only the value b .

TABLE 2
List of Characteristic Values
 $X_{Rm} \leq kb$ for the Rigid Wall Boundary Condition
[Characteristic Eq. (41)] and $b/a = 2.0$

m	X_{Rm}	m	X_{Rm}
0	0	20	63.6113567
1	3.8317060	21	66.7532267
2	7.0155867	22	69.8950718
3	10.1734681	23	73.0368952
4	13.3236919	24	76.1786996
5	16.4706301	25	79.3204872
6	19.6158585	26	82.4622599
7	22.7600844	27	85.6040194
8	25.9036721	28	88.7457671
9	29.0468285	29	91.8875042
10	32.1896799	30	95.0292318
11	35.3323076	31	98.1709507
12	38.4747662	32	101.3126618
13	41.6170942	33	104.4543658
14	44.7593190	34	107.5960633
15	47.9014609	35	110.7377548
16	51.0435352	36	113.8794408
17	54.1855536	37	117.0211219
18	57.3275254	38	120.1627983
19	60.4694578	39	123.3044705

values in Table 1 to check orthogonality. From Eq. (33) we note immediately that if the characteristic values are zeros of \mathcal{J}_1 , then both terms in the equation are identically zero. Thus the characteristic functions derivable from the assumption of absolutely rigid walls are orthogonal and the relatively simple Eq. (16) may be used for calculation of the expansion coefficients.

For infinitely flexible boundary conditions, we likewise immediately note that the pertinent characteristic values, the zeros of \mathcal{J}_0 , result in both terms of Eq. (33) being identically zero. So the expansion of the velocity potential field inside the cylinder may, for infinitely flexible boundary conditions, as well as absolutely rigid boundary conditions, be obtained in the relatively simple formulation pertinent to orthogonal functions. A table of appropriate characteristic values for this infinitely flexible boundary condition, using the values shown in Table 1, is given in Table 3.

For liquid boundary conditions, the appropriate characteristic values X_{Lm} indicated by Eq. (64) are summed, according to Eqs. (61) and (63), up to

$$Y = b\sqrt{k_1^2 - k_2^2}$$

where k_1 is the wave number of the contained liquid and k_2 is the wave number of the boundary liquid. Our standard reference conditions are $k_1/k_2 = 4$ and $b = 20\lambda_1$ with $\lambda_1 = 0.15$ cm, so for this case $Y = 121.673$. The appropriate characteristic values are given in Table 4.

Since these values are neither zeros of \mathcal{J}_0 or \mathcal{J}_1 , Eq. (33) is obviously not identically zero by inspection. As a matter of fact, it is generally true that the characteristic functions will not be mutually orthogonal if the boundary conditions depend on the characteristic value.

If we use Table 4 and calculate $\mathcal{J}_0(X_{Lm})$ and $\mathcal{J}_1(X_{Lm})$ with the standardized value of b , we

TABLE 3
List of Characteristic Values $X_{Fm} \leq kb$ that are zeros of $\mathcal{J}_0(X_{Fm})$ for the Infinitely Flexible Boundary Condition [Characteristic Eq. (49)] and $b/a = 2.0$

m	X_{Fm}	m	X_{Fm}
1	2.4048256	21	65.1899648
2	5.5200781	22	68.3314693
3	8.6537279	23	71.4729816
4	11.7915344	24	74.6145006
5	14.9309177	25	77.7560256
6	18.0710640	26	80.8975559
7	21.2116366	27	84.0390908
8	24.3524715	28	87.1806298
9	27.4934791	29	90.3221726
10	30.6346065	30	93.4637188
11	33.7758202	31	96.6052680
12	36.9170983	32	99.7468199
13	40.0584258	33	102.8883742
14	43.1997917	34	106.0299309
15	46.3411884	35	109.1714896
16	49.4826099	36	112.3130503
17	52.6240518	37	115.4546126
18	55.7655108	38	118.5961766
19	58.9069839	39	121.7377421
20	62.0484692	40	124.8793089

TABLE 4
List of Characteristic Values $X_{Lm} \leq Y$ for the Liquid Boundary Condition [Characteristic Eq. (64)] and $b/a = 2.0$

m	X_{Lm}	m	X_{Lm}
1	2.2716377	21	63.8405807
2	5.2211344	22	66.9679868
3	8.2022980	23	70.0963105
4	11.2055952	24	73.2254264
5	14.2292985	25	76.3552248
6	17.2712781	26	79.4856088
7	20.3289243	27	82.6164906
8	23.3996145	28	85.7477895
9	26.4809976	29	88.8794289
10	29.5710924	30	92.0113338
11	32.6682830	31	95.1434277
12	35.7712728	32	98.2756279
13	38.8790273	33	101.4078399
14	41.9907212	34	104.5399468
15	45.1056940	35	107.6717908
16	48.2234141	36	110.8031348
17	51.3434505	37	113.9335679
18	54.4654514	38	117.0622018
19	57.5891272	39	120.1859282
20	60.7142374		

obtain Table 5 from Eq. (33) where the combination is such that the first characteristic value is checked for orthogonality in turn with each successive one, that is, the first with the second, the first with the third, the first with the fourth, etc. This amounts to defining $\ell = 1$ in Eq. (33).

Before commenting on Table 5 we shall determine the characteristic values X_{Em} for elastic boundary conditions using the standardized parameters shown in Table 1. In this case we use Eq. (89) with the roots summed from $0 \leq X_{Em} < Y_s$. The reference parameters from Table 1 yield $Y_s = 109.474$, and the characteristic values smaller than this value are listed in Table 6. From this table of characteristic values for elastic boundary conditions and the reference parameters, we again check for orthogonality, as was done for Table 5 for liquid boundary conditions, and obtain Table 7 where again the check is for each value in turn with the first.

Tables 5 and 7 indicate that the characteristic functions for both the liquid boundary condition and the elastic boundary condition are nonorthogonal, as might have been expected. However, it does not seem trivial or unduly heuristic to state that they are *almost* orthogonal. In any event, it would be interesting to calculate and compare the expansion coefficients K_{0m} obtained by the relatively simple Eq. (16), which invoked orthogonality, and the more exact Eq. (38), the latter being properly terminated after a finite number of terms, as previously shown.

Table 8 is a comparison of the expansion coefficients calculated by both methods for the liquid boundary condition reference parameters, and Table 9 is the same comparison for the elastic boundary condition reference parameters.

TABLE 5

Orthogonality Check of the Characteristic Functions Listed in Table 4. The Values of Table 4 are Used in Evaluating Eq. (33), Which Would Equal Zero for Orthogonality.

m	Evaluation of Eq. (33)	m	Evaluation of Eq. (33)
1	—	21	$+1.520180 \times 10^{-7}$
2	-1.269465×10^{-7}	22	-1.531461
3	+1.501627	23	+1.547735
4	-1.632731	24	-1.569518
5	+1.697591	25	+1.597487
6	-1.720454	26	-1.632527
7	+1.718015	27	+1.678582
8	-1.701534	28	-1.728905
9	+1.677856	29	+1.793230
10	-2.038622	30	-1.873832
11	+1.624821	31	+1.972802
12	-1.599700	32	-2.097020
13	+1.576982	33	+2.256007
14	-1.557219	34	-2.465297
15	+1.540742	35	+2.752281
16	-1.527754	36	-3.170842
17	+1.518400	37	+3.846300
18	-1.512808	38	-5.170171
19	+1.511116	39	+9.726968
20	-1.513498		

TABLE 6

List of Characteristic Values $X_{Em} < Y_s$ for the Elastic Boundary Condition [Characteristic Eq. (89)] and $b/a = 2.0$

m	X_{Em}	m	X_{Em}
1	3.0413911	19	60.3961131
2	6.5283908	20	63.5395907
3	9.8273980	21	66.6826014
4	13.0557922	22	69.8251471
5	16.2518595	23	72.9672093
6	19.4306369	24	76.1087436
7	22.5991233	25	79.2496705
8	25.7609959	26	82.3898569
9	28.9183657	27	85.5290817
10	32.0725284	28	88.6669664
11	35.2243216	29	91.8028211
12	38.3743096	30	94.9352565
13	41.5228853	31	98.0610040
14	44.6703291	32	101.1700866
15	47.8168454	33	104.2115035
16	50.9625847	34	106.5524618
17	54.1076584	35	107.9510042
18	57.2521485		

It is obvious that the numerical values obtained for the expansion coefficients by the assumption of orthogonality are generally changed but little from their actual values. (Although the last few elastic wall coefficients have large errors, they will be seen to contribute little to the final result.)

The final check on the suitability of using expansion coefficients calculated by the simple method valid for orthogonal functions is a comparison of both the average relative pressure $\langle p \rangle_{rel}$ and the average relative phase difference $\langle \theta \rangle_{rel}$ calculated by the two sets of coefficients. Tables 10 and 11 are the result of these calculations for the liquid boundary reference conditions and Tables 12 and 13 are the same comparison for the elastic wall boundary reference conditions. It is obvious that no real differentiation of the results can be made and that invoking orthogonality of the characteristic functions simplifies the calculations while introducing no effective error, at least for $b/a = 2$.

TABLE 7

Orthogonality Check of the Characteristic Functions Listed in Table 6. The Values of Table 6 are Used in Evaluating Eq. (33), Which Would Equal Zero for Orthogonality.

m	Evaluation of Eq. (89)	m	Evaluation of Eq. (89)
1	-	19	- 5.86770×10^{-5}
2	+ 11.16391×10^{-5}	20	+ 5.96176
3	- 9.95115	21	- 6.09159
4	+ 8.97192	22	+ 6.26297
5	- 8.22789	23	- 6.48415
6	+ 7.65611	24	+ 6.76699
7	- 7.20909	25	- 7.12880
8	+ 6.85694	26	+ 7.59572
9	- 6.64260	27	- 8.20884
10	+ 6.34402	28	+ 9.03244
11	- 6.16285	29	- 10.20153
12	+ 6.02141	30	+ 11.94970
13	- 5.91372	31	- 14.85767
14	+ 5.83666	32	+ 20.68132
15	- 5.78804	33	- 38.29343
16	+ 5.76666	34	+151.58271
17	- 5.77224	35	- 66.44633
18	+ 5.80541		

Additional calculations show that the error introduced by the approximation of orthogonality is even less for $b/a > 2$. However, the error increases as b/a approaches 1, at a greater rate for the elastic than for the liquid boundary conditions. In later calculations in this report with the parameter b/a , both the actual and the orthogonal-assumption expansion coefficients, as well as graphs, are compared for $b/a < 2$.

It may be noted that the orthogonality (or near-orthogonality) of the sequence of characteristic functions ensures that there are no complex characteristic values if r , k , q , and n are real. For if, say, $R_m = u + iv$, then $u - iv = R_n$ would also have to be a characteristic function by symmetry. (The characteristic functions would be complex conjugates of each other, as would the characteristic values.) Then orthogonality would require that

TABLE 8

Comparison of Liquid Boundary Expansion Coefficients K_{Lm} Obtained by Assuming Orthogonality [Eq. (16)] with the Actual K_{Lm} Values Obtained Using the Exact Method [Eq. (38)] and $b/a = 2.0$

m	K_{Lm} (Orth. Assump.)	K_{Lm} (Actual)	Relative Error (re Actual)
1	+0.7016619	+0.7016466	+0.0000217
2	+0.6946078	+0.6945457	+0.0000895
3	-0.1551839	-0.1551602	+0.0001531
4	-0.5036120	-0.5034236	+0.0003741
5	+0.0447238	+0.0446840	+0.0008928
6	+0.4150456	+0.4148227	+0.0005374
7	+0.0034498	+0.0034203	+0.0086066
8	-0.3591414	-0.3588310	+0.0008650
9	-0.0281100	-0.0281205	-0.0003730
10	+0.3195555	+0.3193022	+0.0007933
11	+0.0416518	+0.0415708	+0.0019474
12	-0.2897809	-0.2894450	+0.0011606
13	-0.0493929	-0.0493879	+0.0001014
14	+0.2664664	+0.2662270	+0.0008993
15	+0.0539082	+0.0537956	+0.0020930
16	-0.2476499	-0.2473100	+0.0013743
17	-0.0565419	-0.0565328	+0.0001606
18	+0.2320947	+0.2318738	+0.0009525
19	+0.0580382	+0.0579030	+0.0023354
20	-0.2189810	-0.2186361	+0.0015772
21	-0.0588300	-0.0588218	+0.0001397
22	+0.2077433	+0.2075363	+0.0009976
23	+0.0591800	+0.0590240	+0.0026427
24	-0.1979790	-0.1976210	+0.0018116
25	-0.0592541	-0.0592484	+0.0000965
26	+0.1893926	+0.1891914	+0.0010635
27	+0.0591619	+0.0589820	+0.0030515
28	-0.1817621	-0.1813764	+0.0021267
29	-0.0589801	-0.0589763	+0.0000631
30	+0.1749157	+0.1747074	+0.0011924
31	+0.0587673	+0.0585530	+0.0036590
32	-0.1687168	-0.1682744	+0.0026290
33	-0.0585770	-0.0585709	+0.0001037
34	+0.1630505	+0.1628042	+0.0015130
35	+0.0584744	+0.0581954	+0.0047953
36	-0.1578094	-0.1572207	+0.0037444
37	-0.0585826	-0.0585447	+0.0006466
38	+0.1528488	+0.1523702	+0.0031411
39	+0.0594298	+0.0587811	+0.0110368

$$\int_0^b r(u^2 + v^2) dr = 0$$

which is inconsistent with the statement that r , u , and v are real.

TABLE 9
Comparison of Elastic Boundary
Expansion Coefficients K_{Em} Obtained by
Assuming Orthogonality [Eq. (16)] with the
Actual K_{Em} Values Obtained Using the Exact
Method [Eq. (38)] and $b/a = 2.0$

m	K_{Em} (Orth. Assump.)	K_{Em} (Actual)	Relative Error (re Actual)
1	+1.0266836	+1.0267832	-0.0000970
2	+0.3956044	+0.3950305	+0.0014528
3	-0.5153298	-0.5145621	+0.0014919
4	-0.2341204	-0.2347660	-0.0027501
5	+0.3992444	+0.3999285	-0.0017105
6	+0.1794007	+0.1784297	+0.0054418
7	-0.3390867	-0.3379713	+0.0033004
8	-0.1505190	-0.1515411	-0.0067446
9	+0.3002692	+0.3013158	-0.0034737
10	+0.1321559	+0.1308594	+0.0099083
11	-0.2724367	-0.2709951	+0.0053197
12	-0.1192285	-0.1205983	-0.0113585
13	+0.2511771	+0.2525801	-0.0055548
14	+0.1095285	+0.1078649	+0.0154233
15	-0.2342299	-0.2323967	+0.0078879
16	-0.1019304	-0.1037114	-0.0171723
17	+0.2202946	+0.2221320	-0.0082714
18	+0.0957968	+0.0936446	+0.0229825
19	-0.2085599	-0.2061787	+0.0115493
20	-0.0907414	-0.0930989	-0.0253233
21	+0.1984868	+0.2009515	-0.0122652
22	+0.0865216	+0.0836075	+0.0348547
23	-0.1896973	-0.1864125	+0.0176211
24	-0.0829896	-0.0863160	-0.0385380
25	+0.1819104	+0.1854755	-0.0192215
26	+0.0800767	+0.0756883	+0.0579790
27	-0.1748948	-0.1696998	+0.0306132
28	-0.0778215	-0.0833048	-0.0658225
29	+0.1684097	+0.1746527	-0.0357452
30	+0.0765399	+0.0677138	+0.1303452
31	-0.1619917	-0.1494347	+0.0840305
32	-0.0780996	-0.0936788	-0.1663039
33	+0.1519948	+0.1750994	-0.1319512
34	+0.1360407	-0.0094748	+15.3581715
35	+0.0354620	+0.0832140	-0.5738464

A sufficient condition for completeness of the sequence of characteristic functions derived as solutions of the Liouville-type equation is that they satisfy boundary conditions such that

$$r \mathcal{G}_0 \left(r \frac{X_{0m}}{b} \right) \mathcal{G}'_0 \left(r \frac{X_{0m}}{b} \right) \Big|_{r=0}^{r=b} = 0.$$

In our cases this requirement is obviously satisfied when the X_{0m} are the zeros of \mathcal{G}_1 as in absolutely rigid boundary conditions, as well as when the X_{0m} are the zeros of \mathcal{G}_0 , as in infinitely flexible boundary conditions. While the lower limit satisfies the equality for all the boundary conditions considered here, the upper limit does not. Rather than attempting to prove completeness mathematically so that the expansion of Eq. (10) may be made, we will resort to a physical argument. The notion of completeness here concerns the least-squares representation of a function by a series expansion of characteristic functions. In our case we note that the characteristic functions for both absolutely rigid and infinitely flexible boundary conditions are complete. From a physical standpoint we would expect the type of boundary condition to become relatively immaterial as b/a increases, and in fact for reasonable values of the dimensionless quantity $z \lambda/a^2$ we would expect, for large values of b/a , that all the boundary conditions would agree with the free-field values. If these predictions are borne out we can be reasonably certain that the characteristic function expansions for liquid and elastic boundary conditions are valid representations. To demonstrate that this is not true for the reference parameter $b/a = 2$, we plot Figs. 3 through 10 which show $\langle p \rangle_{\text{rel}}$ and $\langle \theta \rangle_{\text{rel}}$, respectively, for the four boundary conditions (rigid, flexible, liquid, and elastic) considered in detail. Obviously there is little agreement among the plots and no particular coincidence with the free-field ($b/a = \infty$) calculation ($ka = 20\pi$, or $a = 10\lambda$, for all these plots). Figures 11 and 12 are composite presentations, respectively, of $\langle p \rangle_{\text{rel}}$ and $\langle \theta \rangle_{\text{rel}}$ for the four boundary conditions and the reference parameters, with the exception that $b/a = 5$ in these plots, compared with the free-field result for $ka = 20\pi$; Figs. 13 and 14 are the same but with $b/a = 10$. In the former case ($b/a = 5$) coincidence is being approached, while in the latter ($b/a = 10$) we apparently have justification of our assumption. (Recall that we are changing only the value of b .)

TABLE 10
 Comparison of Average Relative Pressure Values
 $(\langle p \rangle_{rel})_L$ Obtained Using Orthogonal Assumption and Actual K_{Lm}
 Values from Table 8 in Eqs. 20 and 24 for the Liquid Boundary Condition
 [Characteristic Eq. (64)] and $b/a = 2.0$

$z \frac{\lambda}{a^2}$ (Dimensionless)	$(\langle p \rangle_{rel})_L$ (Orth. Assump.)	$(\langle p \rangle_{rel})_L$ (Actual)	Relative Error (re Actual)
0.0	0.9895775	0.9894456	+0.0001334
0.1	0.9306396	0.9305719	+0.0000728
0.2	0.9018492	0.9018035	+0.0000508
0.3	0.8832659	0.8832215	+0.0000503
0.4	0.8747904	0.8747423	+0.0000550
0.5	0.8601329	0.8600888	+0.0000513
0.6	0.8296854	0.8296640	+0.0000258
0.7	0.8454234	0.8453774	+0.0000545
0.8	0.8156356	0.8156078	+0.0000340
0.9	0.8024712	0.8024510	+0.0000251
1.0	0.8094636	0.8094384	+0.0000311
2.0	0.7535671	0.7535548	+0.0000162
3.0	0.7475792	0.7475292	+0.0000668
4.0	0.5320858	0.5321009	-0.0000285
5.0	0.5033542	0.5033521	+0.0000043
6.0	0.3703530	0.3703732	-0.0000546
7.0	0.2964656	0.2964915	-0.0000873
8.0	0.4134798	0.4134609	+0.0000458
9.0	0.3812747	0.3813003	-0.0000671
10.0	0.5912150	0.5912050	+0.0000171

TABLE 11
 Comparison of Average Relative Phase-Difference Values
 $(\langle \theta \rangle_{rel})_L$ Obtained Using Orthogonal Assumption and Actual K_{Lm}
 Values from Table 8 in Eqs. (21) and (24) for the Liquid Boundary Condition
 [Characteristic Eq. (64)] and $b/a = 2.0$

$z \frac{\lambda}{a^2}$ (Dimensionless)	$(\langle \theta \rangle_{rel})_L$ (Orth. Assump.)	$(\langle \theta \rangle_{rel})_L$ (Actual)	Relative Error (re Actual)
0.0	0.0000006	0.0000006	0
0.1	0.0770784	0.0770483	+0.0003907
0.2	0.1104181	0.1103926	+0.0002308
0.3	0.1358862	0.1358591	+0.0001993
0.4	0.1639416	0.1639192	+0.0001367
0.5	0.1836409	0.1836184	+0.0001226
0.6	0.2061965	0.2061710	+0.0001238
0.7	0.2209007	0.2208823	+0.0000832
0.8	0.2617586	0.2617183	+0.0001541
0.9	0.2418164	0.2418140	+0.0000100
1.0	0.2425141	0.2425331	-0.0000786
2.0	0.3661808	0.3661959	-0.0000412
3.0	0.7017445	0.7016980	+0.0000663
4.0	0.7916116	0.7916051	+0.0000082
5.0	0.7776839	0.7777139	-0.0000386
6.0	1.0905651	1.0904750	+0.0000826
7.0	0.6155605	0.6156242	-0.0001034
8.0	0.6405180	0.6405112	+0.0000106
9.0	0.4942622	0.4943238	-0.0001246
10.0	0.5903329	0.5903391	-0.0000104

TABLE 12
 Comparison of Average Relative Pressure Values
 $(\langle p \rangle_{rel})_E$ Obtained Using Orthogonal Assumption and Actual K_{Em}
 Values from Table 9 in Eqs. (20) and (24) for the Elastic Boundary Condition
 [Characteristic Eq. (89)] and $b/a = 2.0$

$z \frac{\lambda}{a^2}$ (Dimensionless)	$(\langle p \rangle_{rel})_E$ (Orth. Assump.)	$(\langle p \rangle_{rel})_E$ (Actual)	Relative Error (re Actual)
0.0	0.9717788	0.9713188	+0.0004736
0.1	0.9141165	0.9142742	-0.0001725
0.2	0.8860098	0.8864551	-0.0005023
0.3	0.8667967	0.8662562	+0.0006240
0.4	0.8564165	0.8562606	+0.0001821
0.5	0.8415938	0.8420237	-0.0005106
0.6	0.8190483	0.8186038	+0.0005429
0.7	0.8225790	0.8221697	+0.0004978
0.8	0.8094269	0.8097581	-0.0004089
0.9	0.7846205	0.7844757	+0.0001846
1.0	0.7762643	0.7759440	+0.0004127
2.0	0.7059880	0.7055973	+0.0005538
3.0	0.7464714	0.7462238	+0.0003319
4.0	0.7666435	0.7664073	+0.0003082
5.0	0.6782722	0.6783252	-0.0000781
6.0	0.7197391	0.7197888	-0.0000690
7.0	0.8061243	0.8058819	+0.0003008
8.0	0.7915121	0.7917809	-0.0003396
9.0	0.7181985	0.7187899	-0.0008227
10.0	0.8622688	0.8627789	-0.0005911

TABLE 13
 Comparison of Average Relative Phase-Difference Values
 $(\langle \theta \rangle_{rel})_E$ Obtained Using Orthogonal Assumption and Actual K_{Em}
 Values from Table 9 in Eqs. (21) and (24) for the Elastic Boundary Condition
 [Characteristic Eq. (89)] and $b/a = 2.0$

$z \frac{\lambda}{a^2}$ (Dimensionless)	$(\langle \theta \rangle_{rel})_E$ (Orth. Assump.)	$(\langle \theta \rangle_{rel})_E$ (Actual)	Relative Error (re Actual)
0.0	0	0	0
0.1	0.0778414	0.0784568	-0.0078441
0.2	0.1151891	0.1146869	+0.0043793
0.3	0.1422784	0.1418842	+0.0027785
0.4	0.1659318	0.1665204	-0.0035344
0.5	0.1894090	0.1893459	+0.0003332
0.6	0.2217272	0.2213196	+0.0018414
0.7	0.2228230	0.2230320	-0.0009370
0.8	0.2655853	0.2657002	-0.0004324
0.9	0.2644061	0.2635660	+0.0031874
1.0	0.2681320	0.2679827	+0.0005574
2.0	0.4333332	0.4338638	-0.0012228
3.0	0.5311679	0.5318601	-0.0013016
4.0	0.8584935	0.8591407	-0.0007333
5.0	0.9762409	0.9768278	-0.0006009
6.0	0.9276615	0.9286576	-0.0010726
7.0	1.1607084	1.1611076	-0.0003438
8.0	1.4857913	1.4862842	-0.0003316
9.0	1.6592534	1.6596663	-0.0002488
10.0	1.7931229	1.7934281	-0.0001702

INTRODUCTION OF ABSORPTION

In the immediately preceding report on free-field diffraction (4), absorption was introduced merely by replacing the wave number k by $k^* = k_{00} - i\alpha_{00}$.* To introduce absorption into the guided mode formulation of this report, we may, as in the previous report, substitute a complex wave number for the parameter k . To an apparent first-order approximation, we will also assume that the characteristic values X_{0m} are not themselves modified by attenuation in the medium or the walls, but that only propagation in the modes across and down the tube is affected. That is, in Eq. (24) only the exponential term will require modification.

We write

$$k_{00}^* = k_{00} - i\alpha_{00} \quad q_{0m}^* = q_{0m}^M - i\alpha_{0m}$$

$$\left(\frac{X_{0m}}{b}\right)^2 = (k_{00}^*)^2 - (q_{0m}^*)^2 \quad (90)$$

and obtain from separately equating the real and the imaginary parts

$$k_{00}^2 - \alpha_{00}^2 = \left(\frac{X_{0m}}{b}\right)^2 + (q_{0m}^M)^2 - \alpha_{0m}^2$$

and

$$\alpha_{00}k_{00} = \alpha_{0m}q_{0m}^M. \quad (91)$$

We use the second relation in Eq. (91) to eliminate α_{0m} from the first relation and obtain

$$X_{0m} = b \sqrt{k_{00}^2 - (q_{0m}^M)^2 + \alpha_{00}^2 \left(\frac{k_{00}^2}{(q_{0m}^M)^2} - 1\right)}, \quad (92)$$

or, finally, the modified q_{0m} , i.e., q_{0m}^M , is given by

$$2(q_{0m}^M)^2 = k_{00}^2 - \alpha_{00}^2 - \left(\frac{X_{0m}}{b}\right)^2$$

$$+ \left(\left(\frac{X_{0m}}{b}\right)^4 + k_{00}^4 + \alpha_{00}^4\right)$$

*In this notation, the star superscript refers only to a complex value, not to the complex conjugate of an already complex number.

$$+ 2k_{00}^2 \alpha_{00}^2 + 2\left(\frac{X_{0m}}{b}\right)^2 \alpha_{00}^2$$

$$- 2\left(\frac{X_{0m}}{b}\right)^2 k_{00}^2)^{1/2}. \quad (93)$$

The exponential in Eq. (24) is now written

$$e^{-i\left((k_{00} - q_{0m}) + \left(1 - \frac{k_{00}}{q_{0m}}\right)\alpha_{00}\right)z} \quad (94)$$

where k_{00} and α_{00} are given as plane-wave free-field propagation parameters of the contained liquid.

We note that in this manner the X_{0m} are real, as previously, and the new q_{0m} are also real. Returning to our assumption that the procedure outlined above is a first-order-type approximation, we note that for the limiting situations of absolutely rigid and infinitely flexible boundary conditions the use of the theorem stating that there are no pure imaginary or complex zeroes of \mathcal{J}_0 or \mathcal{J}_1 indicates that no approximation is involved in our method of introduction of absorption for the fluid contained in absolutely rigid or infinitely flexible walls. That is, in Eq. (8) (the characteristic equation) we essentially have written the relation

$$\begin{aligned} &\text{Impedance} \\ &\text{of liquid} \\ &\text{(in radial} \\ &\text{direction)} \end{aligned} = -i\omega\rho \frac{\mathcal{J}_0(X)}{X\mathcal{J}_1(X)}$$

and equated this to the impedance Z of the wall so that

$$- \frac{i\omega\rho \mathcal{J}_0(X)}{X\mathcal{J}_1(X)} = Z_{\text{wall}}. \quad (95)$$

If the wall impedance is pure real we have attenuation, while a pure imaginary impedance results in propagation. For absolutely rigid walls Z goes to ∞ , and for infinitely flexible walls Z goes to 0. Obviously, for both these limiting cases we can only have the characteristic value X real inasmuch as Bessel functions of complex argument are in general themselves complex. We may note in passing that the left-hand side of Eq. (95) resembles the cotangent function, so the

procedures used in the sections devoted to absolutely rigid and infinitely flexible boundaries may be replaced by finding the zeroes and infinities, respectively, of this quotient.

For the liquid and elastic boundary conditions we find the right-hand side of Eq. (95) replaced by a function which, if allowed to become complex, then requires complex values of X . So our procedure for introducing absorption into these conditions is only an approximation.* Because absorption was introduced in the contained liquid at a relatively late stage of the development, we find that in order to equate impedances across the boundary we now demand the simultaneous introduction of a related absorption for the wall material. Recalling that

$$Y \equiv b\sqrt{k_1^2 - k_2^2}$$

we now find

$$Y = b\sqrt{k_1^2 - 2ik_1\alpha_1 - \alpha_1^2 - k_2^2 + 2ik_2\alpha_2 + \alpha_2^2}.$$

The real part yields

$$Y = b\sqrt{k_1^2 - \alpha_1^2 - k_2^2 + \alpha_2^2}$$

and the imaginary part

$$k_1\alpha_1 = k_2\alpha_2.$$

We demanded that Y be real, so substitution gives

$$Y = b\sqrt{k_1^2 - \alpha_1^2 - k_2^2 + \left(\frac{k_1}{k_2}\alpha_1\right)^2}. \quad (96)$$

*We will not in this report present a more rigorous introduction of absorption but will delay it to a future report, since even with restrictions to frequencies far removed from relaxation effects involving bulk viscosity or chemical reactions, it would appear necessary to ascribe a viscosity to the fluid and thus negate any simplifying assumption concerning the transverse component of pressure or particle velocity at the boundary. Indeed, apparently one becomes involved with simultaneous solutions to a diffusion (parabolic) equation as well as a wave or hyperbolic equation. In any event, the simple introduction of a complex propagation constant, without implying viscosity, leads to attenuation, and for relatively small attenuations it could not result in characteristic values X_{0m} much changed from those resulting from real propagation constants. The characteristic functions would not be orthogonal for a complex impedance, but we recall that they were not orthogonal anyway for liquid and elastic boundary conditions—though, being nearly so, they did not significantly change (for $b \geq 2a$) the expansion coefficients K_{0m} from their values obtained by invoking orthogonality.

This restriction above is innocuous, albeit not particularly desirable. It has no particular significance other than that the assumption of X_{0m} unchanged implies that Y is unchanged.

Utilizing the previous equations with the exponential as modified in Eq. (94) and with the new q_{0m}^M given by Eq. (93), we calculate $\langle p \rangle_{rel}$ and $\langle \theta \rangle_{rel}$ as before, but for the absorption parameter $\alpha \equiv \alpha_{00} = 0, 0.01, 0.1, 1.0, \text{ and } 10.0$. Because the 0.01 and 0.1 plots are almost indistinguishable from $\alpha = 0$, we plot only the values $\alpha = 0, 1.0, \text{ and } 10.0$ for each of the boundary conditions. Figure 15 is a plot of $\langle p \rangle_{rel}$ for absolutely rigid boundaries for the α parameter values 0, 1.0, and 10.0. Figure 16 shows $\langle \theta \rangle_{rel}$ for absolutely rigid boundaries plotted in the same way over the same ranges of $z\lambda/a^2$ (dimensionless) and for the same absorption parameter values. It should be remarked again that, unless otherwise noted, all graphs in this report are for the standard reference parameters given in Table 1. Thus, the figures are for $b/a = 2$ and $ka = 20\pi$. In a similar fashion, Figs. 17 and 18 show $\langle p \rangle_{rel}$ and $\langle \theta \rangle_{rel}$, respectively, for infinitely flexible boundary conditions with the absorption parameter varied; Figs. 19 and 20 are for liquid boundary conditions with additional standard reference conditions $\rho_2/\rho_1 = 7$ and $k_1/k_2 = 4$; and the last boundary condition considered here, elastic walls, is plotted in Figs. 21 and 22 and includes the further additional standard reference parameter of the Poisson's ratio $\nu = 0.325$.

The most noticeable feature of these absorption parameter plots is the marked smoothing of the pressure and phase plots caused by the introduction of absorption in this, for the latter two boundary conditions, first-degree-approximation manner. (All the graphs in this report will be discussed more fully in a later section.)

ADDITIONAL PARAMETERS

We have already shown graphs comparing the four boundary conditions for the radius ratio $b/a = 2$ with the free field and for $b/a = 5$ and $b/a = 10$. The absorption parameter was also varied for the reference value $b/a = 2$. These plots were all for $k_1a = 20\pi$ and, where applica-

ble, $k_1/k_2 = 4$. We now turn our attention to a variation of b/a , where we have previously noted that most of the change due to this variable occurs for the smaller values of this variable. We have also alluded to the increasing differences to be expected in a comparison of the actual expansion coefficients with those obtained by erroneously using the simplification of orthogonality for the liquid and elastic boundary cases. Our primary interest is in a comparison of both $\langle p \rangle_{rel}$ and $\langle \theta \rangle_{rel}$ calculated using expansion coefficients obtained by the two different methods.

For $b/a = 1.25$ we have tabulated values and proportional differences in Table 14 for $\langle p \rangle_{rel}{}_L$, in Table 15 for $\langle \theta \rangle_{rel}{}_L$, in Table 16 for $\langle p \rangle_{rel}{}_E$, and in Table 17 for $\langle \theta \rangle_{rel}{}_E$. Obviously, no significant error is caused by the orthogonal assumption for the liquid boundary, but differences as large as 3 percent occur for $\langle p \rangle_{rel}{}_E$ and 8 percent for $\langle \theta \rangle_{rel}{}_E$.

Additional calculations indicate that the liquid boundary case involves no appreciable error even for $b/a = 1$, as shown in Table 18 for $\langle p \rangle_{rel}{}_L$ and Table 19 for $\langle \theta \rangle_{rel}{}_L$. But here the insignificant difference is not caused by a small change in K_{Lm} but rather by the decreasing contribution of the higher m values. As seen in Table 20 there is an appreciable difference (as large as 88 percent) between the actual K_{Lm} and the orthogonal assumption K_{Lm} , for $b/a = 1$, which is not reflected in the $\langle p \rangle_{rel}{}_L$ and $\langle \theta \rangle_{rel}{}_L$ values.

Table 21 compares the two sets of expansion coefficients K_{Em} for the elastic boundary situation, with $b/a = 1$ being the only parameter changed from the standard reference values. We find some coefficients changed by almost 100 percent. The corresponding $\langle p \rangle_{rel}{}_E$ and $\langle \theta \rangle_{rel}{}_E$ for selected values of $z\lambda/a^2$ are tabulated in Tables 22 and 23, respectively. The greatest difference in $\langle p \rangle_{rel}{}_E$ is 25 percent, and that in $\langle \theta \rangle_{rel}{}_E$ is 1000 percent.

TABLE 14
Comparison of Average Relative Pressure Values
 $\langle p \rangle_{rel}{}_L$ Obtained Using Orthogonal Assumption and Actual K_{Lm} Values
(Calculated from Eqs. (16) and (38), Respectively) in Eqs. (20) and (24)
for the Liquid Boundary Condition [Characteristic Eq. (64)] and $b/a = 1.25$

$z \frac{\lambda}{a^2}$ (Dimensionless)	$\langle p \rangle_{rel}{}_L$ (Orth. Assump.)	$\langle p \rangle_{rel}{}_L$ (Actual)	Relative Error (re Actual)
0.0	0.9899171	0.9897142	+ 0.0002050
0.1	0.9243691	0.9242909	- 0.0000846
0.2	0.9078447	0.9077375	+ 0.0001182
0.3	0.8630293	0.8629577	+ 0.0000829
0.4	0.8492456	0.8491806	+ 0.0000766
0.5	0.8432466	0.8431503	+ 0.0001142
0.6	0.8374968	0.8374500	+ 0.0000559
0.7	0.8681471	0.8680264	+ 0.0001390
0.8	0.8379808	0.8379386	+ 0.0000504
0.9	0.8691401	0.8690317	+ 0.0001247
1.0	0.8595755	0.8594977	+ 0.0000905
2.0	0.9192813	0.9192201	+ 0.0000666
3.0	0.8537115	0.8536319	+ 0.0000932
4.0	0.8981722	0.8980542	+ 0.0001314
5.0	0.8490684	0.8489840	+ 0.0000993
6.0	0.8523115	0.8522883	+ 0.0000273
7.0	0.8460231	0.8459170	+ 0.0001254
8.0	0.8144340	0.8143755	+ 0.0000718
9.0	0.8222387	0.8221836	+ 0.0000671
10.0	0.8244292	0.8243614	+ 0.0000823

TABLE 15

Comparison of Average Relative Phase-Difference Values
 $(\langle \theta \rangle_{rel})_L$ Obtained Using Orthogonal Assumption and Actual K_{Lm} Values
 (Calculated from Eqs. (16) and (38), Respectively) in Eqs. (21) and (24)
 for the Liquid Boundary Condition [Characteristic Eq. (64)] and $b/a = 1.25$

$z \frac{\lambda}{a^2}$ (Dimensionless)	$(\langle \theta \rangle_{rel})_L$ (Orth. Assump.)	$(\langle \theta \rangle_{rel})_L$ (Actual)	Relative Error (re Actual)
0.0	0	0	0
0.1	0.0751249	0.0751140	+0.0001446
0.2	0.1237556	0.1237194	+0.0002922
0.3	0.1485767	0.1485352	+0.0002797
0.4	0.1511827	0.1511792	+0.0000228
0.5	0.1409557	0.1409701	-0.0001024
0.6	0.1517650	0.1517736	-0.0000569
0.7	0.1850660	0.1850342	+0.0001715
0.8	0.1947565	0.1947661	-0.0000492
0.9	0.2136579	0.2136648	-0.0000324
1.0	0.2358251	0.2358388	-0.0000580
2.0	0.4669629	0.4669691	-0.0000133
3.0	0.7005599	0.7005384	+0.0000307
4.0	0.9307200	0.9307649	-0.0000482
5.0	1.1635297	1.1635811	-0.0000442
6.0	1.4359258	1.4359296	-0.0000027
7.0	1.7188279	1.7188191	+0.0000051
8.0	1.9325513	1.9325491	+0.0000012
9.0	2.2348147	2.2348432	-0.0000128
10.0	2.4549971	2.4549533	+0.0000179

TABLE 16

Comparison of Average Relative Pressure Values
 $(\langle p \rangle_{rel})_E$ Obtained Using Orthogonal Assumption and Actual K_{Em} Values
 (Calculated from Eqs. (16) and (38), Respectively) in Eqs. (20) and (24)
 for the Elastic Boundary Condition [Characteristic Eq. (89)] and $b/a = 1.25$

$z \frac{\lambda}{a^2}$ (Dimensionless)	$(\langle p \rangle_{rel})_E$ (Orth. Assump.)	$(\langle p \rangle_{rel})_E$ (Actual)	Relative Error (re Actual)
0.0	0.6762827	0.6866799	-0.0151414
0.1	0.6155481	0.6204182	-0.0078496
0.2	0.6168034	0.6300323	-0.0209972
0.3	0.5994986	0.6123391	-0.0209696
0.4	0.5761935	0.5789443	-0.0047513
0.5	0.5441485	0.5531761	-0.0163195
0.6	0.5133055	0.5122106	-0.0021376
0.7	0.5171981	0.5165782	+0.0012001
0.8	0.4799800	0.4934086	-0.0272160
0.9	0.4636831	0.4638596	-0.0003805
1.0	0.4690766	0.4788756	-0.0204625
2.0	0.3481575	0.3457400	+0.0069924
3.0	0.5582870	0.5599304	-0.0029350
4.0	0.5983060	0.6011824	-0.0047848
5.0	0.3676897	0.3698082	-0.0057286
6.0	0.4284766	0.4369658	-0.0194274
7.0	0.6318598	0.6455171	-0.0211572
8.0	0.4911429	0.5046498	-0.0267649
9.0	0.3236569	0.3209491	+0.0084369
10.0	0.4989774	0.5006685	-0.0033777

TABLE 17
 Comparison of Average Relative Phase-Difference Values
 $(\langle \theta \rangle_{rel})_E$ Obtained Using Orthogonal Assumption and Actual K_{Em} Values
 (Calculated from Eqs. (16) and (38), Respectively) in Eqs. (21) and (24)
 for the Elastic Boundary Condition [Characteristic Eq. (89)] and $b/a = 1.25$

$z \frac{\lambda}{a^2}$ (Dimensionless)	$(\langle \theta \rangle_{rel})_E$ (Orth. Assump.)	$(\langle \theta \rangle_{rel})_E$ (Actual)	Relative Error (re Actual)
0.0	0	0	0
0.1	0.1380550	0.1360894	+0.0144435
0.2	0.2118209	0.2298612	-0.0784834
0.3	0.3249062	0.3154815	+0.0298741
0.4	0.4181617	0.4242684	-0.0143934
0.5	0.4845435	0.4945054	-0.0201451
0.6	0.5506718	0.5411030	+0.0176838
0.7	0.5859817	0.6076427	-0.0356476
0.8	0.6900229	0.6831681	+0.0100337
0.9	0.6527385	0.6541685	-0.0021860
1.0	0.7507075	0.7521207	-0.0018790
2.0	1.0479946	1.0799276	-0.0295695
3.0	1.5272789	1.5271199	+0.0001041
4.0	2.2624835	2.2558020	+0.0029619
5.0	2.8991612	2.8799479	+0.0066714
6.0	3.1144023	3.1207704	-0.0020406
7.0	3.7961330	3.7927269	+0.0008981
8.0	4.5533582	4.5694361	-0.0035186
9.0	4.9727837	4.9992754	-0.0052991
10.0	5.2715110	5.2596523	+0.0025465

TABLE 18
 Comparison of Average Relative Pressure Values
 $(\langle p \rangle_{rel})_L$ Obtained Using Orthogonal Assumption and Actual K_{Lm} Values
 (Calculated from Eqs. (16) and (38), Respectively) in Eqs. (20) and (24)
 for the Liquid Boundary Condition [Characteristic Eq. (64)] and $b/a = 1.0$

$z \frac{\lambda}{a^2}$ (Dimensionless)	$(\langle p \rangle_{rel})_L$ (Orth. Assump.)	$(\langle p \rangle_{rel})_L$ (Actual)	Relative Error (re Actual)
0.0	0.9981645	0.9998849	-0.0017206
0.1	0.9744380	0.9753644	-0.0009499
0.2	0.9478367	0.9485705	-0.0007736
0.3	0.9233720	0.9239012	-0.0005728
0.4	0.9019077	0.9024089	-0.0005554
0.5	0.8810601	0.8813703	-0.0003520
0.6	0.8653565	0.8658056	-0.0005188
0.7	0.8473875	0.8477187	-0.0003907
0.8	0.8420991	0.8427221	-0.0007393
0.9	0.8169883	0.8173123	-0.0003965
1.0	0.7959366	0.7960492	-0.0001414
2.0	0.6731596	0.6732681	-0.0001612
3.0	0.8379450	0.8383262	-0.0004548
4.0	0.9657948	0.9666361	-0.0008703
5.0	0.7894673	0.7897891	-0.0004075
6.0	0.6606877	0.6604517	+0.0003574
7.0	0.8855006	0.8862457	-0.0008408
8.0	0.9431363	0.9437847	-0.0006870
9.0	0.7642870	0.7643782	-0.0001193
10.0	0.6711493	0.6707567	+0.0005853

TABLE 19
 Comparison of Average Relative Phase-Difference Values
 $(\langle \theta \rangle_{rel})_L$ Obtained Using Orthogonal Assumption and Actual K_{Lm} Values
 (Calculated from Eqs. (16) and (38), Respectively) in Eqs. (21) and (24)
 for the Liquid Boundary Condition [Characteristic Eq. (64)] and $b/a = 1.0$

$z \frac{\lambda}{a^2}$ (Dimensionless)	$(\langle \theta \rangle_{rel})_L$ (Orth. Assump.)	$(\langle \theta \rangle_{rel})_L$ (Actual)	Relative Error (re Actual)
0.0	0.0000006	0.0000006	0
0.1	0.0905143	0.0909282	-0.0045518
0.2	0.1556971	0.1560929	-0.0025352
0.3	0.2104748	0.2108481	-0.0017705
0.4	0.2576192	0.2578053	-0.0007220
0.5	0.3012797	0.3014043	-0.0004134
0.6	0.3475494	0.3479874	-0.0012587
0.7	0.3771373	0.3771603	-0.0000609
0.8	0.4225055	0.4228402	-0.0007913
0.9	0.4680654	0.4686056	-0.0011527
1.0	0.4854230	0.4857166	-0.0006043
2.0	0.7208829	0.7207918	+0.0001264
3.0	1.0179109	1.0181569	-0.0002417
4.0	1.4538678	1.4533953	+0.0003251
5.0	1.9759632	1.9764646	-0.0002537
6.0	2.1794069	2.1789635	+0.0002035
7.0	2.4786985	2.4787000	-0.0000006
8.0	2.9542018	2.9542190	-0.0000058
9.0	3.4332652	3.4333348	-0.0000203
10.0	3.6757460	3.6760906	-0.0000937

TABLE 20

Comparison of Liquid Boundary Expansion
 Coefficients K_{Lm} Obtained by Assuming Ortho-
 gonality [Eq. (16)] with the Actual K_{Lm} Values
 Obtained Using the Exact Method [Eq. (38)] and
 $b/a = 1.0$

m	K_{Lm} (Orth. Assump.)	K_{Lm} (Actual)	Relative Error (re Actual)
1	+1.5592724	+1.5599775	-0.0004520
2	-0.9336714	-0.9360733	-0.0025660
3	+0.6403251	+0.6447437	-0.0068532
4	-0.4624958	-0.4688900	-0.0136369
5	+0.3467280	+0.3549177	-0.0230748
6	-0.2680057	-0.2778048	-0.0352733
7	+0.2123773	+0.2236380	-0.0503523
8	-0.1716642	-0.1842819	-0.0684699
9	+0.1409130	+0.1548213	-0.0898346
10	-0.1170241	-0.1321886	-0.1147187
11	+0.0979923	+0.1144071	-0.1434768
12	-0.0824768	-0.1001631	-0.1765752
13	+0.0695511	+0.0885593	-0.2146379
14	-0.0585517	-0.0789664	-0.2585236
15	+0.0489824	+0.0709336	-0.3094618
16	-0.0404466	-0.0641313	-0.3693159
17	+0.0325891	+0.0583154	-0.4411572
18	-0.0250121	-0.0533050	-0.5307736
19	+0.0170344	+0.0489757	-0.6521863
20	-0.0053318	-0.0452071	-0.8820580

TABLE 21

Comparison of Elastic Boundary Expansion
 Coefficients K_{Em} Obtained by Assuming Ortho-
 gonality [Eq. (16)] with the Actual K_{Em} Values
 Obtained Using the Exact Method [Eq. (38)] and
 $b/a = 1.0$

m	K_{Em} (Orth. Assump.)	K_{Em} (Actual)	Relative Error (re Actual)
1	+0.6847004	+0.7285022	-0.0601258
2	-0.2541044	-0.3201611	-0.2063232
3	+0.1438355	+0.2264065	-0.3647026
4	-0.0965672	-0.1942744	-0.5029339
5	+0.0713326	+0.1842075	-0.6127596
6	-0.0561096	-0.1850984	-0.6968662
7	+0.0462064	+0.1931193	-0.7607366
8	-0.0394569	-0.2071299	-0.8095065
9	+0.0347496	+0.2274224	-0.8472022
10	-0.0314822	-0.2555165	-0.8767901
11	+0.0293366	+0.2945913	-0.9004158
12	-0.0281958	-0.3508499	-0.9196358
13	+0.0281567	+0.4372198	-0.9356006
14	-0.0297171	-0.5849160	-0.9491943
15	+0.0346552	+0.8916582	-0.9611340
16	-0.0527891	-1.8700824	-0.9717718
17	+0.2748274	+4.6615750	-0.9410441
18	-0.0610809	-4.1532538	-0.9852932

Returning to the graphs for the b/a parameter varied between 1 and 2 we have, for rigid boundaries, $\langle p \rangle_{\text{rel}}$ plotted in Figs. 23 and $\langle \theta \rangle_{\text{rel}}$ in Fig. 24. Figures 25 and 26 show $\langle p \rangle_{\text{rel}}$ and $\langle \theta \rangle_{\text{rel}}$, respectively, for infinitely flexible boundary conditions. The results for liquid boundary conditions proved to be independent of whether the coefficients were obtained in the correct manner or by means of the orthogonal simplification and are shown as $\langle p \rangle_{\text{rel}}$ in Fig. 27 and $\langle \theta \rangle_{\text{rel}}$ in Fig. 28. Figures 29 and 30 show $\langle p \rangle_{\text{rel}}$ and $\langle \theta \rangle_{\text{rel}}$, respectively, for elastic boundary conditions and are the only graphs which differentiate between the actual calculations and those obtained by orthogonal simplification. (The values for $b/a = 1.5$ and 2.0 are so nearly identical that no differentiation can be made between the two methods of calculation on Figs. 29 and 30.) For the (b) part of each figure (i.e., $1 \leq z\lambda/a^2 \leq 10$) we note that the variation in the actual curve for $b/a = 1$ is so rapid that only the portion $5.0 \leq z\lambda/a^2 \leq 5.5$ is sketched in detail; for other regions on this curve only the envelope is indicated.

With this last group of figures, we have exhausted the parameters that can be varied and compared for all of the four boundary conditions. For the liquid and elastic walls, we can next vary the ratio of the wave number for the contained liquid and for the wall material. Figures 31 and 32 show $\langle p \rangle_{\text{rel}}$ and $\langle \theta \rangle_{\text{rel}}$ for liquid walls and k_1/k_2 values of 3, 4, and 5. Figures 33 and 34 are for the same variation of parameters for elastic walls. The ratio of densities ρ_2/ρ_1 is also at our disposal and we select values of 6, 7, and 8 for this in Figs. 35 and 36, which are for liquid boundary conditions, and in Figs. 37 and 38, which apply to elastic boundary conditions. The only parameter remaining is Poisson's ratio ν for the elastic walls, and $\langle p \rangle_{\text{rel}}$ and $\langle \theta \rangle_{\text{rel}}$ are plotted for $\nu = 0.300$, 0.325 , and 0.350 in Figs. 39 and 40, respectively.

DISCUSSION AND APPLICATION

In earlier sections of the report we have shown that the proper expansion coefficients for the nonorthogonal characteristic functions are

essentially the same as those obtained by wrongly assuming orthogonality, and the resulting calculations of $\langle p \rangle_{\text{rel}}$ and $\langle \theta \rangle_{\text{rel}}$ for the liquid and elastic boundary conditions are essentially unchanged in the correct formulation from the approximation of orthogonality (for $b \geq 2a$). From Figs. 3 through 10 we note that none of the boundary conditions for $b/a = 2$ are in essential agreement with the free-field calculations for the same radiating piston. But for $b/a = 5$ in Figs. 11 and 12 the graphs are becoming quite similar, while for $b/a = 10$ in Figs. 13 and 14 the graphs for all the boundary conditions just about coincide with free-field calculations over the distances z considered.

If we compare the various boundary condition plots for $b/a = 2$ we note that for $0 < z\lambda/a^2 \leq 1$ the $\langle p \rangle_{\text{rel}}$ plots are quite similar; the same is true for the $\langle \theta \rangle_{\text{rel}}$ plots, although one might say that $\langle \theta \rangle_{\text{rel}}$ for infinitely flexible boundary conditions is generally out of phase with the other boundary conditions over this range of distance. The same plots for $1 \leq z\lambda/a^2 \leq 10$ indicate that infinitely flexible and liquid boundary conditions are similar up to about $z\lambda/a^2 = 5$, as are the absolutely rigid and elastic boundary conditions. While there is a general tendency toward similarity of the four plots at $z\lambda/a^2 = 5$, for greater $z\lambda/a^2$ values $\langle \theta \rangle_{\text{rel}}$ separates, with the rigid and elastic conditions forming one similar pair and the flexible and liquid conditions another. But for $\langle p \rangle_{\text{rel}}$, while it could be said that the liquid and flexible continue with some similarity, it is obvious that the elastic diverges from the rigid and, in fact, begins to resemble infinitely flexible boundary conditions. The general trends toward increasing or decreasing values are perhaps more significant in this appraisal than the absolute values. In any event, it apparently is necessary to carefully specify the boundary conditions appropriate to a given experiment.

We will return to the discussion of tube-to-crystal radius ratio b/a as a parameter later; for now we shall direct our attention to absorption. Figures 15 and 16 indicate that for rigid boundary conditions neither $\langle p \rangle_{\text{rel}}$ nor $\langle \theta \rangle_{\text{rel}}$ are particularly affected by the inclusion of a realistic intrinsic absorption in the contained liquid.

TABLE 22

Comparison of Average Relative Pressure Values
 $(\langle p \rangle_{rel})_E$ Obtained Using Orthogonal Assumption and Actual K_{Em} Values
 (Calculated from Eqs. (16) and (38), Respectively) in Eqs. (20) and (24)
 for the Elastic Boundary Condition [Characteristic Eq. (89)] and $b/a = 1.0$

$z \frac{\lambda}{a^2}$ (Dimensionless)	$(\langle p \rangle_{rel})_E$ (Orth. Assump.)	$(\langle p \rangle_{rel})_E$ (Actual)	Relative Error (re Actual)
0.0	0.0865885	0.1149452	-0.2466977
0.1	0.0837691	0.0885871	-0.0543867
0.2	0.0819398	0.0837064	-0.0211038
0.3	0.0816765	0.1026259	-0.2041334
0.4	0.0791261	0.0844068	-0.0625626
0.5	0.0771040	0.0703626	+0.0958097
0.6	0.0778171	0.0967713	-0.1958666
0.7	0.0755567	0.0841316	-0.1019345
0.8	0.0742354	0.0670090	+0.1078425
0.9	0.0754615	0.0907023	-0.1680305
1.0	0.0738765	0.0857666	-0.1386335
2.0	0.0810237	0.0763331	+0.0614479
3.0	0.0739906	0.0652305	+0.1342936
4.0	0.0757399	0.0779204	-0.0279841
5.0	0.0794552	0.0935181	-0.1503765
6.0	0.0741046	0.0896573	-0.1734676
7.0	0.0840508	0.0966090	-0.1299905
8.0	0.0717685	0.0660596	+0.0864209
9.0	0.0825636	0.0740020	+0.1156933
10.0	0.0742248	0.0820247	-0.0950918

TABLE 23

Comparison of Average Relative Phase-Difference Values
 $(\langle \theta \rangle_{rel})_E$ Obtained Using Orthogonal Assumption and Actual K_{Em} Values
 (Calculated from Eqs. (16) and (38), Respectively) in Eqs. (21) and (24)
 for the Elastic Boundary Condition [Characteristic Eq. (89)] and $b/a = 1.0$

$z \frac{\lambda}{a^2}$ (Dimensionless)	$(\langle \theta \rangle_{rel})_E$ (Orth. Assump.)	$(\langle \theta \rangle_{rel})_E$ (Actual)	Relative Error (re Actual)
0.0	0	0	0
0.1	0.1164774	0.0123768	10.4109544
0.2	0.2429197	0.3906022	0.3780892
0.3	0.3374536	0.3773222	0.1056622
0.4	0.4170587	0.2355805	0.7703445
0.5	0.5266520	0.6172168	0.1467309
0.6	0.6133799	0.6556577	0.0644815
0.7	0.6812442	0.4752492	0.4334463
0.8	0.7721171	0.7757266	0.0046530
0.9	0.8697393	0.9672980	0.1008569
1.0	0.9410286	0.7772928	0.2106489
2.0	1.7700447	1.6318643	0.0846764
3.0	2.8077192	2.9059464	0.0228021
4.0	3.5623730	3.6924945	0.0352395
5.0	4.5911729	4.6815573	0.0193064
6.0	5.3566908	5.3429339	0.0025748
7.0	6.3399993	6.2022560	0.0144352
8.0	7.2382555	7.0272994	0.0300195
9.0	8.1288061	8.1732742	0.0054407
10.0	9.1389897	9.3734856	0.0250169

For the rather large value of $\alpha = 10$ the effect on $\langle p \rangle_{rel}$ is only an additional loss, similar to that found for free-field conditions in the immediately preceding report of this series. The effect on $\langle \theta \rangle_{rel}$ may appear somewhat startling; apparently at $z\lambda/a^2 = 10$ the phase difference with respect to a plane wave is materially reduced by the inclusion of this large absorption value. But this should not really be surprising. We recall that the higher order modes are the least nonplanar in the sense that they are associated with increasingly larger errors in wavelength (but their group velocities are increasingly smaller than plane-wave velocity). And the effect of intrinsic absorption is to preferentially attenuate the higher order, more complex modes. We also recall here that absolutely rigid boundary conditions are the only ones considered in this report for which a plane wave is one of the family of modes possible of propagation.

Figures 17 and 18 indicate that the effect of including absorption in the contained liquid for infinitely flexible boundary conditions is similar to that for rigid boundary conditions, but because the plane-wave mode does not exist for the former, the decrease in phase "error" is not as pronounced. The effect is one of general smoothing in the nature of the curves.

For the liquid boundary conditions as shown in Figs. 19 and 20, not much more can be said of the effect of intrinsic absorption other than that there is a general trend toward smoothing of the curves to a more monotonic variation. For the shorter range of $z\lambda/a^2$ the relative magnitude decrease is generally greater, and the relative phase increase is generally smaller, for the larger absorption, but for larger distances z it is obvious that the only real effect is one of smoothing of the oscillations.

Figures 21 and 22, for elastic boundary conditions, indicate that the statements made above concerning the effect of intrinsic absorption in the liquid for liquid boundary conditions could generally be made also for the elastic boundary conditions. But there is one obvious difference in that, while the smoothing characteristic noted for the other boundary conditions is maintained

for the overall trend of the curves, the introduction of absorption into the elastic boundary condition case results, for the larger absorption coefficient considered, in a much more rapid decrease in $\langle p \rangle_{rel}$ over the larger $z\lambda/a^2$ range.

As has been stated, the limiting boundary condition of absolutely rigid walls (devoid of thermal conductivity and perfectly smooth) does result in one permissible mode being a plane wave. Moreover, as indicated earlier, the situation for $b/a = 1$ (i.e., the transducer completely filling one end of the tube) results in the plane-wave mode being the only permissible one. Figures 23 and 24, with b/a as the parameter, show that $\langle p \rangle_{rel} \equiv 1$ and $\langle \theta \rangle_{rel} \equiv 0$ for this situation ($b/a = 1$). But even so small a change as $b/a = 1.1$ results in a drastic change in the plots of $\langle p \rangle_{rel}$ and $\langle \theta \rangle_{rel}$. (Here we should stress that one does not have uniform piston motion when a transducer completely covers the opening of a hollow right-circular cylinder, so that the ratio b/a would necessarily be greater than unity, even if rigid walls were attainable.) For the shorter range of $z\lambda/a^2$ we find $\langle p \rangle_{rel}$ decreasing faster than free field and then oscillating about free field, while $\langle \theta \rangle_{rel}$ initially increases like free field and then levels off somewhat about 0.05 radian. For the larger $z\lambda/a^2$ range we find that $\langle p \rangle_{rel}$ is oscillating about a value of 0.8 while $\langle \theta \rangle_{rel}$ is oscillating about 0 radian. For $b/a = 1.2$, however, we find $\langle p \rangle_{rel}$ decreasing faster than free field and then demonstrating a general leveling off, while $\langle \theta \rangle_{rel}$ starts off like free field, levels off at about 0.15 radian near $z\lambda/a^2 = 1$, and then, like the curve for $b/a = 1.1$, oscillates about 0 radian. At this point it should be remarked that these last two plots for which $\langle \theta \rangle_{rel}$ becomes negative are the only ones as yet which could result in an apparent phase velocity being smaller than (or an apparent group velocity being greater than) the plane-wave sound speed. For $b/a = 1.5$ as with $b/a = 2$, both $\langle p \rangle_{rel}$ and $\langle \theta \rangle_{rel}$ approximate the free-field curves over the short $z\lambda/a^2$ range.

But $\langle p \rangle_{rel}$ portrays a sharp minimum near $z\lambda/a^2 = 5.5$ and then climbs sharply; $\langle \theta \rangle_{rel}$ simultaneously climbs very sharply near $z\lambda/a^2 = 5.5$ before assuming its gradual increase.

Figures 25 and 26, with b/a as parameter, are plotted for infinitely flexible boundary conditions. Over the short range and for $b/a = 1$, $\langle p \rangle_{\text{rel}}$ decreases faster than free field, but for the larger b/a value it generally shows increasing resemblance to free field ($b/a = 1.2$ appears to be an exception). The behavior of $\langle \theta \rangle_{\text{rel}}$ over the shorter $z\lambda/a^2$ range is more regular with the parameter b/a . Here we find the curve for $b/a = 1$ portraying the greatest ratio of increase in $\langle \theta \rangle_{\text{rel}}$, with the curves for successively larger values of b/a showing a monotonic tendency to closer agreement with free field. Over the larger $z\lambda/a^2$ range we find the relative phase behavior continuing in the same manner, and the behavior of $\langle p \rangle_{\text{rel}}$ for various values of b/a approaches bedlam but generally remains above the free-field value, except for $b/a = 2$ where $\langle p \rangle_{\text{rel}}$ is beginning to resemble free field.

Liquid boundary conditions with b/a as parameter are shown in Figs. 27 and 28. These figures are not sufficiently detailed to note differences between the curves as calculated by the erroneous, but simplifying, assumption of orthogonality and by the correct (actual) procedure. Here again we find a general tendency for $\langle p \rangle_{\text{rel}}$ to oscillate about a constant value after an initial decrease (except for $b/a = 2$, which again is beginning to resemble free field), while $\langle \theta \rangle_{\text{rel}}$ tends to separate for the various values of the b/a parameter. The trend in $\langle \theta \rangle_{\text{rel}}$ is again for the $b/a = 1$ curve to be the most different from the plane-wave curve, with increasing b/a values leading to $\langle \theta \rangle_{\text{rel}}$ converging on the free-field plot.

The last boundary condition considered is the most realistic for a metal tube, that is, the elastic solid boundary condition. Figures 29 and 30 show the effect of the b/a parameter for this case. For the first time the differences between the correct (actual) curves and the ones calculated with the assumption of orthogonality are apparent in the curves for which $b/a < 1.5$. We also note that the differences are greater for these elastic boundary conditions. Here we find $\langle p \rangle_{\text{rel}}$ generally assuming a constant value for each b/a , with the variation increasing with $z\lambda/a^2$ and the constant value increasing with

b/a . For the phase plots, however, we find that $\langle \theta \rangle_{\text{rel}}$ has the greatest rate of increase for the smaller values of b/a ; that is, $b/a = 1$ has the largest phase correction to a plane wave, with the correction decreasing with increasing b/a until, at the value $b/a = 2$, it begins to approximate free-field conditions over the distances plotted. Obviously those individuals who attempt to minimize the apparent sound speed discrepancies with respect to plane-wave values by purposely choosing $b/a = 1$, in the mistaken assumption that their boundary conditions approximate absolutely rigid walls and thus permit only the plane-wave mode, could not have selected a worse b/a parameter. These plots, it should be recalled, are for a realistic metal wall with a density seven times that of the contained liquid, a sound speed four times that of the contained liquid, and Poisson's ratio $\nu = 0.325$. All calculations, except for the parameter being varied, are for the standard reference conditions in Table 1.

The next parameter varied is the wavenumber (or unconfined plane-wave sound speed) ratio k_1/k_2 of the contained liquid to the wall material. We select values of $k_1/k_2 = 3, 4,$ and 5 . Figures 31 and 32 are for liquid boundary conditions. Obviously the variation of this parameter has very little effect on the curves, which cannot be distinguished over the major portion of the $z\lambda/a^2$ range and, as usual, oscillate about the free-field curve.

Figures 33 and 34 are for the parameter k_1/k_2 for elastic boundary conditions. Unlike the liquid boundary condition, the effect here is pronounced and can be summarized by noting that the $\langle p \rangle_{\text{rel}}$ plots are generally similar, with the curves for the larger parameter values beginning at lower $\langle p \rangle_{\text{rel}}$ values and then all tending to merge toward the end of the $z\lambda/a^2$ range at a value well above free field, showing the effect of coherent reflections. The $\langle \theta \rangle_{\text{rel}}$ plots are likewise generally similar, roughly approximating the free-field curve until the reflections become important, and with the phase relative to a plane wave increasing with k_1/k_2 .

Varying the density ratio ρ_2/ρ_1 of the wall material and the confined liquid again results in

little differentiation for the values $\rho_2/\rho_1 = 6$, 7, and 8 in the case of liquid boundary conditions (see Figs. 35 and 36).

The density ratio parameter variation for elastic boundary conditions is shown in Figs. 37 and 38. Here we note that the behavior is similar to the k_1/k_2 variation effect for elastic walls. Again $\langle p \rangle_{\text{rel}}$ begins with values that are dependent on the parameter values; the curve for the larger density ratio is the farthest below free field. All the curves end with general merging at $z\lambda/a^2 = 10$ at a value above free field. The curves for $\langle \theta \rangle_{\text{rel}}$ tend initially to oscillate about the free-field value but appear to be heading for phase differences (from plane-wave values) that are greater than the free field is from the plane-wave value at $z\lambda/a^2 = 10$. The greater density apparently has the greater anomaly.

Figures 39 and 40 indicate the effect of varying the Poisson's ratio parameter ν for elastic boundary conditions. Here again we find minor differences in $\langle p \rangle_{\text{rel}}$ over the shorter $z\lambda/a^2$ range and an eventual merging at the greatest distance considered. Conversely, $\langle \theta \rangle_{\text{rel}}$ values show little difference up to $z\lambda/a^2 = 1$, beyond which there is a gradual divergence of the ν parameter plots, with the smaller Poisson's ratio contributing a slightly larger phase discrepancy from plane-wave values.

As discussed in Ref. 4, the intrinsic absorption coefficient α of the contained liquid can be experimentally determined most readily from the equation

$$\alpha = \frac{1}{(X_2 - X_1)} \ln \left(\frac{A_1}{A_2} \right)$$

where $X_2 - X_1$ represents a sufficiently small distance interval and

$$\frac{A_2}{A_1} = \left(\frac{N_2}{N_1} \right) \left(\frac{D_1}{D_2} \right)$$

is obtained from the measured amplitudes N and the diffraction amplitude D . The latter two quantities are obtained from

$$N_2 = N_1 e^{-\nu(X_2 - X_1)}$$

and

$$D_2 = D_1 e^{-\delta(X_2 - X_1)}$$

where we have assumed no interaction, i.e.,

$$\alpha = \nu - \delta,$$

and we note that both ν and δ may be either positive or negative depending on the distances involved.

Similarly, the application of these current calculations to sound speed measurements is adequately detailed in the immediately preceding report of this series. In the case of guided propagation, however, the advantages accruing from increasing path in free-field propagation are non-existent, and the utilization of differential path techniques must be applied with even more judicious selection of operating distances.

Of all the boundary conditions considered in this report, the one which is believed to most adequately approximate a thick-walled metal tube containing a liquid is the formulation for an elastic solid wall. For this situation we find the choice of $b/a = 1$ to be an unusually inept selection, and for values of $b/a > 2$ the predicted effect is essentially the same as that for free-field propagation from a similar source (for $ka = 20\pi$) up to at least $z\lambda/a^2 = 10$, which corresponds, for $a = 10\lambda$, to $z = 150$ cm. It should be recalled that the formulation in this report deals with nonterminated situations or with terminations wherein the effects of such may be time-separated, such as by the use of pulsing techniques.

CONCLUSIONS

As was shown also for free-field diffraction (finite size, plane-parallel source) in an earlier report (4), appreciable errors in the measurement of sound speed and sound absorption may be attributed to either neglect in applying appropriate corrections to guided mode propagation measurements or to improper selection of geometric parameters so that corrections are not precluded. In particular, the elastic solid boundary conditions, which are considered to be those most appropriate to the situation of a liquid contained within a thick-walled metal tube, are shown to result in maximum anomalies in sound speed determination for the situation of a transducer completely filling one end of the tube. For tube-to-transducer radius ratios greater than 2, the

effect for this boundary condition closely approximates (to ranges of $z\lambda/a^2 \approx 10$) that of free-field propagation from a finite transducer.

FUTURE WORK

The next report of this series will deal with propagation within liquid cylinders contained in shells, both liquid and elastic. Subsequent reports will (a) introduce viscosity in order to more precisely specify appropriate boundary conditions and deal with viscous absorption, (b) introduce an elastic termination to the open end of the liquid cylinder, resulting in iterative reflections, especially for continuous waves, and (c) correlate the theoretical predictions with recent experimental findings. A report on a more adequate representation of free-field phenomena at $z = 0$, including point-source approximations, is also anticipated.

ACKNOWLEDGMENTS

The author wishes to thank Dr. R. L. Steinberger for suggesting that this work be published, Mr. R. E. McGill both for programming the calculations for NAREC and for generous assistance with the mathematics, and Mr. W. F. Walker and Mr. L. P. La Lumiere for plotting the graphs. Mr. R. E. McGill will publish shortly a report on the programming methods he evolved and utilized. Appreciation is also acknowledged to Dr. B. L. Snavely for the stimulating course in acoustic wave propagation at The Catholic University of America which the author was fortunate enough to attend.

REFERENCES

1. Del Grosso, V.A., NRL Report 4002, June 1952
2. Greenspan, M., and Tschiegg, C.E., *J. Research Natl. Bur. Standards* 59:249 (1957)
3. Wilson, W.D., *J. Acous. Soc. Am.* 31(No. 8): 1067-1072 (1959)
4. Del Grosso, V.A., NRL Report 6026, Jan. 1964
5. Del Grosso, V.A., NRL Report 4439, Dec. 1954
6. Lord Rayleigh, "The Theory of Sound," (2nd ed. revised and enlarged, London:MacMillan, 1894) 1st American ed., New York:Dover, 1945
7. Krasnooshkin, P., *Compt. Rend. USSR* 27: 214 (1940)
8. Krasnooshkin, P.E., *J. Phys. USSR* 7:(No. 2)80 (1943)
9. Krasnooshkin, P.E., *Phys. Rev.* 65:190 (1944)
10. Kirchhoff, *Pogg. Ann.* 134:177 (1868)
11. Van Itterbeek, A., and Verhaegen, L., *Nature* 167:477 (1951)
12. Bell, J.F.W., *Proc. Phys. Soc. (London)* B63:958 (1950)
13. Morse, P.M., "Vibration and Sound," 2nd ed., New York:McGraw Hill, 1948
14. Hartig, H.E., and Swanson, C.E., *Phys. Rev.* 54:618 (1938)
15. Jacobi, W.J., *J. Acous. Soc. Am.* 21(No. 2): 120-127 (1949)
16. Biot, M.A., *J. Appl. Phys.* 23:997 (1952)
17. Lin, T.C., and Morgan, C.W., *J. Acous. Soc. Am.* 28:1165 (1956)
18. Pochhammer, L., *J. Reine Angew. Math. (Crelle)* 81:324 (1876)
19. Chree, C., *Quart. J. Math.* 21:287 (1886)
20. Green, H.C., *Phil. Mag.* 45:907 (1923)
21. Boyle, R.W., and Froman, D., *Nature* 126: 602 (1930)
22. Field, G.S., *Can. J. Research* 5:131 (1931)
23. Field, G.S., *Nature* 128:117 (1931)
24. Field, G.S., and Boyle, R.W., *Can. J. Research* 6:192 (1932)
25. Boyle, R.W., Field, G.S., and Froman, D.K., *Nature* 129:693A (1932)
26. Vance, C.B., *Phys. Rev.* 39:737 (1932)
27. Fisher, C.B., and Field, G.S., *Can. J. Research* 7:548 (1932)
28. Boyle, R.W., Froman, D.K., and Field, G.S., *Can. J. Research* 6:102 (1932)
29. Norton, G.A., *Phys. Rev.* 44:951A (1933)
30. Field, G.S., *Can. J. Research* 11:254 (1934)
31. Norton, G.A., *J. Acous. Soc. Am.* 7:16(1935)
32. Hulswit, W.H., Jr., and Spence, B.J., *Phys. Rev.* 52:256A (1937)
33. Hulswit, W.H., Jr., *J. Acous. Soc. Am.* 9:224 (1938)
34. May, J., *Proc. Phys. Soc.* 50:553 (1938)
35. Field, G.S., *Can. J. Research* 17A:197 (1939)

36. Field, G.S., *Can. J. Research* 17A:141 (1939)
37. Benfield, A.E., Emslie, A.G., and Huntington, H.B., "On the Theory and Performance of Liquid Delay Lines," MIT Rad. Lab. Report 792 (1945)
38. Sharpless, T.K., *Electronics* 20(No. 11):134 (1947)
39. Fay, R.E., Brown, R.L., and Fortier, O.V., *J. Acous. Soc. Am.* 19:850 (1947)
40. McSkimin, H.J., *J. Acous. Soc. Am.* 20:418 (1948)
41. Huntington, H.B., *J. Acous. Soc. Am.* 20:424 (1948)
42. Redwood, M., *Proc. Phys. Soc. (London)* B70:721 (1957)
43. Redwood, M., "Mechanical Waveguides," London:Pergamon, 1960
44. Carome, E.F., and Witting, J.M., *J. Acous. Soc. Am.* 33:187 (1961)
45. Carome, E.F., Witting, J.M., and Fleury, P.A., *J. Acous. Soc. Am.* 33:1417 (1961)
46. Carome, E.F., and Lastovka, J.B., *J. Acous. Soc. Am.* 35:645 (1963)
47. Lastovka, J.B., and Carome, E.F., *J. Acous. Soc. Am.* 35:1279 (1963)
48. Elco, R.A., and Hughes, W.F., "Acoustic Waveguide Mode Interference and Damping in Viscous Fluids," in "Proceedings of the Fourth International Congress on Acoustics, Part I," August 21-28, 1962, Copenhagen, Denmark

APPENDIX A

TIME CONVENTION FOR AN OUTGOING WAVE

The function appropriate to an outgoing wave with the time convention $e^{-i\omega t}$ is $\mathcal{H}_0^{(1)} = \mathcal{J}_0 + i\mathcal{N}_0$ when $r > 0$. This leads directly, for example, to the characteristic equation (Eq. (62)) for a liquid boundary condition:

$$\frac{\mathcal{J}_0(X)}{X \mathcal{J}_1(X)} = \frac{\rho_2}{\rho_1} \frac{\mathcal{H}_0^{(1)}(\sqrt{X^2 - Y^2})}{\sqrt{X^2 - Y^2} \mathcal{H}_1^{(1)}(\sqrt{X^2 - Y^2})} \quad (97)$$

The requirement that the velocity potential in the second (boundary) medium vanish as the distance r perpendicular to the acoustic source axis approaches ∞ , plus the fact that $\mathcal{H}_0^{(1)}$ vanishes for an infinite complex argument with the imaginary part positive, since

$$\mathcal{H}_m^{(1)}(y) \rightarrow \sqrt{\frac{2}{\pi y}} e^{iy - \frac{\pi i}{2}(m + \frac{1}{2})} \quad (98)$$

as the distance z parallel to the source axis approaches ∞ , requires that

$$Y^2 > X^2.$$

So we write

$$\frac{\mathcal{J}_0(X)}{X \mathcal{J}_1(X)} = \frac{\rho_2}{\rho_1} \frac{\mathcal{H}_0^{(1)}(i\sqrt{Y^2 - X^2})}{i\sqrt{Y^2 - X^2} \mathcal{H}_1^{(1)}(i\sqrt{Y^2 - X^2})}. \quad (99)$$

Since

$$\mathcal{K}_m(y) = \frac{\pi i}{2} e^{\frac{im\pi}{2}} \mathcal{H}_m^{(1)}(iz), \quad (100)$$

with

$$\mathcal{K}_m(y) \rightarrow \sqrt{\frac{\pi}{2y}} e^{-y} \text{ as } z \rightarrow \infty, \quad (101)$$

we may rewrite (89) as

$$\frac{\mathcal{J}_0(X)}{X \mathcal{J}_1(X)} = \frac{\rho_2}{\rho_1} \frac{\mathcal{K}_0(\sqrt{Y^2 - X^2})}{\sqrt{Y^2 - X^2} \mathcal{K}_1(\sqrt{Y^2 - X^2})}. \quad (102)$$

The appropriate characteristic values X for the standard reference conditions (Table 1) are given in Table 4. We note that the Hankel functions $\mathcal{H}_m^{(1)}$ and $\mathcal{H}_m^{(2)}$ have complex values for real arguments, but $i\mathcal{H}_0^{(1)}(iy)$, $-\mathcal{H}_1^{(1)}(iy)$, $-i\mathcal{H}_0^{(2)}(-iy)$, and $-\mathcal{H}_1^{(2)}(-iy)$ are real for positive y . Also

$$\mathcal{H}_0^{(1)}(iy) = -\mathcal{H}_0^{(2)}(-iy) \quad (103)$$

and

$$\mathcal{H}_1^{(1)}(iy) = \mathcal{H}_1^{(2)}(-iy). \quad (104)$$

The Hankel functions are the only unmodified Bessel functions that vanish for an infinite complex argument. The modified Bessel Functions \mathcal{K}_n are real and vanish exponentially at infinity. They are defined in terms of $\mathcal{H}_n^{(1)}$ only and are sometimes called hyperbolic Bessel functions.

If we had chosen the time convention $e^{i\omega t}$, an outgoing wave would apparently be represented by

$$e^{i\omega t} e^{-iq_0 m z} \mathcal{H}_0^{(2)}\left(r \frac{X_0 m}{b}\right) \quad (105)$$

where

$$\mathcal{H}_0^{(2)} = \mathcal{J}_0 - i\mathcal{N}_0.$$

This would lead directly to another characteristic equation for a liquid boundary condition:

$$\frac{\mathcal{J}_0(X)}{X \mathcal{J}_1(X)} = \frac{\rho_2}{\rho_1} \frac{\mathcal{H}_0^{(2)}(\sqrt{X^2 - Y^2})}{\sqrt{X^2 - Y^2} \mathcal{H}_1^{(2)}(\sqrt{X^2 - Y^2})}. \quad (106)$$

As

$$\mathcal{H}_0^{(1)}(z) \rightarrow e^{iz} \sqrt{\frac{2}{i\pi z}} \quad (107)$$

for infinitely large z , so also does

$$\mathcal{H}_0^{(2)}(z) \rightarrow e^{-iz} \sqrt{\frac{2i}{\pi z}} \text{ as } z \rightarrow \infty. \quad (108)$$

But here we note that $\mathcal{H}_0^{(2)}$ vanishes for an infinite complex argument with the imaginary part *nega-*

tive. If we choose the same limits as before, i.e., $Y^2 > X^2$ – which corresponds to $q_{0m}^2 > k^2$ and further requires that $C_2 > C_1$ (or $k_1 > k_2$) for Y real—we have a pure imaginary argument which is positive, so

$$\frac{\mathcal{J}_0(X)}{X \mathcal{J}_1(X)} = \frac{\rho_2}{\rho_1} \frac{H_0^{(2)}(i\sqrt{Y^2 - X^2})}{i\sqrt{Y^2 - X^2} H_1^{(2)}(i\sqrt{Y^2 - X^2})} \tag{109}$$

The simplest way to rectify this is to substitute $-i$ for i , which amounts to defining the argument of $H_0^{(2)}$ in (105) as negative. This step leads directly, using (107) and (108), to

$$\frac{\mathcal{J}_0(X)}{X \mathcal{J}_1(X)} = \frac{\rho_2}{\rho_1} \frac{H_0^{(1)}(i\sqrt{Y^2 - X^2})}{i\sqrt{Y^2 - X^2} H_1^{(1)}(i\sqrt{Y^2 - X^2})}$$

which is just the characteristic equation we used for the $e^{-i\omega t}$ time convention. Thus, the set of roots X would be identical to that shown in

Table 4, and the succeeding calculations based on these roots would follow exactly as before.

At this point, it might prove enlightening to *not* change the sign of the argument in (109) but to follow the calculations blindly from this point on. The resulting roots are given in Table A1, along with the correct roots repeated from Table 4. With this wrong time convention, then, $\langle p \rangle_{rel}$ is calculated both by (erroneously) invoking orthogonality and by the correct procedure and is listed in Table A2; $\langle \theta \rangle_{rel}$ is similarly shown in Table A3. With the time convention used both correctly and incorrectly ($\langle p \rangle_{rel}$)_L values for the orthogonal assumption are calculated for outgoing waves and are compared in Table A4, and ($\langle \theta \rangle_{rel}$)_L values are similarly compared in Table A5. Finally, ($\langle p \rangle_{rel}$)_L values for the actual case with the time convention handled correctly and incorrectly are compared in Table A6, and ($\langle \theta \rangle_{rel}$)_L values are similarly compared in Table A7. Without belaboring the issue further, the effect of careless handling of the limits of functions is obvious.

TABLE A1

Comparison of Characteristic Values $X_{Lm} \leq Y$ Obtained by Using the Correct [Eq. (62)] and Incorrect [Eq. (109)] Time Convention in the Characteristic Equation. Calculations are Based on Standard Reference Parameters Shown in Table 1

m	X_{Lm} —correct (From Table 4)	X_{Lm} —incorrect	m	X_{Lm} —correct (From Table 4)	X_{Lm} —incorrect
1	2.2716377	2.5456742	21	63.8405807	66.5372263
2	5.2211344	5.8345490	22	66.9679868	69.6927184
3	8.2022980	9.1249658	23	70.0963105	72.8473568
4	11.2055952	12.3981611	24	73.2254264	76.0012595
5	14.2292985	15.6518249	25	76.3552248	79.1545308
6	17.2712781	18.8875996	26	79.4856088	82.3072641
7	20.3289243	22.1082122	27	82.6164906	85.4595453
8	23.3996145	25.3163963	28	85.7477895	88.6114550
9	26.4809976	28.5145236	29	88.8794289	91.7630717
10	29.5710924	31.7045325	30	92.0113338	94.9144750
11	32.6682830	34.8879669	31	95.1434277	98.0657501
12	35.7712728	38.0660457	32	98.2756279	101.2169937
13	38.8790273	41.2397301	33	101.4078399	104.3683248
14	41.9907212	44.4097812	34	104.5399468	107.5199028
15	45.1056940	47.5768059	35	107.6717908	110.6719660
16	48.2234141	50.7412913	36	110.8031348	113.8249268
17	51.3434505	53.9036324	37	113.9335679	116.9796742
18	54.4654514	57.0641517	38	117.0622018	120.1393156
19	57.5891272	60.2231152	39	120.1859282	—
20	60.7142374	63.3807447			

TABLE A2

Comparison of Average Relative Pressure Values $(\langle p \rangle_{rel})_L$ Obtained Using Orthogonal Assumption and Actual Values of K_{Lm} and the Incorrect [Eq. (109)] Time Convention. Pressure Values are for the Liquid Boundary Condition and are Based on Standard Reference Parameters Shown in Table 1. (See Table 10 for Correct Time Convention Values.)

$z \frac{\lambda}{a^2}$ (Dimensionless)	$(\langle p \rangle_{rel})_L$ - incorrect (Orth. Assump.)	$(\langle p \rangle_{rel})_L$ - incorrect (Actual)	Relative Error (re Actual)
0.0	0.9893119	0.9894439	-0.0001334
0.1	0.9306673	0.9307352	-0.0000729
0.2	0.9021680	0.9022147	-0.0000517
0.3	0.8828351	0.8828814	-0.0000524
0.4	0.8716027	0.8716449	-0.0000484
0.5	0.8557258	0.8557640	-0.0000447
0.6	0.8381940	0.8382258	-0.0000379
0.7	0.8307657	0.8307995	-0.0000406
0.8	0.8248261	0.8248644	-0.0000464
0.9	0.8053215	0.8053477	-0.0000325
1.0	0.7863048	0.7863138	-0.0000115
2.0	0.7524726	0.7525081	-0.0000473
3.0	0.6416083	0.6416015	+0.0000106
4.0	0.6750847	0.6751106	-0.0000384
5.0	0.5406173	0.5406127	+0.0000085
6.0	0.4759966	0.4759698	+0.0000563
7.0	0.5544776	0.5544712	+0.0000117
8.0	0.7111028	0.7111316	-0.0000404
9.0	0.7762329	0.7762875	-0.0000703
10.0	0.7352137	0.7352249	-0.0000152

TABLE A3

Comparison of Average Relative Phase-Difference Values $(\langle \theta \rangle_{rel})_L$ Obtained Using Orthogonal Assumption and Actual Values of K_{Lm} and the Incorrect [Eq. (109)] Time Convention. Phase-Difference Values are for the Liquid Boundary Condition and are Based on Standard Reference Parameters Shown in Table 1. (See Table 11 for Correct Time Convention Values.)

$z \frac{\lambda}{a^2}$ (Dimensionless)	$(\langle \theta \rangle_{rel})_L$ - incorrect (Orth. Assump.)	$(\langle \theta \rangle_{rel})_L$ - incorrect (Actual)	Relative Error (re Actual)
0.0	0.0000006	0.0000006	0
0.1	0.0770320	0.0770624	-0.0003940
0.2	0.1109370	0.1109651	-0.0002535
0.3	0.1378661	0.1378951	-0.0002106
0.4	0.1603679	0.1603884	-0.0001276
0.5	0.1836590	0.1836803	-0.0001159
0.6	0.2128278	0.2128556	-0.0001307
0.7	0.2161217	0.2161328	-0.0000513
0.8	0.2450991	0.2451190	-0.0000810
0.9	0.2568528	0.2568658	-0.0000505
1.0	0.2757060	0.2757279	-0.0000795
2.0	0.4586840	0.4587147	-0.0000670
3.0	0.6006214	0.6006454	-0.0000398
4.0	0.6731474	0.6731453	+0.0000030
5.0	0.8388133	0.8388583	-0.0000537
6.0	0.6892981	0.6892698	-0.0000410
7.0	0.7115613	0.7115412	+0.0000282
8.0	0.7916429	0.7916281	+0.0000186
9.0	1.0351496	1.0351467	+0.0000029
10.0	1.1512997	1.1513039	-0.0000037

TABLE A4
 Comparison of Average Relative Pressure Values
 $(\langle p \rangle_{rel})_L$ Obtained Using the Orthogonal Assumption Values of K_{Lm} and
 the Correct [Eq. (62)] and Incorrect [Eq. (109)] Time Convention. Pressure
 Values are for the Liquid Boundary Condition and are Based on Standard
 Reference Parameters Shown in Table 1.

$z \frac{\lambda}{a^2}$ (Dimensionless)	$(\langle p \rangle_{rel})_L$ - incorrect (Orth. Assump.; Table A2)	$(\langle p \rangle_{rel})_L$ -correct (Orth. Assump.; Table 10)	Relative Error (re Correct)
0.0	0.9893119	0.9895775	- 0.0002684
0.1	0.9306673	0.9306396	+ 0.0000298
0.2	0.9021680	0.9018492	+ 0.0003535
0.3	0.8828351	0.8832659	- 0.0004877
0.4	0.8716027	0.8747904	- 0.0036440
0.5	0.8557258	0.8601329	- 0.0051237
0.6	0.8381940	0.8296854	+ 0.0102552
0.7	0.8307657	0.8454234	- 0.0176436
0.8	0.8248261	0.8156356	+ 0.0112679
0.9	0.8053215	0.8024712	+ 0.0035519
1.0	0.7863048	0.8094636	- 0.0294527
2.0	0.7524726	0.7535671	- 0.0014545
3.0	0.6416083	0.7475792	- 0.1651645
4.0	0.6750847	0.5320858	+ 0.2687516
5.0	0.5406173	0.5033542	+ 0.0740296
6.0	0.4759966	0.3703530	+ 0.2852511
7.0	0.5544776	0.2964656	+ 0.8702932
8.0	0.7111028	0.4134798	+ 0.7198006
9.0	0.7762329	0.3812747	+ 1.0358888
10.0	0.7352137	0.5912150	+ 0.2435640

TABLE A5
 Comparison of Average Relative Phase-Difference Values
 $(\langle \theta \rangle_{rel})_L$ Obtained Using the Orthogonal Assumption Values of K_{Lm} and
 the Correct [Eq. (62)] and Incorrect [Eq. (109)] Time Convention. Phase-
 Difference Values are for the Liquid Boundary Condition and are Based on
 Standard Reference Parameters Shown in Table 1.

$z \frac{\lambda}{a^2}$ (Dimensionless)	$(\langle \theta \rangle_{rel})_L$ - incorrect (Orth. Assump.; Table A3)	$(\langle \theta \rangle_{rel})_L$ -correct (Orth. Assump.; Table 11)	Relative Error (re Correct)
0.0	0.0000006	0.0000006	0
0.1	0.0770320	0.0770784	- 0.0006020
0.2	0.1109370	0.1104181	+ 0.0046994
0.3	0.1378661	0.1358862	+ 0.0145703
0.4	0.1603679	0.1639416	- 0.0217986
0.5	0.1836590	0.1836409	+ 0.0000986
0.6	0.2128278	0.2061965	+ 0.0321601
0.7	0.2161217	0.2209007	- 0.0216342
0.8	0.2450991	0.2617586	- 0.0636445
0.9	0.2568528	0.2418164	+ 0.0621811
1.0	0.2757060	0.2425141	+ 0.1368659
2.0	0.4586840	0.3661808	+ 0.2526165
3.0	0.6006214	0.7017445	- 0.1441024
4.0	0.6731474	0.7916116	- 0.1496494
5.0	0.8388133	0.7776839	+ 0.0786044
6.0	0.6892981	1.0905651	- 0.3679441
7.0	0.7115613	0.6155605	+ 0.1559567
8.0	0.7916429	0.6405180	+ 0.2359147
9.0	1.0351496	0.4942622	+ 1.0943329
10.0	1.1512997	0.5903329	+ 0.9502550

TABLE A6

Comparison of Average Relative Pressure Values
 $(\langle p \rangle_{rel})_L$ Obtained Using the Actual Values of K_{Lm} and the Correct [Eq. (62)] and Incorrect [Eq. (109)] Time Convention. Pressure Values are for the Liquid Boundary Condition and are Based on Standard Reference Parameters Shown in Table 1.

$z \frac{\lambda}{a^2}$ (Dimensionless)	$(\langle p \rangle_{rel})_L$ -incorrect (Actual Table A2)	$(\langle p \rangle_{rel})_L$ -correct (Actual Table 10)	Relative Error (re Correct)
0.0	0.9894439	0.9894456	- 0.0000017
0.1	0.9307352	0.9305719	+ 0.0001755
0.2	0.9022147	0.9018035	+ 0.0004560
0.3	0.8828814	0.8832215	- 0.0003851
0.4	0.8716449	0.8747423	- 0.0035409
0.5	0.8557640	0.8600888	- 0.0050283
0.6	0.8382258	0.8296640	+ 0.0103196
0.7	0.8307995	0.8453774	- 0.0172407
0.8	0.8248644	0.8156078	+ 0.0113493
0.9	0.8053477	0.8024510	+ 0.003610
1.0	0.7863138	0.8094384	- 0.0285687
2.0	0.7525081	0.7535548	- 0.0013890
3.0	0.6416015	0.7475292	- 0.1417038
4.0	0.6751106	0.5321009	+ 0.2687643
5.0	0.5406127	0.5033521	+ 0.0740249
6.0	0.4759698	0.3703732	+ 0.2851086
7.0	0.5544712	0.2964915	+ 0.8701082
8.0	0.7111316	0.4134609	+ 0.7199489
9.0	0.7762875	0.3813003	+ 1.0358953
10.0	0.7352249	0.5912050	+ 0.2436040

TABLE A7

Comparison of Average Relative Phase-Difference Values
 $(\langle \theta \rangle_{rel})_L$ Obtained Using the Actual Values of K_{Lm} and the Correct [Eq. (62)] and Incorrect [Eq. (109)] Time Convention. Pressure Values are for the Liquid Boundary and are Based on Standard Reference Parameters Shown in Table 1.

$z \frac{\lambda}{a^2}$ (Dimensionless)	$(\langle \theta \rangle_{rel})_L$ -incorrect (Actual; Table A3)	$(\langle \theta \rangle_{rel})_L$ -correct (Actual; Table 11)	Relative Error (re Actual)
0.0	0.0000006	0.0000006	0
0.1	0.0770624	0.0770483	+ 0.0001830
0.2	0.1109651	0.1103926	+ 0.0051860
0.3	0.1378951	0.1358591	+ 0.0149861
0.4	0.1603884	0.1639192	- 0.0215399
0.5	0.1836803	0.1836184	+ 0.0003371
0.6	0.2128556	0.2061710	+ 0.0324226
0.7	0.2161328	0.2208823	- 0.0215024
0.8	0.2451190	0.2617183	- 0.0634243
0.9	0.2568658	0.2418140	+ 0.0622454
1.0	0.2757279	0.2425331	+ 0.1368671
2.0	0.4587147	0.3661959	+ 0.2526484
3.0	0.6006454	0.7016980	- 0.1440115
4.0	0.6731453	0.7916051	- 0.496451
5.0	0.8388583	0.7777139	+ 0.0786207
6.0	0.6892698	1.0904750	- 0.3679178
7.0	0.7115412	0.6156242	+ 0.1558045
8.0	0.7916281	0.6405112	+ 0.2359317
9.0	1.0351467	0.4943238	+ 1.0940661
10.0	1.1513039	0.5903391	+ 0.9502416

APPENDIX B

REDEFINITION OF VECTOR DISPLACEMENT POTENTIAL Ψ

In the formulation for elastic solid boundary conditions we have used the displacement vector

$$\mathbf{s} = \nabla\Phi + \nabla_{\mathbf{x}}\Psi$$

where, because of axial symmetry, we have only the single θ component of Ψ , denoted by the scalar Ψ . Our Ψ is a solution to

$$\frac{\partial^2 \Psi}{\partial r^2} + \frac{1}{r} \frac{\partial \Psi}{\partial r} - \frac{\Psi}{r^2} + \frac{\partial^2 \Psi}{\partial z^2} = \frac{1}{C_s^2} \frac{\partial^2 \Psi}{\partial t^2},$$

which we call a pseudo-wave equation because of the extraneous term $-\frac{\Psi}{r^2}$. (The development in the text utilized this potential Ψ and carried it through straightforwardly.)

An alternate procedure consists of redefining the potential used, such that

$$\Psi = -\frac{\partial \bar{\Psi}}{\partial r}, \quad (110)$$

where $\bar{\Psi}$ is a solution to the wave equation

$$\frac{\partial^2 \bar{\Psi}}{\partial r^2} + \frac{1}{r} \frac{\partial \bar{\Psi}}{\partial r} + \frac{\partial^2 \bar{\Psi}}{\partial z^2} = \frac{1}{C_s^2} \frac{\partial^2 \bar{\Psi}}{\partial t^2}. \quad (111)$$

The scalar potential Φ remains unchanged. The displacement vector components then become (cf. Eq. (78))

$$\begin{aligned} s_r &= \frac{\partial \Phi}{\partial r} + \frac{\partial}{\partial z} \left(\frac{\partial \bar{\Psi}}{\partial r} \right) \\ s_z &= \frac{\partial \Phi}{\partial z} - \frac{1}{r} \frac{\partial}{\partial r} \left(r \frac{\partial \bar{\Psi}}{\partial r} \right). \end{aligned} \quad (112)$$

Using the stresses as defined in Eq. (79), the displacement components as defined above, and the relation between C_s and C_c , we then obtain (cf. Eq. (81))

$$\begin{aligned} \sigma_{rr} &= 2\rho_2 C_s^2 \left(\frac{\partial^2 \Phi}{\partial r^2} + \frac{\partial}{\partial r} \left(\frac{\partial^2 \bar{\Psi}}{\partial r \partial z} \right) \right) \\ &\quad + \rho_2 \left(\frac{\nu}{1-\nu} \right) \frac{\partial^2 \Phi}{\partial t^2} \end{aligned}$$

and

$$\begin{aligned} \sigma_{rz} &= 2\rho_2 C_s^2 \left(\frac{\partial^2 \Phi}{\partial r \partial z} + \frac{\partial}{\partial r} \left(\frac{\partial^2 \bar{\Psi}}{\partial z^2} \right) \right) \\ &\quad - \rho_2 \frac{\partial}{\partial r} \left(\frac{\partial^2 \bar{\Psi}}{\partial t^2} \right). \end{aligned} \quad (113)$$

Writing again the expansions in their correct form, i.e.,

$$\Phi = \Phi_0 K_0 \left(r \sqrt{q_{0m}^2 - k_c^2} \right) e^{-i\omega t} e^{iq_{0m}z} \quad (114)$$

and

$$\bar{\Psi} = \bar{\Psi}_0 K_1 \left(r \sqrt{q_{0m}^2 - k_s^2} \right) e^{-i\omega t} e^{iq_{0m}z},$$

we obtain from the vanishing of tangential stress at the boundary (i.e., $\sigma_{rz} \big|_{r=b} = 0$)

$$\begin{aligned} \frac{\Phi_0}{\bar{\Psi}_0} &= \\ &= \frac{-i(2q_{0m}^2 - k_s^2) \sqrt{q_{0m}^2 - k_s^2} K_1' \left(b \sqrt{q_{0m}^2 - k_s^2} \right)}{2q_{0m} \sqrt{q_{0m}^2 - k_c^2} K_0' \left(b \sqrt{q_{0m}^2 - k_c^2} \right)} \end{aligned} \quad (115)$$

(cf. Eq. (82)).

Following the same steps we then find (cf. Eq. (83))

$$\begin{aligned} \sigma_{rr} \big|_{r=b} e^{i(\omega t - q_{0m}z)} &= \\ &= 2\rho_2 C_s^2 (q_{0m}^2 - k_c^2) \Phi_0 K_0'' \left(b \sqrt{q_{0m}^2 - k_c^2} \right) \\ &\quad + i2\rho_2 C_s^2 q_{0m} (q_{0m}^2 - k_s^2) \bar{\Psi}_0 K_1'' \left(b \sqrt{q_{0m}^2 - k_s^2} \right) \\ &\quad - \rho_2 \omega^2 \left(\frac{\nu}{1-\nu} \right) \Phi_0 K_0 \left(b \sqrt{q_{0m}^2 - k_c^2} \right), \end{aligned} \quad (116)$$

and (cf. Eq. (84))

$$s_r \Big|_{r=b} e^{i(\omega t - q_{0m} z)} = \frac{ik_s^2 \bar{\Psi}_0 \sqrt{q_{0m}^2 - k_s^2} \mathcal{K}'_1(b\sqrt{q_{0m}^2 - k_s^2})}{2q_{0m}} \quad (117)$$

where we eliminated Φ_0 by the relation shown in Eq. (115). Finally (cf. Eq. (86))

$$\begin{aligned} \frac{\sigma_{rr}}{s_r} \Big|_{r=b} &= - \left(\frac{2\rho_2 C_s^2}{k_s^2} \right) \\ &\sqrt{q_{0m}^2 - k_c^2} (2q_{0m}^2 - k_s^2) \frac{\mathcal{K}''_0(b\sqrt{q_{0m}^2 - k_c^2})}{\mathcal{K}'_0(b\sqrt{q_{0m}^2 - k_c^2})} \\ &- \left(\frac{4\rho_2 C_s^2}{k_s^2} \right) q_{0m} \sqrt{q_{0m}^2 - k_s^2} \frac{\mathcal{K}''_1(b\sqrt{q_{0m}^2 - k_s^2})}{\mathcal{K}'_1(b\sqrt{q_{0m}^2 - k_s^2})} \\ &+ \rho_2 C_s^2 (2q_{0m}^2 - k_s^2) \\ &\frac{\left(\frac{\nu}{1-\nu} \right) \mathcal{K}_0(b\sqrt{q_{0m}^2 - k_c^2})}{\sqrt{q_{0m}^2 - k_c^2} \mathcal{K}'_0(b\sqrt{q_{0m}^2 - k_c^2})}. \quad (118) \end{aligned}$$

Up until just before this last equation, the various relations obtained using Ψ could be related to those obtained using $\bar{\Psi}$ by the simple substitution of the original redefinition

$$\Psi = - \frac{\partial \bar{\Psi}}{\partial r}$$

or by the equivalent relation

$$\frac{\bar{\Psi}_0}{\Psi_0} = - \sqrt{q_{0m}^2 - k_s^2} \frac{\mathcal{K}'_1(r\sqrt{q_{0m}^2 - k_s^2})}{\mathcal{K}_1(r\sqrt{q_{0m}^2 - k_s^2})}. \quad (119)$$

From Eq. (118), which is obtained from σ_{rr} and s_r whose respective two forms differ only by the relation given in Eq. (119), we find that the two forms of

$$\frac{\sigma_{rr}}{s_r} \Big|_{r=b}$$

can be equated only if, in addition to the relation (eq. (119)), we have

$$\frac{\mathcal{K}''_1}{\mathcal{K}'_1} = \frac{\mathcal{K}''_0}{\mathcal{K}'_0}. \quad (120)$$

It is rather easily shown that such a relation, with the primes referring to differentiation with respect to the entire argument, is not generally true. Quite irrespective of the validity of Eq. (120), we may simplify Eq. (118) to (cf. Eq. (87))

$$\begin{aligned} \frac{\sigma_{rr}}{s_r} \Big|_{r=b} &= - \frac{2\rho_2 \omega^2}{bk_s^2} + \frac{\rho_2 \omega^2 (2q_{0m}^2 - k_s^2)^2 \mathcal{K}_0(b\sqrt{q_{0m}^2 - k_c^2})}{k_s^4 \sqrt{q_{0m}^2 - k_c^2} \mathcal{K}'_1(b\sqrt{q_{0m}^2 - k_c^2})} + \frac{4\rho_2 \omega^2 q_{0m}^2}{bk_s^4} \\ &- \frac{4\rho_2 \omega^2 q_{0m}^2}{bk_s^4} \left(\frac{(b^2 q_{0m}^2 - b^2 k_s^2 + 2) \mathcal{K}_1(b\sqrt{q_{0m}^2 - k_s^2}) + b\sqrt{q_{0m}^2 - k_s^2} \mathcal{K}_0(b\sqrt{q_{0m}^2 - k_s^2})}{\mathcal{K}'_1(b\sqrt{q_{0m}^2 - k_s^2}) + b\sqrt{q_{0m}^2 - k_s^2} \mathcal{K}'_0(b\sqrt{q_{0m}^2 - k_s^2})} \right), \quad (121) \end{aligned}$$

and using the second boundary condition—i.e.,

$$\frac{\sigma_{rr}}{s_r} \Big|_{r=b} = - \frac{p}{s_r^l} \Big|_{r=b}$$

we obtain

$$\frac{\mathcal{J}_0(X_{0m})}{X_{0m} \mathcal{J}_1(X_{0m})} \frac{\rho_1}{\rho_2} = -\frac{2}{b^2 k_s^2} + \frac{(2q_{0m}^2 - k_s^2)^2 \mathcal{K}_0(b\sqrt{q_{0m}^2 - k_c^2})}{k_s^4 b\sqrt{q_{0m}^2 - k_c^2} \mathcal{K}_1(b\sqrt{q_{0m}^2 - k_c^2})} + \frac{4q_{0m}^2}{b^2 k_s^4} - \frac{4q_{0m}^2}{b^2 k_s^4} \left(\frac{(b^2 q_{0m}^2 - b^2 k_s^2 + 2) \mathcal{K}_1(b\sqrt{q_{0m}^2 - k_s^2}) + b\sqrt{q_{0m}^2 - k_s^2} \mathcal{K}_0(b\sqrt{q_{0m}^2 - k_s^2})}{\mathcal{K}_1(b\sqrt{q_{0m}^2 - k_s^2}) + b\sqrt{q_{0m}^2 - k_s^2} \mathcal{K}_0(b\sqrt{q_{0m}^2 - k_s^2})} \right) \quad (122)$$

which becomes, by the previous definitions,

$$\frac{\mathcal{J}_0(X_{0m})}{X_{0m} \mathcal{J}_1(X_{0m})} \frac{\rho_1}{\rho_2} = -\frac{2}{b^2 k_s^2} + \frac{(2q_{0m}^2 - k_s^2)^2 \mathcal{K}_0(\sqrt{Y_c^2 - X_{0m}^2})}{k_s^4 \sqrt{Y_c^2 - X_{0m}^2} \mathcal{K}_1(\sqrt{Y_c^2 - X_{0m}^2})} + \frac{4q_{0m}^2}{b^2 k_s^4} - \frac{4q_{0m}^2}{b^2 k_s^4} \left(\frac{(b^2 q_{0m}^2 - b^2 k_s^2 + 2) \mathcal{K}_1(\sqrt{Y_s^2 - X_{0m}^2}) + \sqrt{Y_s^2 - X_{0m}^2} \mathcal{K}_0(\sqrt{Y_s^2 - X_{0m}^2})}{\mathcal{K}_1(\sqrt{Y_s^2 - X_{0m}^2}) + \sqrt{Y_s^2 - X_{0m}^2} \mathcal{K}_0(\sqrt{Y_s^2 - X_{0m}^2})} \right). \quad (123)$$

This is finally simplified by combining the last two terms to

$$\frac{\mathcal{J}_0(X_{0m})}{X_{0m} \mathcal{J}_1(X_{0m})} \frac{\rho_1}{\rho_2} = -\frac{2}{b^2 k_s^2} + \frac{(2q_{0m}^2 - k_s^2)^2 \mathcal{K}_0(\sqrt{Y_c^2 - X_{0m}^2})}{k_s^4 \sqrt{Y_c^2 - X_{0m}^2} \mathcal{K}_1(\sqrt{Y_c^2 - X_{0m}^2})} - \frac{4q_{0m}^2}{b^2 k_s^4} \left(\frac{(Y_s^2 - X_{0m}^2 + 1) \mathcal{K}_1(\sqrt{Y_s^2 - X_{0m}^2})}{\mathcal{K}_1(\sqrt{Y_s^2 - X_{0m}^2}) + \sqrt{Y_s^2 - X_{0m}^2} \mathcal{K}_0(\sqrt{Y_s^2 - X_{0m}^2})} \right). \quad (124)$$

Obviously, our unwarranted desire to modify the potential used so as to obtain "true" wave equations did not simplify the resulting expressions.

We note that Eq. (124), as compared with Eq. (89), implies for equality that

$$\mathcal{K}_1^2 + X^2 \mathcal{K}_1^2 - X \mathcal{K}_0 \mathcal{K}_1 - X^2 \mathcal{K}_0^2 = 0 \quad (125)$$

where the argument of the Bessel Functions is X . Equation (125) is the equivalent of Eq. (120).

No physical reason demands that this equation be satisfied. However, the intuitive expectation exists that identical $\langle \phi \rangle_{\text{rel}}$ values would be obtained from the solutions X_{0m} to Eq. (124) when used in Eq. (24) with the K_{0m} from Eq. (38) or Eq. (16), as appropriate, as were obtained from the solutions X_{0m} to Eq. (89).

Additional tables have been prepared to demonstrate the degree of validity of this intuitive expectation. Table B1 compares the roots obtained from the redefined potential equation with the original potential equation for the standardized parameters, including $b/a = 2$. Obviously the roots have not been appreciably changed and consequently, as indicated in Table B2, there is little difference between the original and modified potential in the tabulated values of $(\langle p \rangle_{\text{rel}})_E$ calculated by invoking orthogonality. Similarly the orthogonal assumption values for $(\langle \theta \rangle_{\text{rel}})_E$ are essentially the same for both potentials, as seen in Table B3. Finally, for this comparison of results for both potentials for $b/a = 2$, we see in Table B4 that the actual values of $(\langle p \rangle_{\text{rel}})_E$ for both potentials show close agreement and in Table B5 that the same holds for the actual

$(\langle \theta \rangle_{rel})_E$. The roots for both potentials obtained for $b/a = 1$ are shown in Table B6, where again only a slight difference is noted. Tables B7 through B10 again compare solutions obtained for both the original and the redefined potentials and are, respectively, for the orthogonal assumption

$(\langle p \rangle_{rel})_E$, the orthogonal assumption $(\langle \theta \rangle_{rel})_E$, the actual $(\langle p \rangle_{rel})_E$, and the actual $(\langle \theta \rangle_{rel})_E$. While somewhat larger differences may be found in these latter tables, there is generally satisfactory agreement in the results obtained for the two potentials.

TABLE B1

Comparison of Characteristic Values $X_{Em} \leq Y_S$ Obtained by Using the Original Potential Characteristic Equation (Eq. 89) and the Redefined Potential Characteristic Equation (Eq. 124). Calculations are Based on Standard Reference Parameters Shown in Table 1.

m	X_{Em} - Original Potential	X_{Em} - Redefined Potential
1	3.0413911	3.0416401
2	6.5283908	6.5286045
3	9.8273980	9.8275617
4	13.0557922	13.0559227
5	16.2518595	16.2519678
6	19.4306369	19.4307297
7	22.5991233	22.5992045
8	25.7609959	25.7610685
9	28.9183657	28.9184315
10	32.0725284	32.0725888
11	35.2243216	35.2243777
12	38.3743096	38.3743623
13	41.5228853	41.5229351
14	44.6703291	44.6703767
15	47.8168454	47.8168911
16	50.9625847	50.9626290
17	54.1076584	54.1077017
18	57.2521485	57.2521910
19	60.3961139	60.3961552
20	63.5395907	63.5396328
21	66.6826014	66.6826438
22	69.8251471	69.8251902
23	72.9672093	72.9672536
24	76.1087436	76.1087898
25	79.2496705	79.2497194
26	82.3898569	82.3899096
27	85.5290817	85.5291399
28	88.6669664	88.6670328
29	91.8028211	91.8029004
30	94.9352565	94.9353582
31	98.0610040	98.0611503
32	101.1700866	101.1703499
33	104.2115035	104.2123242
34	106.5524618	106.5583070
35	107.9510042	107.9532132

TABLE B2

Comparison of Average Relative Pressure Values $(\langle p \rangle_{rel})_E$ Obtained by Using the Original Potential and the Redefined Potential with the Orthogonal Assumption K_{Em} . Calculations are Based on Standard Reference Parameters Shown in Table 1.

$z \frac{\lambda}{a^2}$	$(\langle p \rangle_{rel})_E -$ Original Potential (Orthog. Assump.)	$(\langle p \rangle_{rel})_E -$ Redefined Potential (Orthog. Assump.)
0.0	0.9717788	0.9717451
0.1	0.9141165	0.9140872
0.2	0.8860098	0.8859779
0.3	0.8667967	0.8667604
0.4	0.8564165	0.8563953
0.5	0.8415938	0.8415637
0.6	0.8190483	0.8190046
0.7	0.8225790	0.8225615
0.8	0.8094269	0.8094015
0.9	0.7846205	0.7845758
1.0	0.7762643	0.7762408
2.0	0.7059880	0.7059790
3.0	0.7464714	0.7465071
4.0	0.7666435	0.7667065
5.0	0.6782722	0.6783703
6.0	0.7197391	0.7198947
7.0	0.8061243	0.8063043
8.0	0.7915121	0.7916595
9.0	0.7181985	0.7183433
10.0	0.8622688	0.8624221

TABLE B3

Comparison of Average Relative Phase Difference Values $(\langle \theta \rangle_{rel})_E$ Obtained by Using the Original Potential and the Redefined Potential with the Orthogonal Assumption K_{Em} . Calculations are Based on Standard Reference Parameters Shown in Table 1.

$z \frac{\lambda}{a^2}$	$(\langle \theta \rangle_{rel})_E -$ Original Potential (Orthog. Assump.)	$(\langle \theta \rangle_{rel})_E -$ Redefined Potential (Orthog. Assump.)
0.0	0	0
0.1	0.0778414	0.0778460
0.2	0.1151891	0.1151897
0.3	0.1422784	0.1422912
0.4	0.1659318	0.1659428
0.5	0.1894090	0.1894081
0.6	0.2217272	0.2217426
0.7	0.2228230	0.2228506
0.8	0.2655853	0.2655847
0.9	0.2644061	0.2644171
1.0	0.2681320	0.2681761
2.0	0.4333332	0.4334086
3.0	0.5311679	0.5312887
4.0	0.8584935	0.8586492
5.0	0.9762409	0.9764162
6.0	0.9276615	0.9278846
7.0	1.1607084	1.1609503
8.0	1.4857913	1.4859755
9.0	1.6592534	1.6594026
10.0	1.7931229	1.7933139

TABLE B4

Comparison of Average Relative Pressure Values $(\langle p \rangle_{rel})_E$ Obtained by Using the Original Potential and the Redefined Potential with the Actual K_{Em} . Calculations are Based on Reference Parameters Shown in Table 1.

$z \frac{\lambda}{a^2}$	$(\langle p \rangle_{rel})_E -$ Original Potential (Actual)	$(\langle p \rangle_{rel})_E -$ Redefined Potential (Actual)
0.0	0.9713188	0.9712871
0.1	0.9142742	0.9142407
0.2	0.8864551	0.8864216
0.3	0.8662562	0.8662263
0.4	0.8562606	0.8562317
0.5	0.8420237	0.8419908
0.6	0.8186038	0.8185737
0.7	0.8221697	0.8221424
0.8	0.8097581	0.8097230
0.9	0.7844757	0.7844519
1.0	0.7759440	0.7759159
2.0	0.7055973	0.7055677
3.0	0.7462238	0.7462155
4.0	0.7664073	0.7663907
5.0	0.6783252	0.6783201
6.0	0.7197888	0.7198243
7.0	0.8058819	0.8059145
8.0	0.7917809	0.7917614
9.0	0.7187899	0.7187712
10.0	0.8627789	0.8627850

TABLE B5

Comparison of Average Relative Phase Difference Values $(\langle \theta \rangle_{rel})_E$ Obtained by Using the Original Potential and the Redefined Potential with the Actual K_{Em} . Calculations are Based on Standard Reference Parameters Shown in Table 1.

$z \frac{\lambda}{a^2}$	$(\langle \theta \rangle_{rel})_E -$ Original Potential (Actual)	$(\langle \theta \rangle_{rel})_E -$ Redefined Potential (Actual)
0.0	0	0
0.1	0.0784568	0.0784571
0.2	0.1146869	0.1146956
0.3	0.1418842	0.1418927
0.4	0.1665204	0.1665249
0.5	0.1893459	0.1893578
0.6	0.2213196	0.2213288
0.7	0.2230320	0.2230467
0.8	0.2657002	0.2657190
0.9	0.2635660	0.2635845
1.0	0.2679827	0.2680016
2.0	0.4338638	0.4338799
3.0	0.5318601	0.5319063
4.0	0.8591407	0.8592388
5.0	0.9768278	0.9769499
6.0	0.9286576	0.9288154
7.0	1.1611076	1.1613348
8.0	1.4862842	1.4865431
9.0	1.6596663	1.6599775
10.0	1.7934281	1.7938050

TABLE B6

Comparison of Characteristic Values $X_{Em} \leq Y_S$ Obtained by Using the Original Potential Characteristic Equation (Eq. 89) and the Redefined Potential Characteristic Equation (Eq. 124). Calculations are Based on Standard Reference Parameters Shown in Table 1 except $b/a = 1$.

m	X_{Em} - Original Potential	X_{Em} - Redefined Potential
1	3.372720310	3.371880142
2	6.759933220	6.759426420
3	9.994916218	9.994554980
4	13.185228852	13.184944867
5	16.356399672	16.356162144
6	19.517557338	19.517349637
7	22.672755116	22.672566964
8	25.824039488	25.823863699
9	28.972516566	28.972347402
10	32.118778351	32.118610445
11	35.263071969	35.262899253
12	38.405321481	38.405135553
13	41.544976097	41.544762561
14	44.680410535	44.680138032
15	47.806349335	47.805921469
16	50.894362149	50.893176539
17	53.284213185	53.269740691
18	54.370414311	54.366793115

TABLE B7

Comparison of Average Relative Pressure Values $(\langle p \rangle_{rel})_E$ Obtained by Using the Original Potential and the Redefined Potential with the Orthogonal Assumption K_{Em} . Calculations are based on Standard Reference Parameters Shown in Table 1 except $b/a = 1$.

$z \frac{\lambda}{a^2}$	$(\langle p \rangle_{rel})_E$ - Original Potential (Orthog. Assump.)	$(\langle p \rangle_{rel})_E$ - Redefined Potential (Orthog. Assump.)
0.0	0.0865885	0.0862226
0.1	0.0837691	0.0834574
0.2	0.0819398	0.0815891
0.3	0.0816765	0.0813158
0.4	0.0791261	0.0788915
0.5	0.0771040	0.0767549
0.6	0.0778171	0.0774220
0.7	0.0755567	0.0753886
0.8	0.0742354	0.0739218
0.9	0.0754615	0.0749993
1.0	0.0738765	0.0737429
2.0	0.0810237	0.0810802
3.0	0.0739906	0.0737786
4.0	0.0757399	0.0749529
5.0	0.0794552	0.0781979
6.0	0.0741046	0.0732354
7.0	0.0840508	0.0843517
8.0	0.0717685	0.0729076
9.0	0.0825636	0.0832128
10.0	0.0742248	0.0732788

TABLE B8

Comparison of Average Relative Phase Difference $(\langle \theta \rangle_{rel})_E$ Obtained by Using the Original Potential and the Redefined Potential with the Orthogonal Assumption K_{Em} . Calculations are Based on Standard Reference Parameters Shown in Table 1 except $b/a = 1$.

$z \frac{\lambda}{a^2}$	$(\langle \theta \rangle_{rel})_E -$ Original Potential (Orthog. Assump.)	$(\langle \theta \rangle_{rel})_E -$ Redefined Potential (Orthog. Assump.)
0.0	0	0
0.1	0.1164774	0.1165960
0.2	0.2429197	0.2425264
0.3	0.3374536	0.3382476
0.4	0.4170587	0.4173054
0.5	0.5266520	0.5256253
0.6	0.6133799	0.6148207
0.7	0.6812442	0.6821635
0.8	0.7721171	0.7702584
0.9	0.8697393	0.8713507
1.0	0.9410286	0.9430995
2.0	1.7700447	1.7694259
3.0	2.8077192	2.8010887
4.0	3.5623730	3.5561345
5.0	4.5911729	4.5958849
6.0	5.3566908	5.3725154
7.0	6.3399993	7.0155598
8.0	7.2382555	7.2433562
9.0	8.1288061	8.1185271
10.0	9.1389897	9.1231125

TABLE B9

Comparison of Average Relative Pressure Values $(\langle p \rangle_{rel})_E$ Obtained by Using the Original Potential and the Redefined Potential with the Actual K_{Em} . Calculations are Based on Standard Reference Parameters Shown in Table 1 except $b/a = 1$.

$z \frac{\lambda}{a^2}$	$(\langle p \rangle_{rel})_E -$ Original Potential (Actual)	$(\langle p \rangle_{rel})_E -$ Redefined Potential (Actual)
0.0	0.1149452	0.1143217
0.1	0.0885871	0.0886270
0.2	0.0837064	0.0828748
0.3	0.1026259	0.1019088
0.4	0.0844068	0.0855379
0.5	0.0703626	0.0692773
0.6	0.0967713	0.0952813
0.7	0.0841316	0.0860895
0.8	0.0670090	0.0664880
0.9	0.0907023	0.0880094
1.0	0.0857666	0.0880855
2.0	0.0763331	0.0826905
3.0	0.0652305	0.0657404
4.0	0.0779204	0.0688498
5.0	0.0935181	0.0781585
6.0	0.0896573	0.0802315
7.0	0.0966090	0.1057441
8.0	0.0660596	0.0903985
9.0	0.0740020	0.0925368
10.0	0.0820247	0.0671322

TABLE B10

Comparison of Average Relative Phase Difference Values $(\langle\theta\rangle_{rel})_E$ Obtained by Using the Original and the Redefined Potential with the Actual K_{Em} . Calculations are Based on Standard Reference Parameters Shown in Table 1 except $b/a = 1$.

$z \frac{\lambda}{a^2}$	$(\langle\theta\rangle_{rel})_E -$ Original Potential (Actual)	$(\langle\theta\rangle_{rel})_E -$ Redefined Potential (Actual)
0.0	0	0
0.1	-0.0123768	-0.0121608
0.2	+0.3906022	+0.3845634
0.3	0.3773222	0.3867991
0.4	0.2355805	0.2383487
0.5	0.6172168	0.5959548
0.6	0.6556577	0.6736168
0.7	0.4752492	0.4887624
0.8	0.7757266	0.7343813
0.9	0.9672980	0.9886973
1.0	0.7772928	0.8038792
2.0	1.6318643	1.6129921
3.0	2.9059464	2.7563164
4.0	3.6924945	3.5702522
5.0	4.6815573	4.7394374
6.0	5.3429339	5.5420472
7.0	6.2022560	6.4038979
8.0	7.0272994	7.1159801
9.0	8.1732742	7.9348692
10.0	9.3734856	9.0432620

APPENDIX C

SELECTION OF APPROPRIATE BESSEL FUNCTION SOLUTIONS

Reduced wave equations are obtained from Eq. (70) by separating out a harmonic time dependence $e^{-i\omega t}$ so that the axial dependence for outgoing waves is $e^{iq_0 m z}$. The remaining radial dependence for axial symmetry then is

$$\frac{\partial^2 \Phi}{\partial r^2} + \frac{1}{r} \frac{\partial \Phi}{\partial r} + \left[\left(\frac{\omega^2}{C_c^2} - q_n^2 \right) - \frac{0^2}{r^2} \right] \Phi = 0 \quad (126)$$

and

$$\frac{\partial^2 \Psi}{\partial r^2} + \frac{1}{r} \frac{\partial \Psi}{\partial r} - \left[\left(\frac{\omega^2}{C_s^2} - q_n^2 \right) - \frac{1}{r^2} \right] \Psi = 0 \quad (127)$$

where we note that we have only the single θ component of the original vector potential Ψ . Equation (126) is Bessel's equation with parameter

$$\beta_1 = \sqrt{\frac{\omega^2}{C_c^2} - q_n^2}$$

and order zero; its general solution is

$$\Phi = C_1 \mathcal{J}_0(\beta_1 r) + C_2 \mathcal{N}_0(\beta_1 r), \quad (128)$$

and $C_2 \equiv 0$ for our liquid cylinder, which includes $r = 0$. Equation (127) is a modified Bessel's equation with parameter

$$\beta_2 = \sqrt{\frac{\omega^2}{C_s^2} - q_n^2}$$

and order unity; its general solution is

$$\Psi = C_3 \mathcal{I}_1(\beta_2 r) + C_4 \mathcal{K}_1(\beta_2 r), \quad (129)$$

and $C_3 \equiv 0$ for our second (wall) medium, which includes $r = \infty$. We note in passing that $\mathcal{K}_1 \rightarrow \infty$ as $r \rightarrow 0$, but our wall material does not extend to $r = 0$. Thus if our region were the cylinder, we should set $C_4 \equiv 0$ and retain C_3 .

In the liquid boundary case considered earlier in the report, we had only a scalar potential for the wall material, which did not extend to $r = 0$, so that we kept both solutions to Bessel's equation. But for ease of handling, we chose the particular combination of constants

$$C_1 = 1 \quad \text{and} \quad C_2 = i$$

using

$$\Phi = \mathcal{J}_0(\beta_1 r) + i \mathcal{N}_0(\beta_1 r) \equiv \mathcal{H}_0^{(1)}(\beta_1 r). \quad (130)$$

Noting that

$$\beta_1 = \sqrt{k_c^2 - q_n^2} = i \sqrt{q_n^2 - k_c^2} \equiv i \gamma_n,$$

we may write

$$\Phi = \mathcal{H}_0^{(1)}(i \gamma_n r) = -\frac{2i}{\pi} \mathcal{K}_0(\gamma_n r). \quad (131)$$

Thus for the outside region we choose \mathcal{K}_0 (or $\mathcal{H}_0^{(1)}$) for the scalar potential solution and \mathcal{K}_1 for the vector potential solution when it exists.

FIGURES

The following figures illustrate the effect of changing the parameter values shown in Table 1 on calculations of the average pressure relative to plane-wave values $\langle p \rangle_{\text{rel}}$ and of the average phase difference $\langle \theta \rangle_{\text{rel}}$ from plane-wave phase. The calculations of $\langle p \rangle_{\text{rel}}$ and $\langle \theta \rangle_{\text{rel}}$ are compared for four possible conditions that might exist at the boundary of a cylindrical cavity and for the free field associated with the radiating piston. In this report, a liquid cavity in the form of a right cylinder is assumed to be the medium and the geometry for guided mode acoustic energy propagation.

Comparison of each boundary condition with the free field for the standard reference parameters shown in Table 1:

Fig. 3 – $\langle p \rangle_{\text{rel}}$ vs $z\lambda/a^2$ for rigid boundary condition

- (a) $0 \leq z\lambda/a^2 \leq 1$
- (b) $1 \leq z\lambda/a^2 \leq 10$

Fig. 4 – $\langle \theta \rangle_{\text{rel}}$ vs $z\lambda/a^2$ for rigid boundary condition

- (a) $0 \leq z\lambda/a^2 \leq 1$
- (b) $1 \leq z\lambda/a^2 \leq 10$

Fig. 5 – $\langle p \rangle_{\text{rel}}$ vs $z\lambda/a^2$ for infinitely flexible boundary condition

- (a) $0 \leq z\lambda/a^2 \leq 1$
- (b) $1 \leq z\lambda/a^2 \leq 10$

Fig. 6 – $\langle \theta \rangle_{\text{rel}}$ vs $z\lambda/a^2$ for infinitely flexible boundary condition

- (a) $0 \leq z\lambda/a^2 \leq 1$
- (b) $1 \leq z\lambda/a^2 \leq 10$

Fig. 7 – $\langle p \rangle_{\text{rel}}$ vs $z\lambda/a^2$ for liquid boundary condition

- (a) $0 \leq z\lambda/a^2 \leq 1$
- (b) $1 \leq z\lambda/a^2 \leq 10$

Fig. 8 – $\langle \theta \rangle_{\text{rel}}$ vs $z\lambda/a^2$ for liquid boundary condition

- (a) $0 \leq z\lambda/a^2 \leq 1$
- (b) $1 \leq z\lambda/a^2 \leq 10$

Fig. 9 – $\langle p \rangle_{\text{rel}}$ vs $z\lambda/a^2$ for elastic boundary condition

- (a) $0 \leq z\lambda/a^2 \leq 1$
- (b) $1 \leq z\lambda/a^2 \leq 10$

Fig. 10 – $\langle \theta \rangle_{\text{rel}}$ vs $z\lambda/a^2$ for elastic boundary condition

- (a) $0 \leq z\lambda/a^2 \leq 1$
- (b) $1 \leq z\lambda/a^2 \leq 10$

Comparison of the four boundary conditions with the free field for radius ratios $b/a = 5$ and $b/a = 10$ (other reference parameters are as shown in Table 1):

Fig. 11 – $\langle p \rangle_{\text{rel}}$ vs $z\lambda/a^2$ for all four boundary conditions and $b/a = 5$

- (a) $0 \leq z\lambda/a^2 \leq 1$
- (b) $1 \leq z\lambda/a^2 \leq 10$

Fig. 12 – $\langle \theta \rangle_{\text{rel}}$ vs $z\lambda/a^2$ for all four boundary conditions and $b/a = 5$

- (a) $0 \leq z\lambda/a^2 \leq 1$
- (b) $1 \leq z\lambda/a^2 \leq 10$

Fig. 13 – $\langle p \rangle_{\text{rel}}$ vs $z\lambda/a^2$ for all four boundary conditions and $b/a = 10$

- (a) $0 \leq z\lambda/a^2 \leq 1$
- (b) $1 \leq z\lambda/a^2 \leq 10$

Fig. 14 – $\langle \theta \rangle_{\text{rel}}$ vs $z\lambda/a^2$ for all four boundary conditions and $b/a = 10$

- (a) $0 \leq z\lambda/a^2 \leq 1$
- (b) $1 \leq z\lambda/a^2 \leq 10$

Comparison of each boundary condition with the free field for absorption parameter values $\alpha = 0$, $\alpha = 1.0$, and $\alpha = 10.0$ (other reference parameters are as shown in Table 1):

Fig. 15 – $\langle p \rangle_{\text{rel}}$ vs $z\lambda/a^2$ for rigid boundary condition

- (a) $0 \leq z\lambda/a^2 \leq 1$
- (b) $1 \leq z\lambda/a^2 \leq 10$

Fig. 16 – $\langle \theta \rangle_{\text{rel}}$ vs $z\lambda/a^2$ for rigid boundary condition

- (a) $0 \leq z\lambda/a^2 \leq 1$
- (b) $1 \leq z\lambda/a^2 \leq 10$

Fig. 17 – $\langle p \rangle_{\text{rel}}$ vs $z\lambda/a^2$ for infinitely flexible boundary condition

- (a) $0 \leq z\lambda/a^2 \leq 1$
- (b) $1 \leq z\lambda/a^2 \leq 10$

Fig. 18 – $\langle \theta \rangle_{\text{rel}}$ vs $z\lambda/a^2$ for infinitely flexible boundary condition

- (a) $0 \leq z\lambda/a^2 \leq 1$
- (b) $1 \leq z\lambda/a^2 \leq 10$

Fig. 19 – $\langle p \rangle_{\text{rel}}$ vs $z\lambda/a^2$ for liquid boundary condition

- (a) $0 \leq z\lambda/a^2 \leq 1$
- (b) $1 \leq z\lambda/a^2 \leq 10$

Fig. 20 – $\langle \theta \rangle_{\text{rel}}$ vs $z\lambda/a^2$ for liquid boundary condition

- (a) $0 \leq z\lambda/a^2 \leq 1$
- (b) $1 \leq z\lambda/a^2 \leq 10$

Fig. 21 – $\langle p \rangle_{\text{rel}}$ vs $z\lambda/a^2$ for elastic boundary condition

- (a) $0 \leq z\lambda/a^2 \leq 1$
- (b) $1 \leq z\lambda/a^2 \leq 10$

Fig. 22 – $\langle \theta \rangle_{\text{rel}}$ vs $z\lambda/a^2$ for elastic boundary condition

- (a) $0 \leq z\lambda/a^2 \leq 1$
- (b) $1 \leq z\lambda/a^2 \leq 10$

Comparison of each boundary condition with the free field for radius-ratio parameter values $b/a = 1.0$, 1.1 , 1.2 , 1.5 , and 2.0 (other reference parameters are as shown in Table 1):

Fig. 23 – $\langle p \rangle_{\text{rel}}$ vs $z\lambda/a^2$ for rigid boundary condition

- (a) $0 \leq z\lambda/a^2 \leq 1$
- (b) $1 \leq z\lambda/a^2 \leq 10$

Fig. 24 - $\langle \theta \rangle_{\text{rel}}$ vs $z\lambda/a^2$ for rigid boundary condition

- (a) $0 \leq z\lambda/a^2 \leq 1$
- (b) $1 \leq z\lambda/a^2 \leq 10$

Fig. 25 - $\langle p \rangle_{\text{rel}}$ vs $z\lambda/a^2$ for infinitely flexible boundary condition

- (a) $0 \leq z\lambda/a^2 \leq 1$
- (b) $1 \leq z\lambda/a^2 \leq 10$

Fig. 26 - $\langle \theta \rangle_{\text{rel}}$ vs $z\lambda/a^2$ for infinitely flexible boundary condition

- (a) $0 \leq z\lambda/a^2 \leq 1$
- (b) $1 \leq z\lambda/a^2 \leq 10$

Fig. 27 - $\langle p \rangle_{\text{rel}}$ vs $z\lambda/a^2$ for liquid boundary condition

- (a) $0 \leq z\lambda/a^2 \leq 1$
- (b) $1 \leq z\lambda/a^2 \leq 10$

Fig. 28 - $\langle \theta \rangle_{\text{rel}}$ vs $z\lambda/a^2$ for liquid boundary condition

- (a) $0 \leq z\lambda/a^2 \leq 1$
- (b) $1 \leq z\lambda/a^2 \leq 10$

Fig. 29 - $\langle p \rangle_{\text{rel}}$ vs $z\lambda/a^2$ for elastic boundary condition

- (a) $0 \leq z\lambda/a^2 \leq 1$
- (b) $1 \leq z\lambda/a^2 \leq 10$

Fig. 30 - $\langle \theta \rangle_{\text{rel}}$ vs $z\lambda/a^2$ for elastic boundary condition

- (a) $0 \leq z\lambda/a^2 \leq 1$
- (b) $1 \leq z\lambda/a^2 \leq 10$

Comparison of liquid and elastic boundary conditions with the free field for wave-number-ratio parameter values $k_1/k_2 = 3, 4, \text{ and } 5$ (other reference parameters are as shown in Table 1):

Fig. 31 - $\langle p \rangle_{\text{rel}}$ vs $z\lambda/a^2$ for liquid boundary condition

- (a) $0 \leq z\lambda/a^2 \leq 1$
- (b) $1 \leq z\lambda/a^2 \leq 10$

Fig. 32 - $\langle \theta \rangle_{\text{rel}}$ vs $z\lambda/a^2$ for liquid boundary condition

- (a) $0 \leq z\lambda/a^2 \leq 1$
- (b) $1 \leq z\lambda/a^2 \leq 10$

Fig. 33 - $\langle p \rangle_{\text{rel}}$ vs $z\lambda/a^2$ for elastic boundary condition

- (a) $0 \leq z\lambda/a^2 \leq 1$
- (b) $1 \leq z\lambda/a^2 \leq 10$

Fig. 34 - $\langle \theta \rangle_{\text{rel}}$ vs $z\lambda/a^2$ for elastic boundary condition

- (a) $0 \leq z\lambda/a^2 \leq 1$
- (b) $1 \leq z\lambda/a^2 \leq 10$

Comparison of liquid and elastic boundary conditions with the free field for density-ratio parameter values $\rho_2/\rho_1 = 6, 7, \text{ and } 8$ (other reference parameters are as shown in Table 1):

Fig. 35 - $\langle p \rangle_{\text{rel}}$ vs $z\lambda/a^2$ for liquid boundary condition

- (a) $0 \leq z\lambda/a^2 \leq 1$
- (b) $1 \leq z\lambda/a^2 \leq 10$

Fig. 36 - $\langle \theta \rangle_{\text{rel}}$ vs $z\lambda/a^2$ for liquid boundary condition

- (a) $0 \leq z\lambda/a^2 \leq 1$
- (b) $1 \leq z\lambda/a^2 \leq 10$

Fig. 37 - $\langle p \rangle_{\text{rel}}$ vs $z\lambda/a^2$ for elastic boundary condition

- (a) $0 \leq z\lambda/a^2 \leq 1$
- (b) $1 \leq z\lambda/a^2 \leq 10$

Fig. 38 - $\langle \theta \rangle_{\text{rel}}$ vs $z\lambda/a^2$ for elastic boundary condition

- (a) $0 \leq z\lambda/a^2 \leq 1$
- (b) $1 \leq z\lambda/a^2 \leq 10$

Comparison of the elastic boundary condition with the free field for Poisson's-ratio parameter values $\nu = 0.300, 0.325, \text{ and } 0.350$ (other reference parameters are as shown in Table 1):

Fig. 39 - $\langle p \rangle_{\text{rel}}$ vs $z\lambda/a^2$ for elastic boundary condition

- (a) $0 \leq z\lambda/a^2 \leq 1$
- (b) $1 \leq z\lambda/a^2 \leq 10$

Fig. 40 - $\langle \theta \rangle_{\text{rel}}$ vs $z\lambda/a^2$ for elastic boundary condition

- (a) $0 \leq z\lambda/a^2 \leq 1$
- (b) $1 \leq z\lambda/a^2 \leq 10$

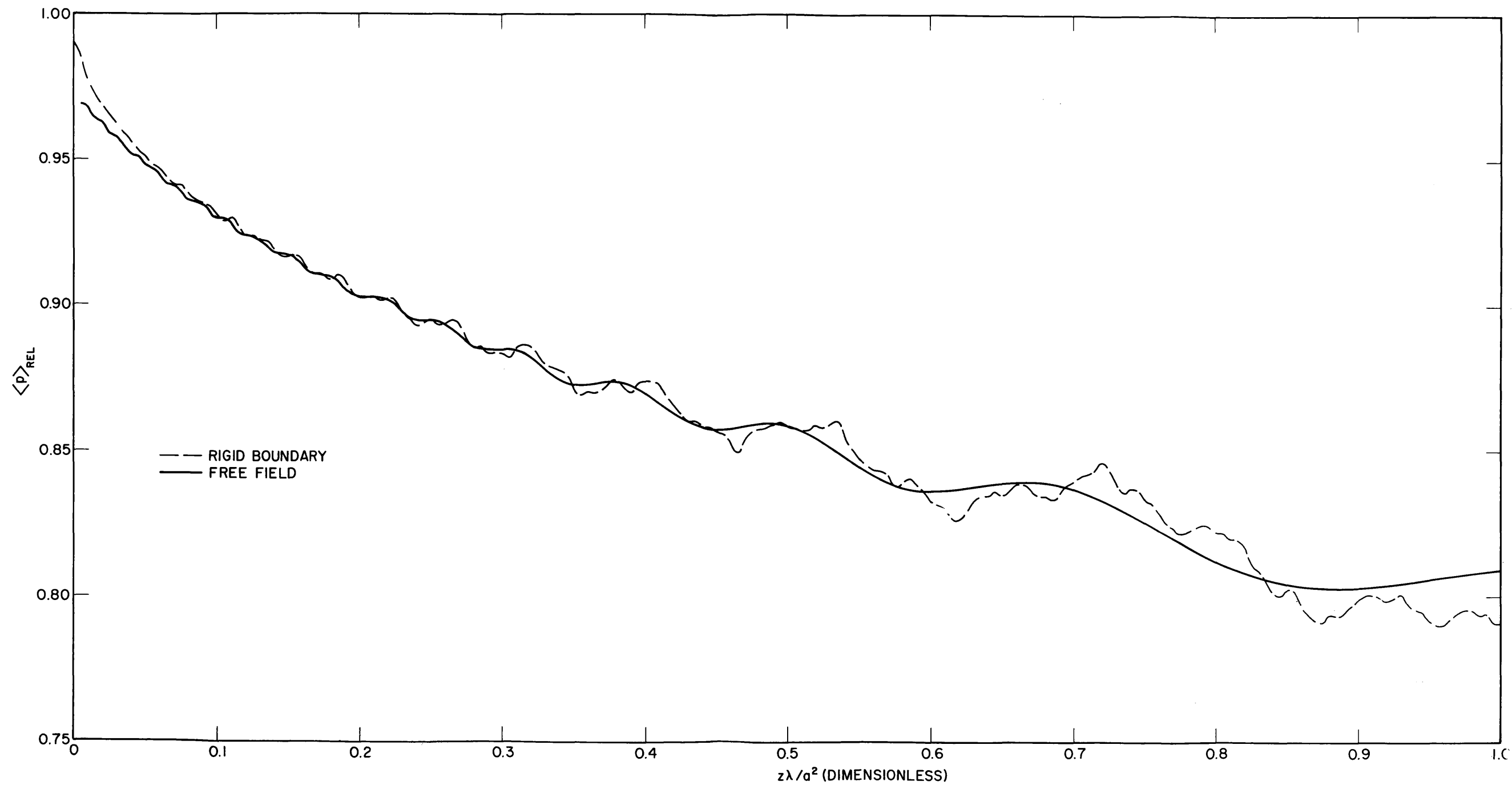


Fig. 3a - Average relative sound pressure $\langle p \rangle_{REL}$ vs $z\lambda/a^2$ for a cylindrical liquid cavity with rigid boundaries. Comparison is between free-field values and rigid boundary values for the standard parameters shown in Table 1 and $0 \leq z\lambda/a^2 \leq 1$.

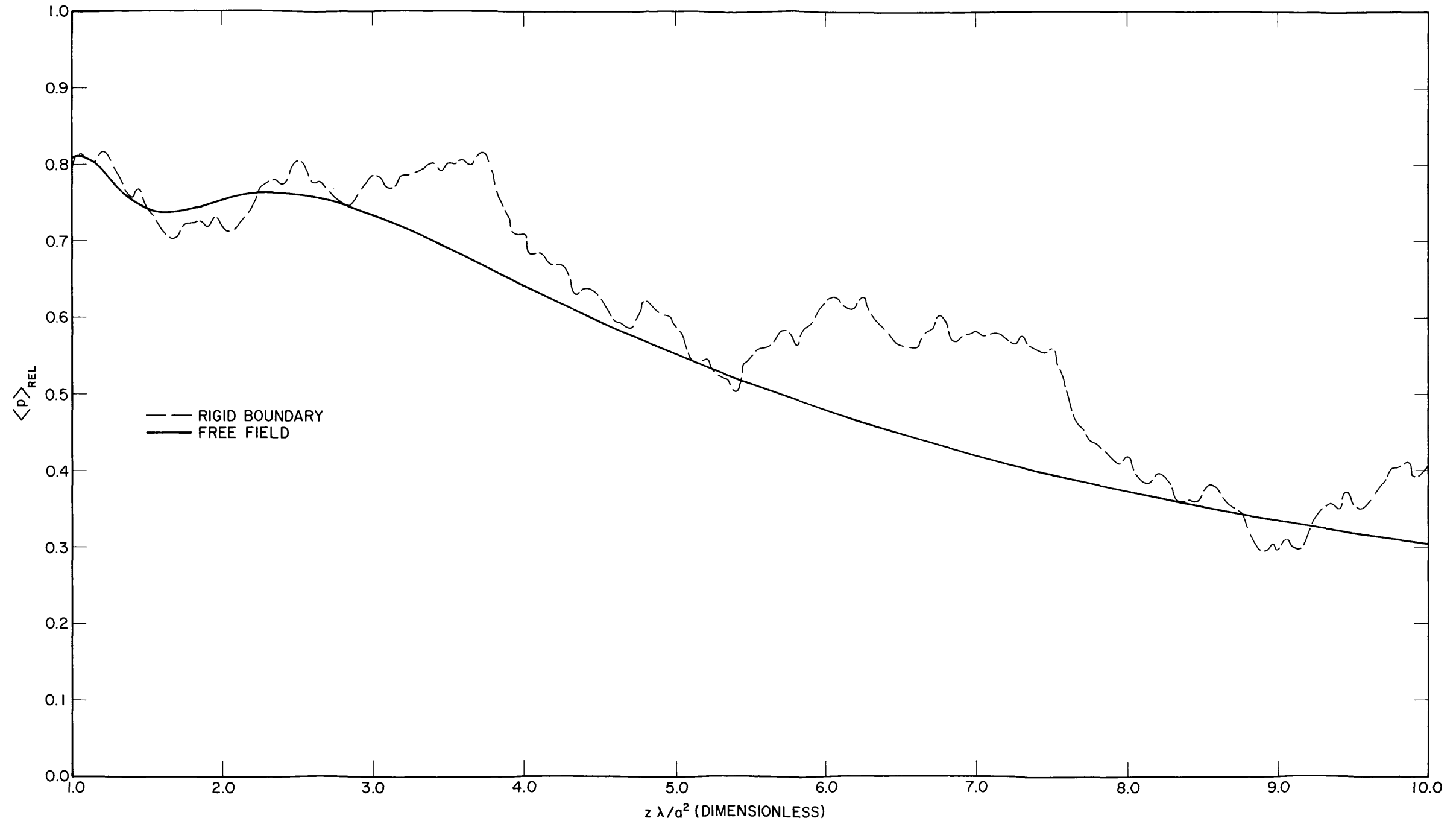


Fig. 3b - Same as Fig. 3a except $1 \leq z \lambda / a^2 \leq 10$

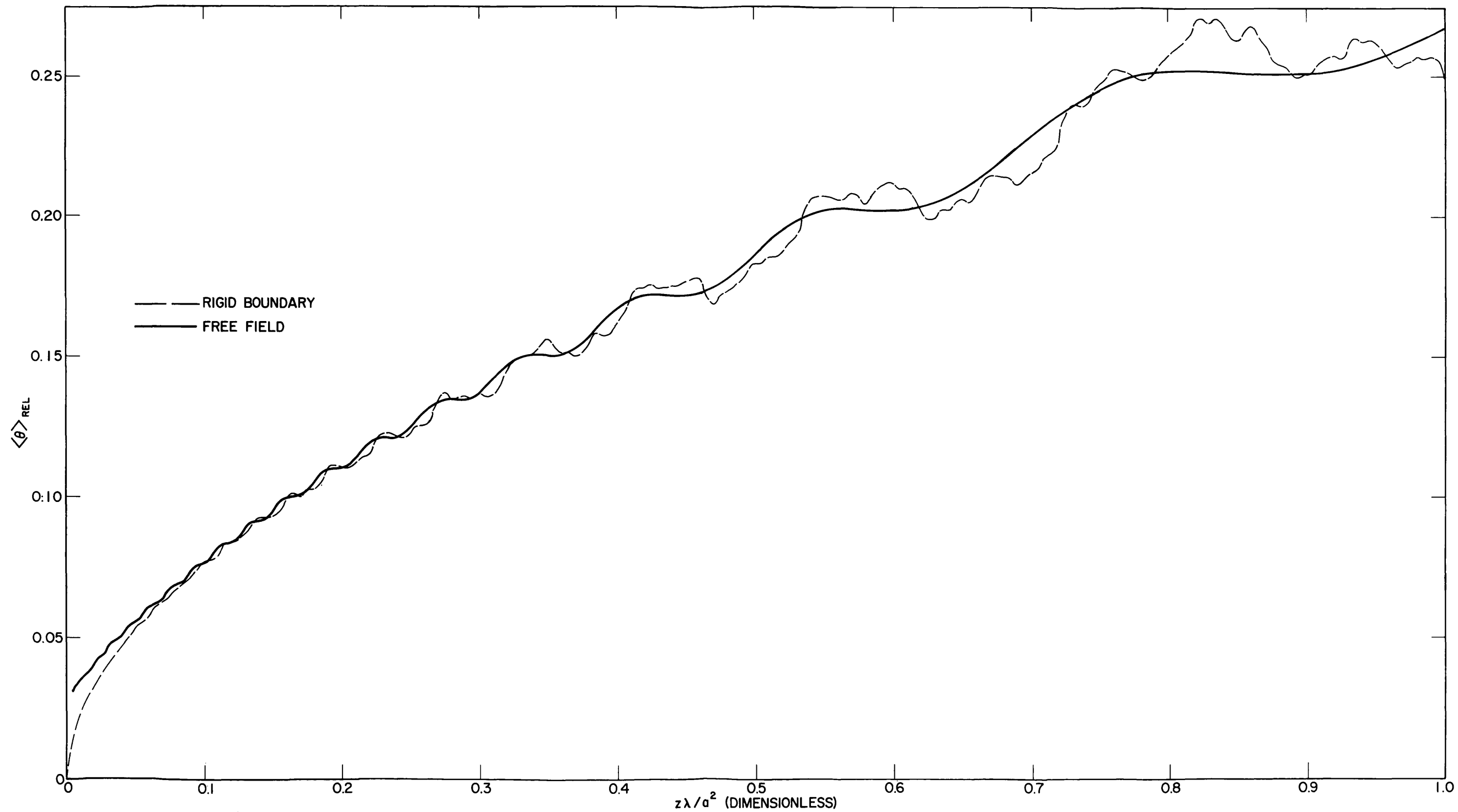
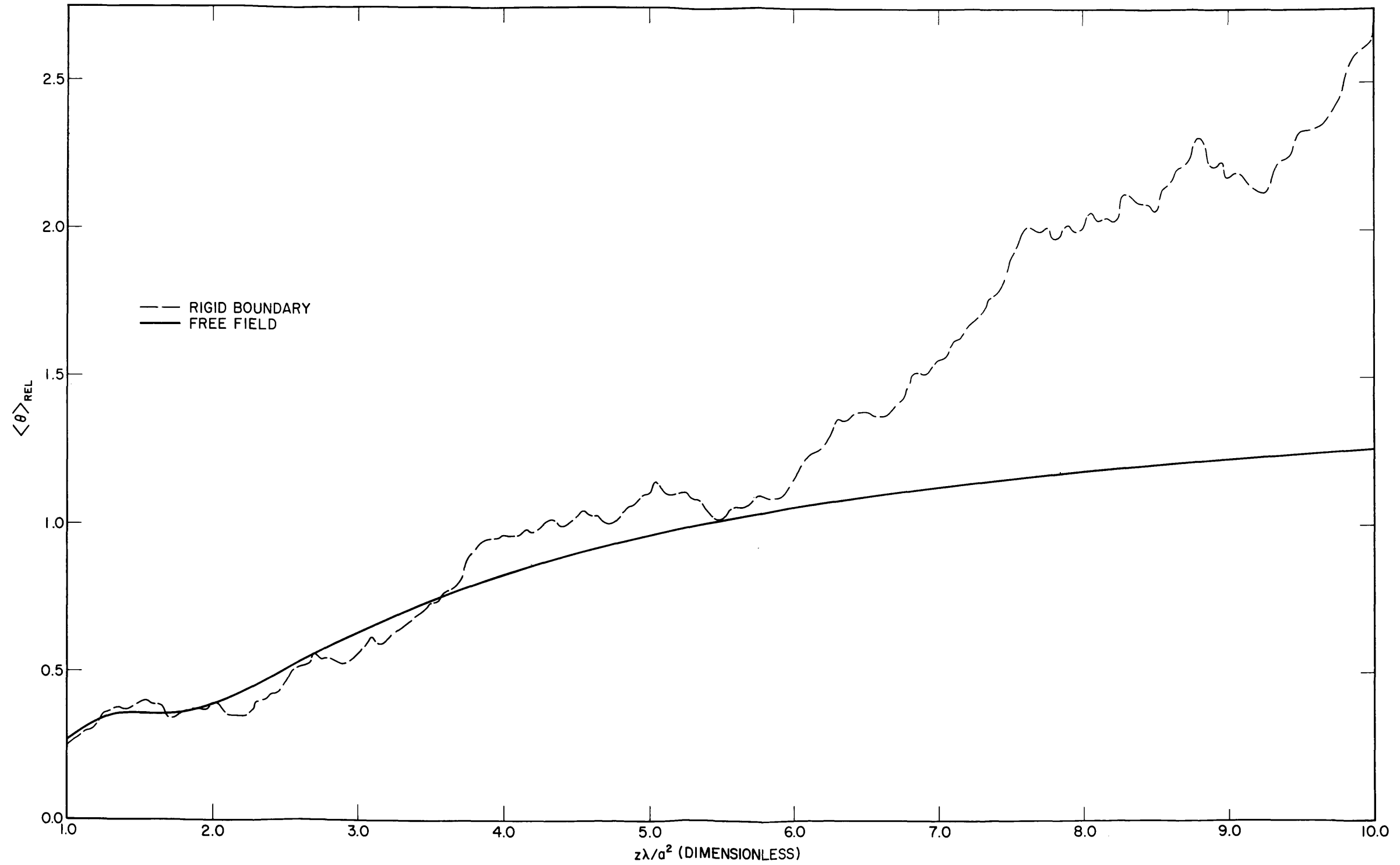


Fig. 4a - Average relative phase difference $\langle \theta \rangle_{REL}$ from plane-wave phase vs $z\lambda/a^2$ for a cylindrical liquid cavity with rigid boundaries. Comparison is between free-field values and rigid boundary values for the standard parameters shown in Table 1 and $0 \leq z\lambda/a^2 \leq 1$.

Fig. 4b - Same as Fig. 4a except $1 \leq z\lambda/a^2 \leq 10$

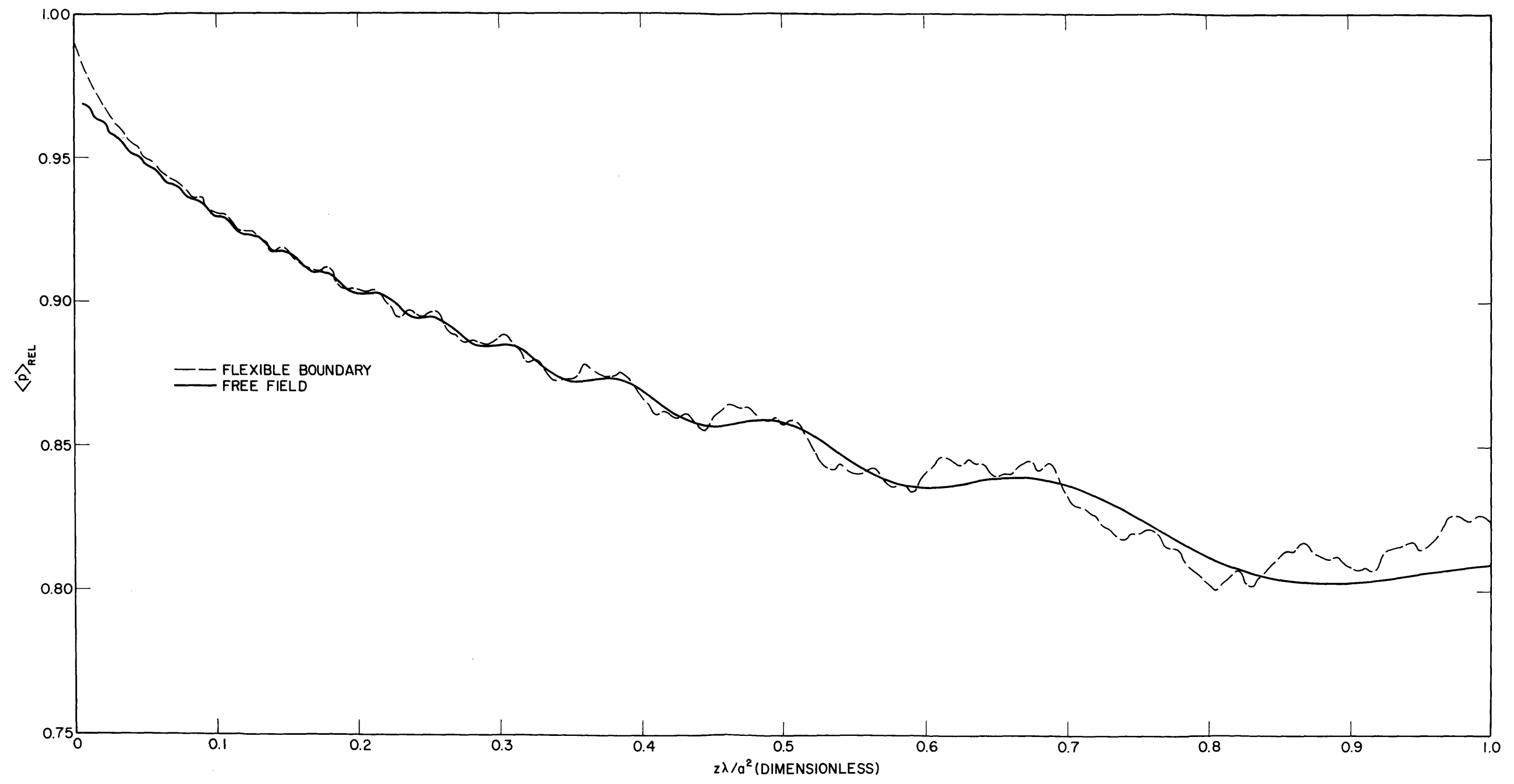
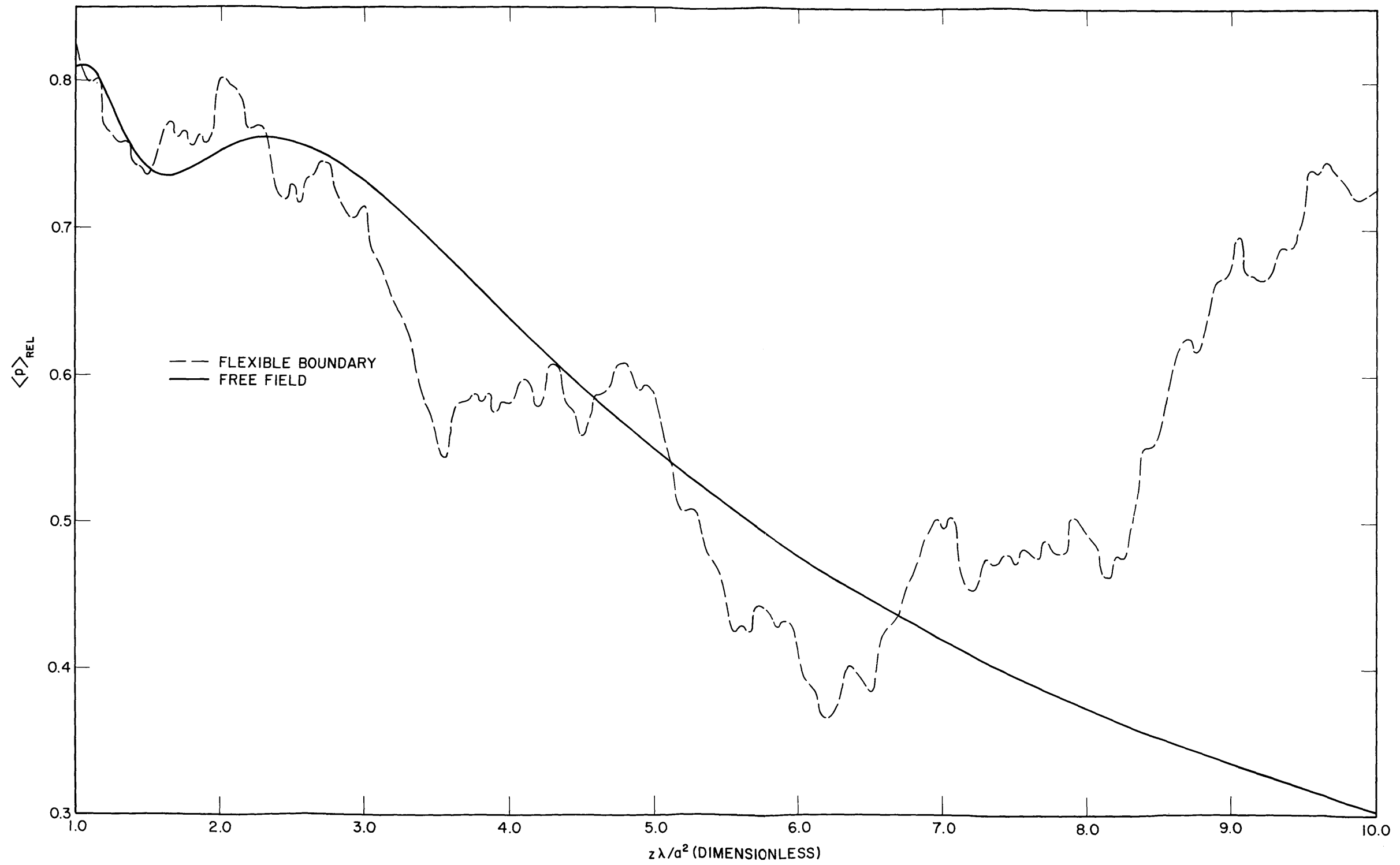


Fig. 5a - Average relative sound pressure $\langle p \rangle_{rel}$ vs $z\lambda/a^2$ for a cylindrical liquid cavity with infinitely flexible boundaries. Comparison is between free-field values and infinitely flexible boundary values for the standard parameters shown in Table 1 and $0 \leq z\lambda/a^2 \leq 1$.

Fig. 5b - Same as Fig. 5a except $1 \leq z\lambda/a^2 \leq 10$

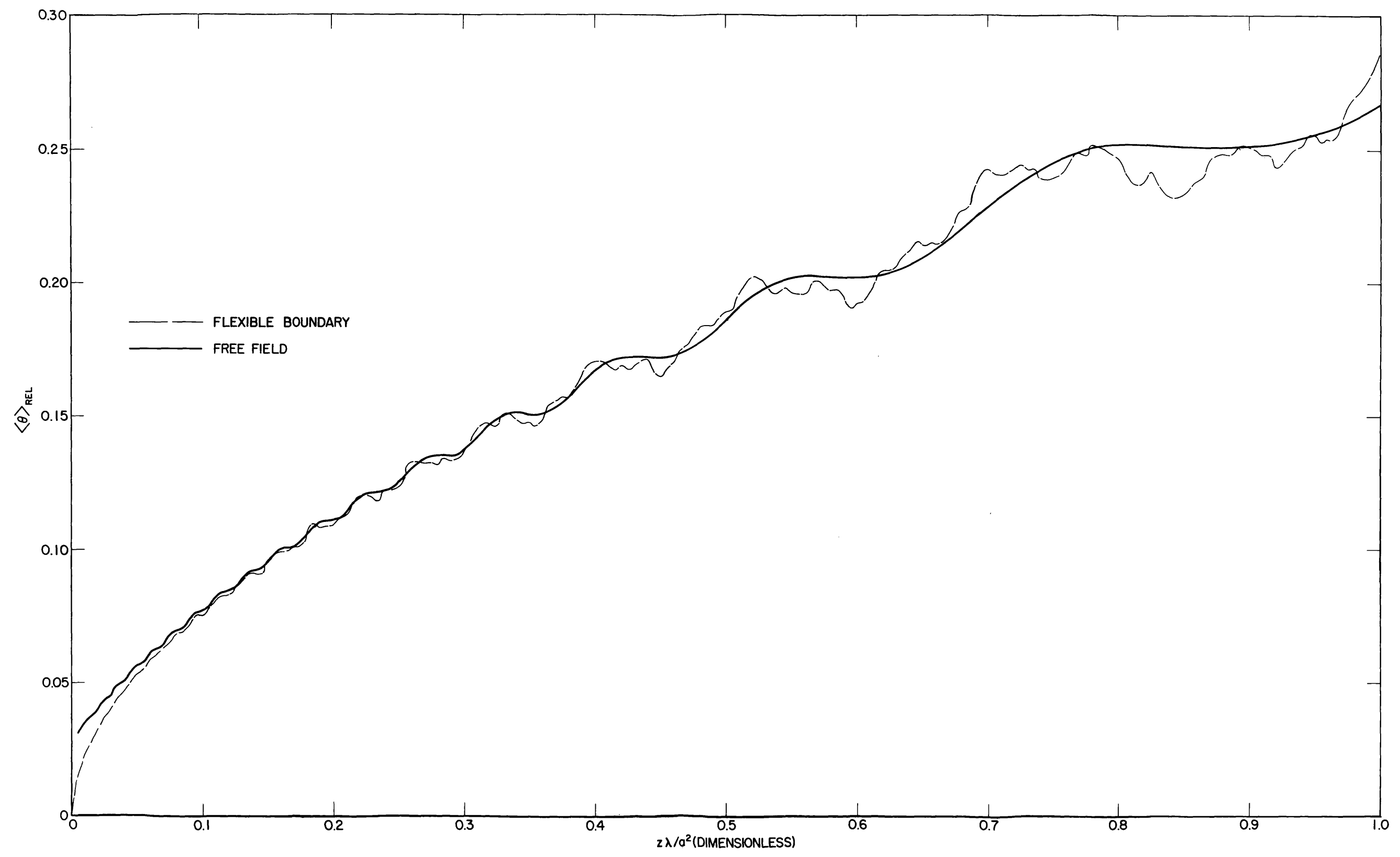


Fig. 6a - Average relative phase difference $\langle \theta \rangle_{REL}$ from plane-wave phase vs $z\lambda/a^2$ for a cylindrical liquid cavity with infinitely flexible boundaries. Comparison is between free-field values and infinitely flexible boundary values for the standard parameters shown in Table 1 and $0 \leq z\lambda/a^2 \leq 1$.

Figure 6

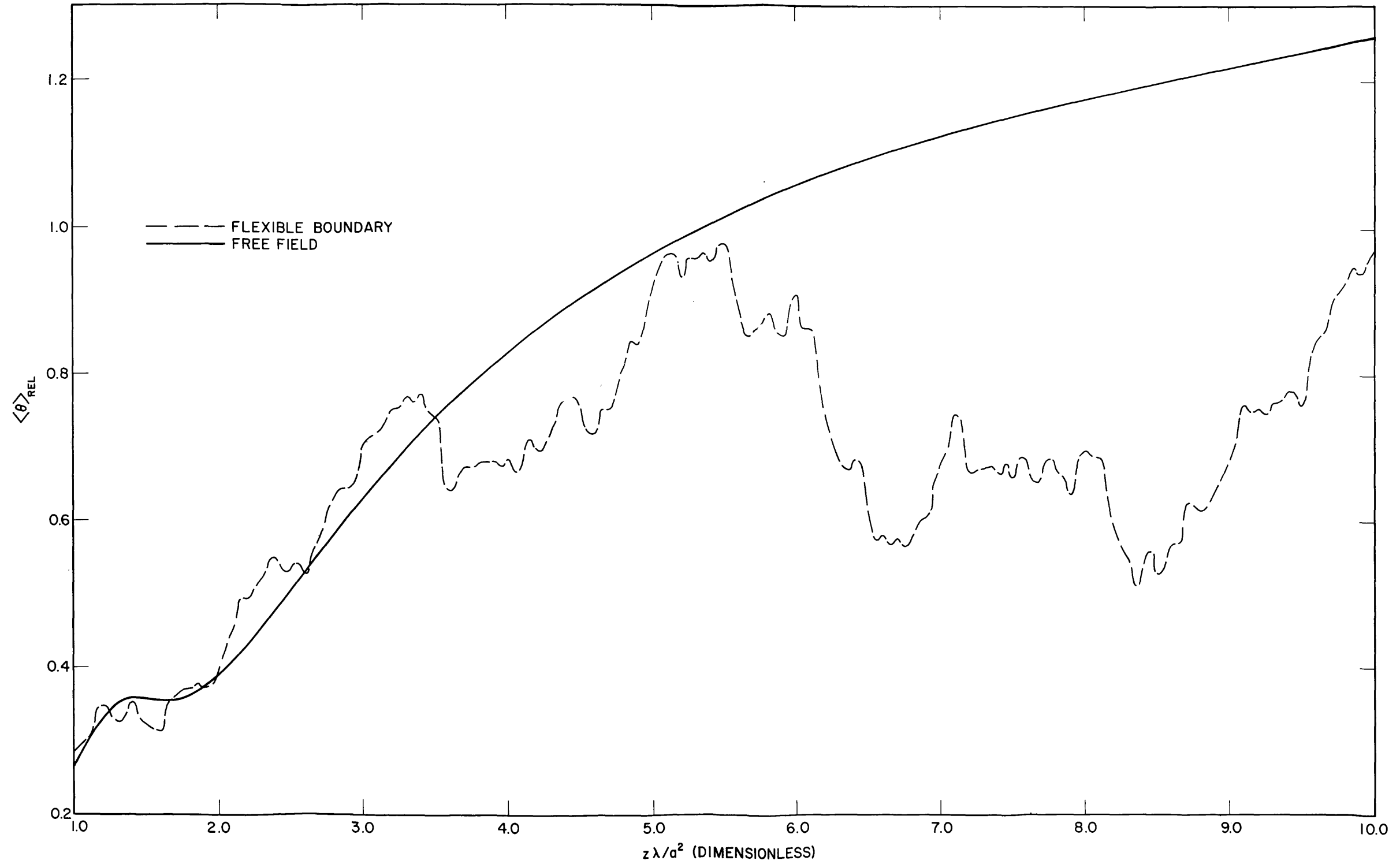


Fig. 6b - Same as Fig. 6a except $1 \leq z\lambda/a^2 \leq 10$

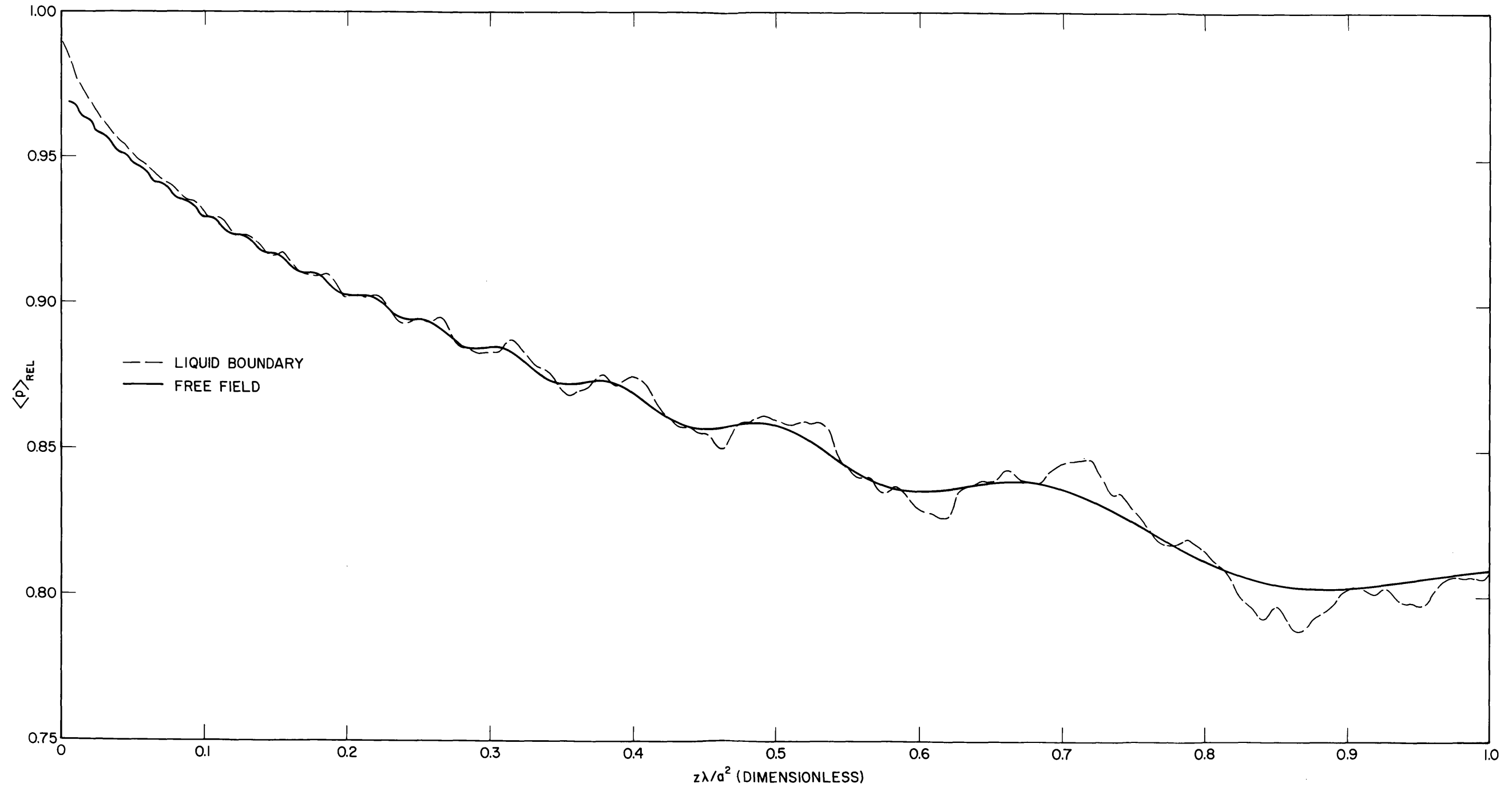
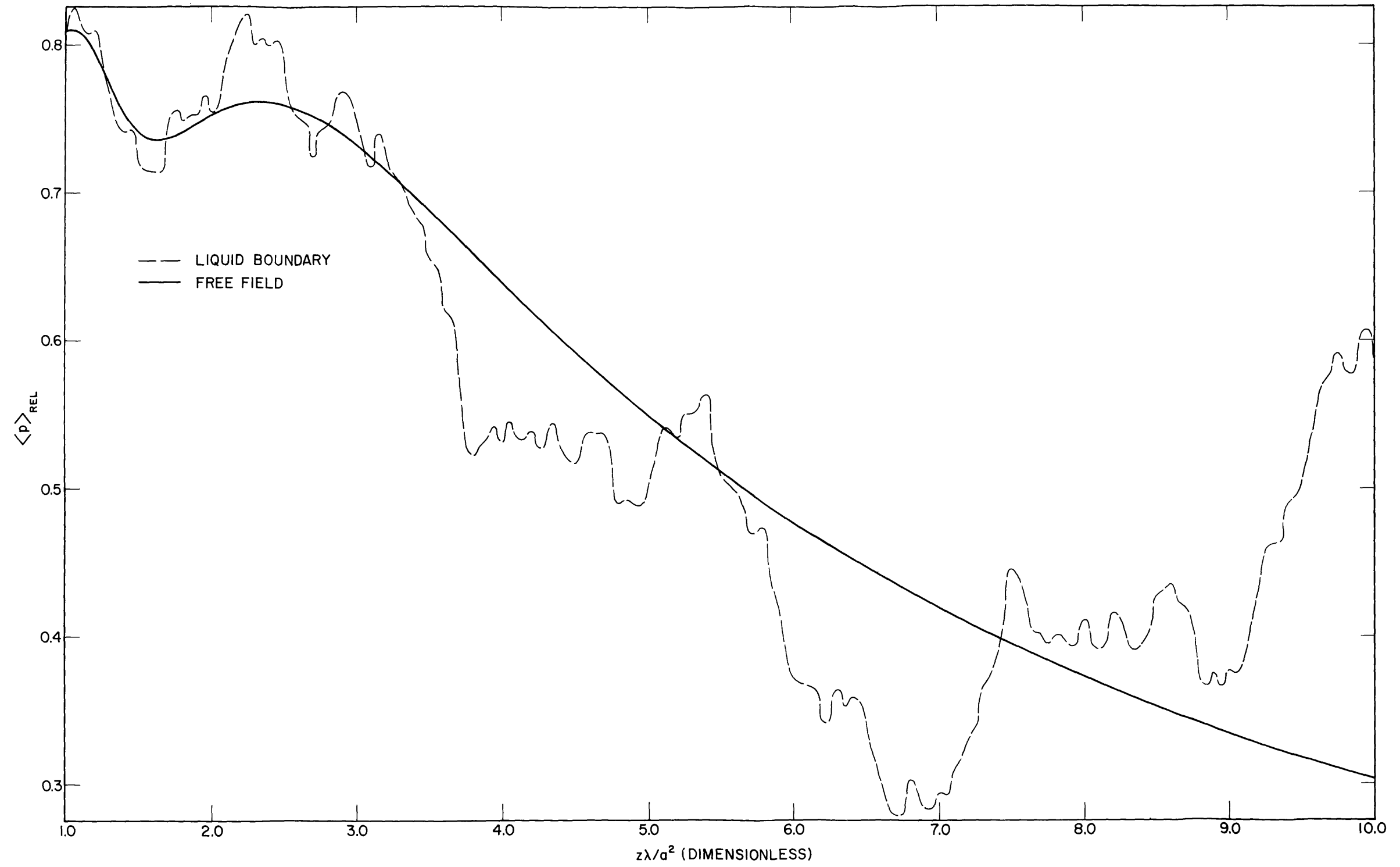


Fig. 7a - Average relative sound pressure $\langle p \rangle_{rel}$ vs $z\lambda/a^2$ for a cylindrical liquid cavity with liquid boundaries. Comparison is between free-field values and liquid boundary values for the standard parameters shown in Table 1 and $0 \leq z\lambda/a^2 \leq 1$.

Fig. 7b - Same as Fig. 7a except $1 \leq z\lambda/a^2 \leq 10$

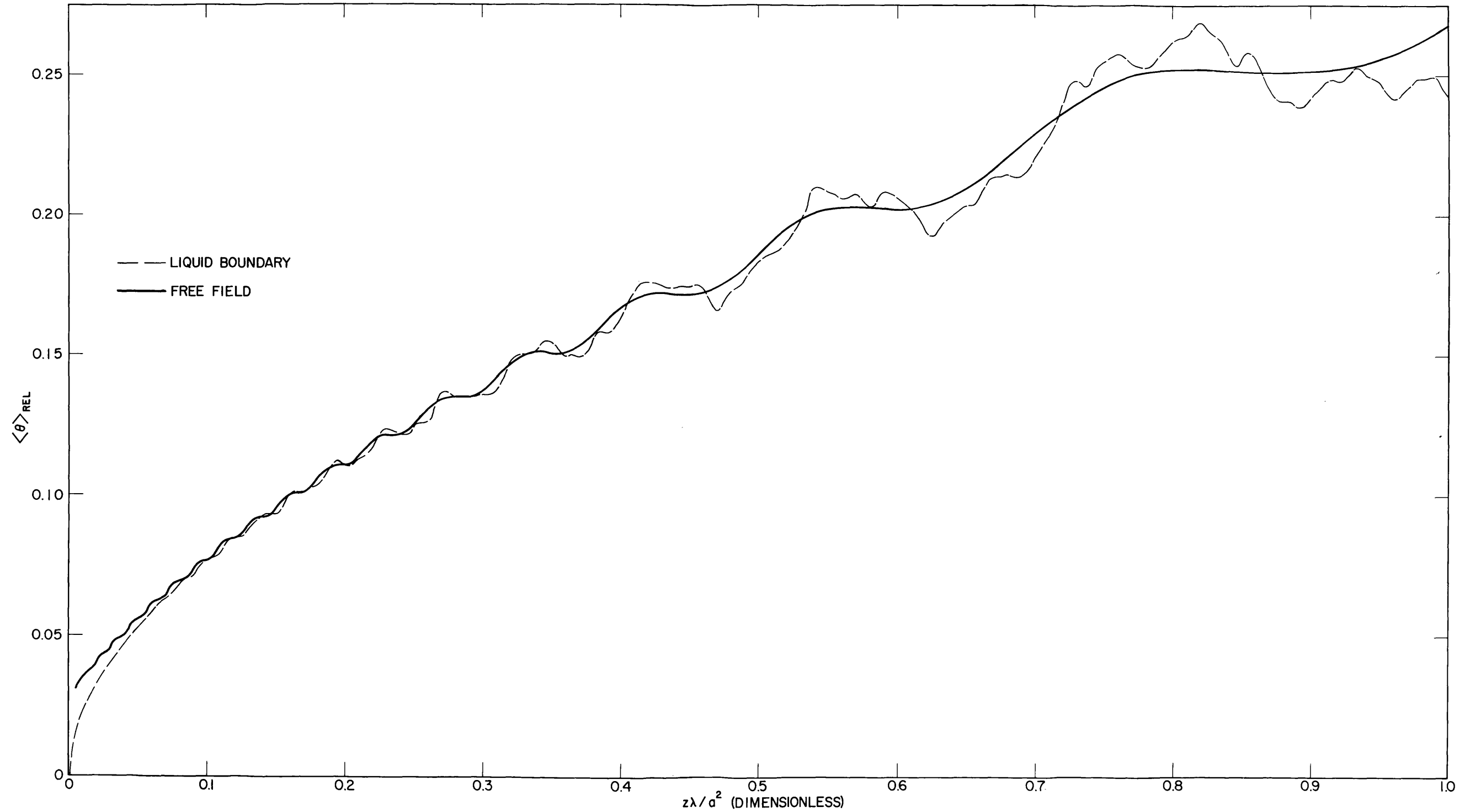
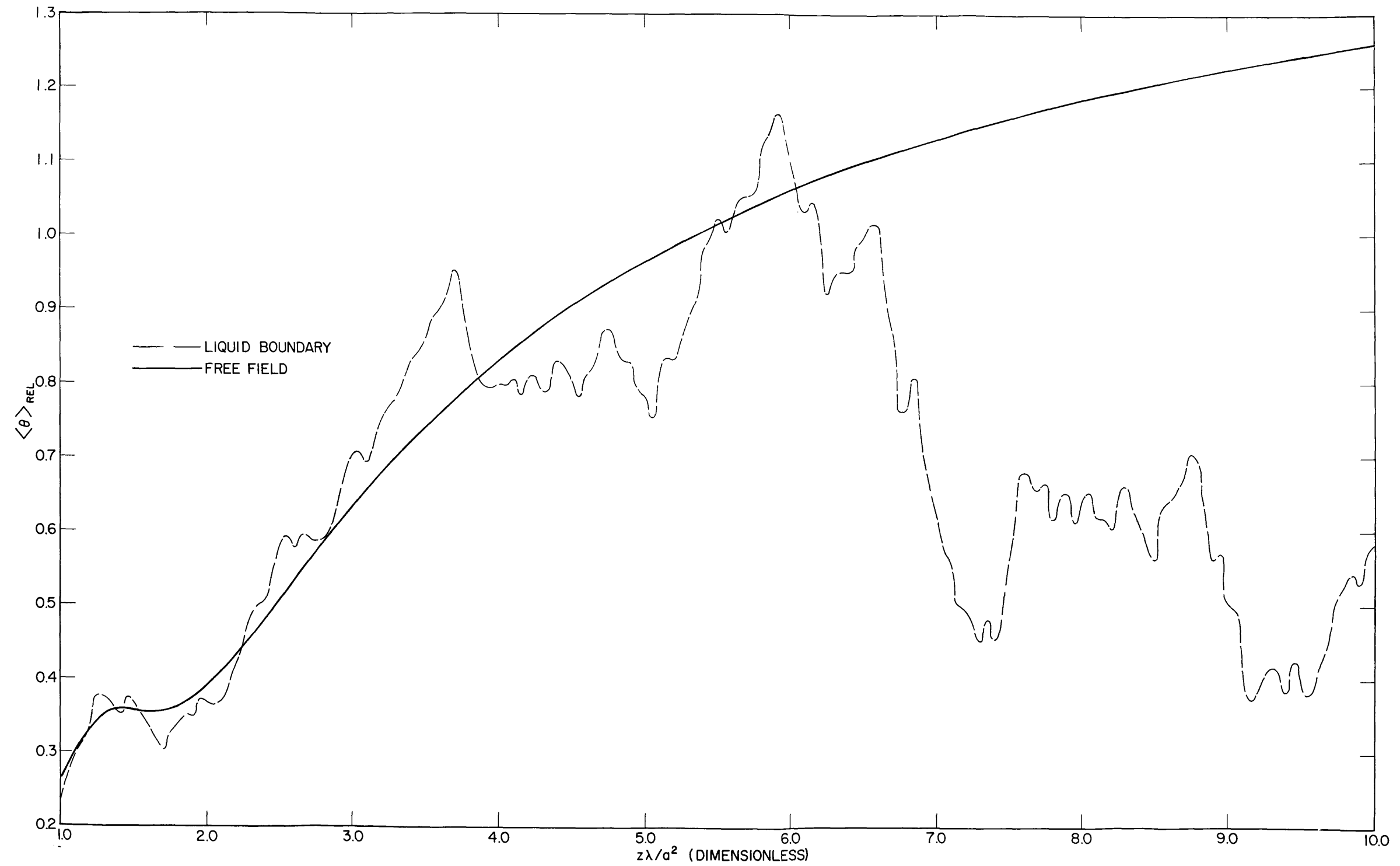


Fig. 8a - Average relative phase difference $\langle \theta \rangle_{rel}$ from plane-wave phase vs $z\lambda/a^2$ for a cylindrical liquid cavity with liquid boundaries. Comparison is between free-field values and liquid boundary values for the standard parameters shown in Table 1 and $0 \leq z\lambda/a^2 \leq 1$.

Fig. 8b - Same as Fig. 8a except $1 \leq z\lambda/a^2 \leq 10$

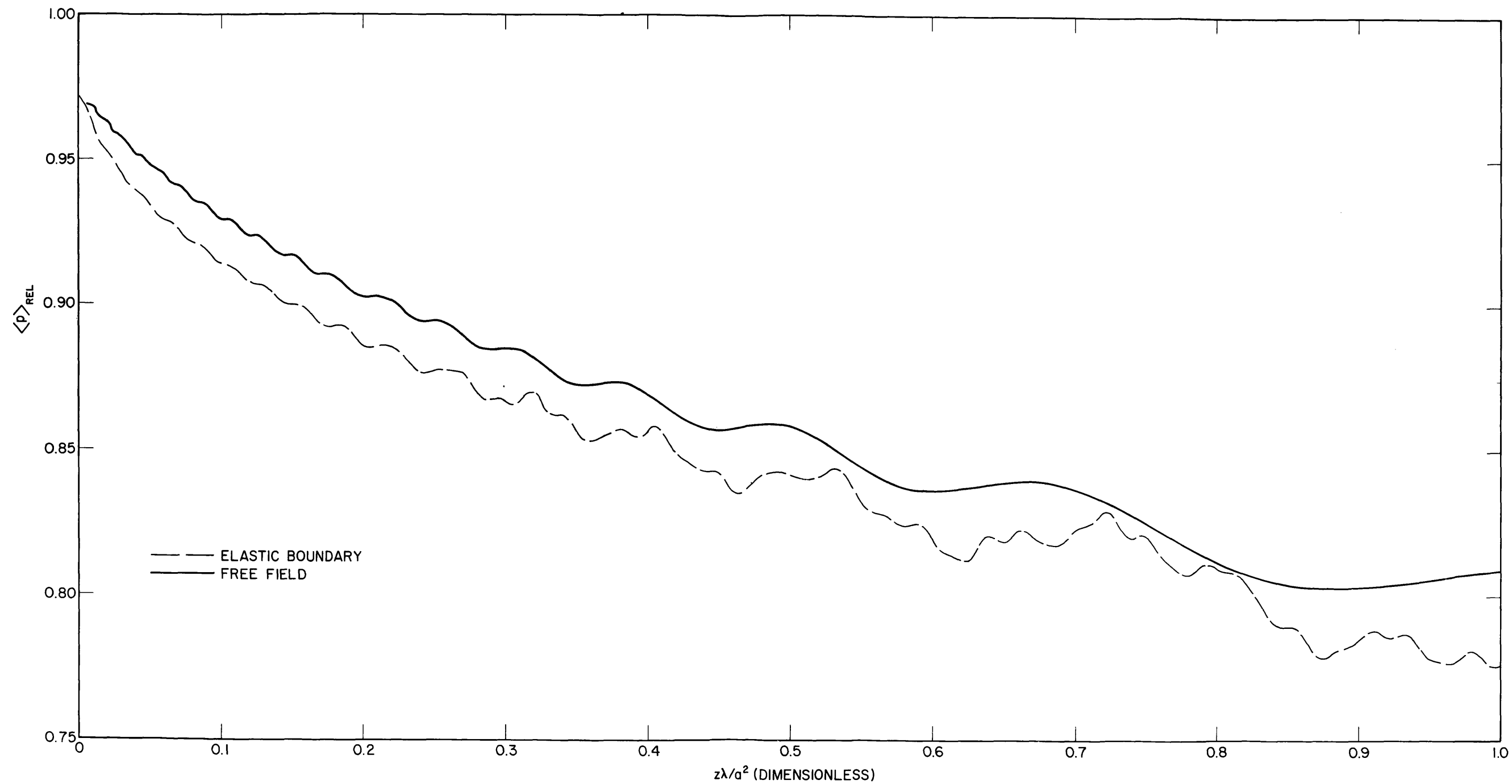
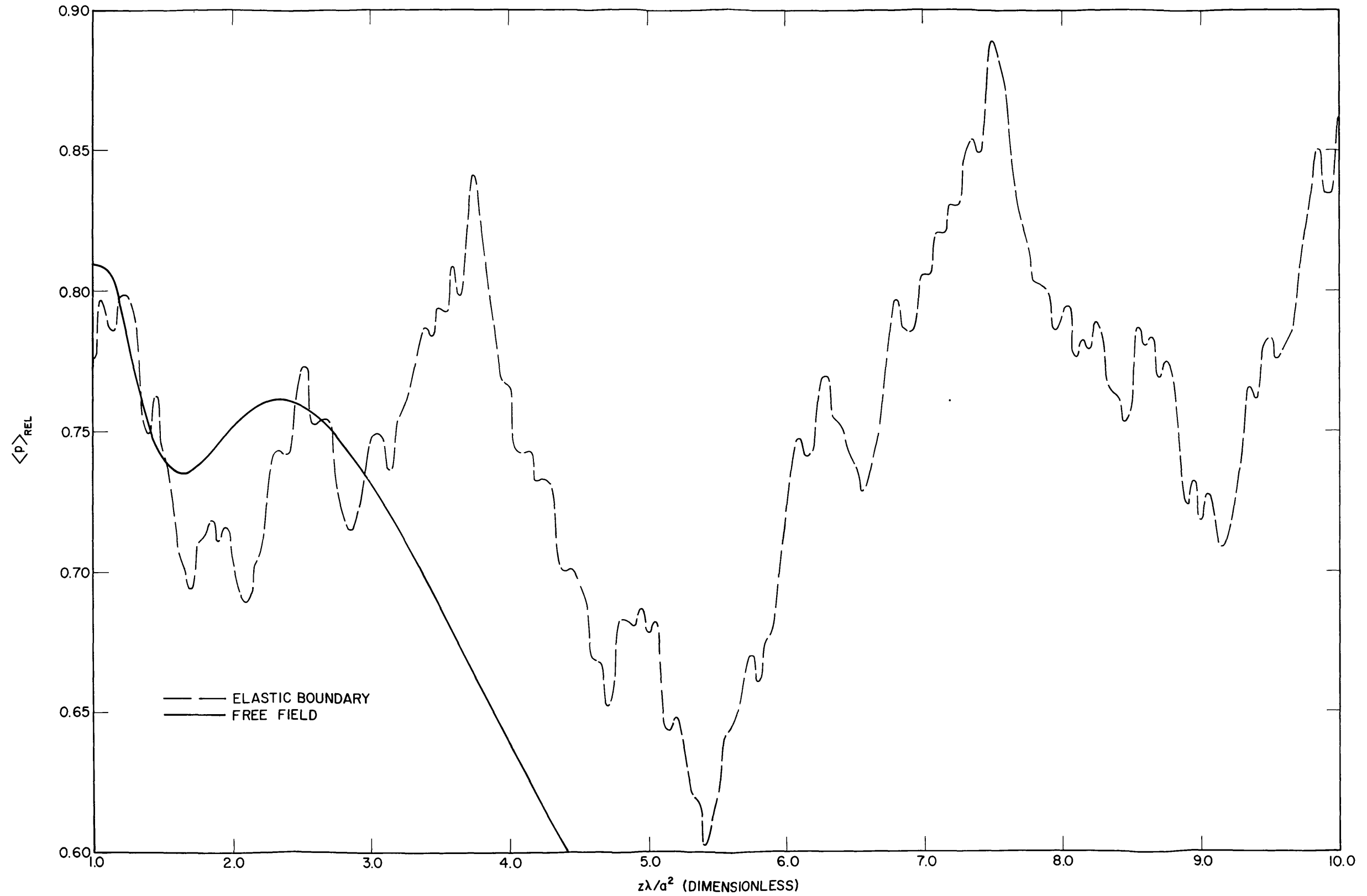


Fig. 9a - Average relative sound pressure $\langle p \rangle_{rel}$ vs $z\lambda/a^2$ for a cylindrical liquid cavity with elastic boundaries. Comparison is between free-field values and elastic boundary values for the standard parameters shown in Table 1 and $0 \leq z\lambda/a^2 \leq 1$.

Fig. 9b - Same as Fig. 9a except $1 \leq z\lambda/a^2 \leq 10$

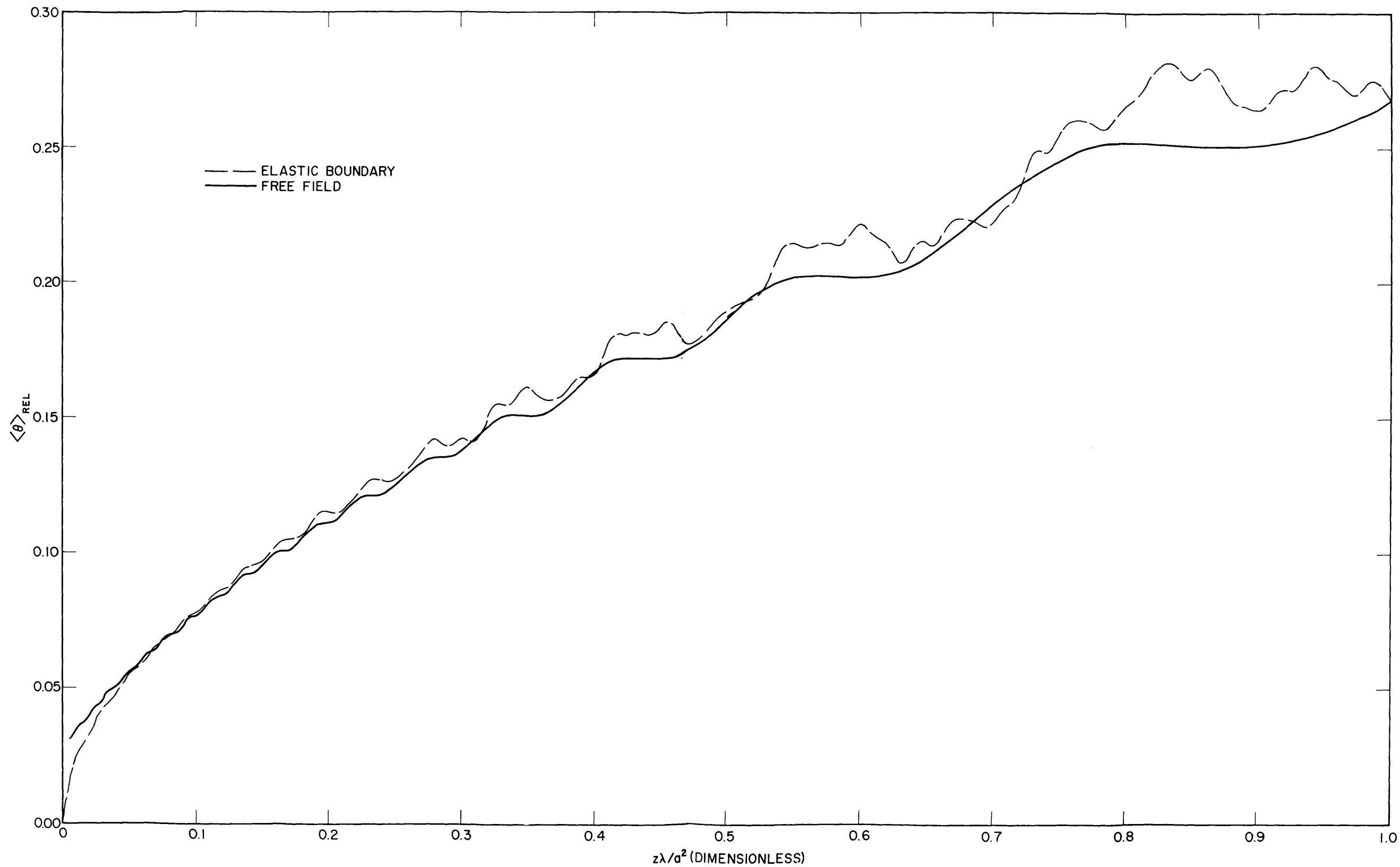
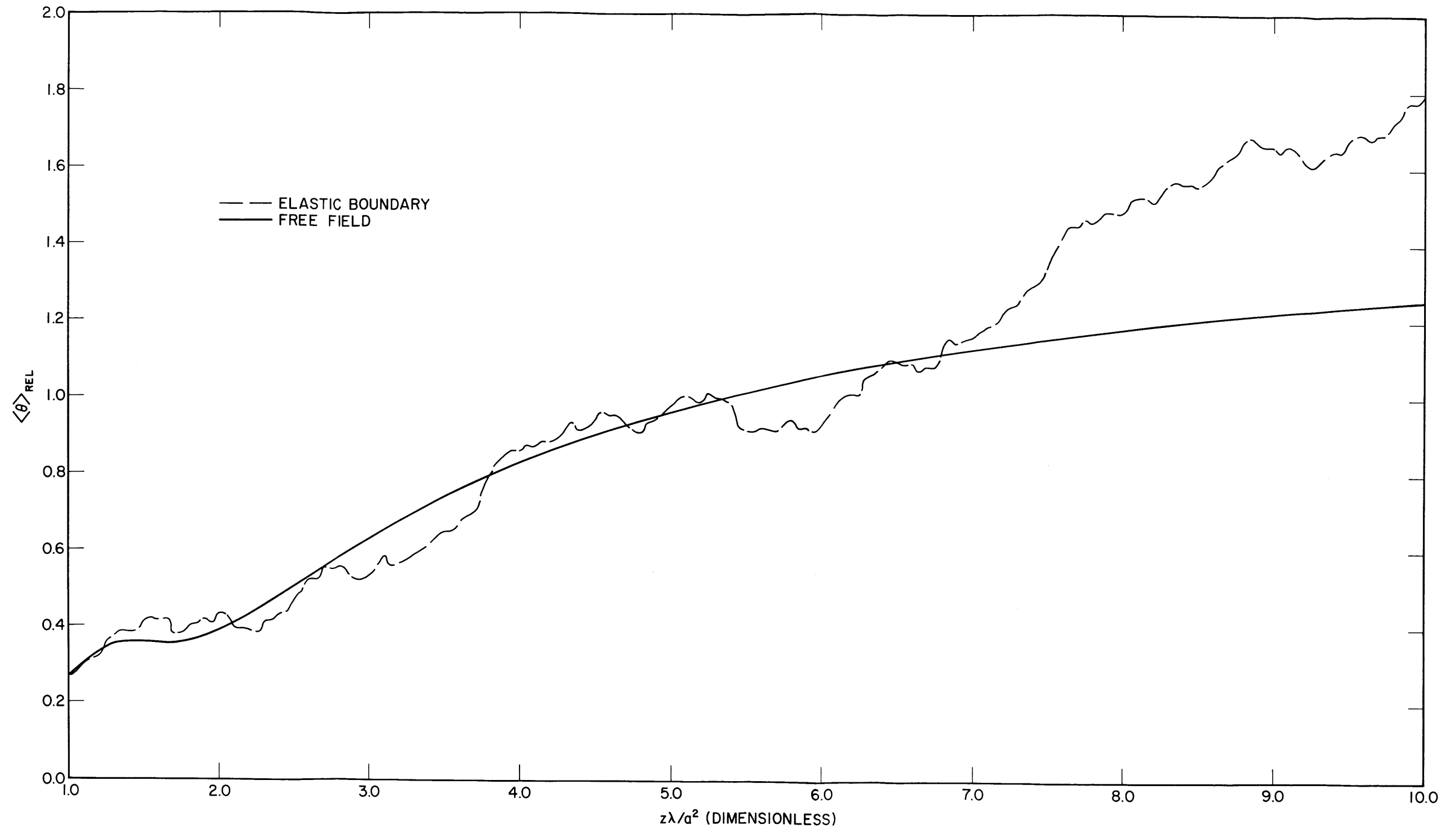


Fig. 10a - Average relative phase difference $\langle \theta \rangle_{REL}$ from plane-wave phase vs $z\lambda/a^2$ for a cylindrical liquid cavity with elastic boundaries. Comparison is between free-field values and elastic boundary values for the standard parameters shown in Table 1 and $0 \leq z\lambda/a^2 \leq 1$.

Fig. 10b - Same as Fig. 10a except $1 \leq z\lambda/a^2 \leq 10$

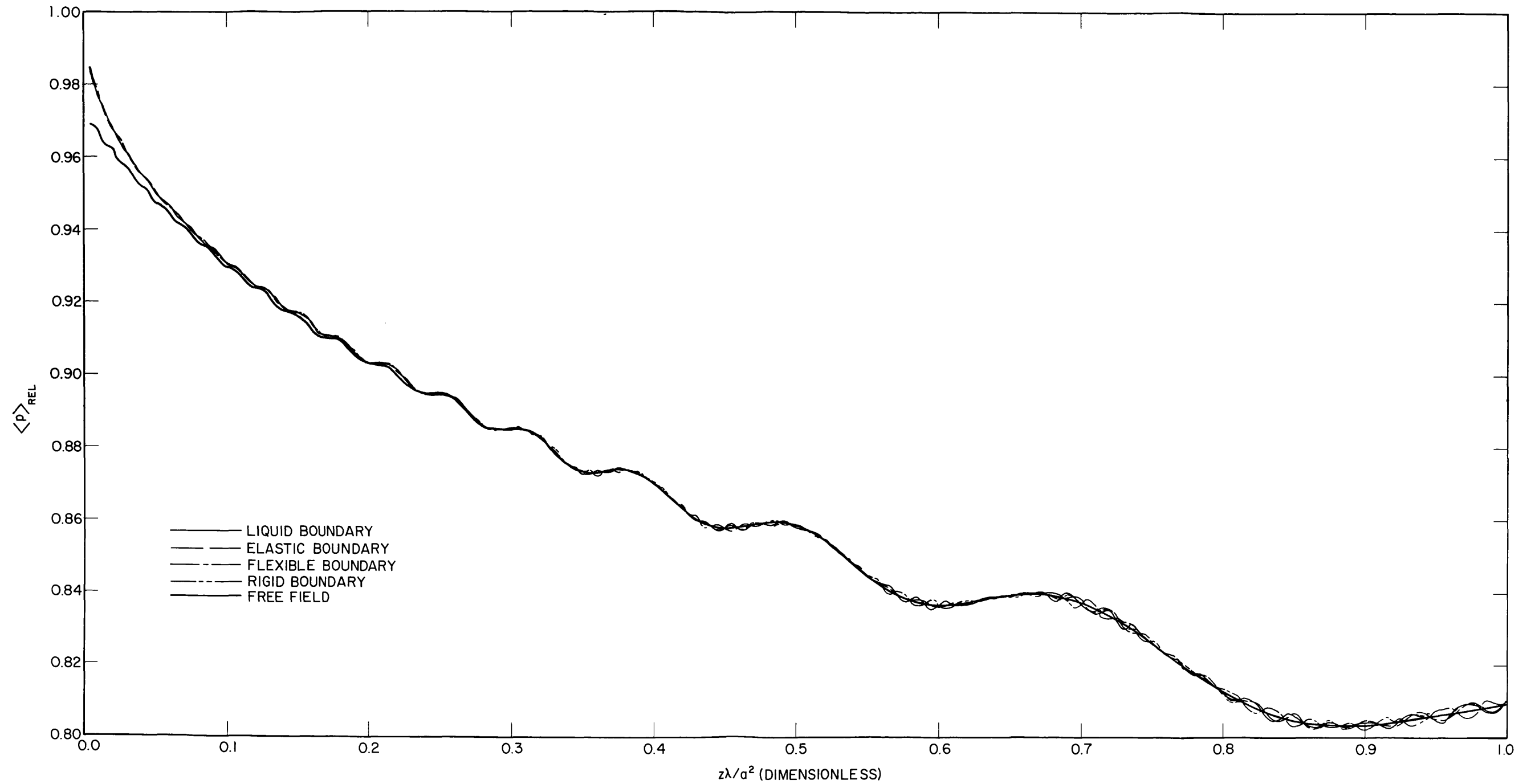
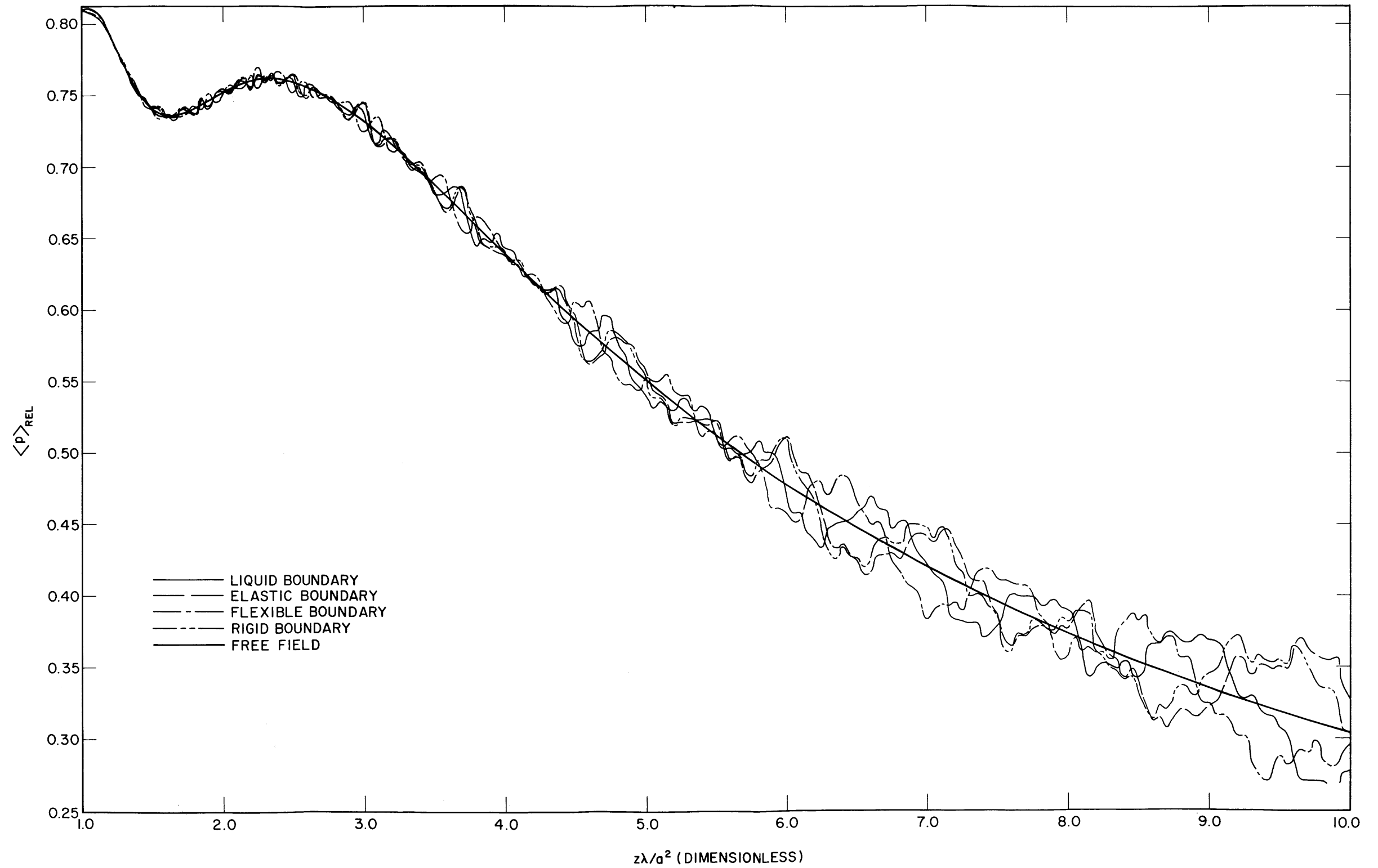


Fig. 11a - Average relative sound pressure $\langle p \rangle_{rel}$ vs $z\lambda/a^2$ for a cylindrical liquid cavity for four boundary conditions. Comparison is between free-field values and rigid, infinitely flexible, liquid, and elastic boundary values for the standard parameters shown in Table 1 (except that $b/a = 5$) and $0 \leq z\lambda/a^2 \leq 1$.

Fig. 11b - Same as Fig. 11a except $1 \leq z\lambda/a^2 \leq 10$

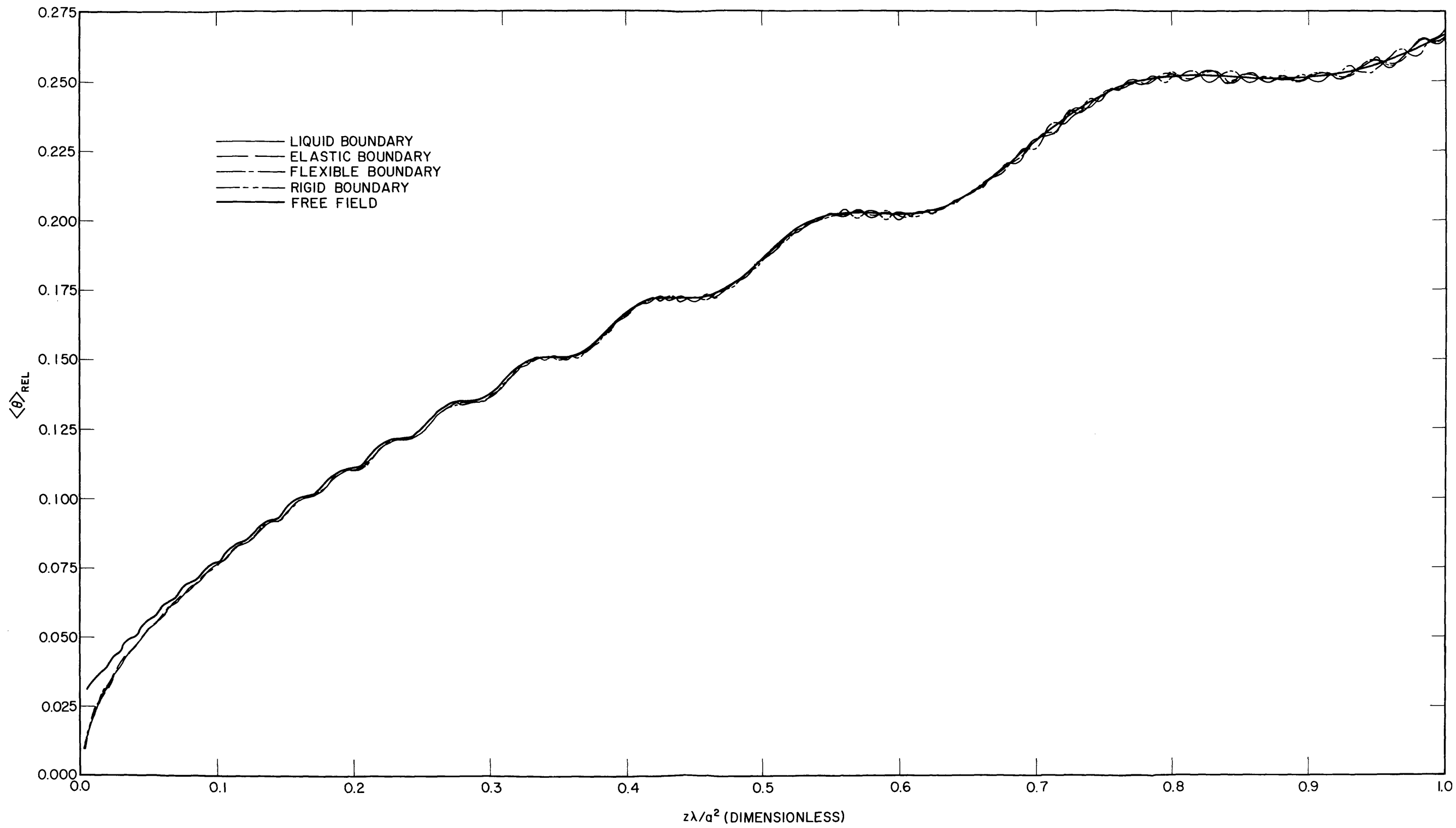
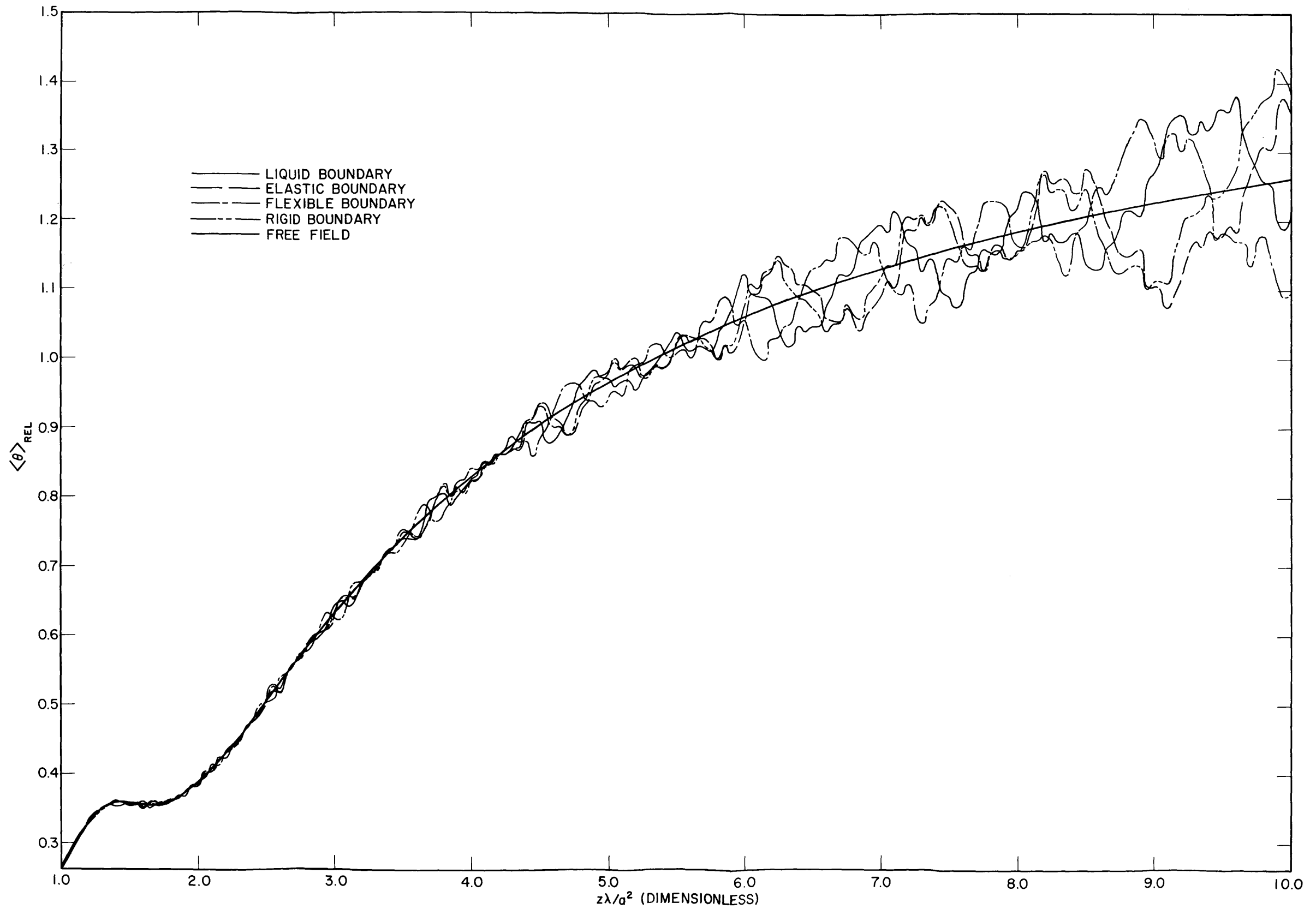


Fig. 12a - Average relative phase difference $\langle \theta \rangle_{REL}$ from plane-wave phase vs $z\lambda/a^2$ for a cylindrical liquid cavity for four boundary conditions. Comparison is between free-field values and rigid, infinitely flexible, liquid, and elastic boundary values for the standard parameters shown in Table 1 (except that $b/a = 5$) and $0 \leq z\lambda/a^2 \leq 1$.

Figure 12

Fig. 12b - Same as Fig. 12a except $1 \leq z\lambda/a^2 \leq 10$

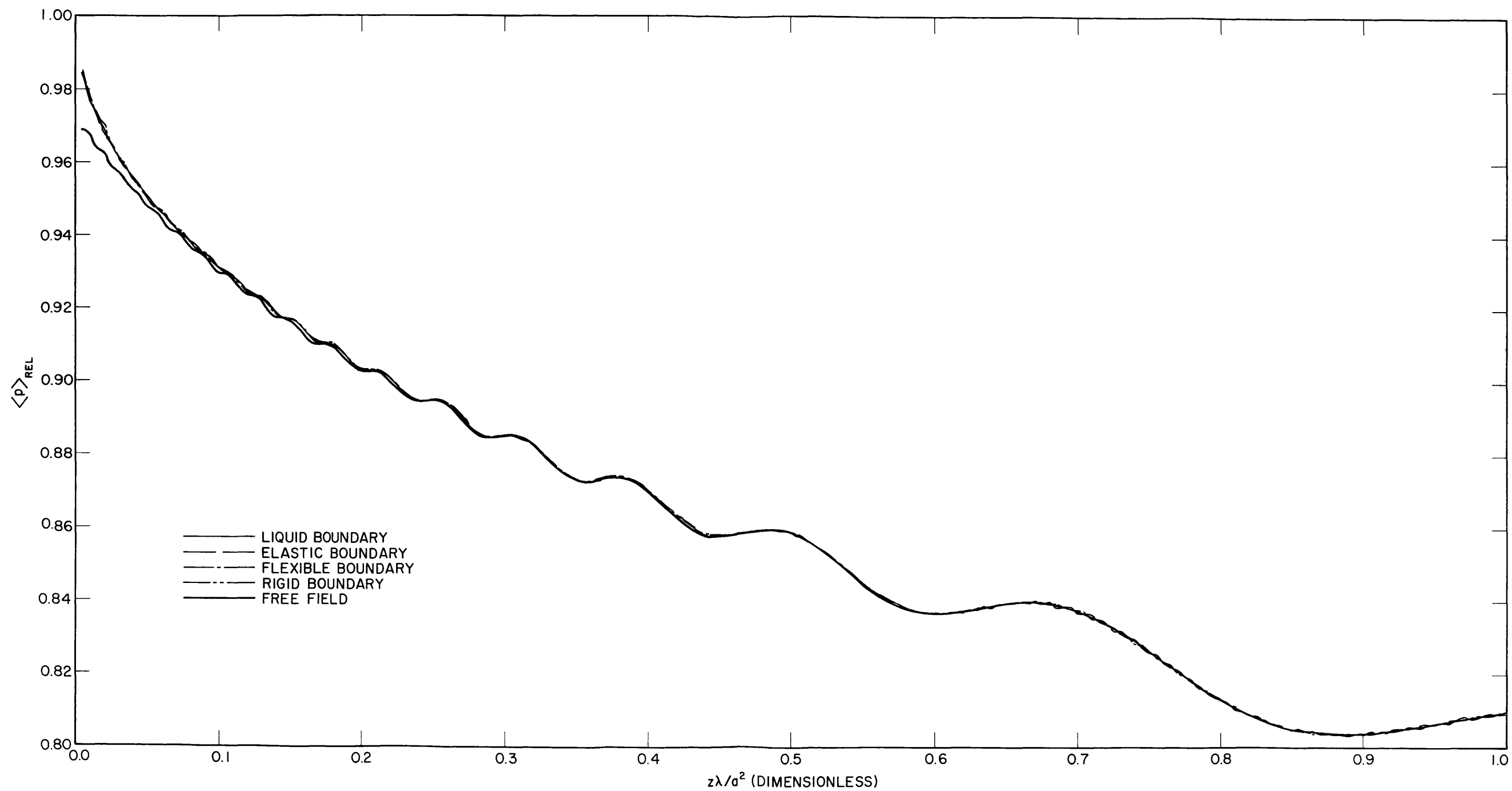


Fig. 13a — Average relative sound pressure $\langle p \rangle_{rel}$ vs $z\lambda/a^2$ for a cylindrical liquid cavity for four boundary conditions. Comparison is between free-field values and rigid, infinitely flexible, liquid, and elastic boundary values for the standard parameters shown in Table 1 (except that $b/a = 10$) and $0 \leq z\lambda/a^2 \leq 1$.

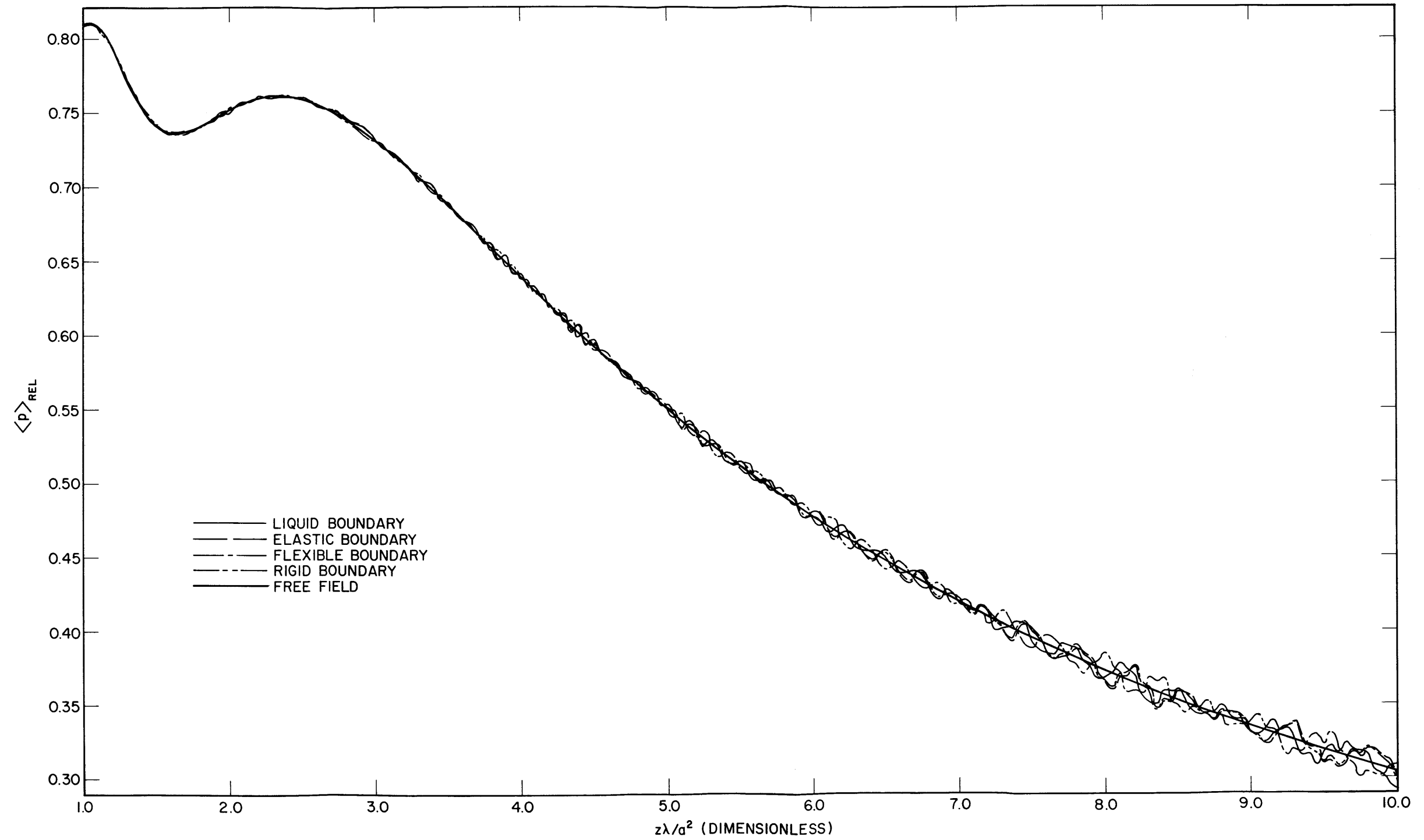


Fig. 13b - Same as Fig. 13a except $1 \leq z\lambda/a^2 \leq 10$

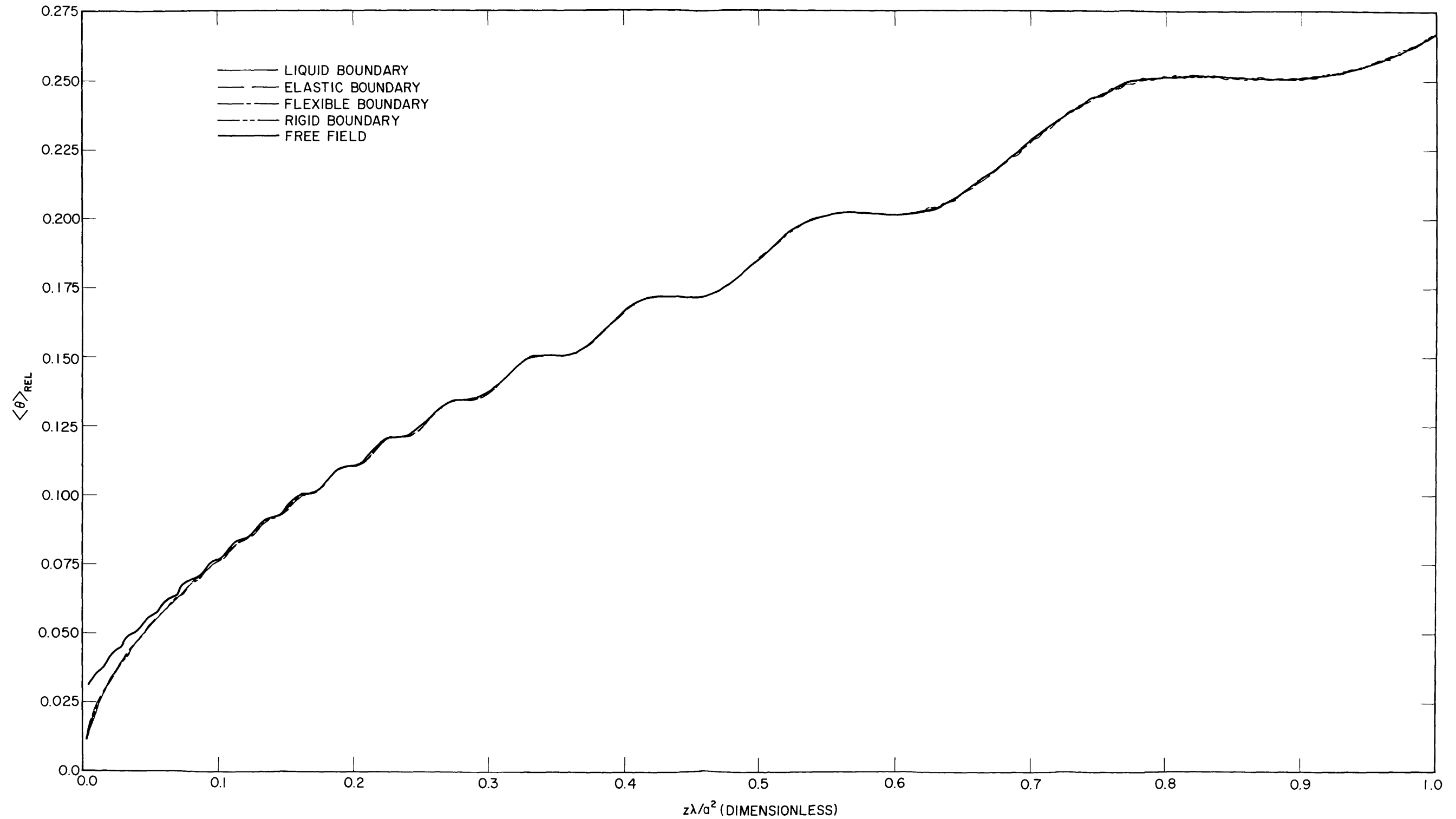
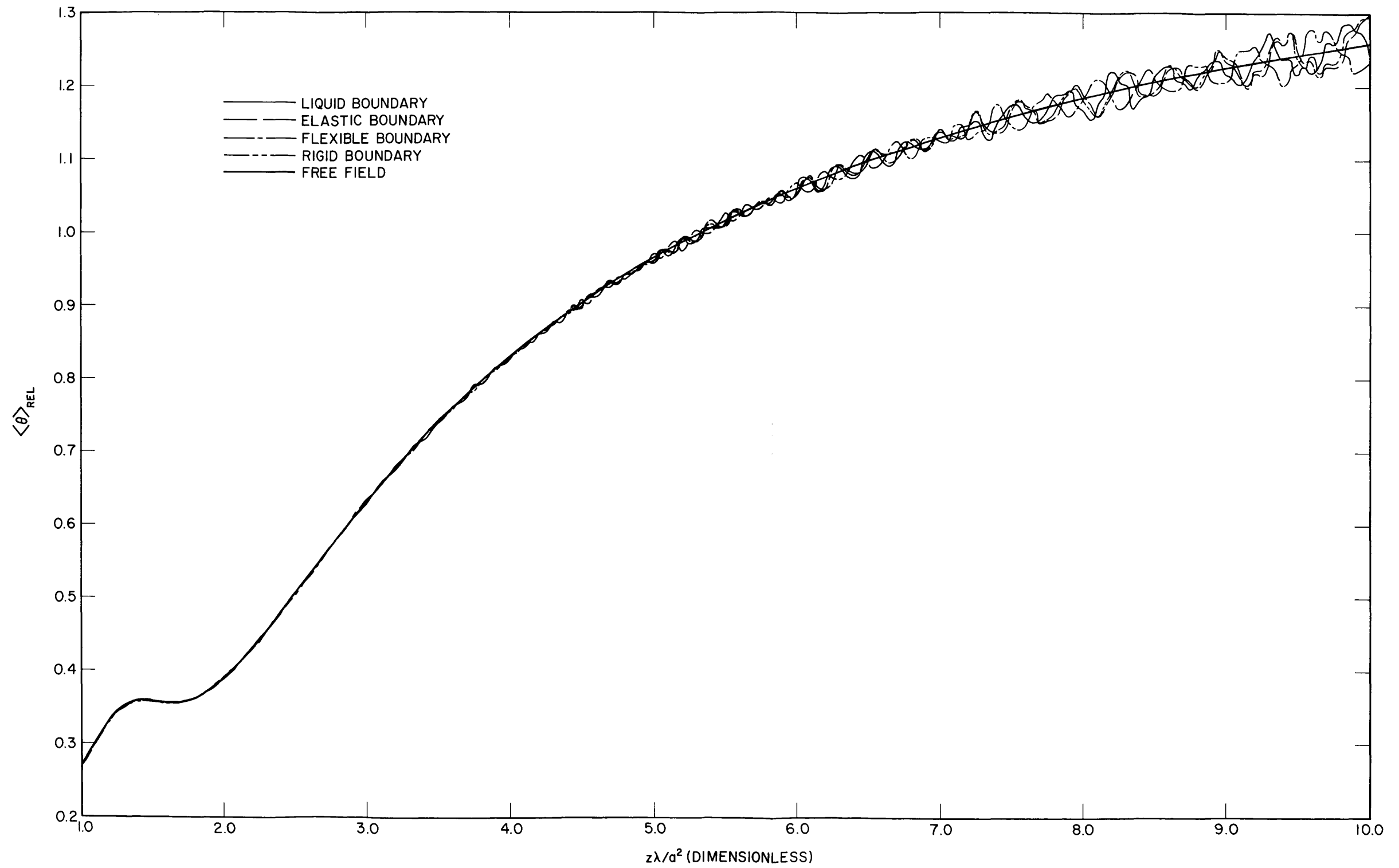


Fig. 14a - Average relative phase difference $\langle \theta \rangle_{REL}$ from plane-wave phase vs $z\lambda/a^2$ for a cylindrical liquid cavity for four boundary conditions. Comparison is between free-field values and rigid, infinitely flexible, liquid, and elastic boundary values for the standard parameters shown in Table 1 (except that $b/a = 10$) and $0 \leq z\lambda/a^2 \leq 1$.

Fig. 14b - Same as Fig. 14a except $1 \leq z\lambda/a^2 \leq 10$

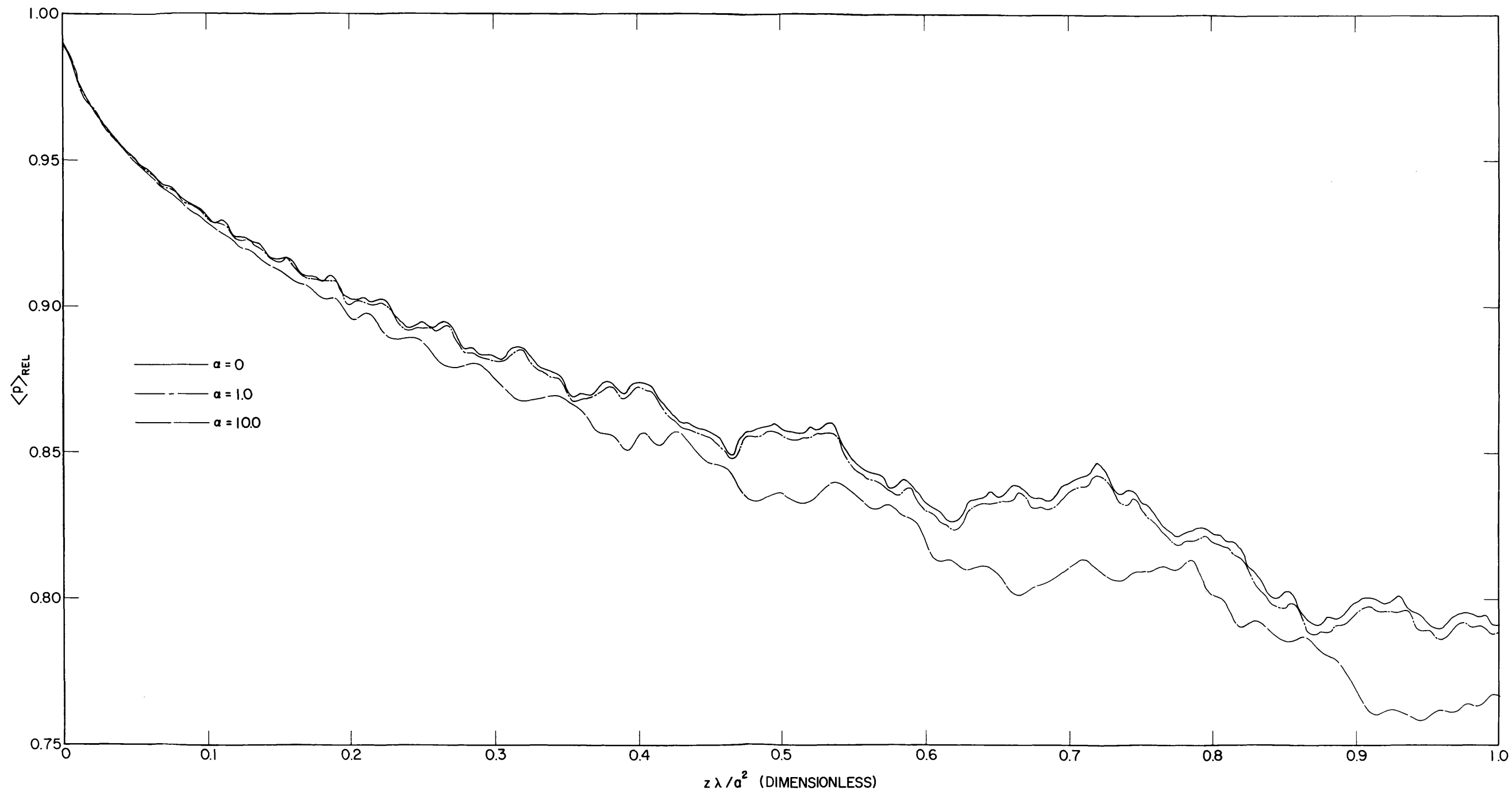
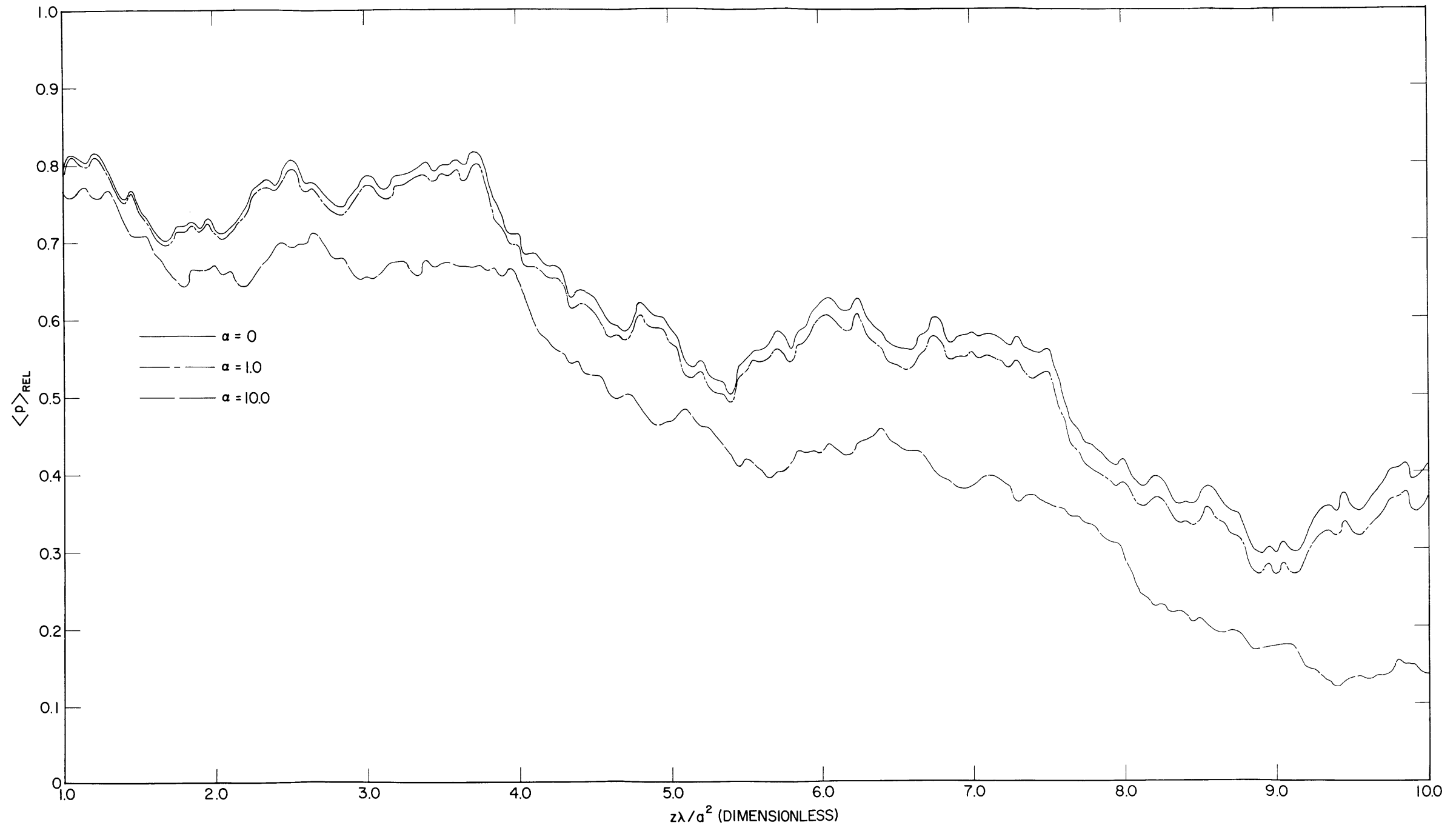


Fig. 15a - Average relative sound pressure $\langle p \rangle_{rel}$ vs $z\lambda/a^2$ for a cylindrical liquid cavity with rigid boundaries. The effect of changing the absorption parameter α on the values of $\langle p \rangle_{rel}$ is shown for the rigid boundary condition. The standard parameters of Table 1 were used (except that α is not restricted to 0) and $0 \leq z\lambda/a^2 \leq 1$.

Fig. 15b - Same as Fig. 15a except $1 \leq z\lambda/a^2 \leq 10$

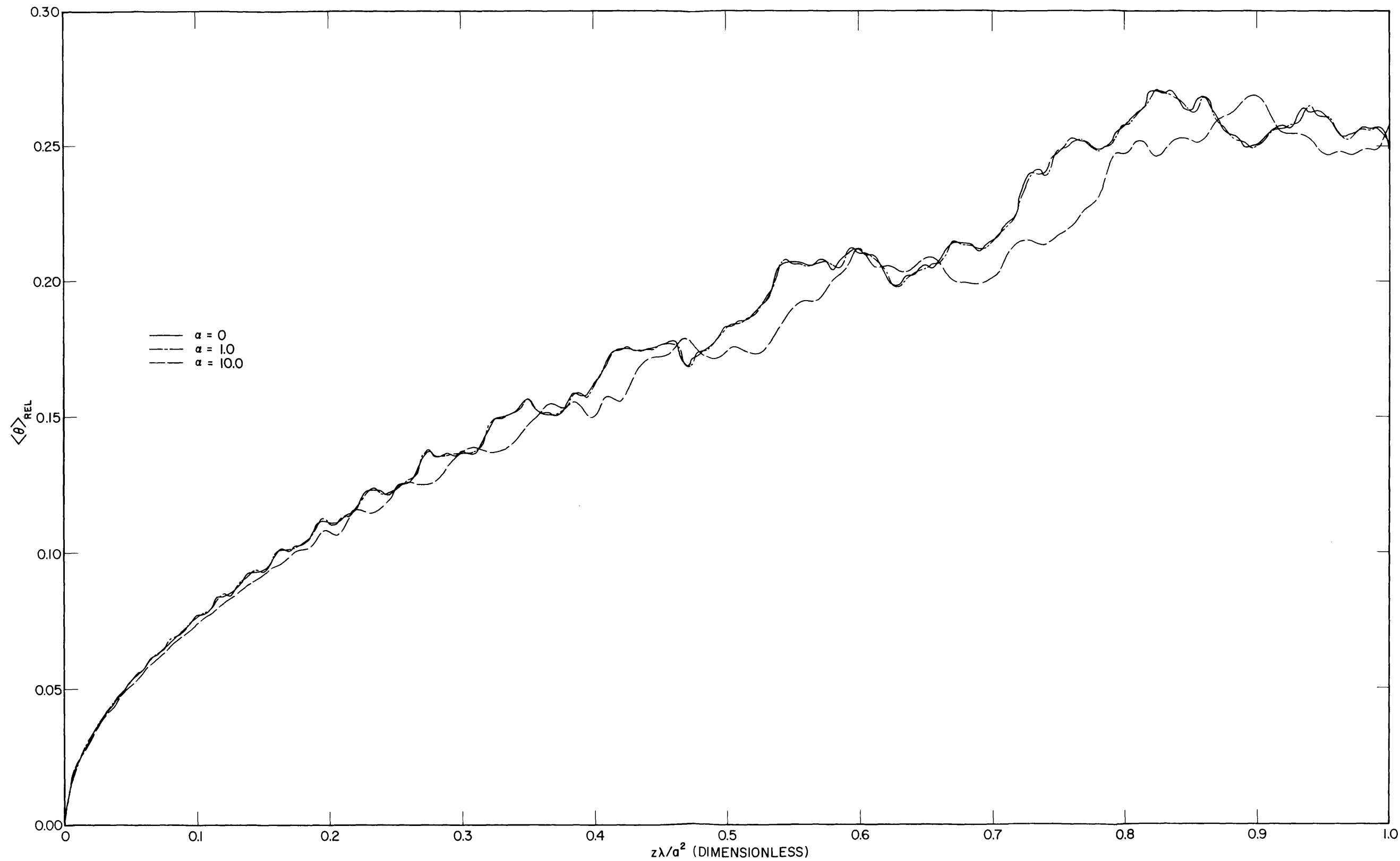
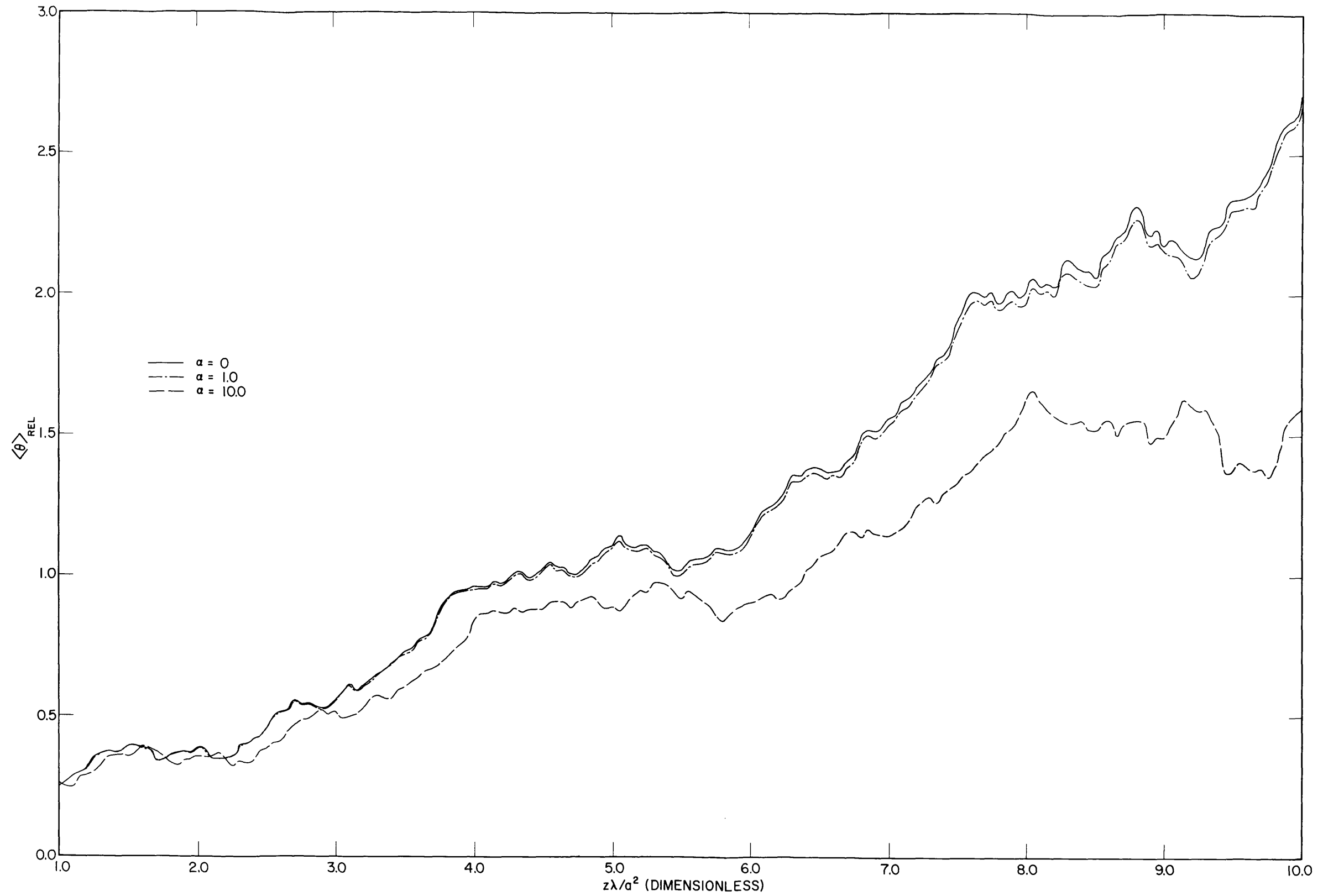


Fig. 16a — Average relative phase difference $\langle \theta \rangle_{REL}$ from plane-wave phase vs $z\lambda/a^2$ for a cylindrical liquid cavity with rigid boundaries. The effect of changing the absorption parameter α on the values of $\langle \theta \rangle_{REL}$ is shown for the rigid boundary condition. The standard parameters of Table 1 were used (except that α is not restricted to 0) and $0 \leq z\lambda/a^2 \leq 1$.

Fig. 16b - Same as Fig. 16a except $1 \leq z\lambda/a^2 \leq 10$

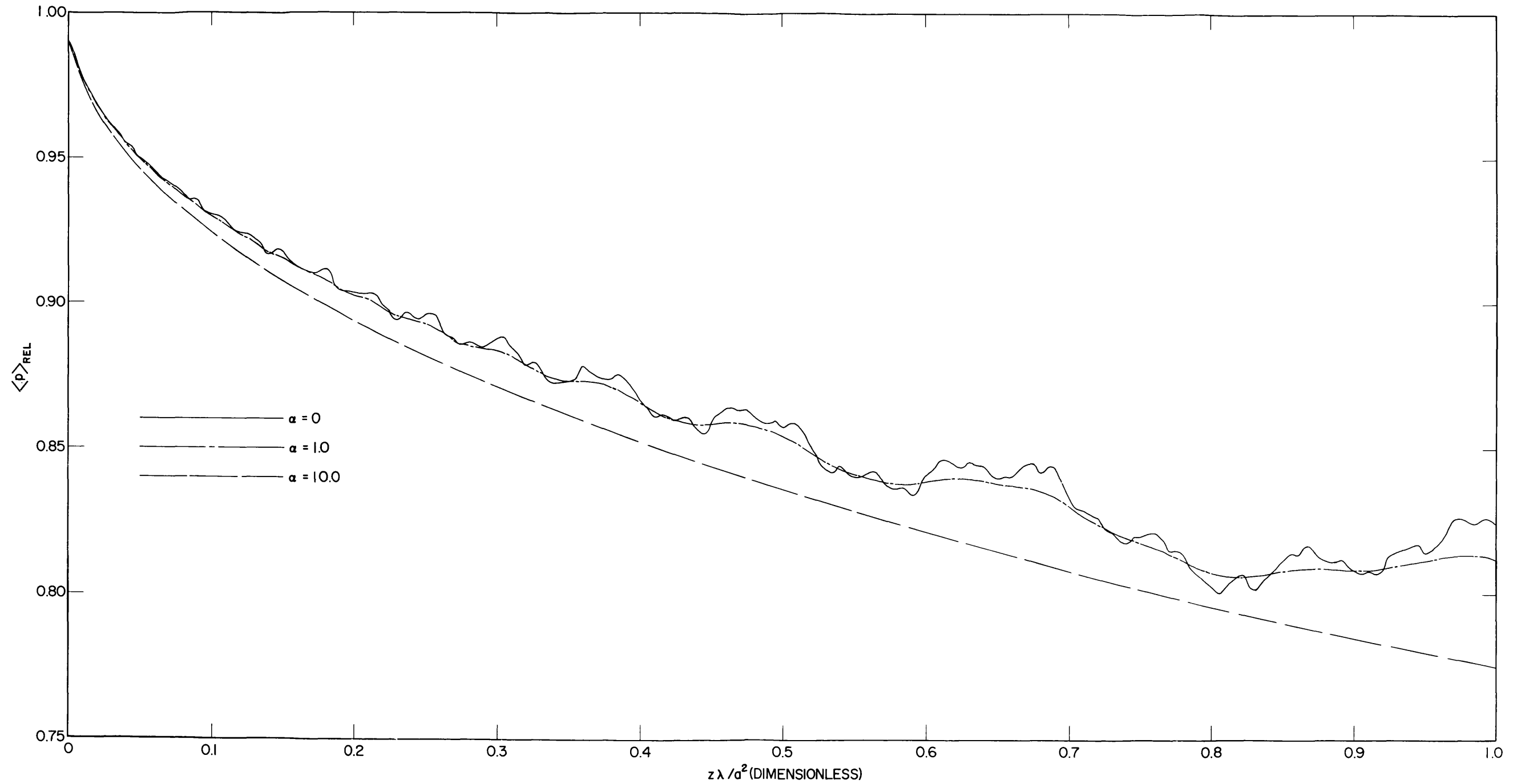
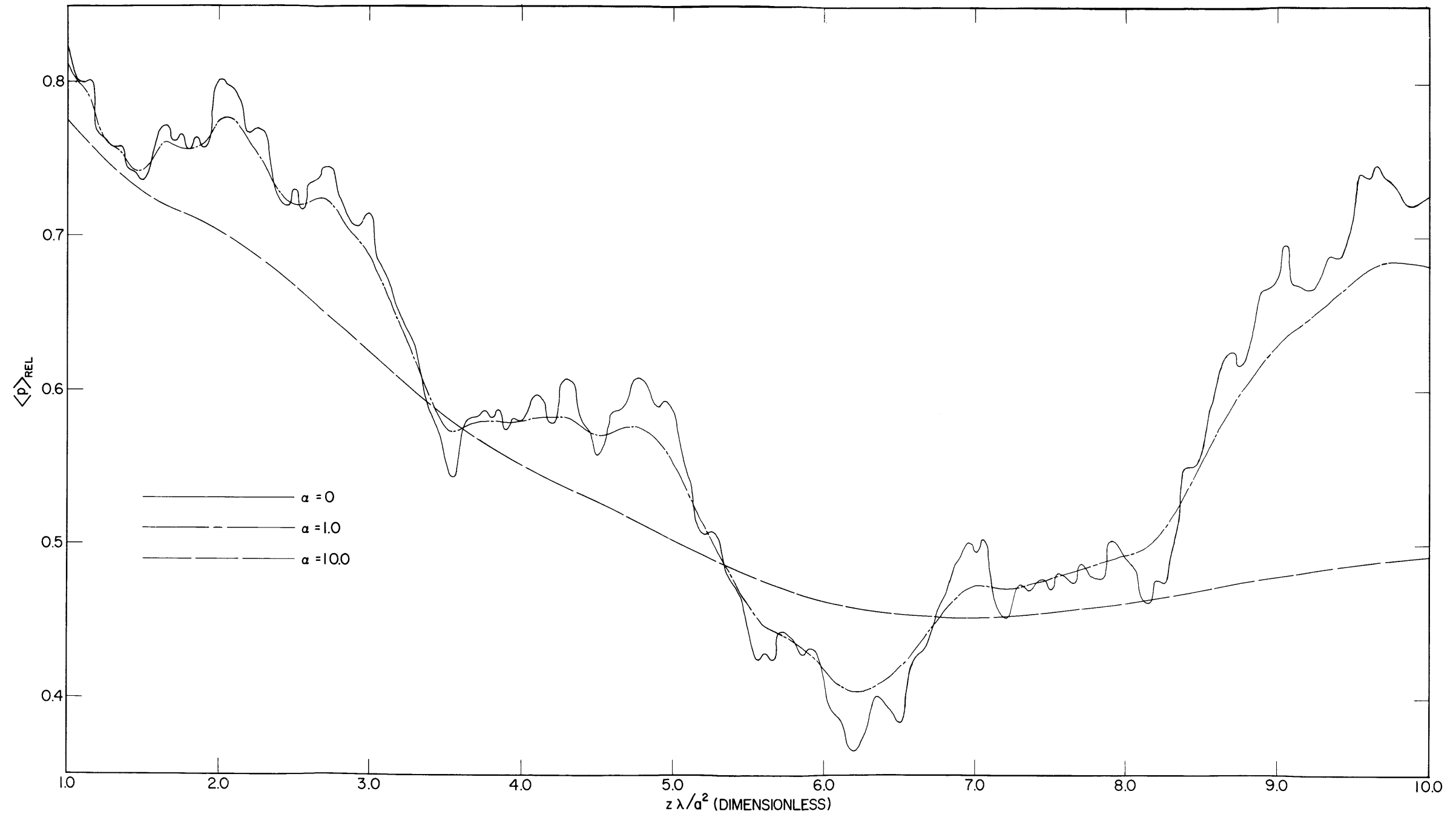


Fig. 17a - Average relative sound pressure $\langle p \rangle_{rel}$ vs $z\lambda/a^2$ for a cylindrical liquid cavity with infinitely flexible boundaries. The effect of changing the absorption parameter α on the values of $\langle p \rangle_{rel}$ is shown for the infinitely flexible boundary condition. The standard parameters of Table I were used (except that α is not restricted to 0) and $0 \leq z\lambda/a^2 \leq 1$.

Fig. 17b - Same as Fig. 17a except $1 \leq z\lambda/a^2 \leq 10$

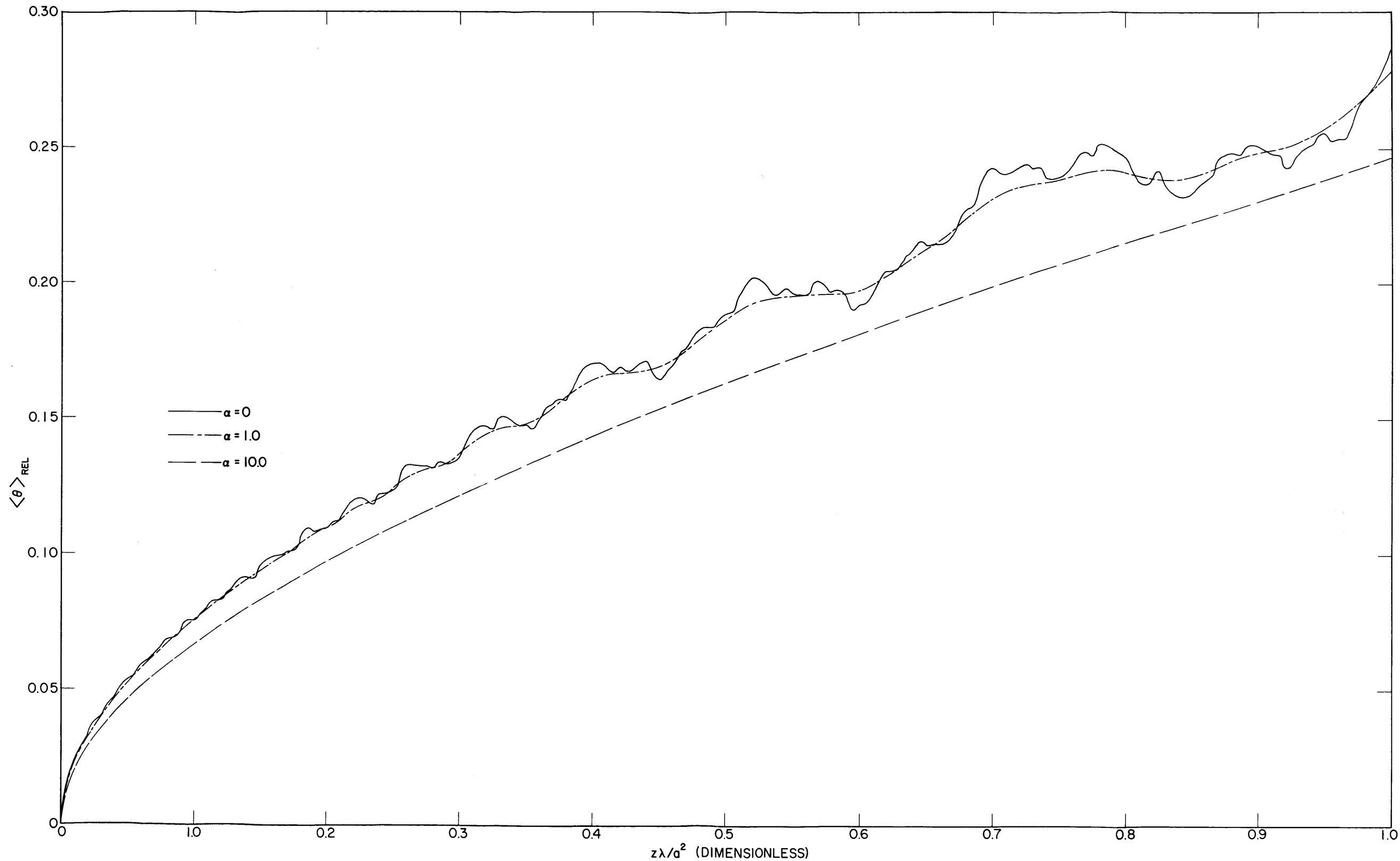
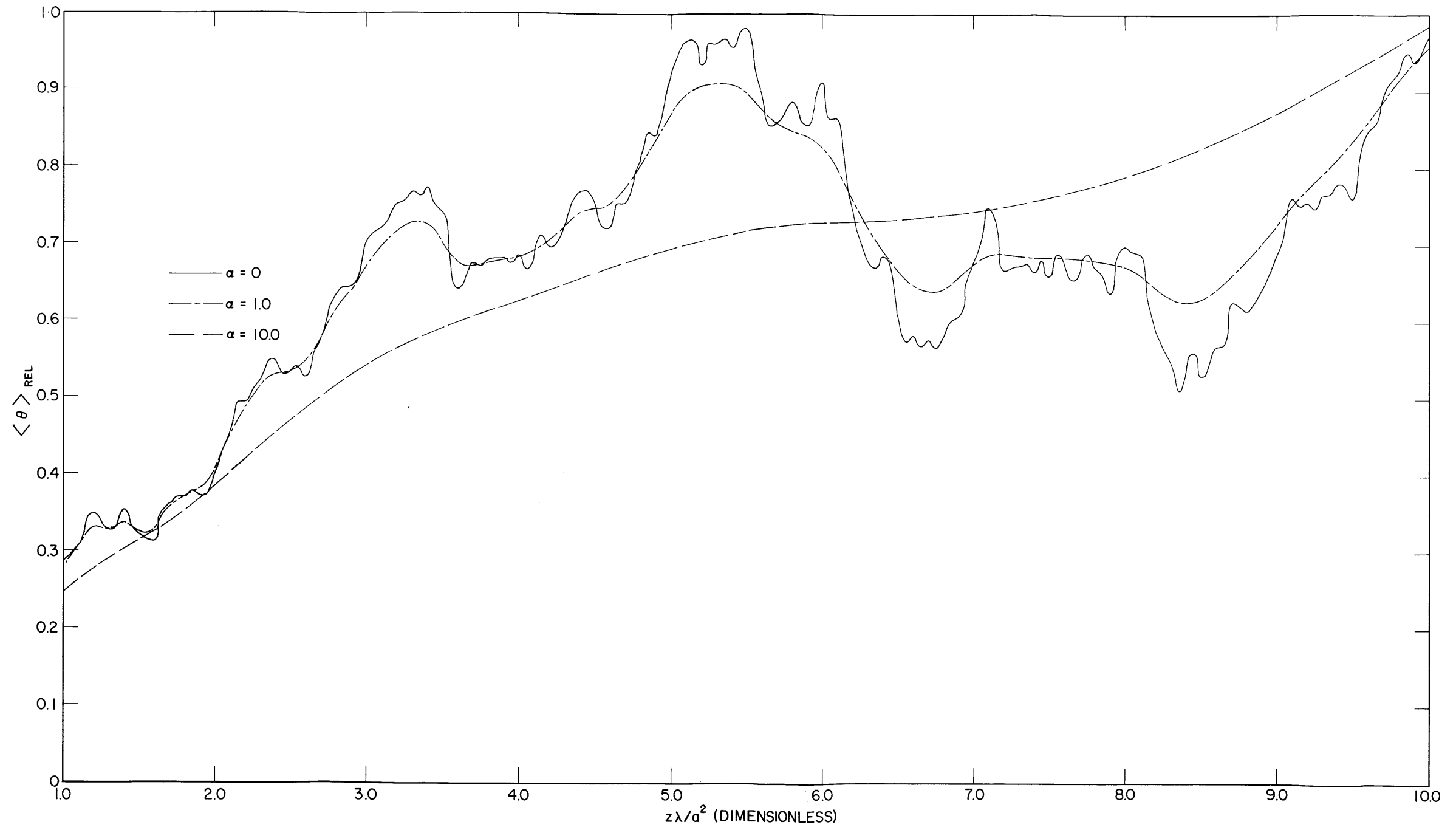


Fig. 18a - Average relative phase difference $\langle \theta \rangle_{REL}$ from plane-wave phase vs $z\lambda/a^2$ for a cylindrical liquid cavity with infinitely flexible boundaries. The effect of changing the absorption parameter α on the values of $\langle \theta \rangle_{REL}$ is shown for the infinitely flexible boundary condition. The standard parameters of Table 1 were used (except that α is not restricted to 0) and $0 \leq z\lambda/a^2 \leq 1$.

Fig. 18b - Same as Fig. 18a except $1 \leq z\lambda/d^2 \leq 10$

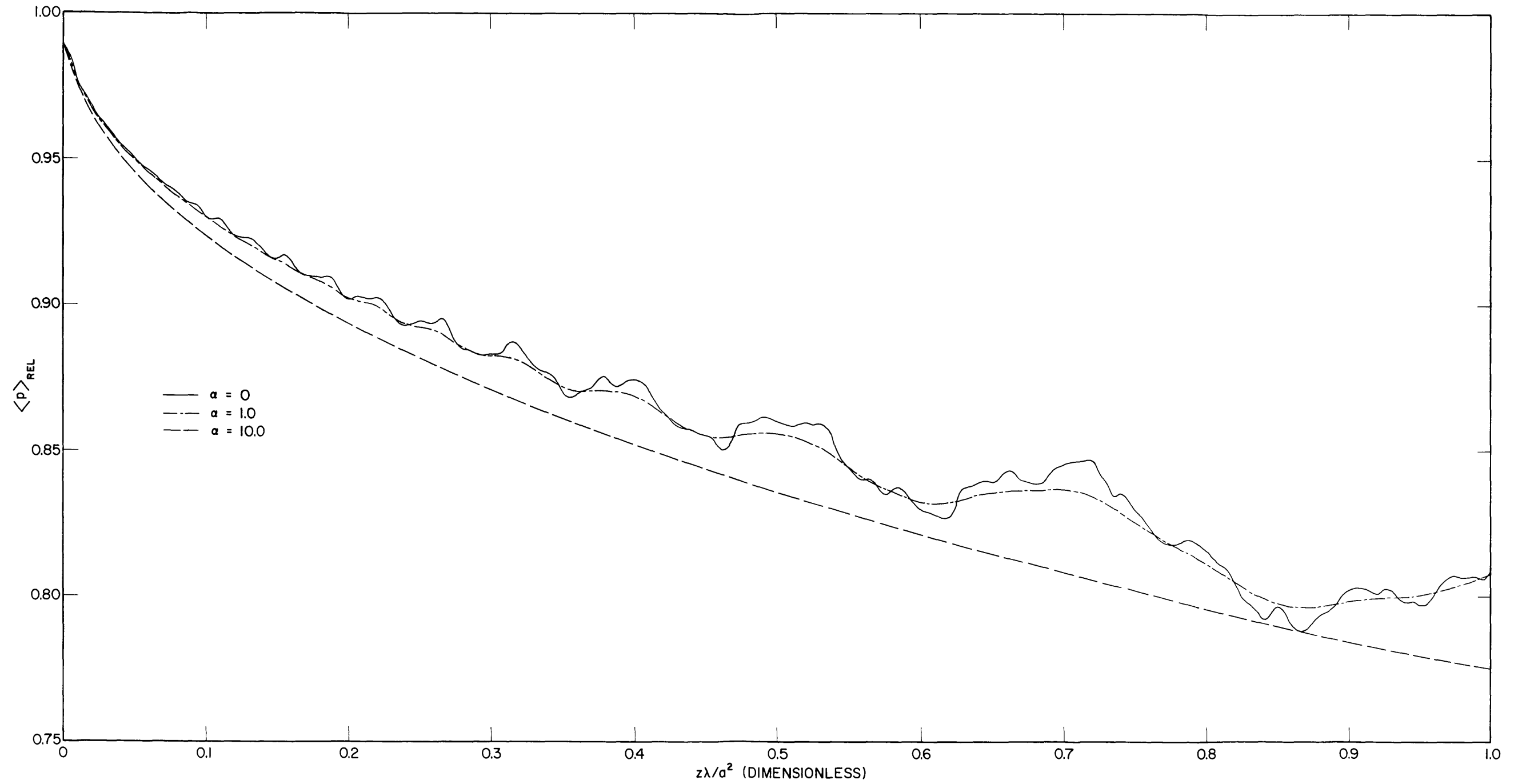


Fig. 19a - Average relative sound pressure $\langle p \rangle_{rel}$ vs $z\lambda/a^2$ for a cylindrical liquid cavity with liquid boundaries. The effect of changing the absorption parameter α on the values of $\langle p \rangle_{rel}$ is shown for the liquid boundary condition. The standard parameters of Table 1 were used (except that α is not restricted to 0) and $0 \leq z\lambda/a^2 \leq 1$.

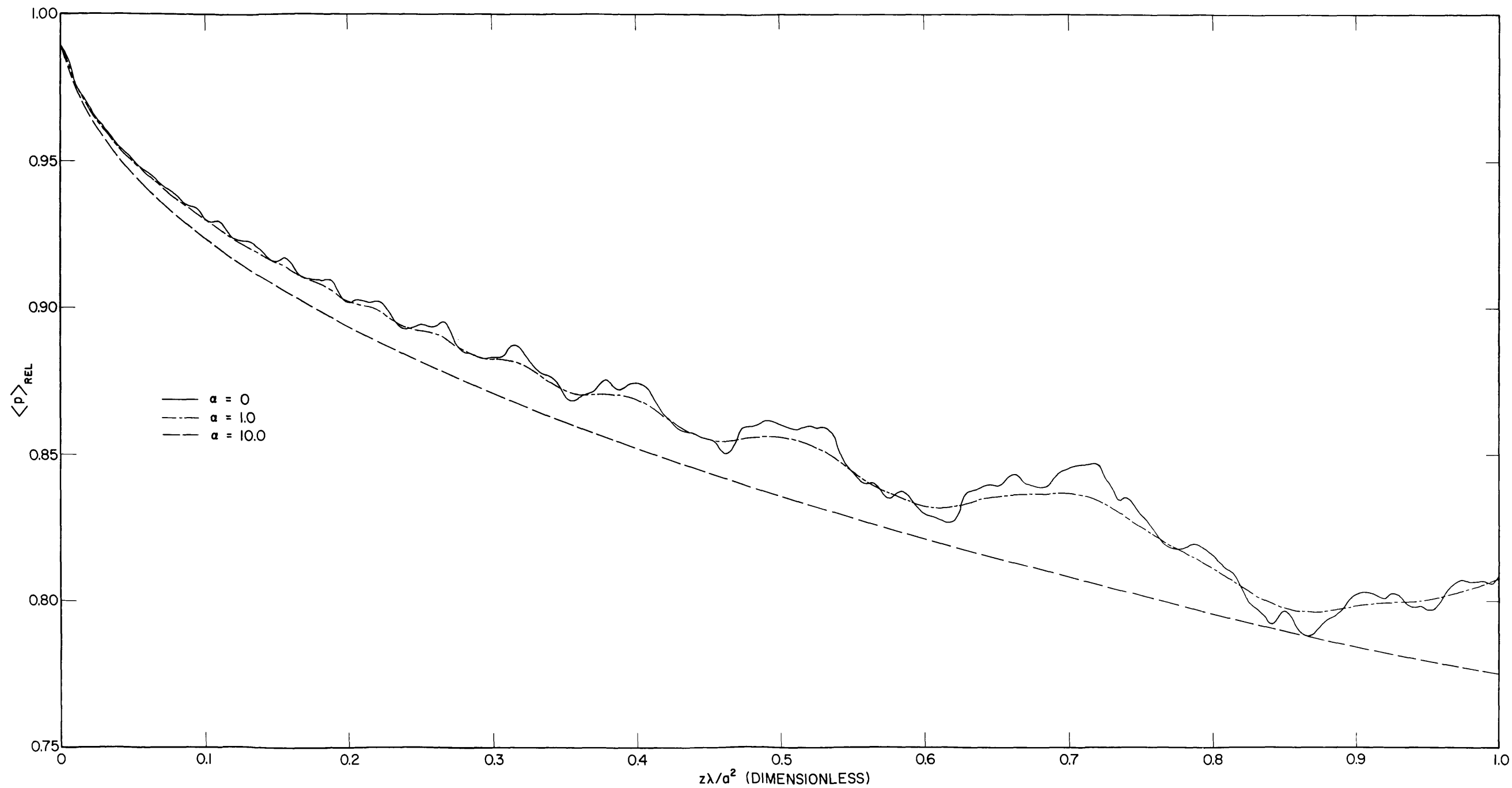
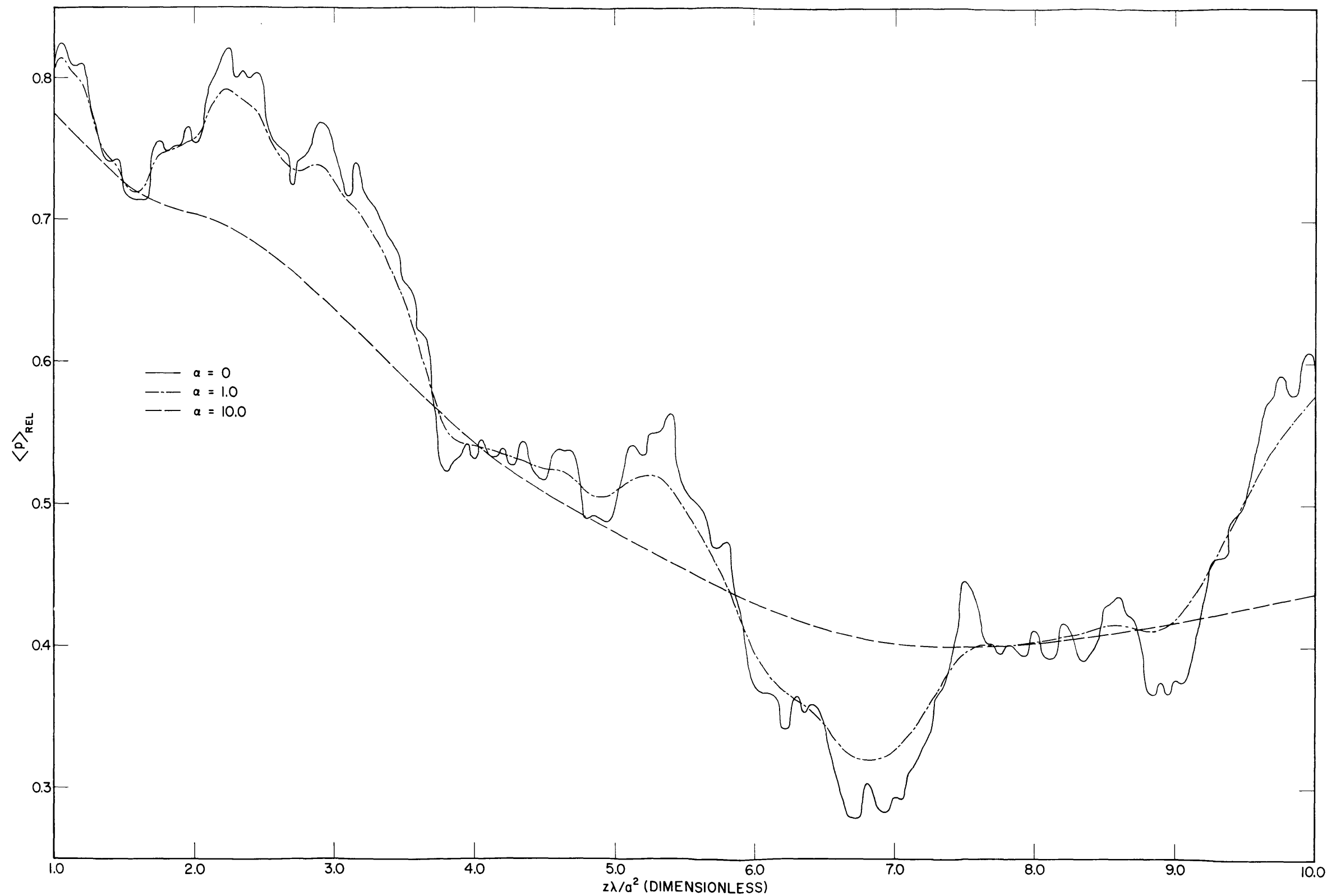


Fig. 19a - Average relative sound pressure $\langle p \rangle_{REL}$ vs $z\lambda/a^2$ for a cylindrical liquid cavity with liquid boundaries. The effect of changing the absorption parameter α on the values of $\langle p \rangle_{REL}$ is shown for the liquid boundary condition. The standard parameters of Table 1 were used (except that α is not restricted to 0) and $0 \leq z\lambda/a^2 \leq 1$.

Fig. 19b - Same as Fig. 19a except $1 \leq z\lambda/a^2 \leq 10$

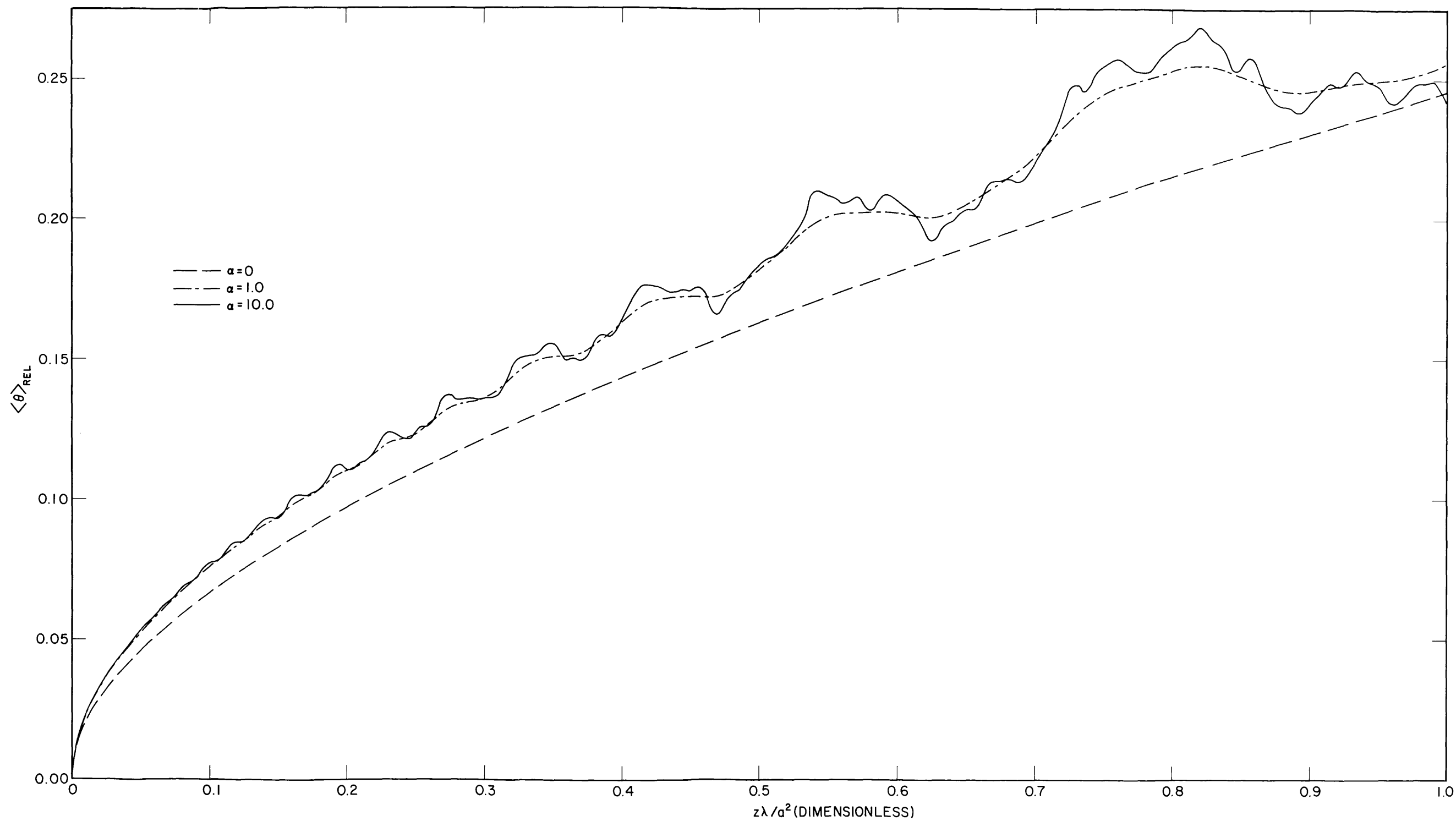
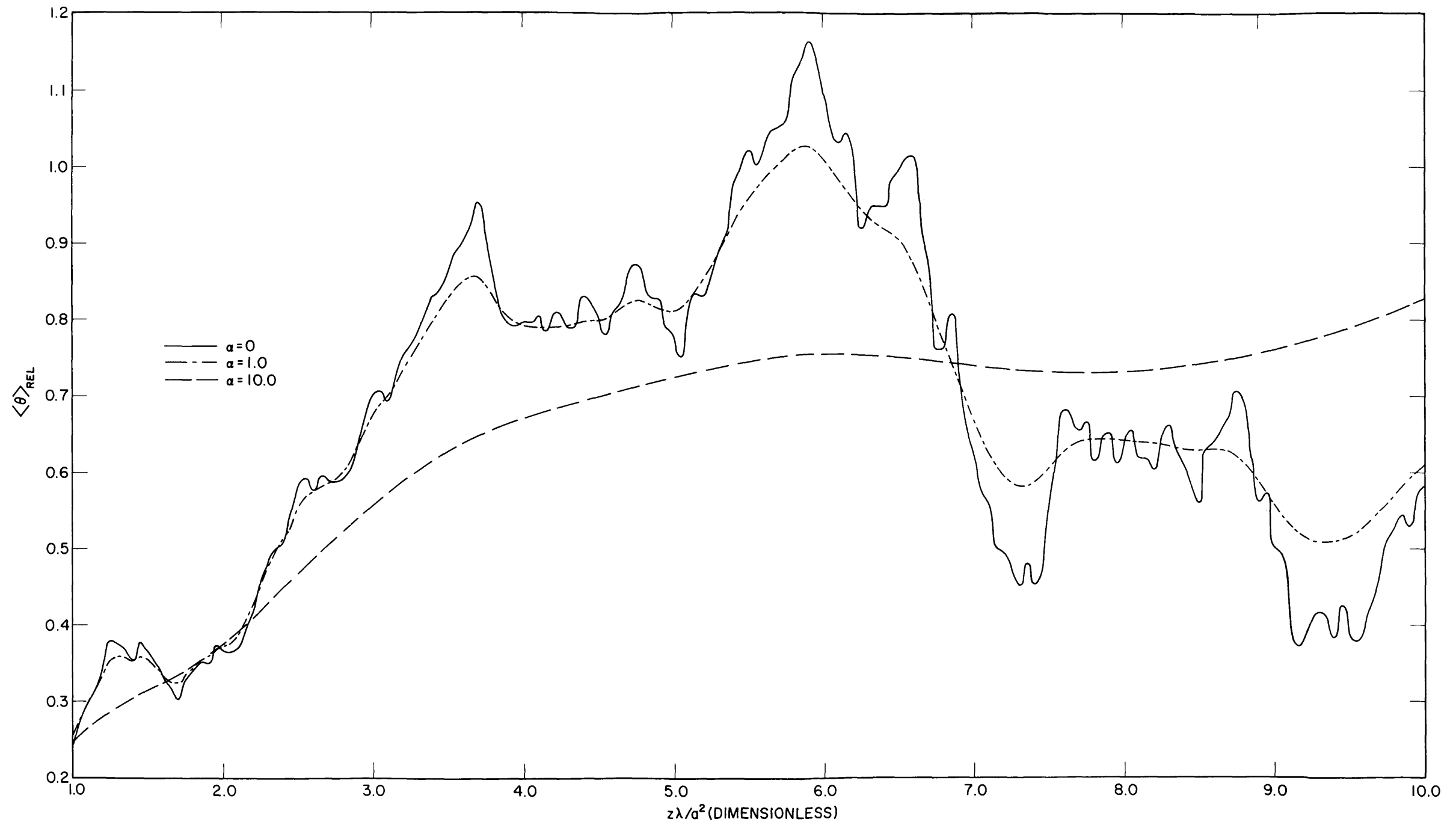


Fig. 20a - Average relative phase difference $\langle \theta \rangle_{rel}$ from plane-wave phase vs $z\lambda/a^2$ for a cylindrical liquid cavity with liquid boundaries. The effect of changing the absorption parameter α on the values of $\langle \theta \rangle_{rel}$ is shown for the liquid boundary condition. The standard parameters of Table I were used (except that α is not restricted to 0) and $0 \leq z\lambda/a^2 \leq 1$.

Fig. 20b - Same as Fig. 20a except $1 \leq z\lambda/a^2 \leq 10$

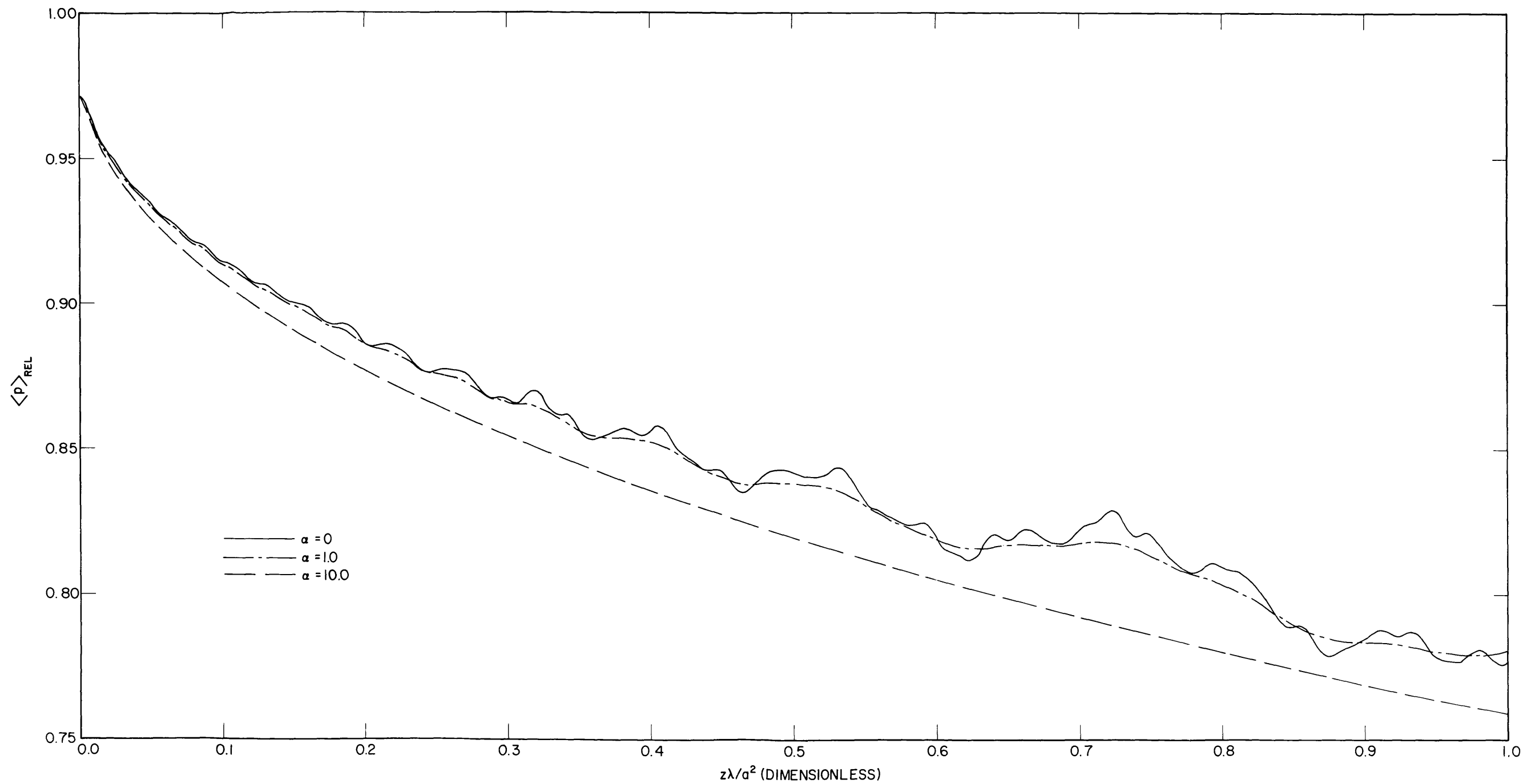
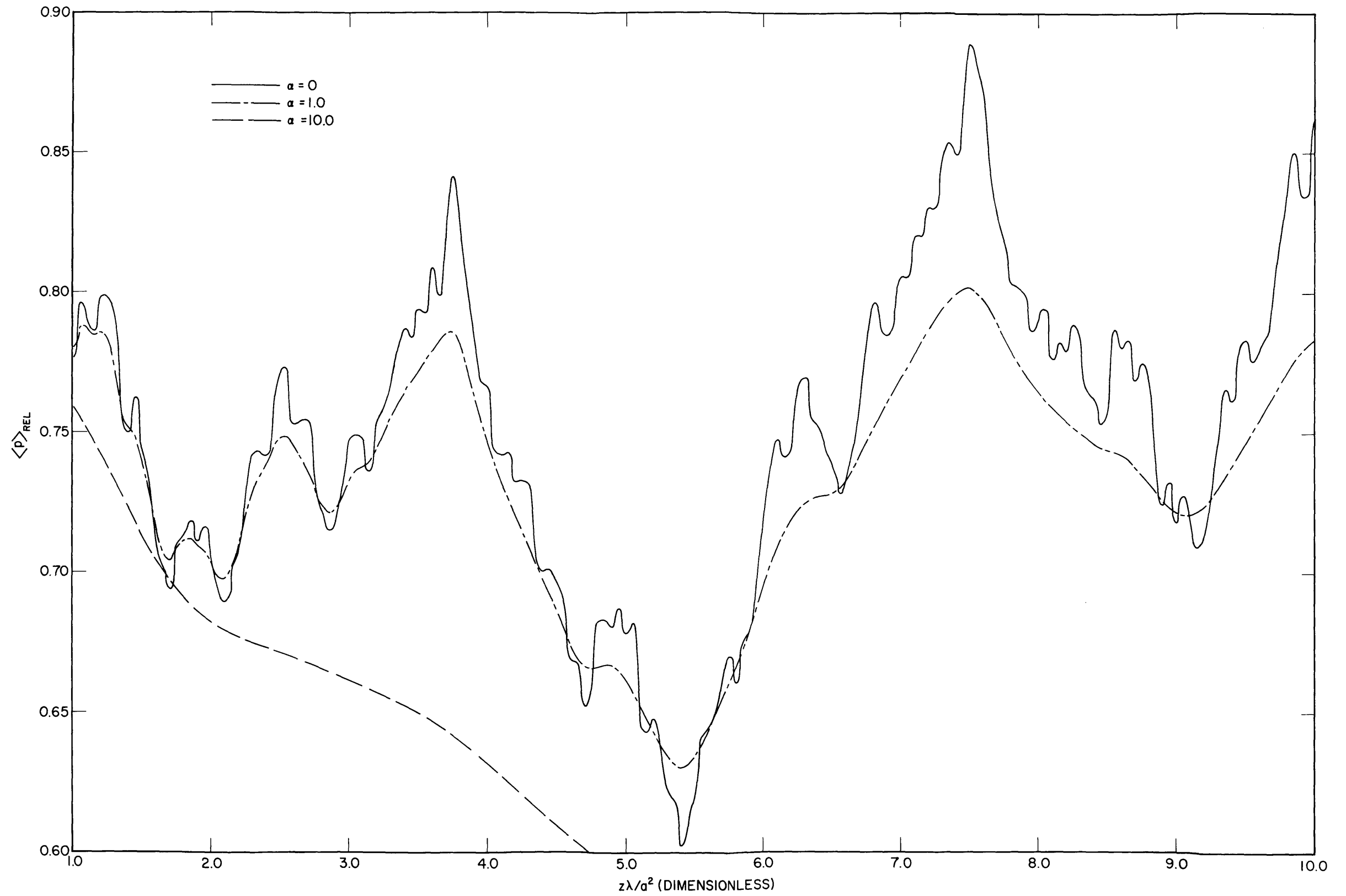


Fig. 21a - Average relative sound pressure $\langle p \rangle_{rel}$ vs $z\lambda/a^2$ for a cylindrical liquid cavity with elastic boundaries. The effect of changing the absorption parameter α on the values of $\langle p \rangle_{rel}$ is shown for the elastic boundary condition. The standard parameters of Table 1 were used (except that α is not restricted to 0) and $0 \leq z\lambda/a^2 \leq 1$.

Fig. 21b - Same as Fig. 21a except $1 \leq z\lambda/a^2 \leq 10$

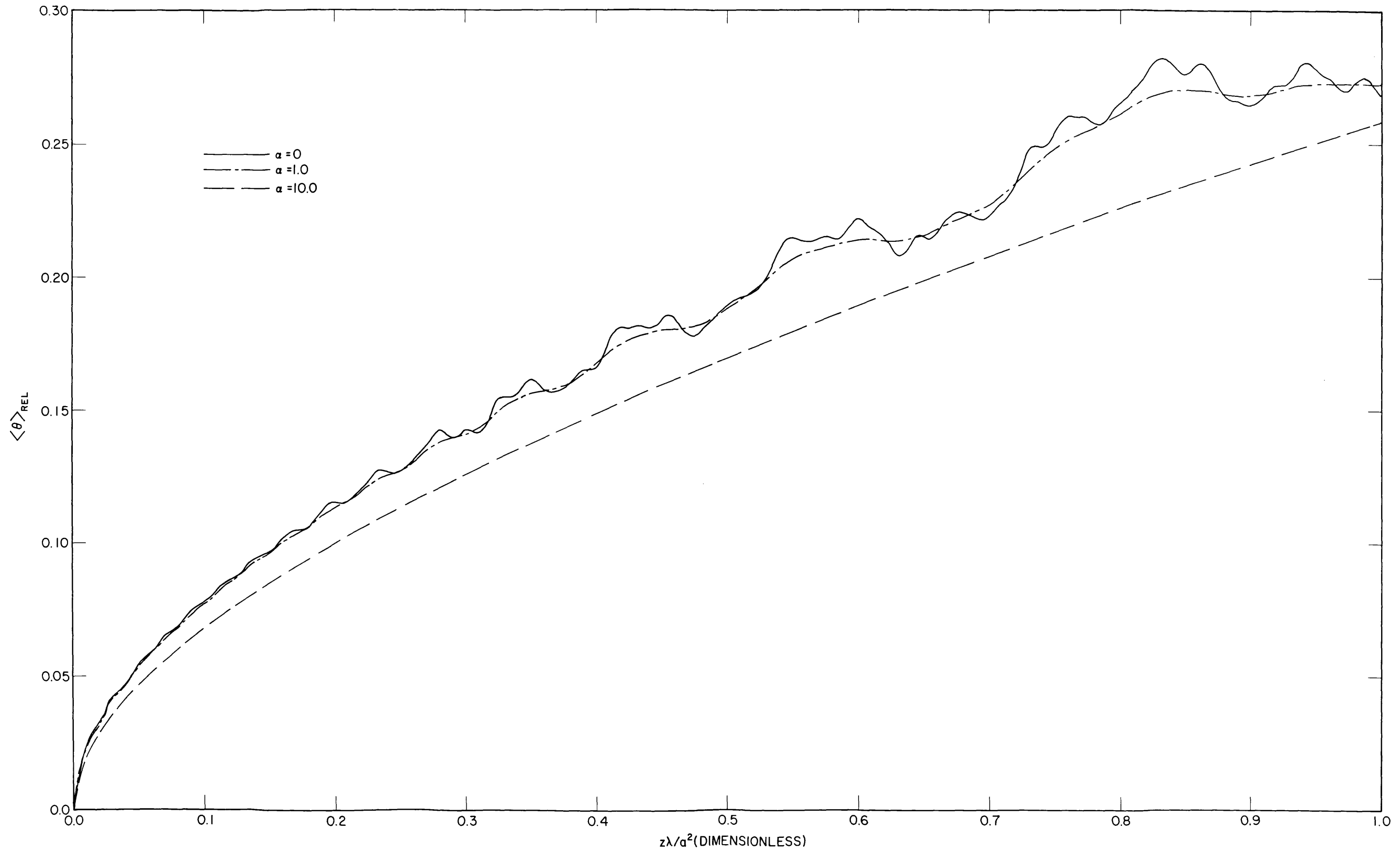
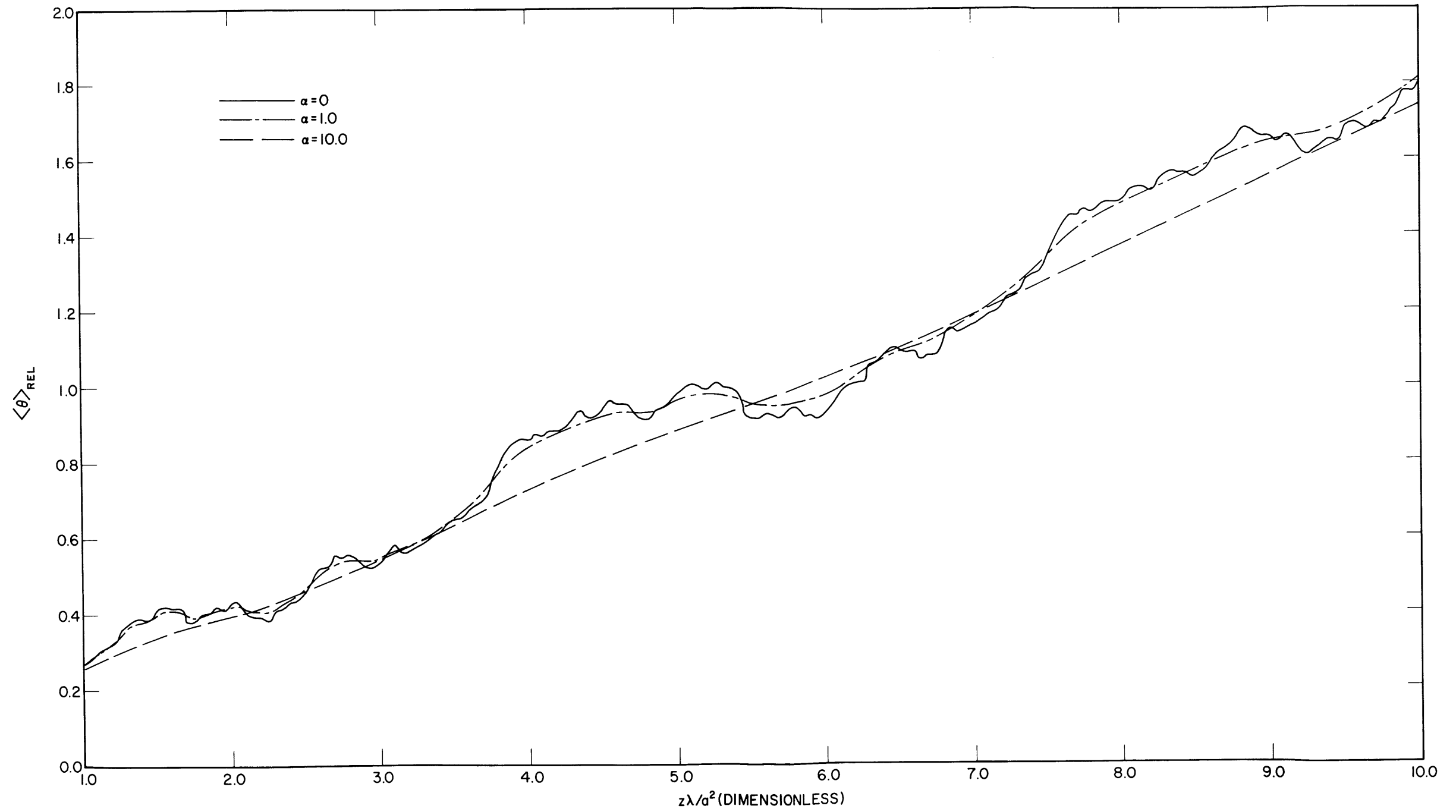


Fig. 22a - Average relative phase difference $\langle \theta \rangle_{rel}$ from plane-wave phase vs $z\lambda/a^2$ for a cylindrical liquid cavity with elastic boundaries. The effect of changing the absorption parameter α on the values of $\langle \theta \rangle_{rel}$ is shown for the elastic boundary condition. The standard parameters of Table 1 were used (except that α is not restricted to 0) and $0 \leq z\lambda/a^2 \leq 1$.

Fig. 22b - Same as Fig. 22a except $1 \leq z\lambda/a^2 \leq 10$

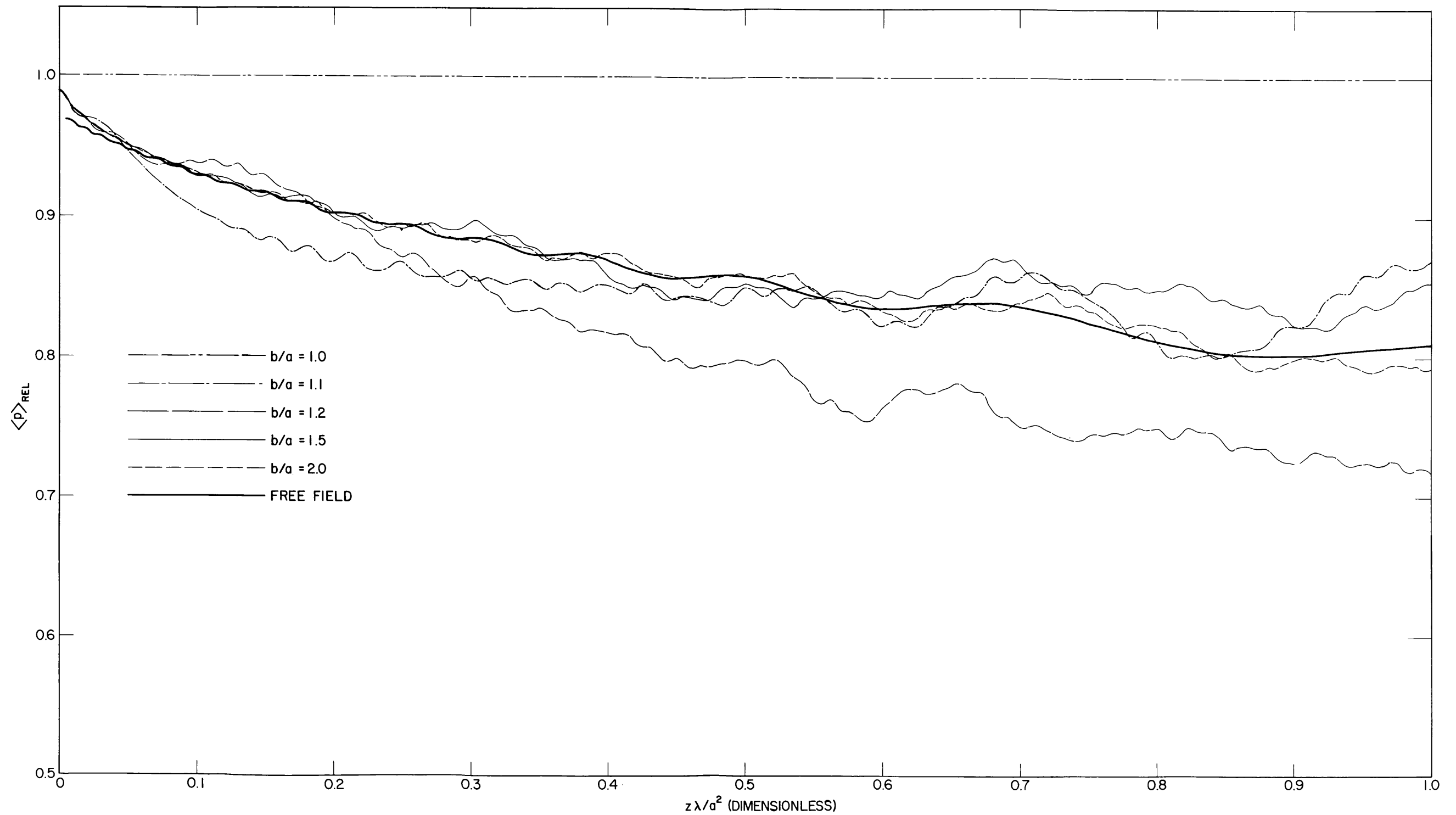
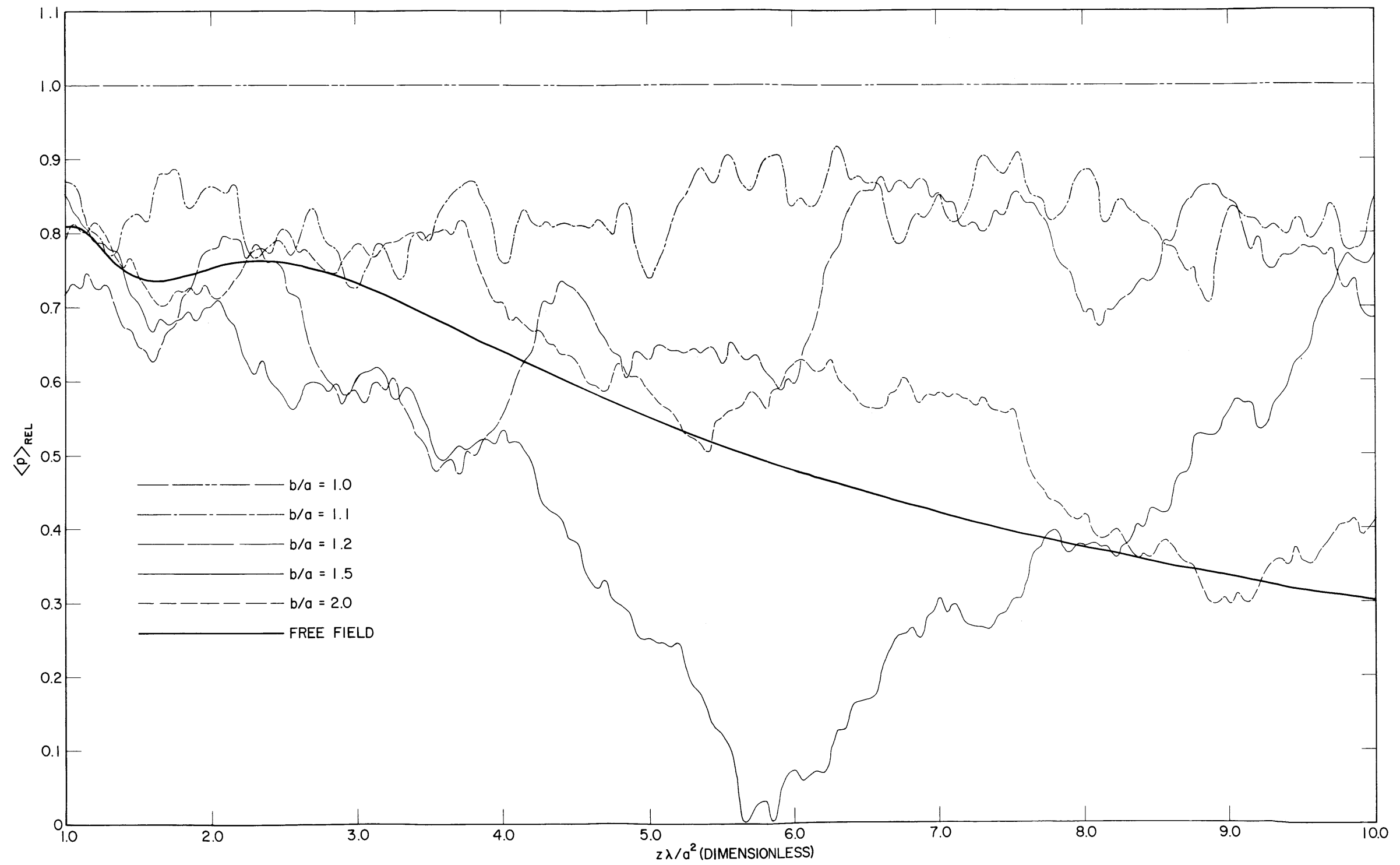


Fig. 23a - Average relative sound pressure $\langle p \rangle_{rel}$ vs $z\lambda/a^2$ for a cylindrical liquid cavity with rigid boundaries. The effect of changing the radius-ratio parameter b/a on the values of $\langle p \rangle_{rel}$ is shown for the rigid boundary condition. The standard parameters of Table 1 were used (except that b/a is not restricted to 2) and $0 \leq z\lambda/a^2 \leq 1$.

Fig. 23b - Same as Fig. 23a except $1 \leq z\lambda/d^2 \leq 10$

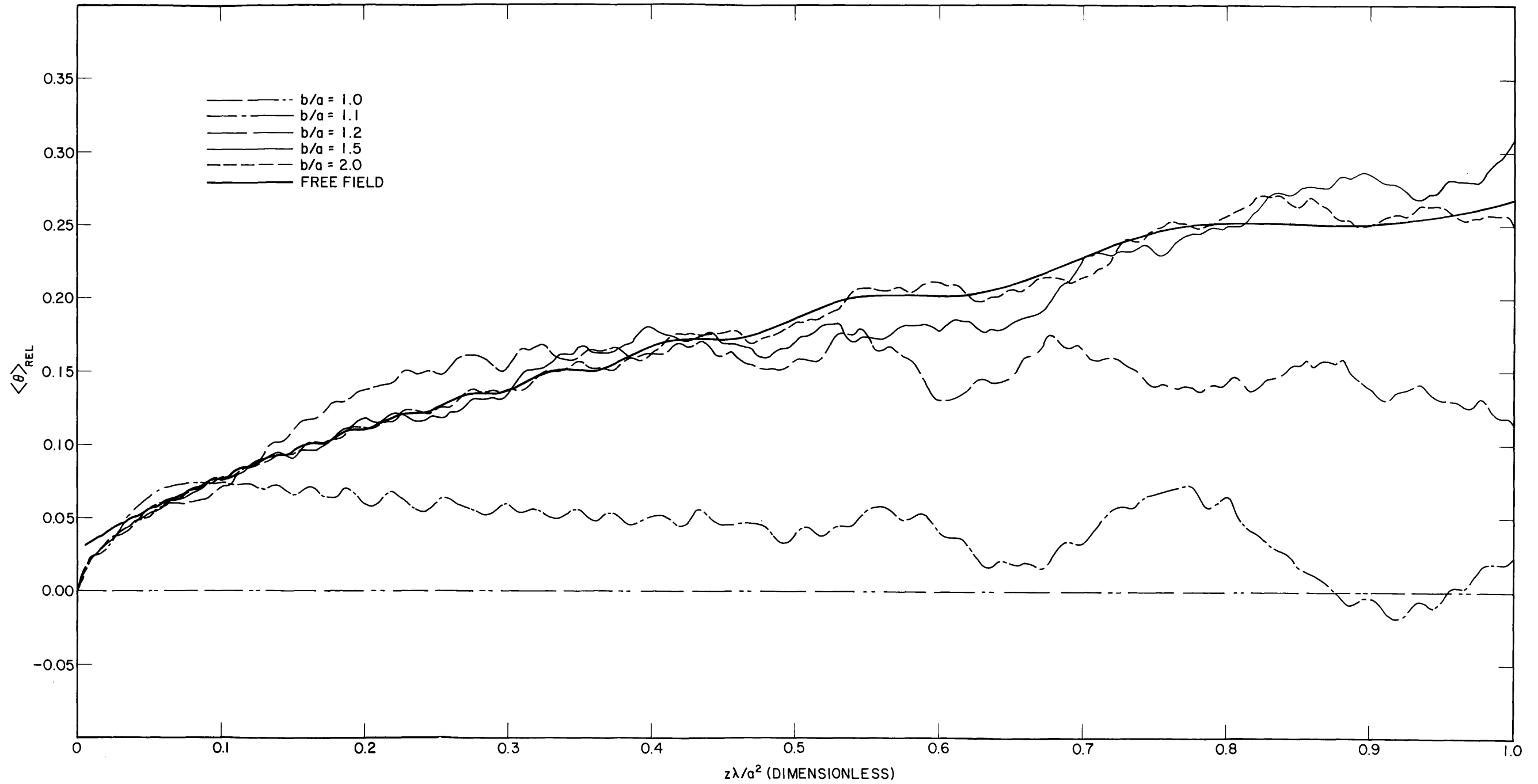
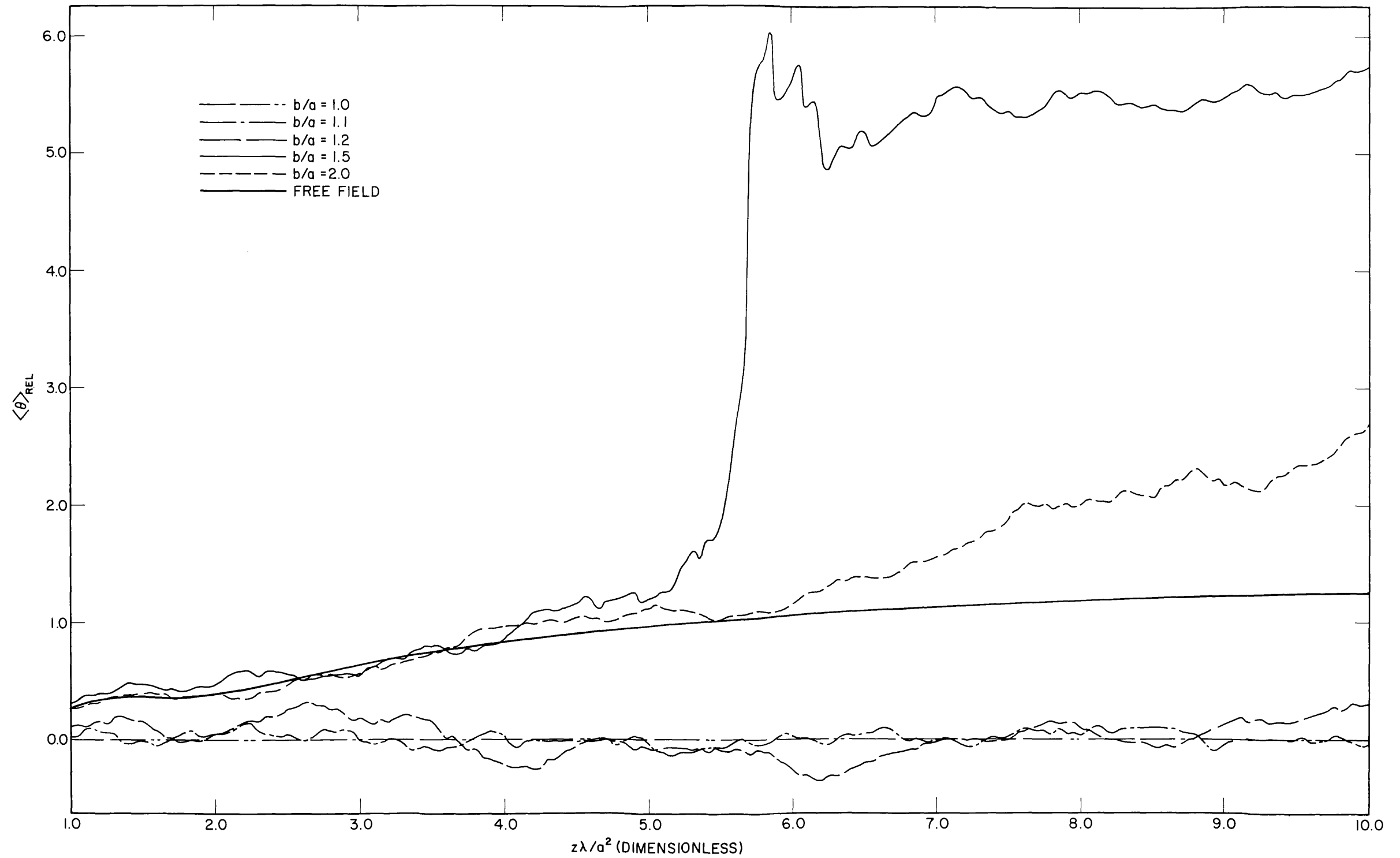


Fig. 24a - Average relative phase difference $\langle \theta \rangle_{rel}$ from plane-wave phase vs $z\lambda/a^2$ for a cylindrical liquid cavity with rigid boundaries. The effect of changing the radius-ratio parameter b/a on the values of $\langle \theta \rangle_{rel}$ is shown for the rigid boundary condition. The standard parameters of Table 1 were used (except that b/a is not restricted to 2) and $0 \leq z\lambda/a^2 \leq 1$.

Fig. 24b - Same as Fig. 24a except $1 \leq z\lambda/a^2 \leq 10$

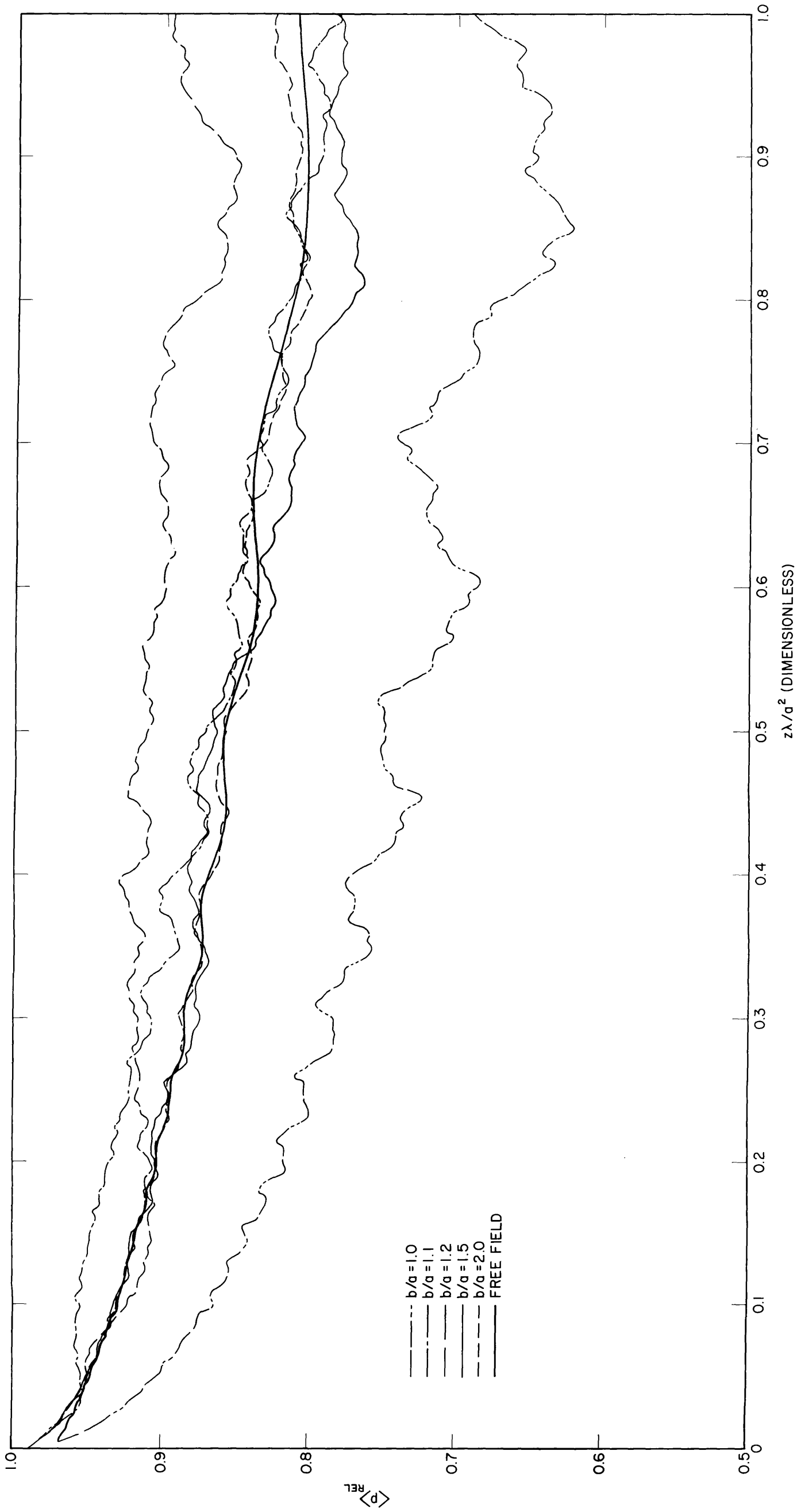
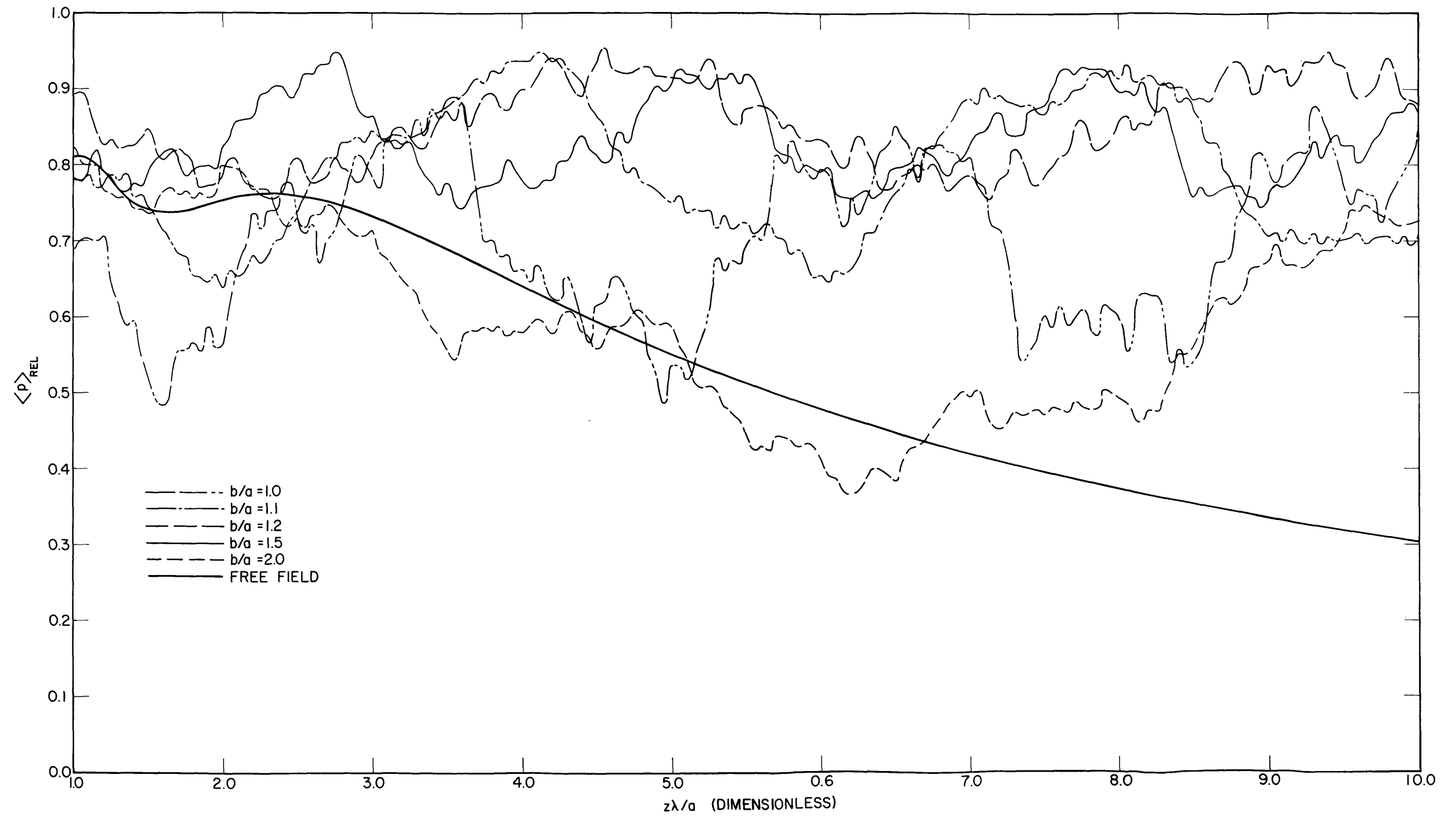


Fig. 25a - Average relative sound pressure $\langle p \rangle_{rel}$ vs $z\lambda/a^2$ for a cylindrical liquid cavity with infinitely flexible boundaries. The effect of changing the radius-ratio parameter b/a on the values of $\langle p \rangle_{rel}$ is shown for the infinitely flexible boundary condition. The standard parameters of Table 1 were used (except that b/a is not restricted to 2) and $0 \leq z\lambda/a^2 \leq 1$.

Fig. 25b - Same as Fig. 25a except $1 \leq z\lambda/a^2 \leq 10$

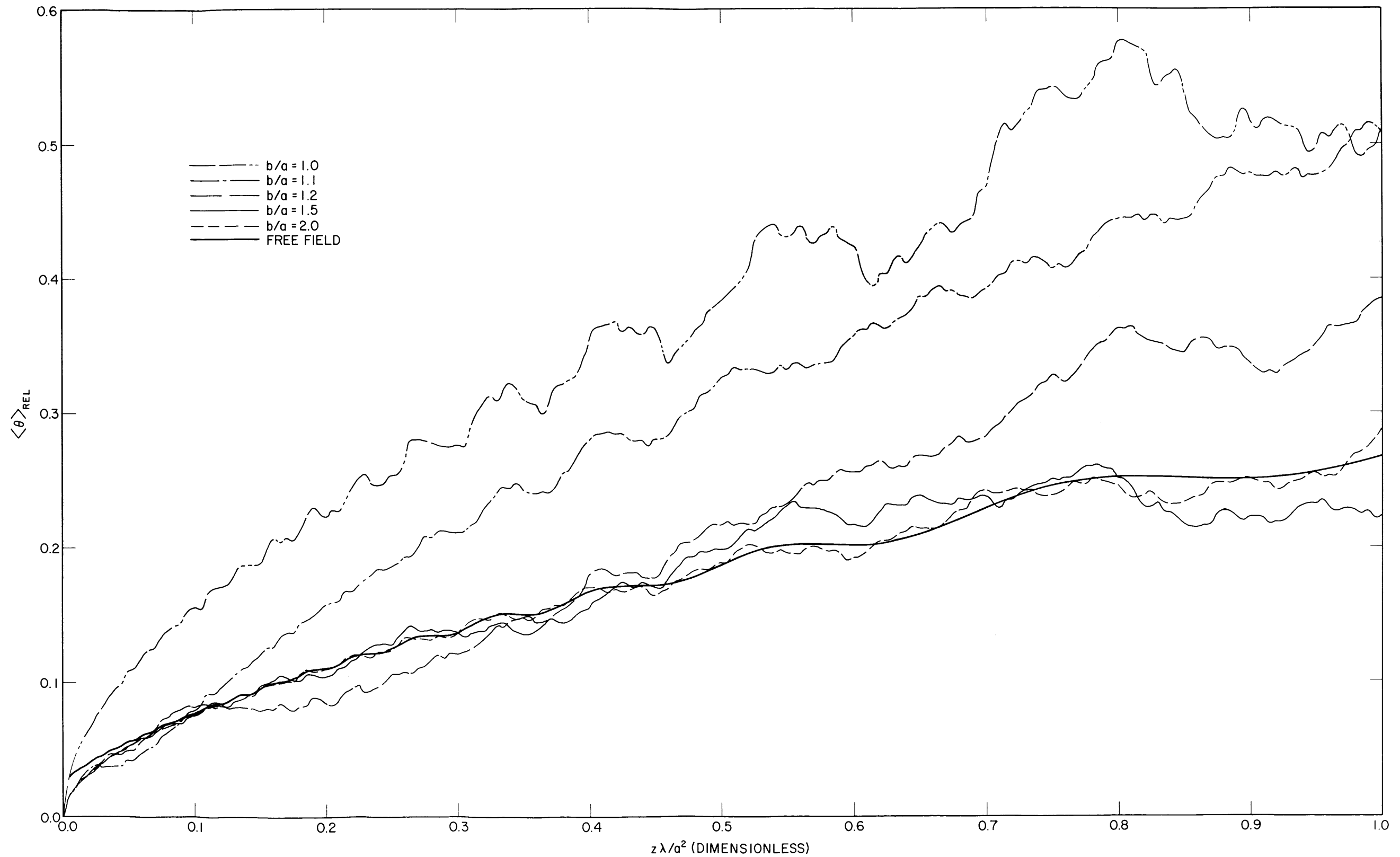


Fig. 26a - Average relative phase difference $\langle \theta \rangle_{REL}$ from plane-wave phase vs $z\lambda/a^2$ for a cylindrical liquid cavity with infinitely flexible boundaries. The effect of changing the radius-ratio parameter b/a on the values of $\langle \theta \rangle_{REL}$ is shown for the infinitely flexible boundary condition. The standard parameters of Table 1 were used (except that b/a is not restricted to 2) and $0 \leq z\lambda/a^2 \leq 1$.

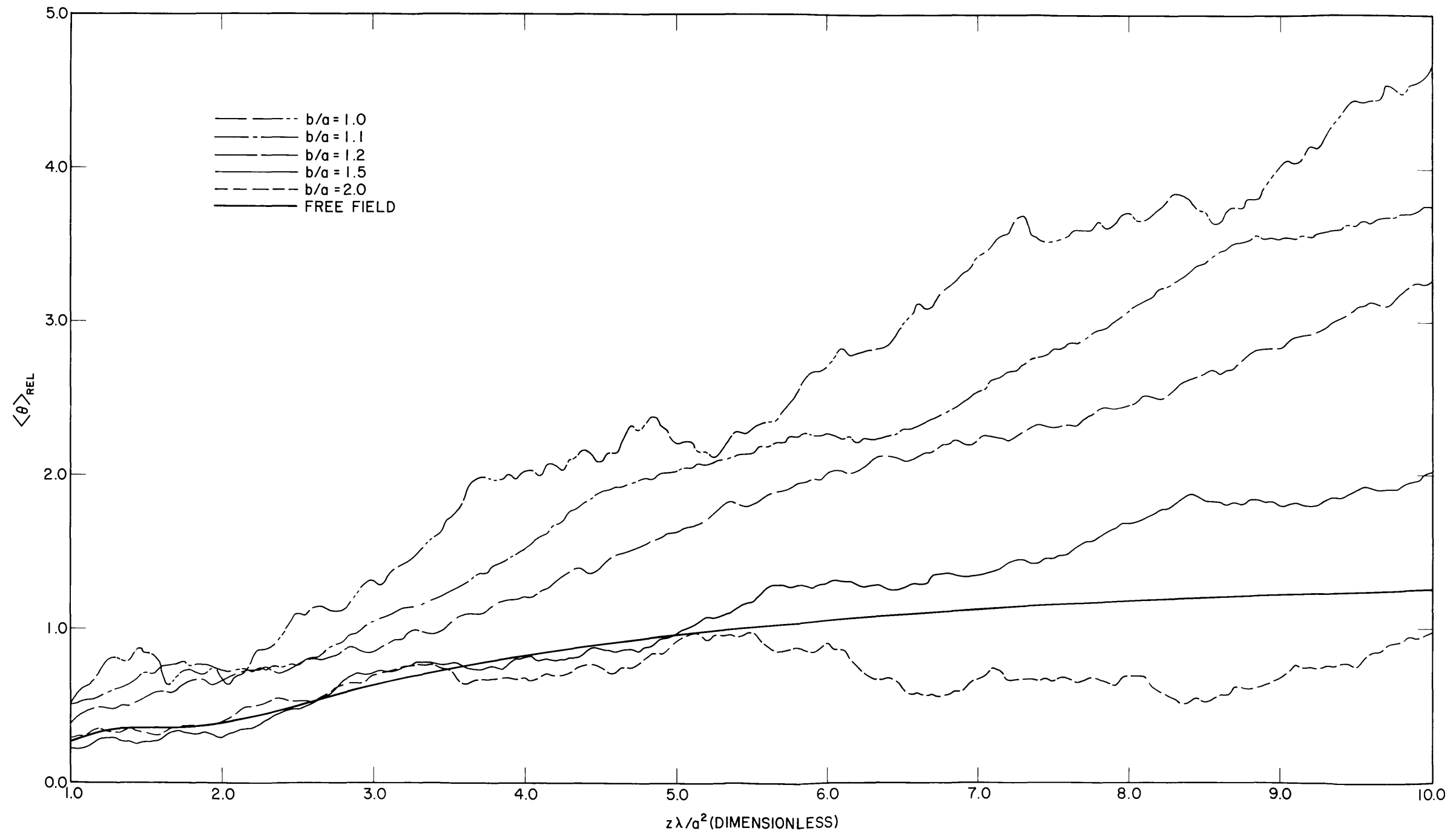


Fig. 26b - Same as Fig. 26a except $1 \leq z\lambda/a^2 \leq 10$.

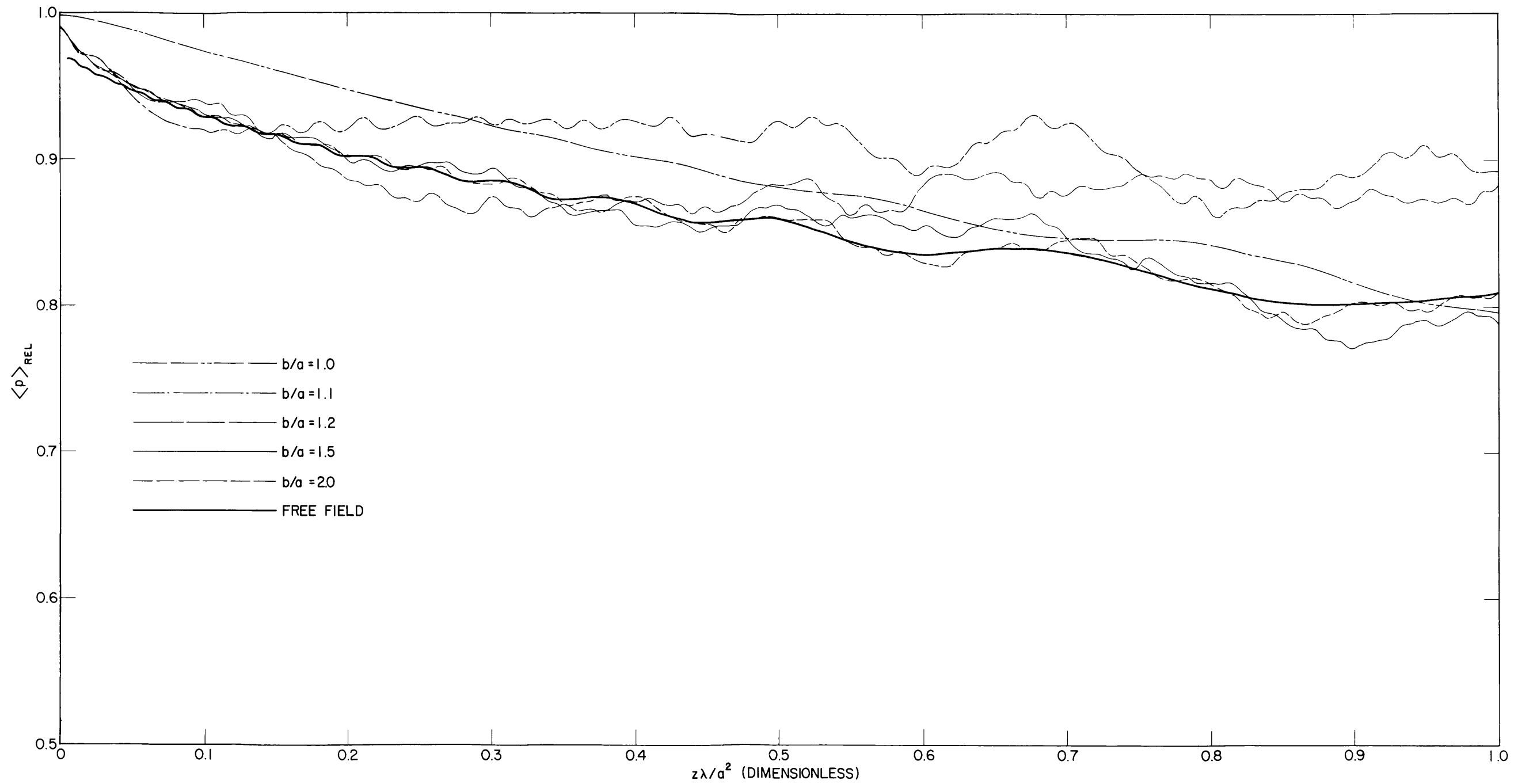
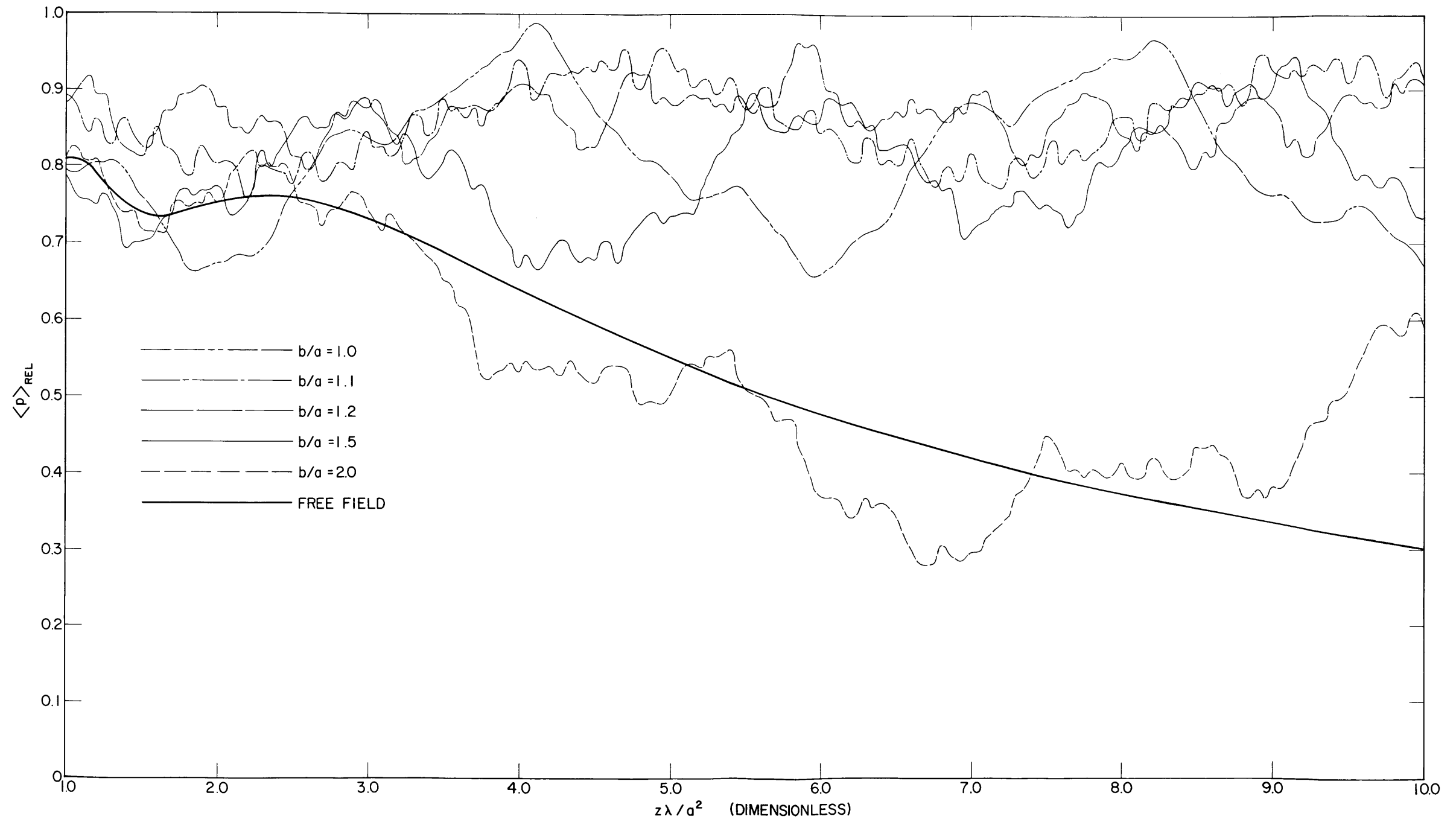


Fig. 27a - Average relative sound pressure $\langle p \rangle_{REL}$ vs $z\lambda/a^2$ for a cylindrical liquid cavity with liquid boundaries. The effect of changing the radius-ratio parameter b/a on the values of $\langle p \rangle_{REL}$ is shown for the liquid boundary condition. The standard parameters of Table 1 were used (except that b/a is not restricted to 2) and $0 \leq z\lambda/a^2 \leq 1$.

Fig. 27b - Same as Fig. 27a except $1 \leq z\lambda/a^2 \leq 10$

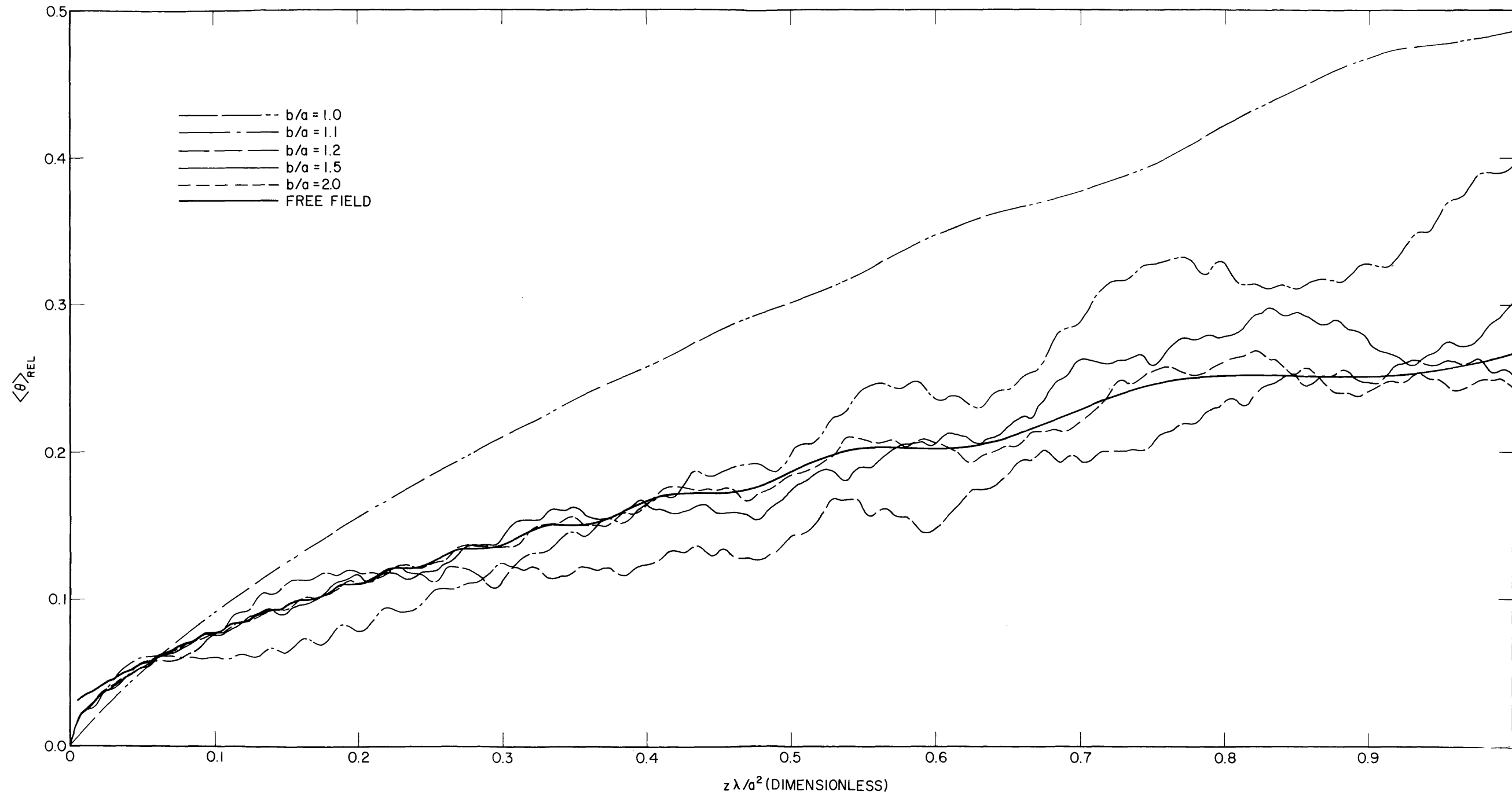
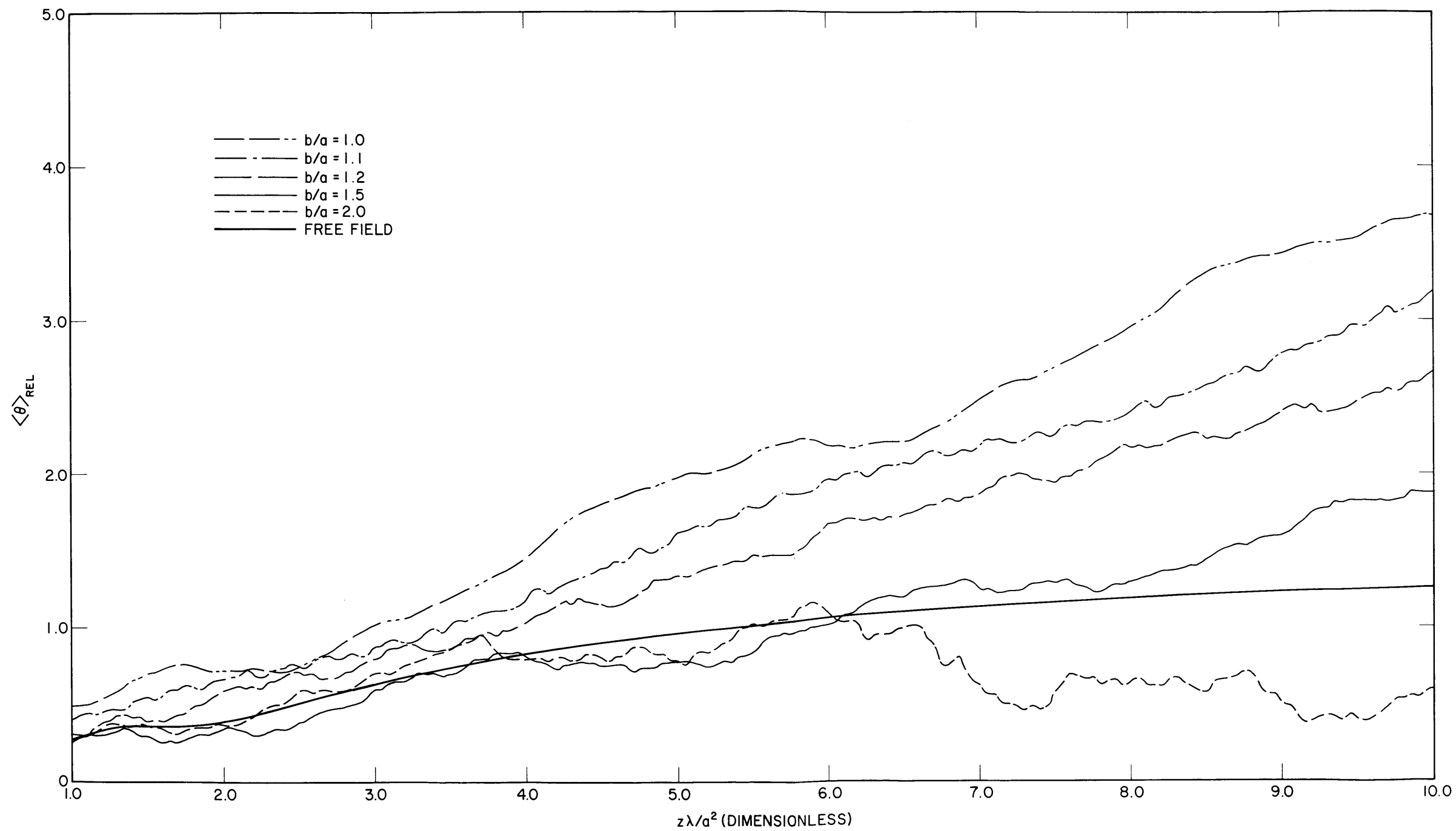


Fig. 28a - Average relative phase difference $\langle \theta \rangle_{rel}$ from plane-wave phase vs $z\lambda/a^2$ for a cylindrical liquid cavity with liquid boundaries. The effect of changing the radius-ratio parameter b/a on the values of $\langle \theta \rangle_{rel}$ is shown for the liquid boundary condition. The standard parameters of Table 1 were used (except that b/a is not restricted to 2) and $0 \leq z\lambda/a^2 \leq 1$.

Fig. 28b - Same as Fig. 28a except $1 \leq z\lambda/a^2 \leq 10$

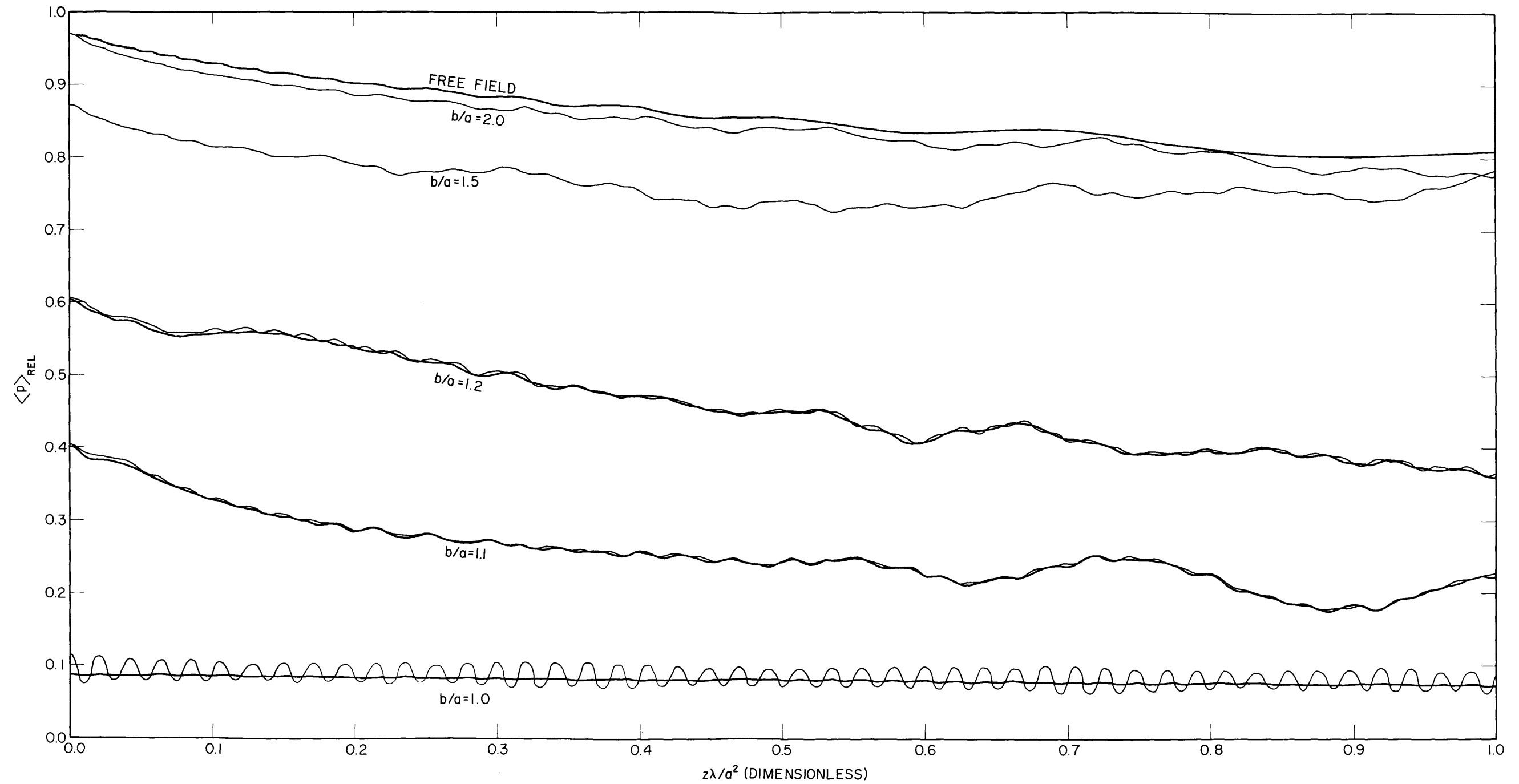


Fig. 29a - Average relative sound pressure $\langle p \rangle_{REL}$ vs $z\lambda/a^2$ for a cylindrical liquid cavity with elastic boundaries. The effect of changing the radius-ratio parameter b/a on the values of $\langle p \rangle_{REL}$ is shown for the elastic boundary condition. The standard parameters of Table 1 were used (except that b/a is not restricted to 2) and $0 \leq z\lambda/a^2 \leq 1$. Light-weight lines indicate actual solutions; heavy-weight lines, orthogonal assumption solutions.

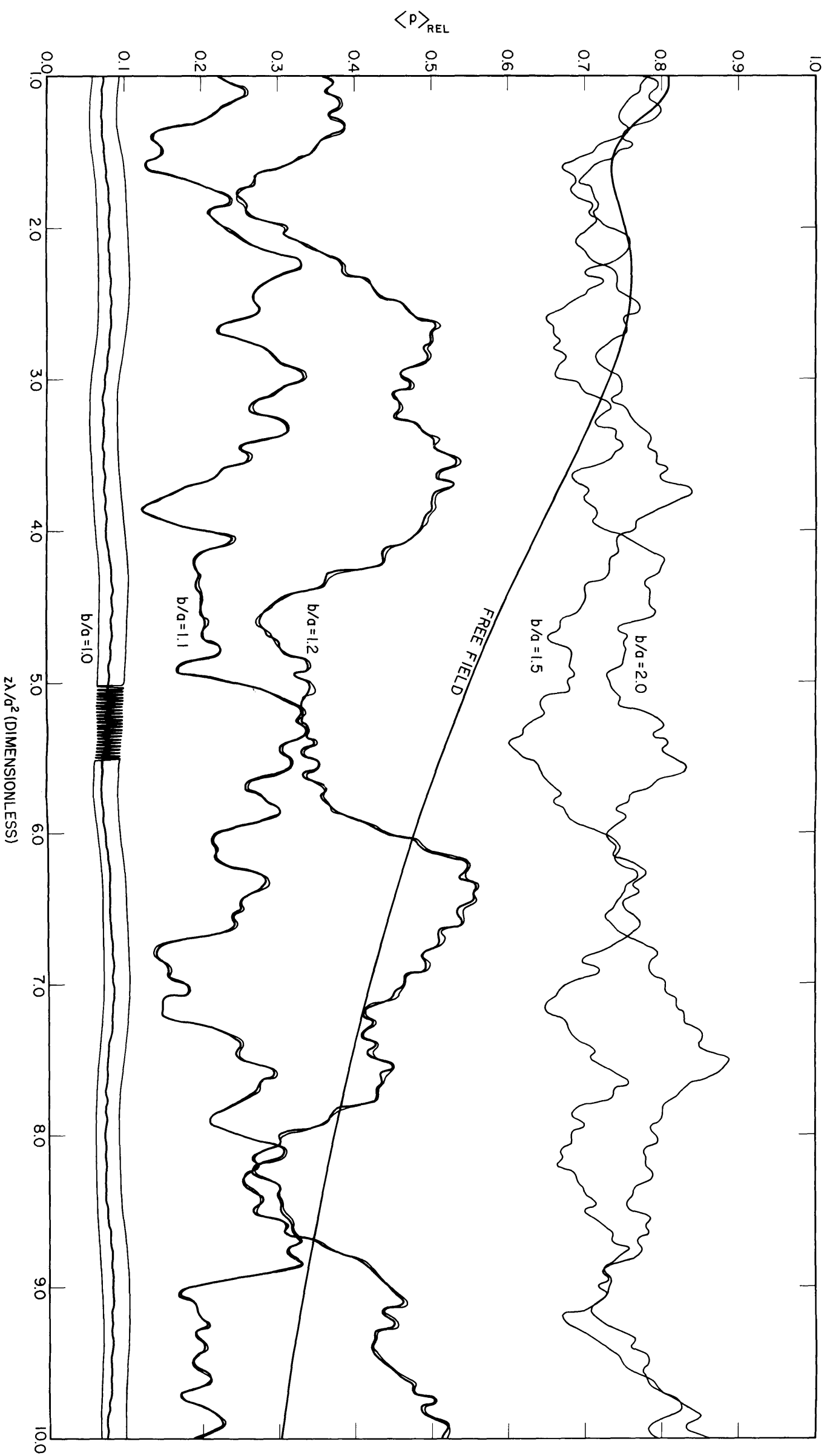


Fig. 29b — Same as Fig. 29a except $1 \leq z\lambda/a^2 \leq 10$. Light-weight lines indicate actual solutions; heavy-weight lines, orthogonal assumption solutions

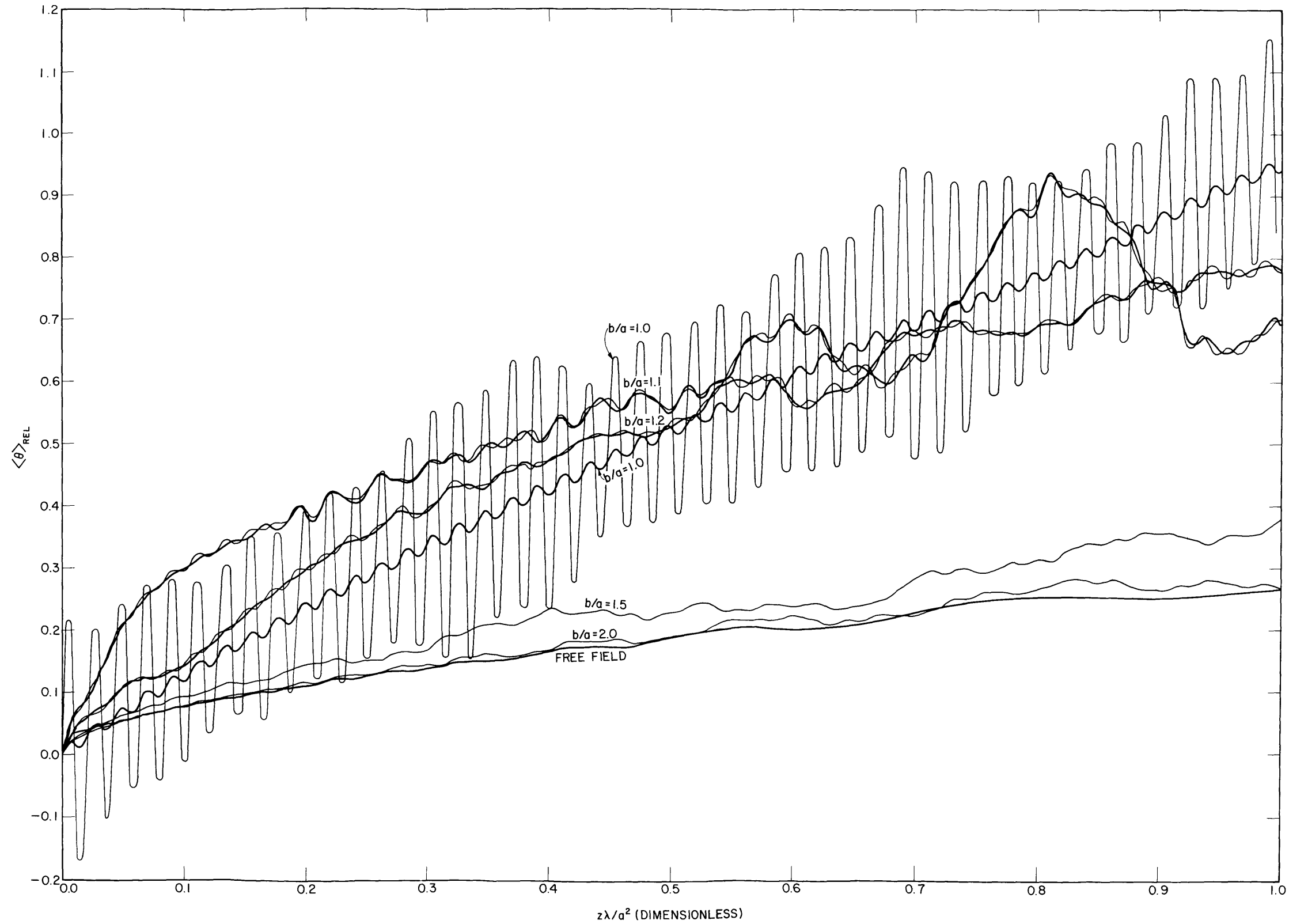


Fig. 30a - Average relative phase difference $\langle \theta \rangle_{rel}$ from plane-wave phase vs $z\lambda/a^2$ for a cylindrical liquid cavity with elastic boundaries. The effect of changing the radius-ratio parameter b/a on the values of $\langle \theta \rangle_{rel}$ is shown for the elastic boundary condition. The standard parameters of Table I were used (except that b/a is not restricted to 2) and $0 \leq z\lambda/a^2 \leq 1$. Light-weight lines indicate actual solutions; heavy-weight lines, orthogonal assumption solutions.

Figure 30

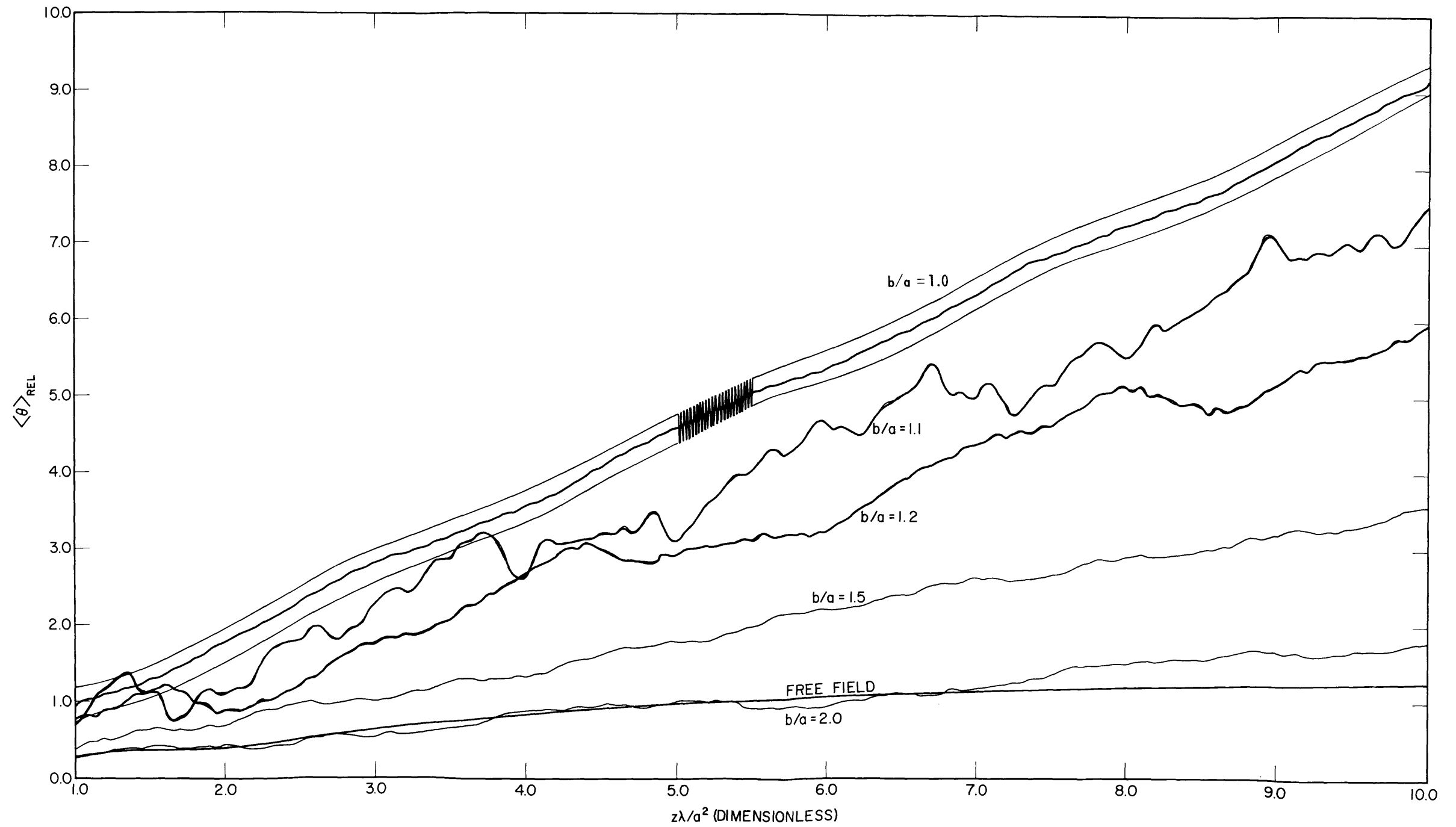


Fig. 30b - Same as Fig. 30a except $1 \leq z\lambda/a^2 \leq 10$. Light-weight lines indicate actual solutions; heavy-weight lines, orthogonal assumption solutions.

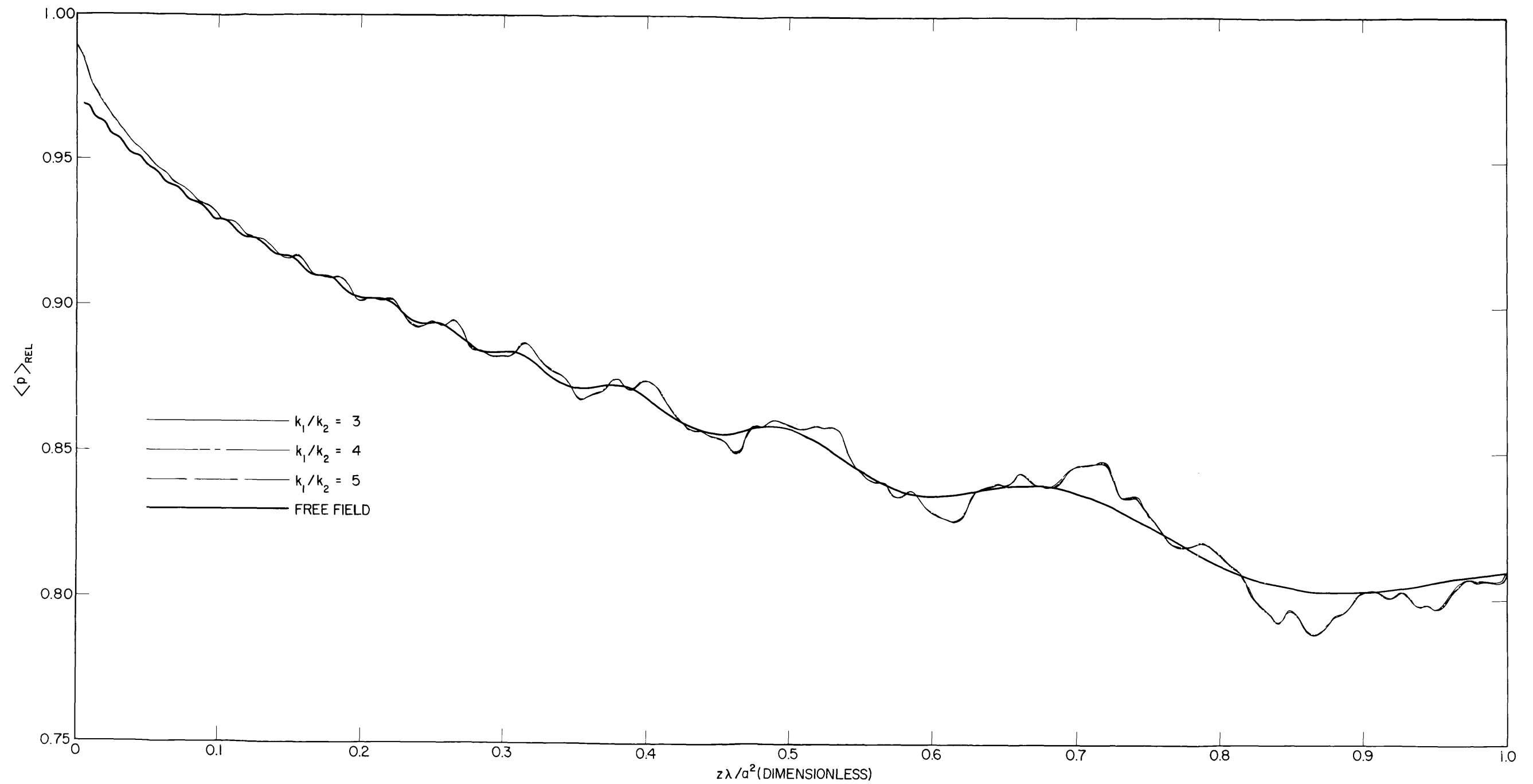
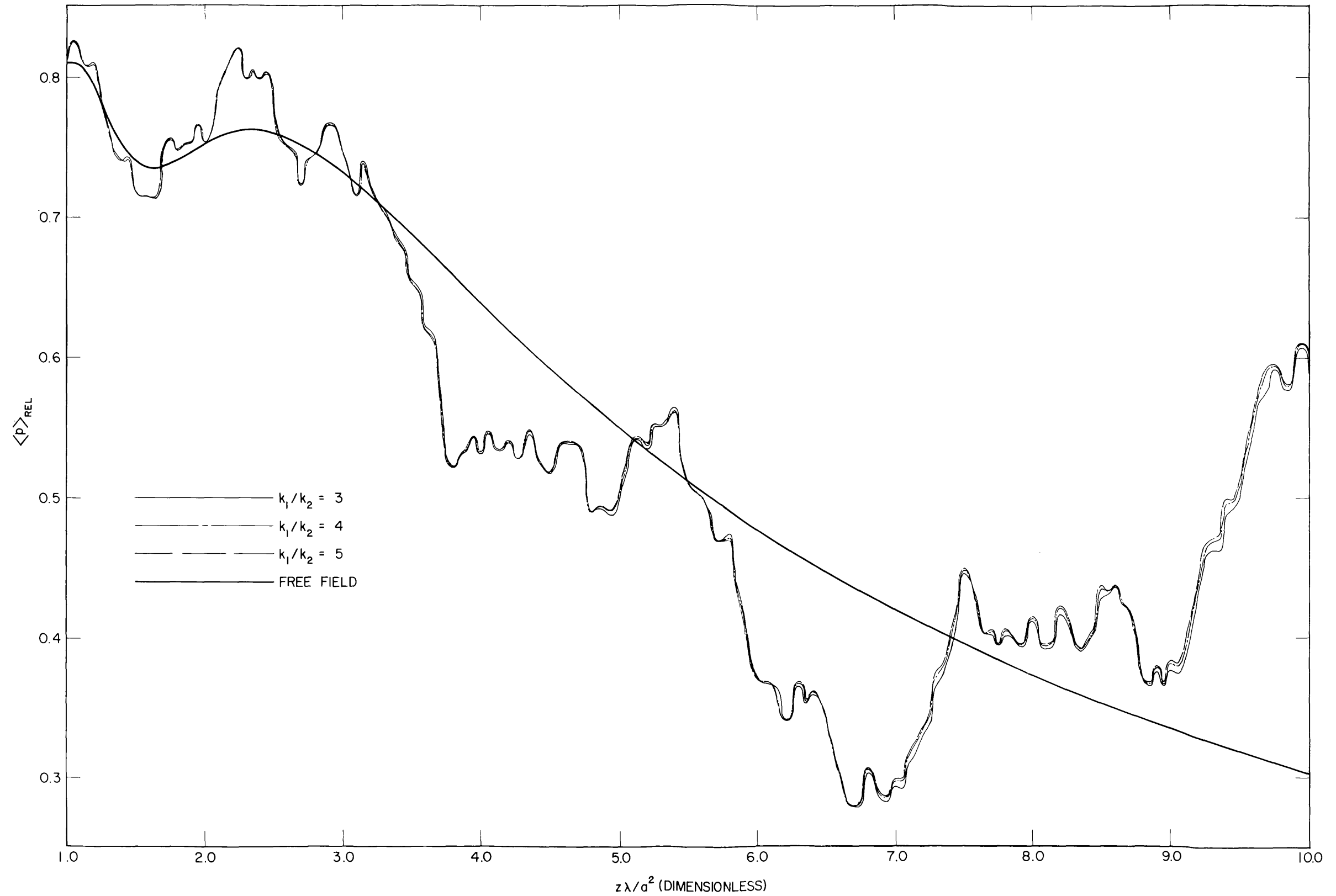


Fig. 31a - Average relative sound pressure $\langle p \rangle_{rel}$ vs $z\lambda/a^2$ for a cylindrical liquid cavity with liquid boundaries. The effect of changing the wave-number-ratio parameter k_1/k_2 on the values of $\langle p \rangle_{rel}$ is shown for the liquid boundary condition. The standard parameters of Table 1 were used (except that k_1/k_2 is not restricted to 4) and $0 \leq z\lambda/a^2 \leq 1$.

Fig. 31b - Same as Fig. 31a except $1 \leq z\lambda/a^2 \leq 10$

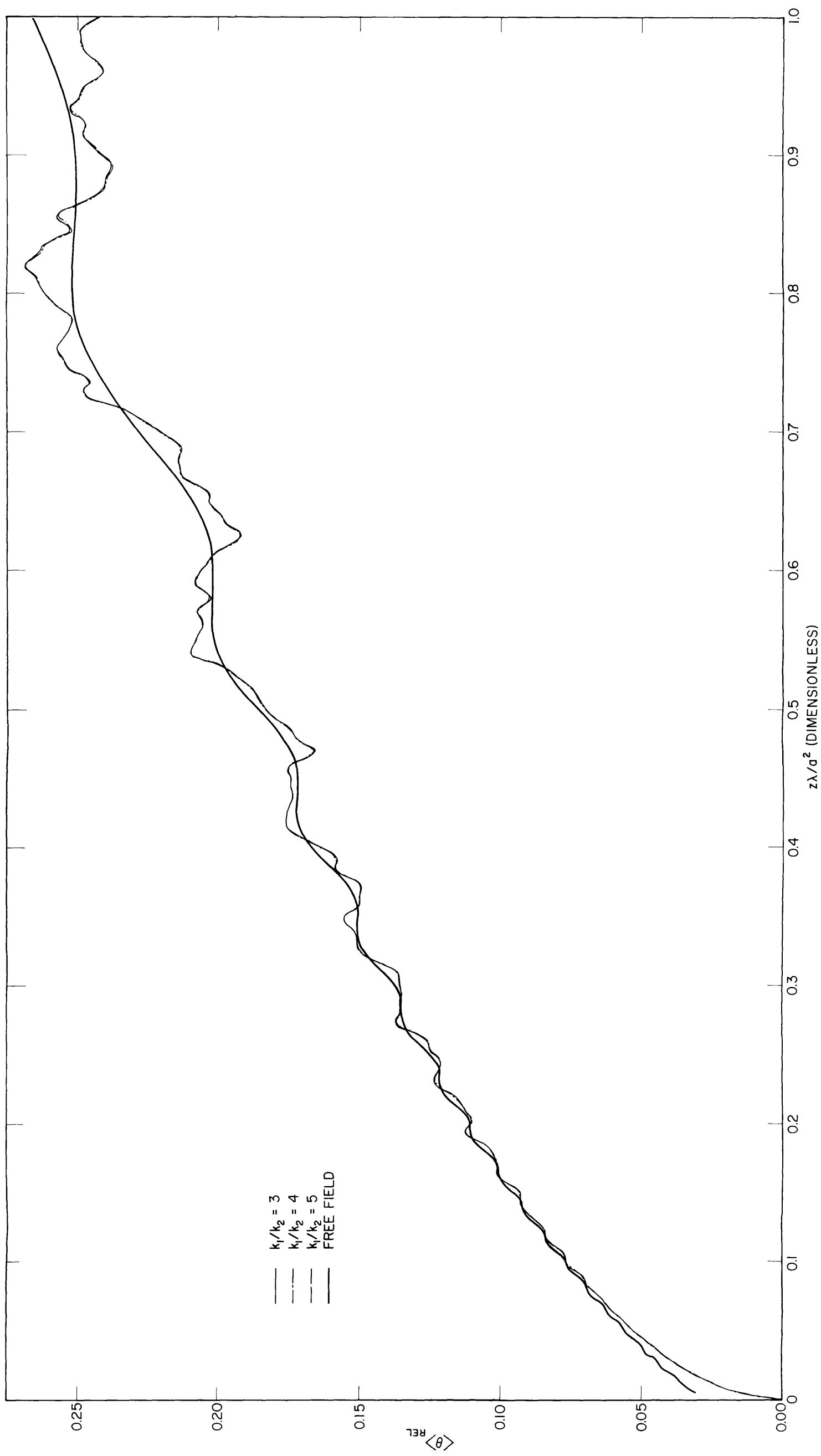
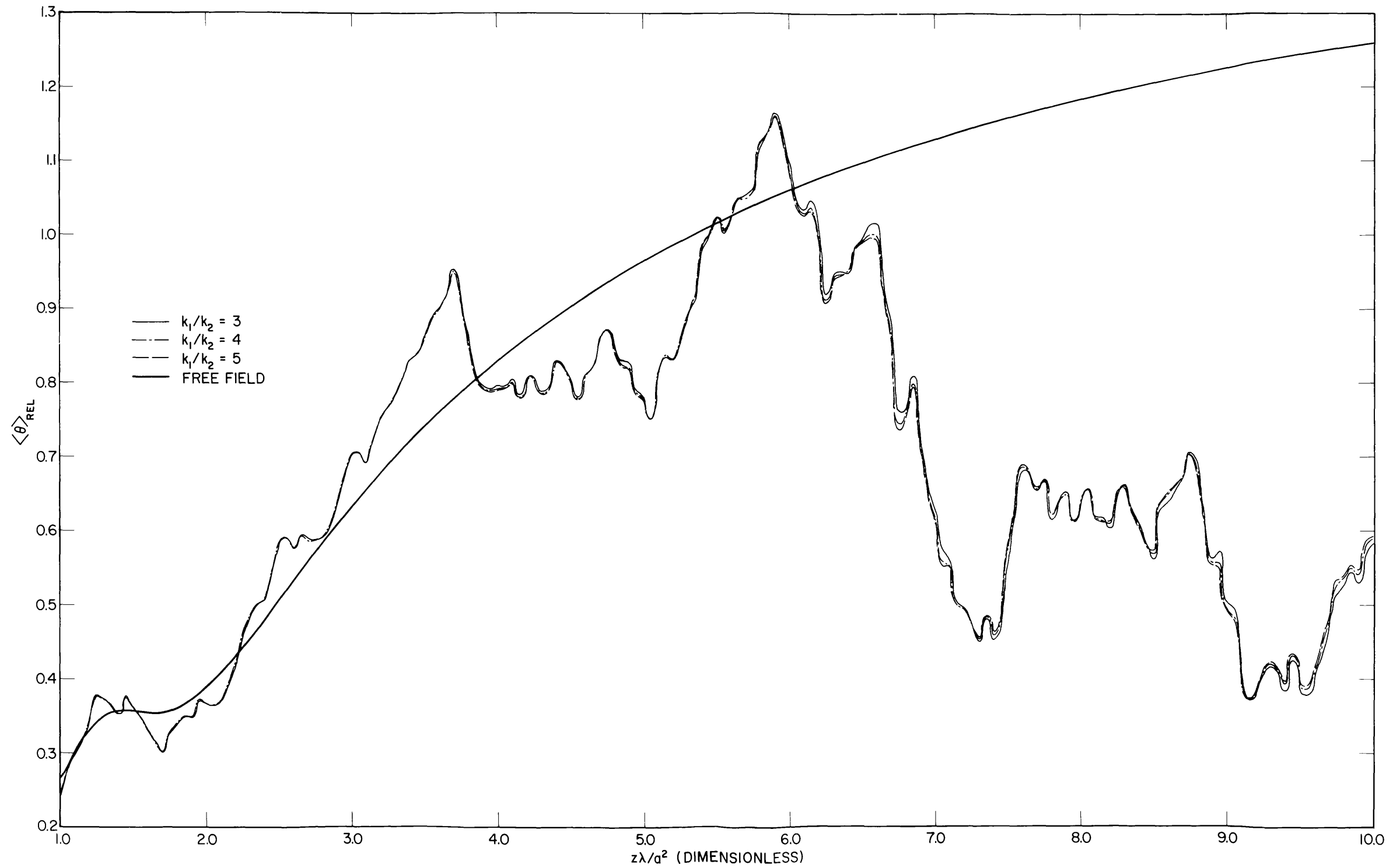


Fig. 32a — Average relative phase difference $\langle \theta \rangle_{REL}$ from plane-wave phase vs $z\lambda/a^2$ for a cylindrical liquid cavity with liquid boundaries. The effect of changing the wave-number-ratio parameter k_1/k_2 on the values of $\langle \theta \rangle_{REL}$ is shown for the liquid boundary condition. The standard parameters of Table 1 were used (except that k_1/k_2 is not restricted to 4) and $0 \leq z\lambda/a^2 \leq 1$.

Fig. 32b - Same as Fig. 32a except $1 \leq z\lambda/a^2 \leq 10$

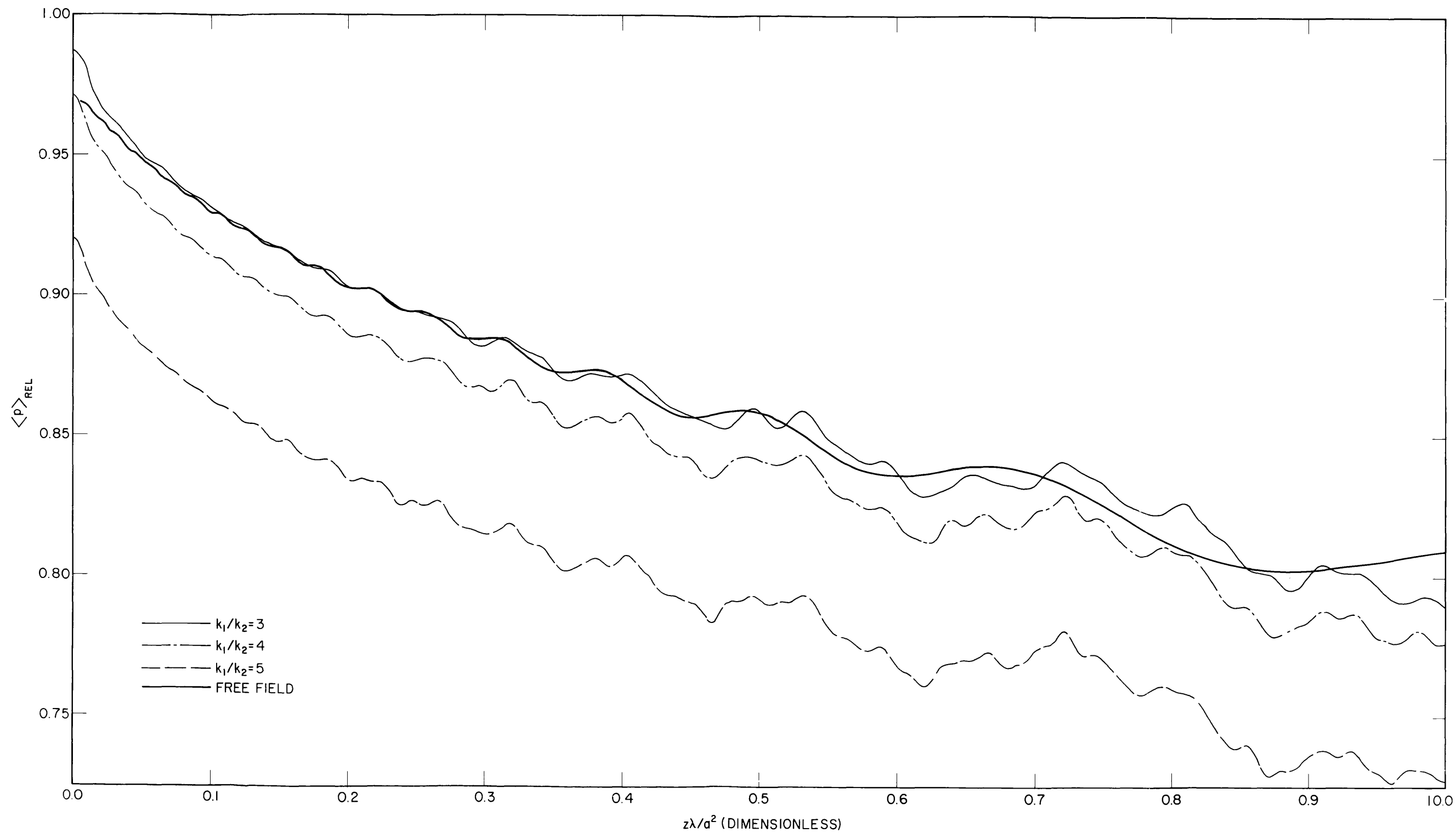
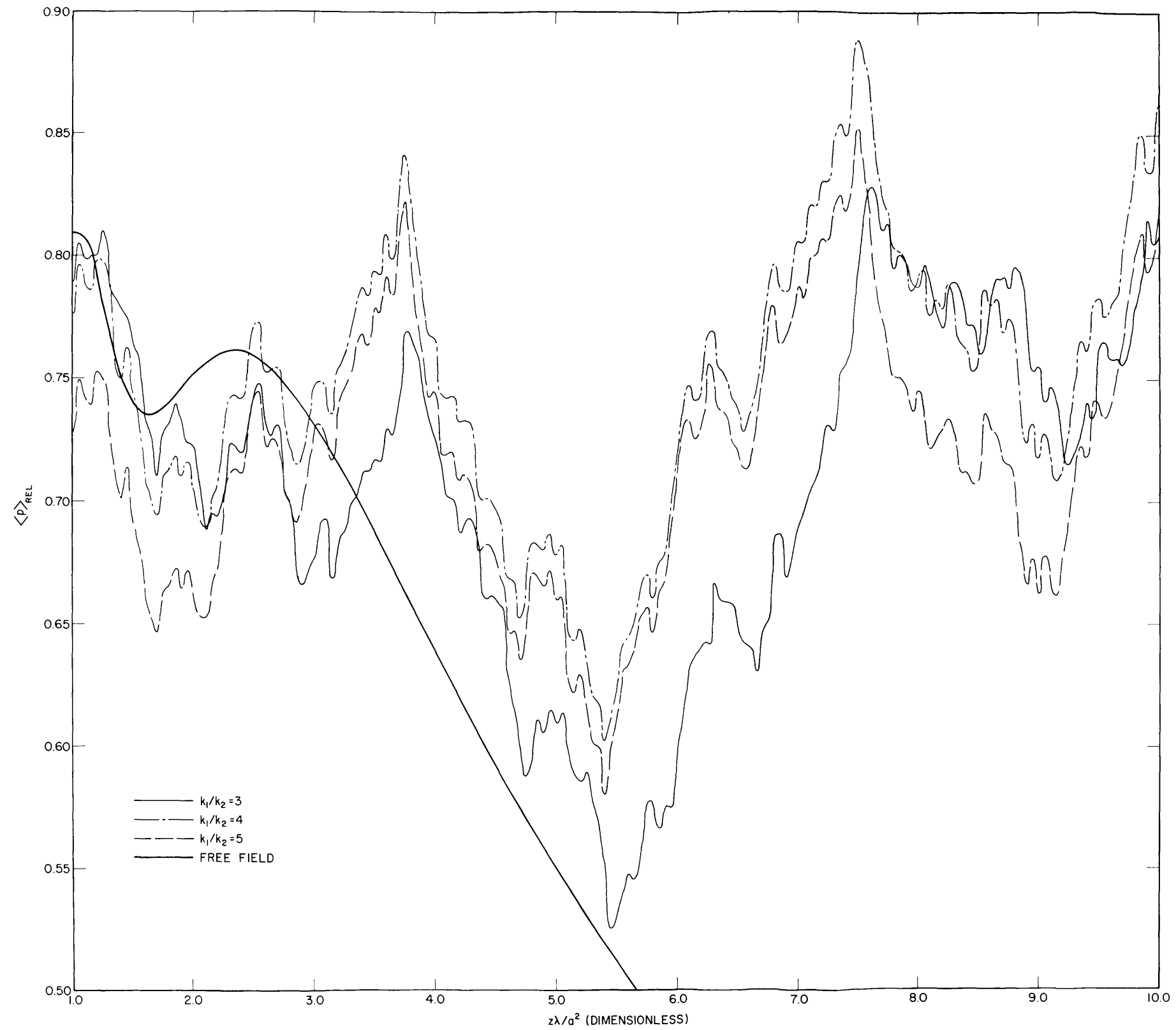


Fig. 33a — Average relative sound pressure $\langle p \rangle_{rel}$ vs $z\lambda/a^2$ for a cylindrical liquid cavity with elastic boundaries. The effect of changing the wave-number-ratio parameter k_1/k_2 on the values of $\langle p \rangle_{rel}$ is shown for the elastic boundary condition. The standard parameters of Table 1 were used (except that k_1/k_2 is not restricted to 4) and $0 \leq z\lambda/a^2 \leq 1$.

Fig. 33b - Same as Fig. 33a except $1 \leq z\lambda/a^2 \leq 10$

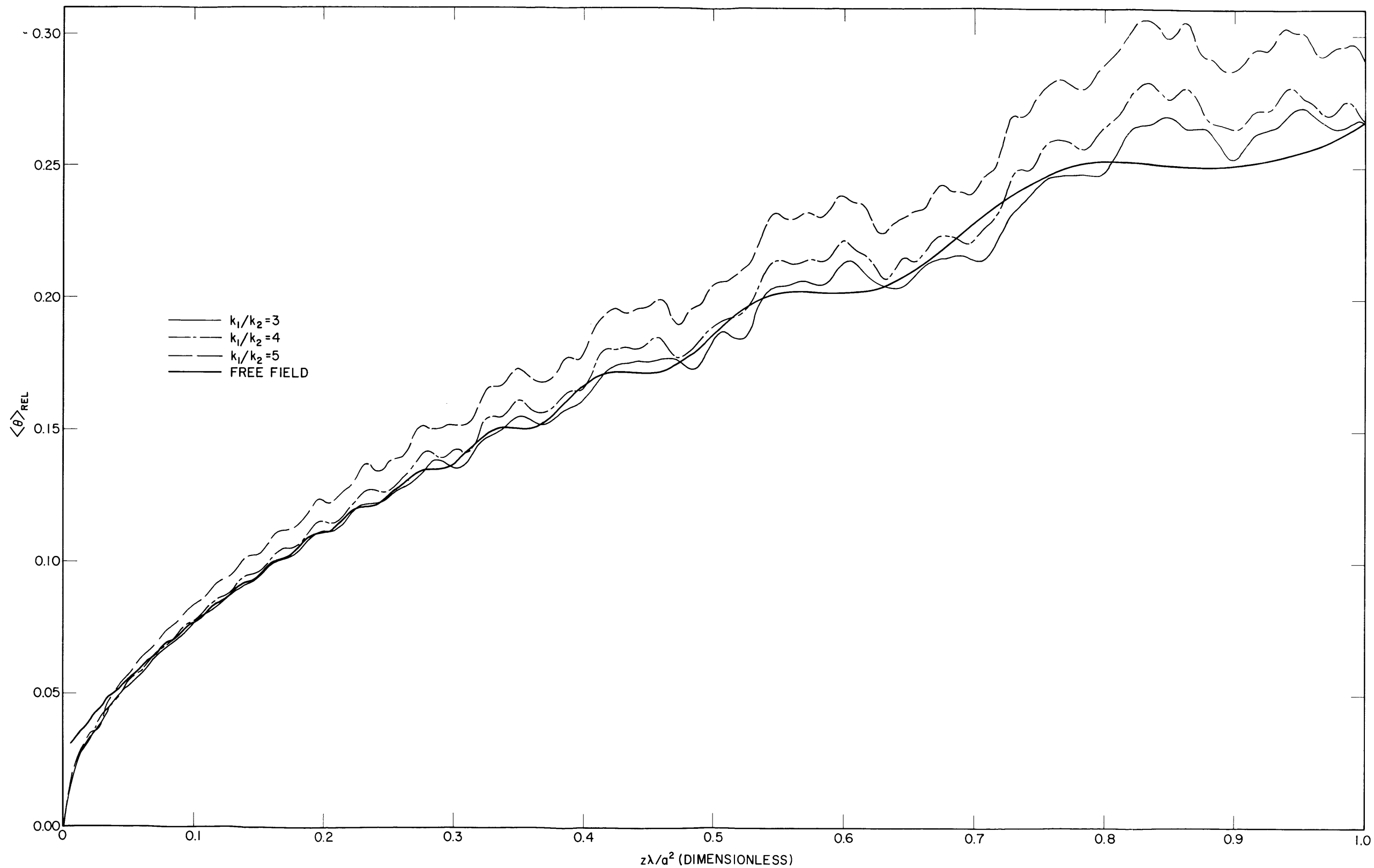
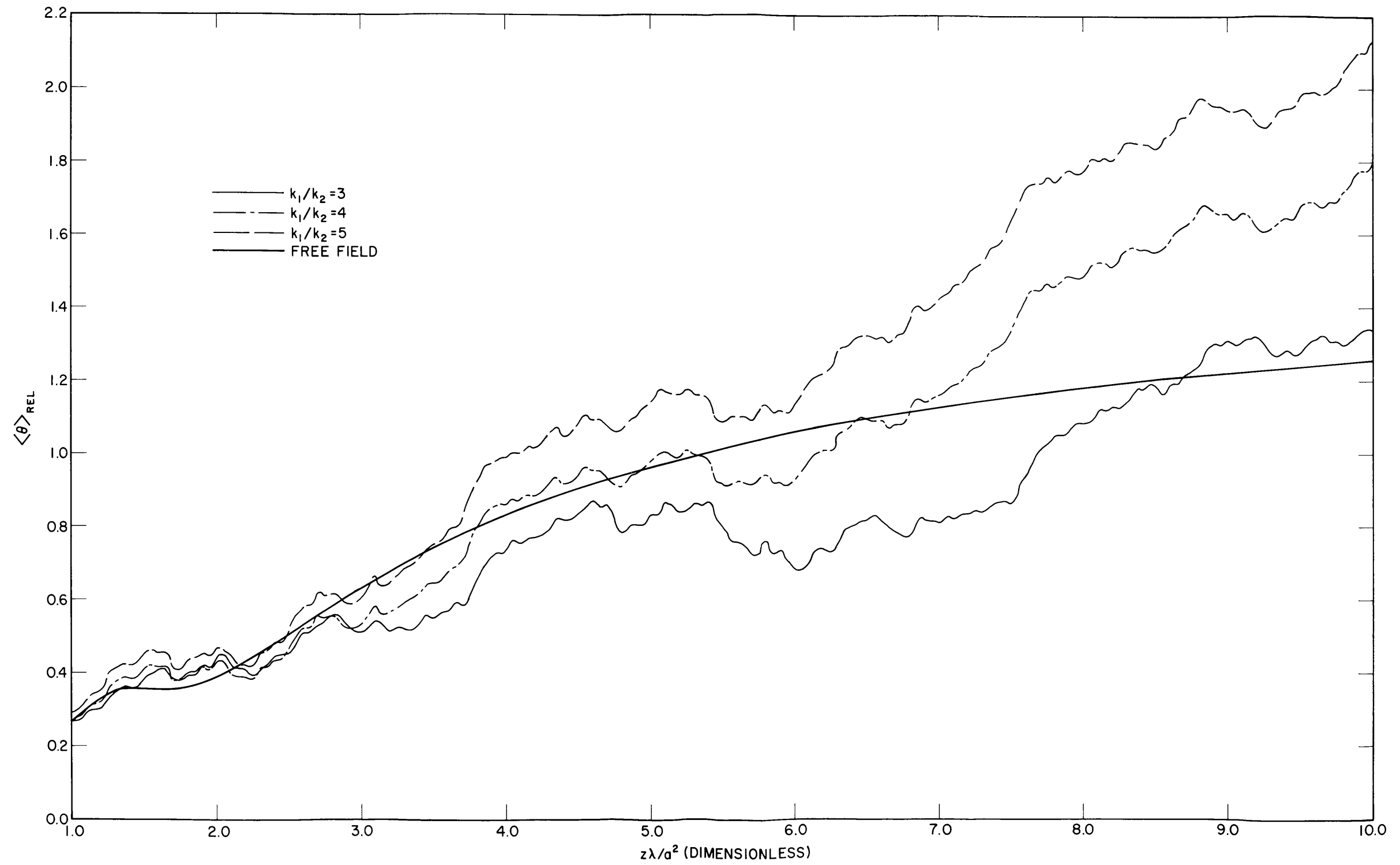


Fig. 34a - Average relative phase difference $\langle \theta \rangle_{rel}$ from plane-wave phase vs $z\lambda/a^2$ for a cylindrical liquid cavity with elastic boundaries. The effect of changing the wave-number-ratio parameter k_1/k_2 on the values of $\langle \theta \rangle_{rel}$ is shown for the elastic boundary condition. The standard parameters of Table 1 were used (except that k_1/k_2 is not restricted to 4) and $0 \leq z\lambda/a^2 \leq 1$.

Fig. 34b - Same as Fig. 34a except $1 \leq z\lambda/a^2 \leq 10$

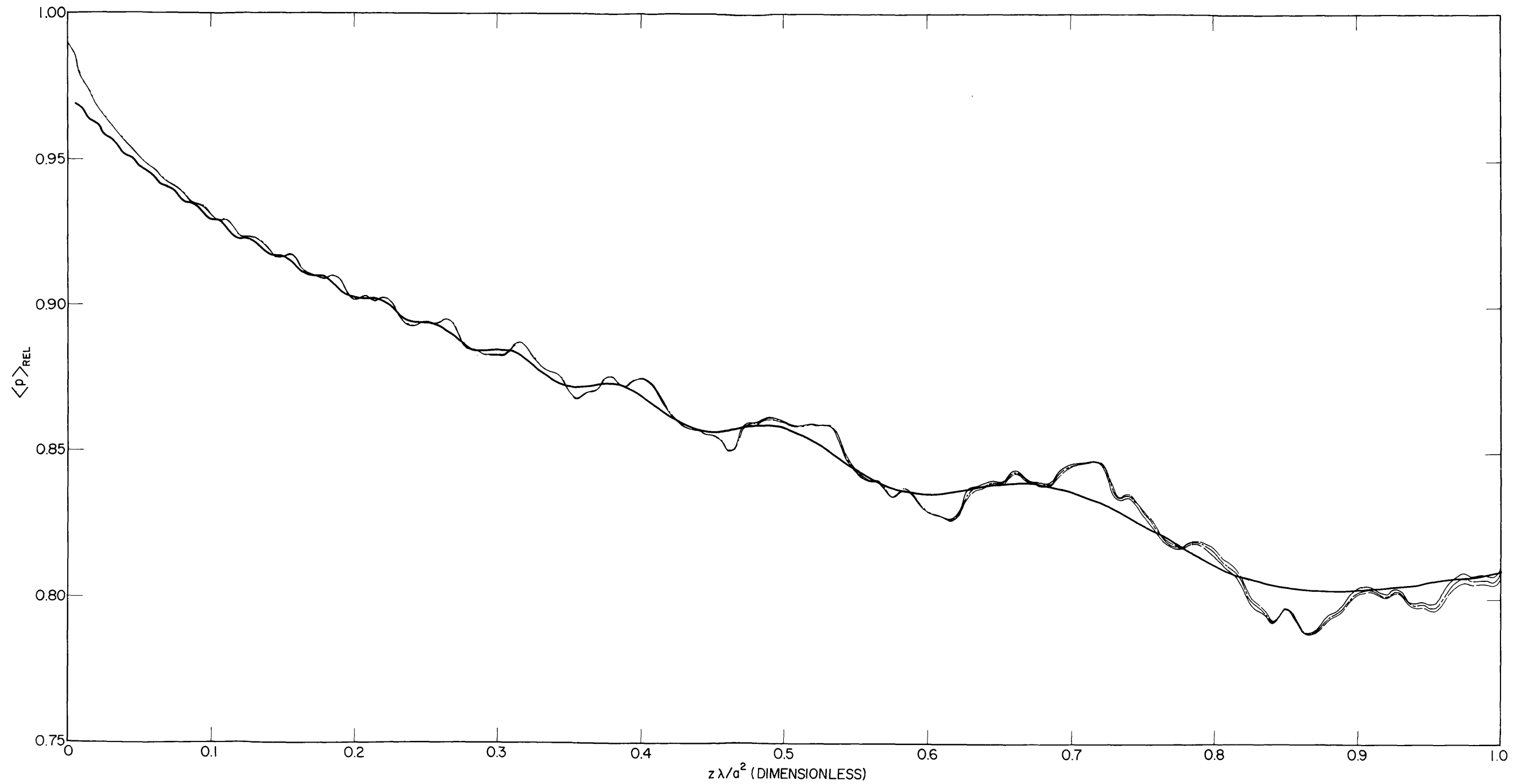
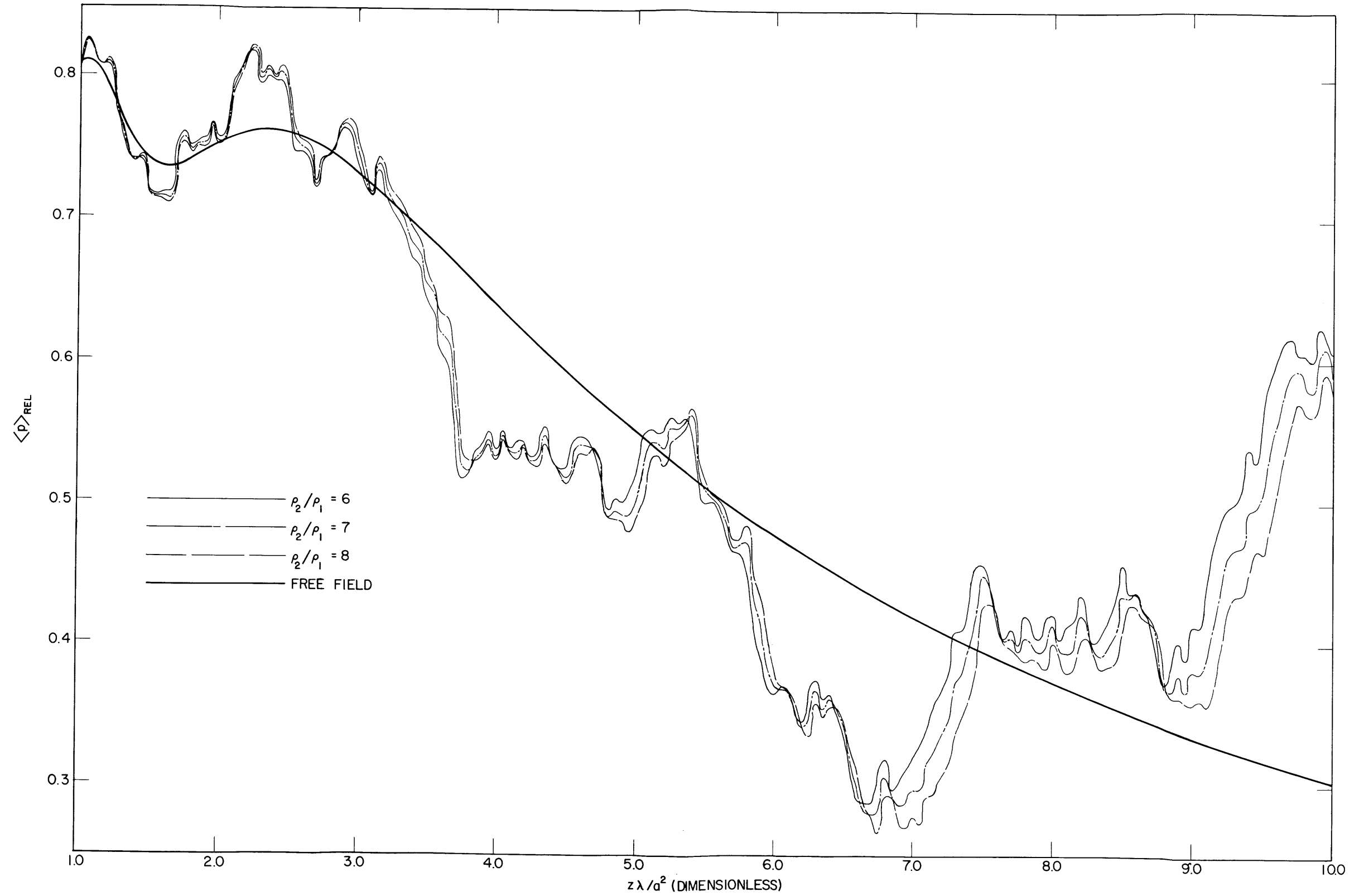


Fig. 35a — Average relative sound pressure $\langle p \rangle_{rel}$ vs $z\lambda/a^2$ for a cylindrical liquid cavity with liquid boundaries. The effect of changing the density-ratio parameter ρ_2/ρ_1 on the values of $\langle p \rangle_{rel}$ is shown for the liquid boundary condition. The standard parameters of Table 1 were used (except that ρ_2/ρ_1 is not restricted to 7) and $0 \leq z\lambda/a^2 \leq 1$.

Fig. 35b - Same as Fig. 35a except $1 \leq z\lambda/a^2 \leq 10$

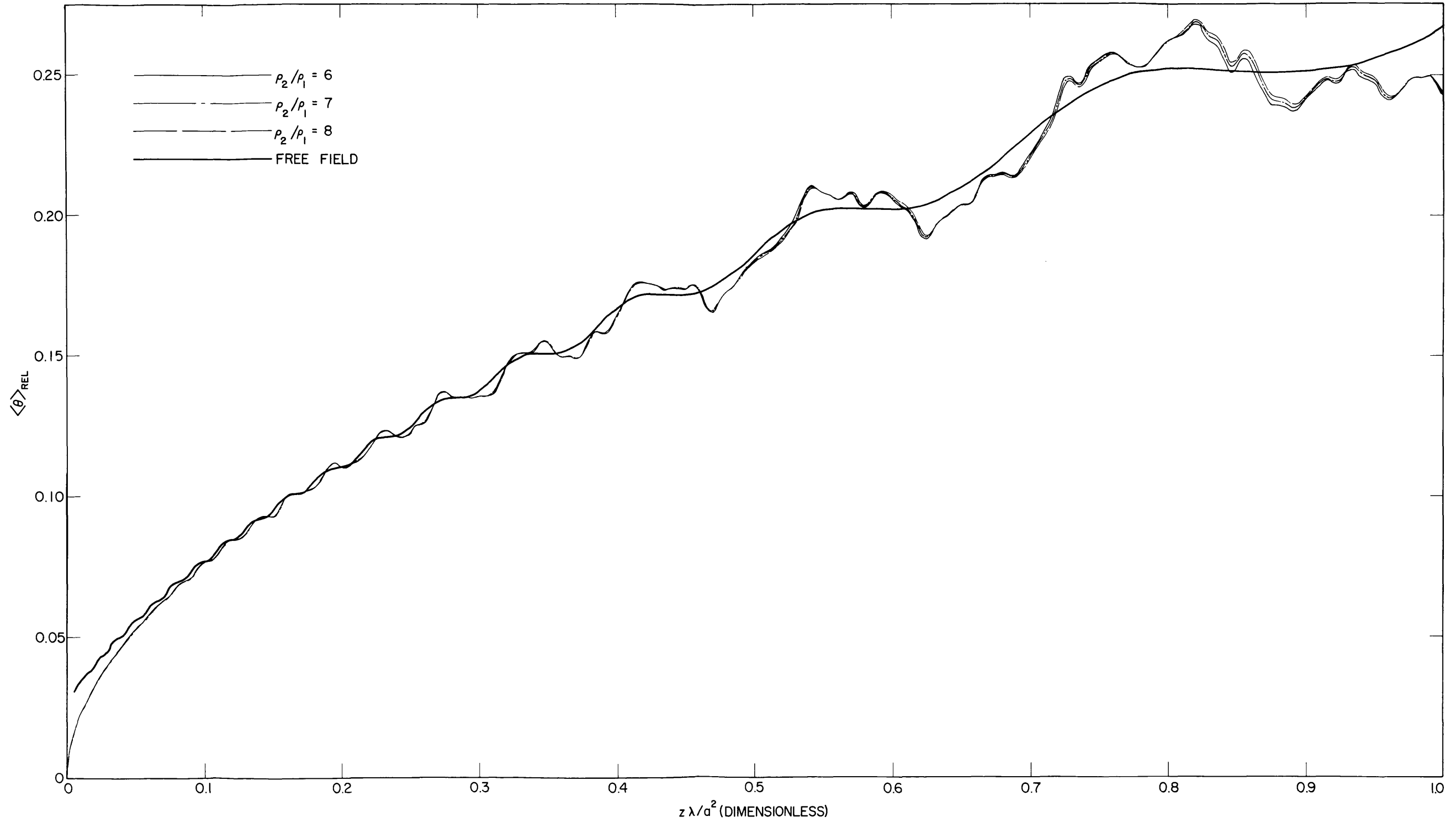
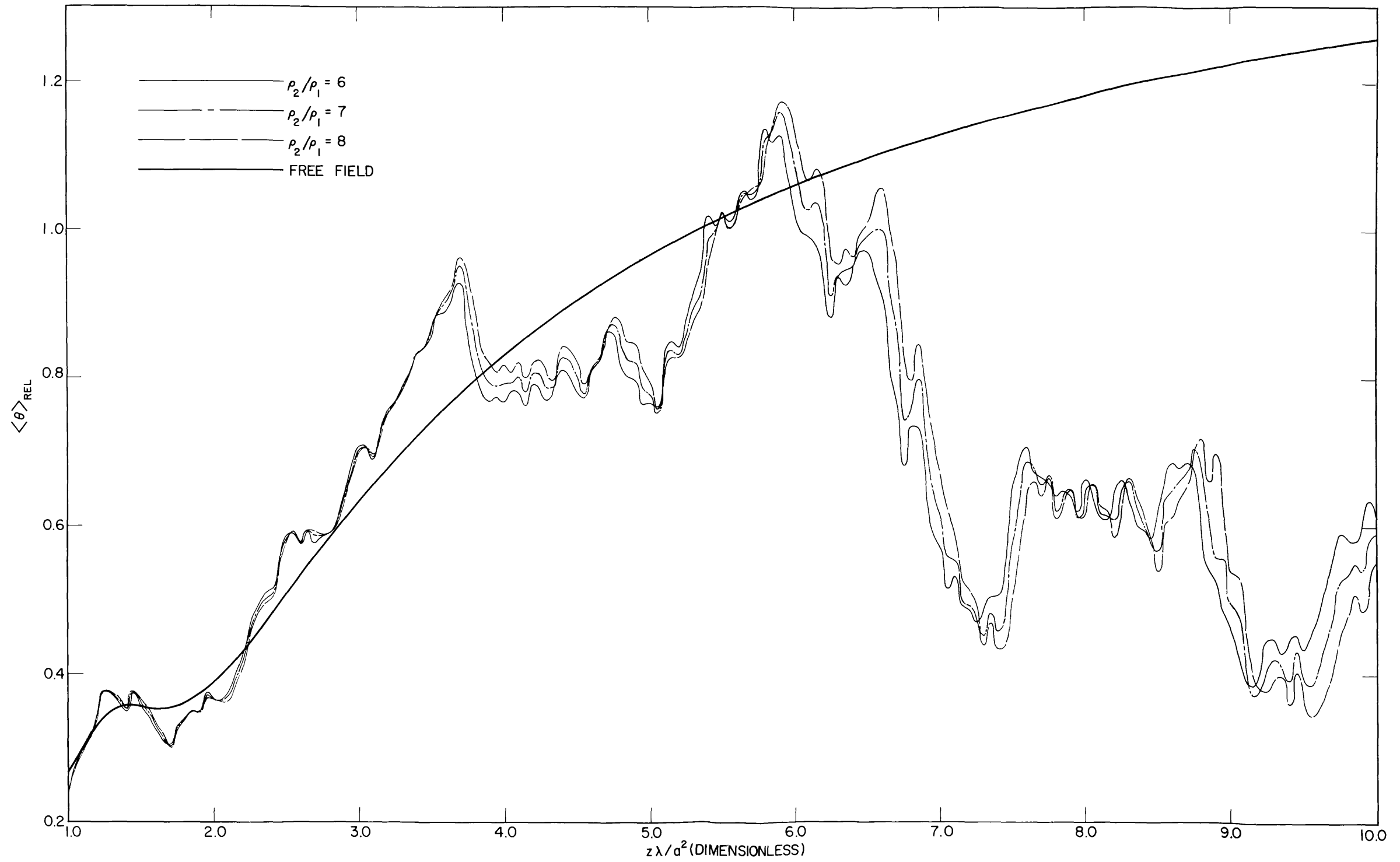


Fig. 36a - Average relative phase difference $\langle \theta \rangle_{\text{REL}}$ from plane-wave phase vs $z\lambda/a^2$ for a cylindrical liquid cavity with liquid boundaries. The effect of changing the density-ratio parameter ρ_2/ρ_1 on the values of $\langle \theta \rangle_{\text{REL}}$ is shown for the liquid boundary condition. The standard parameters of Table I were used (except that ρ_2/ρ_1 is not restricted to 7) and $0 \leq z\lambda/a^2 \leq 1$.

Fig. 36b - Same as Fig. 36a except $1 \leq z\lambda/a^2 \leq 10$

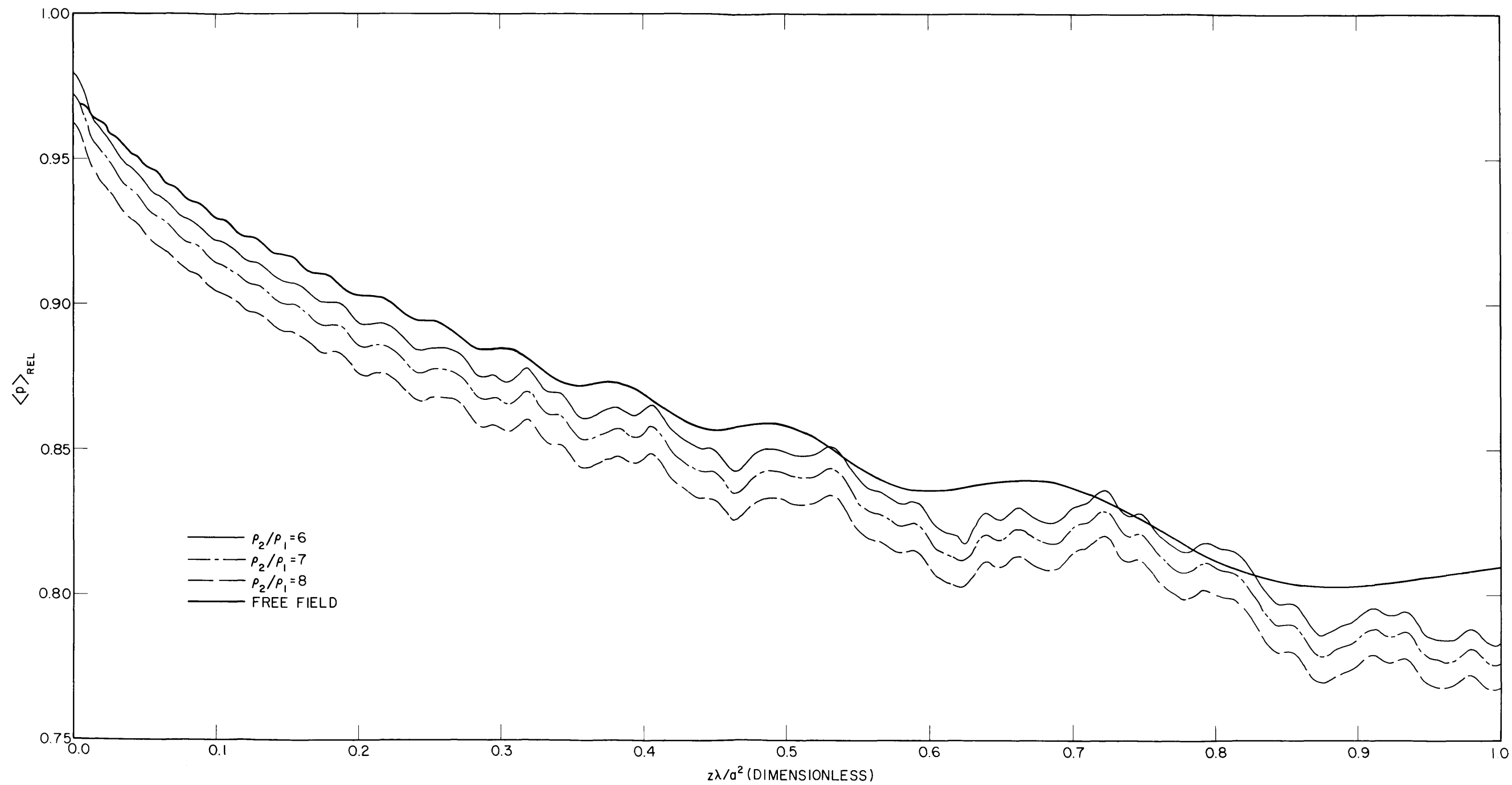
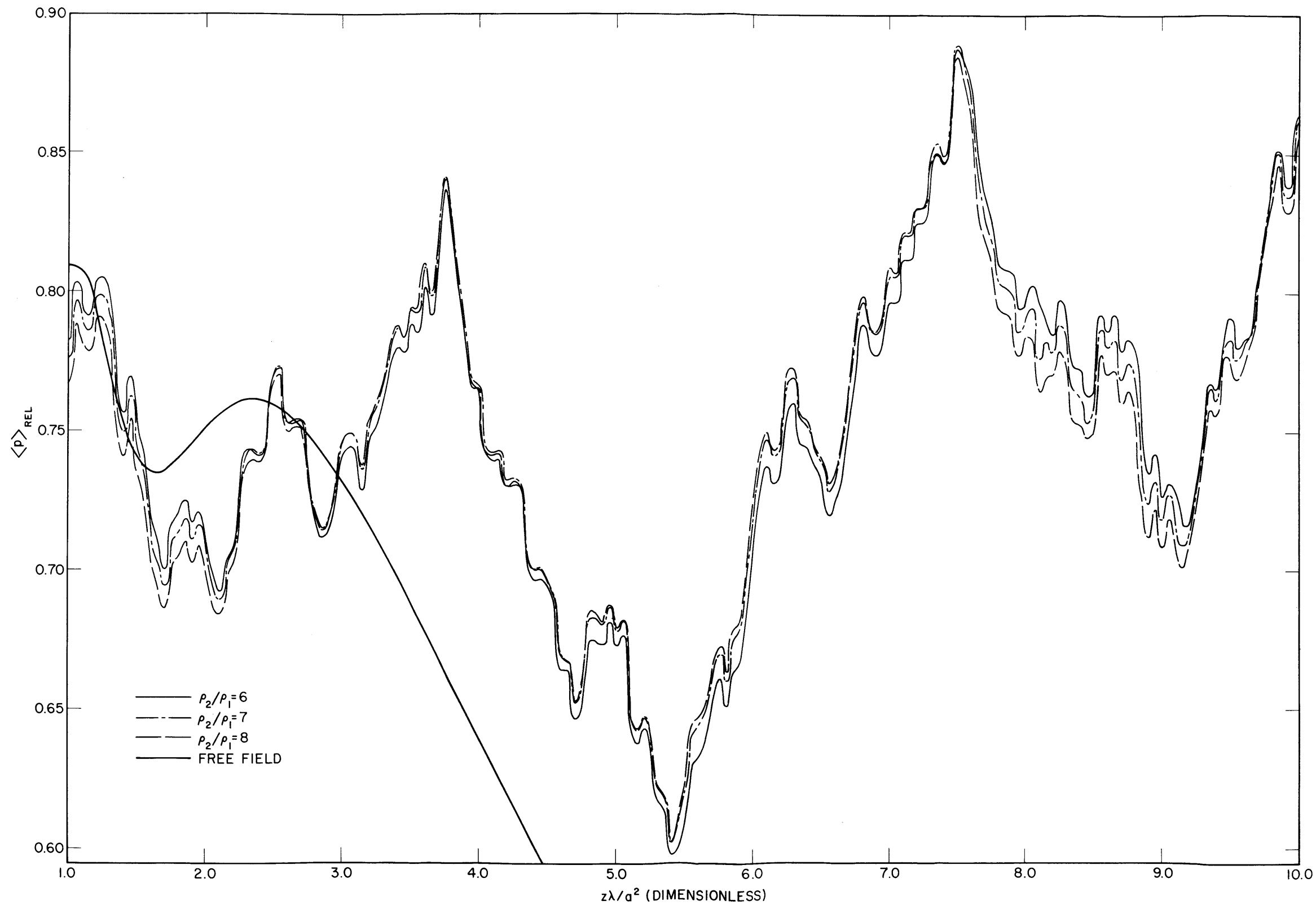


Fig. 37a - Average relative sound pressure $\langle p \rangle_{rel}$ vs $z\lambda/a^2$ for a cylindrical liquid cavity with elastic boundaries. The effect of changing the density-ratio parameter ρ_2/ρ_1 on the values of $\langle p \rangle_{rel}$ is shown for the elastic boundary condition. The standard parameters of Table 1 were used (except that ρ_2/ρ_1 is not restricted to 7) and $0 \leq z\lambda/a^2 \leq 1$.

Fig. 37b - Same as Fig. 37a except $1 \leq z\lambda/a^2 \leq 10$

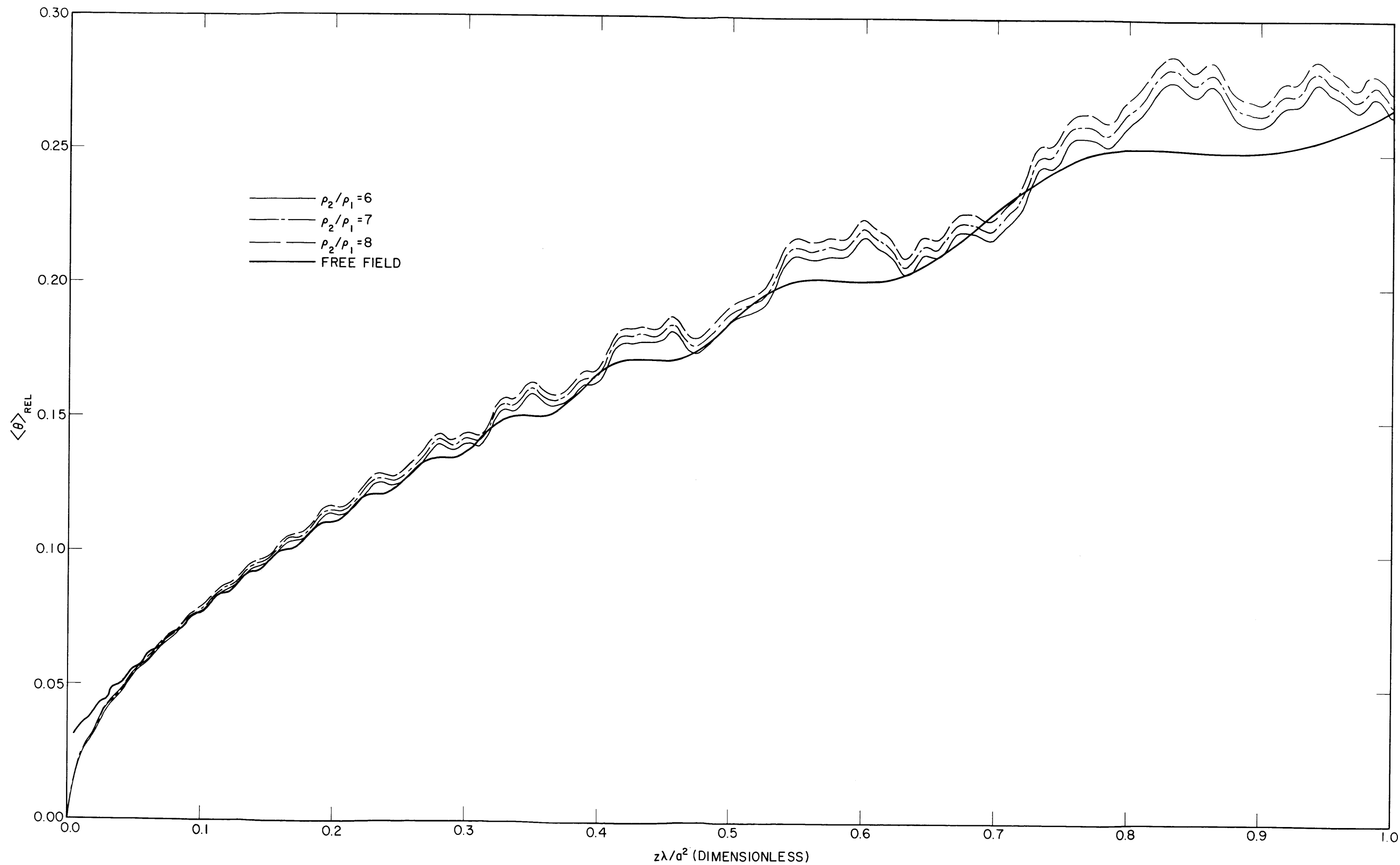
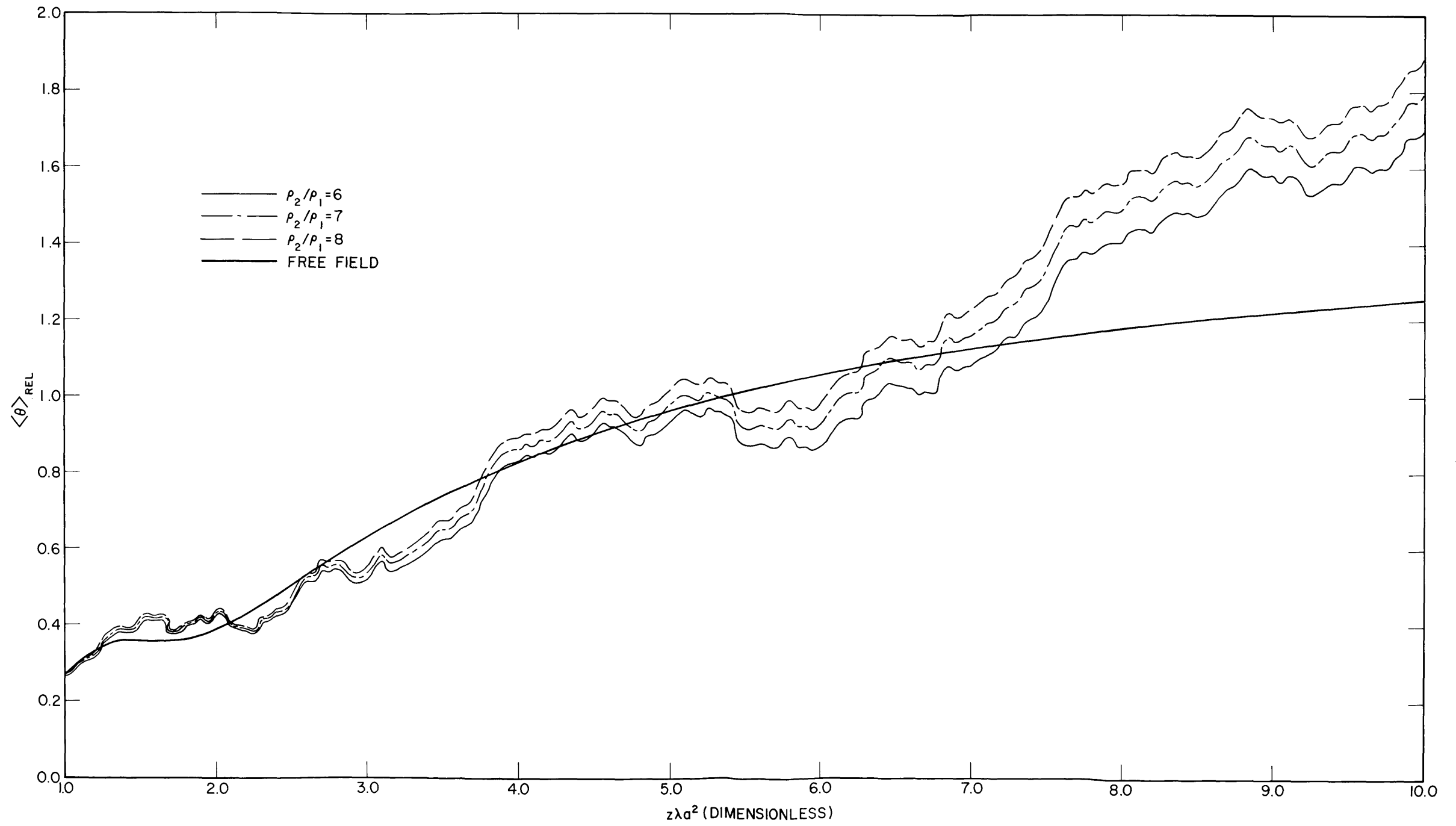


Fig. 38a — Average relative phase difference $\langle \theta \rangle_{\text{REL}}$ from plane-wave phase vs $z\lambda/a^2$ for a cylindrical liquid cavity with elastic boundaries. The effect of changing the density-ratio parameter ρ_2/ρ_1 on the values of $\langle \theta \rangle_{\text{REL}}$ is shown for the elastic boundary condition. The standard parameters of Table I were used (except that ρ_2/ρ_1 is not restricted to 7) and $0 \leq z\lambda/a^2 \leq 1$.

Fig. 38b - Same as Fig. 38a except $1 \leq z\lambda/a^2 \leq 10$

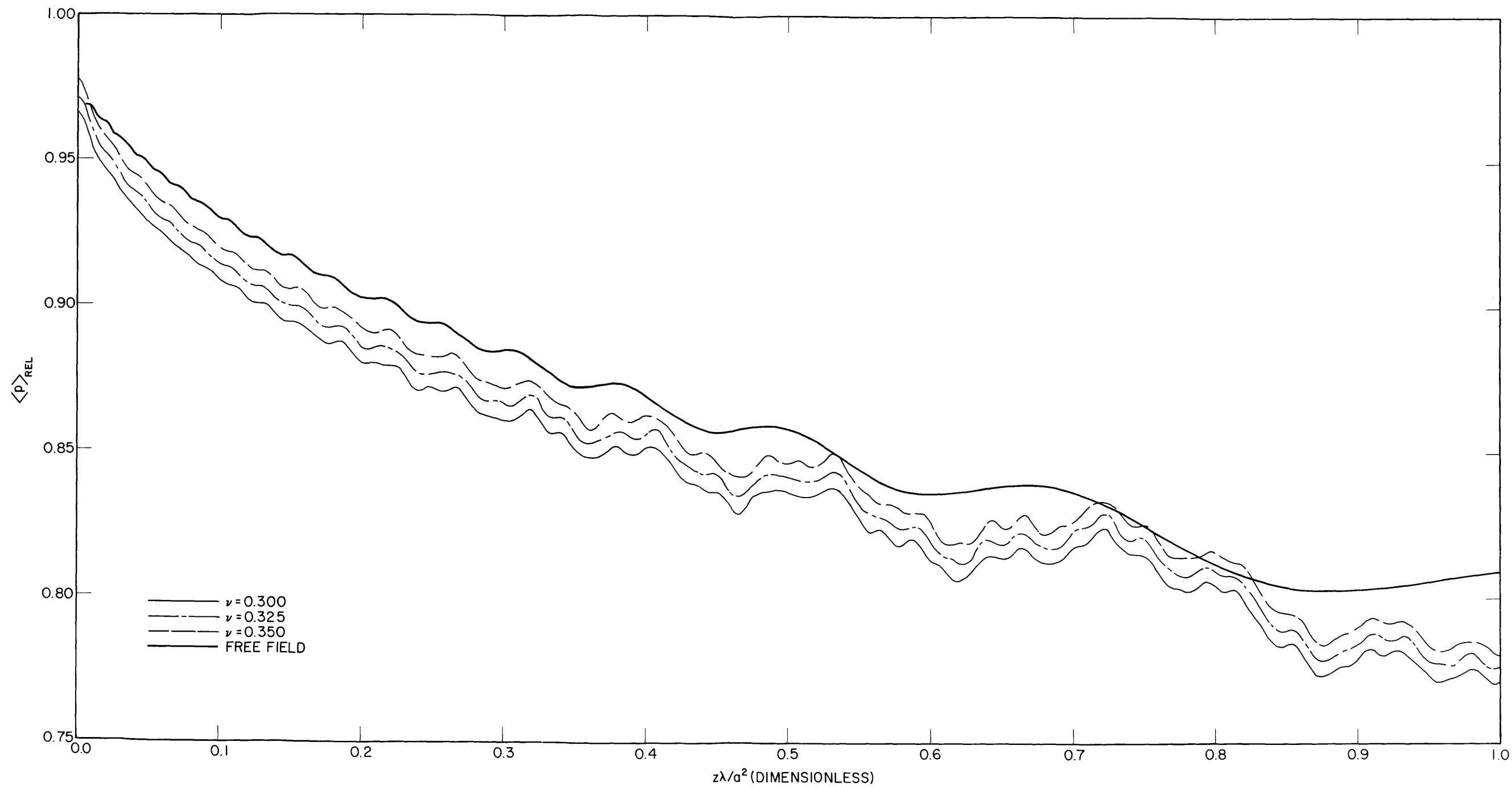
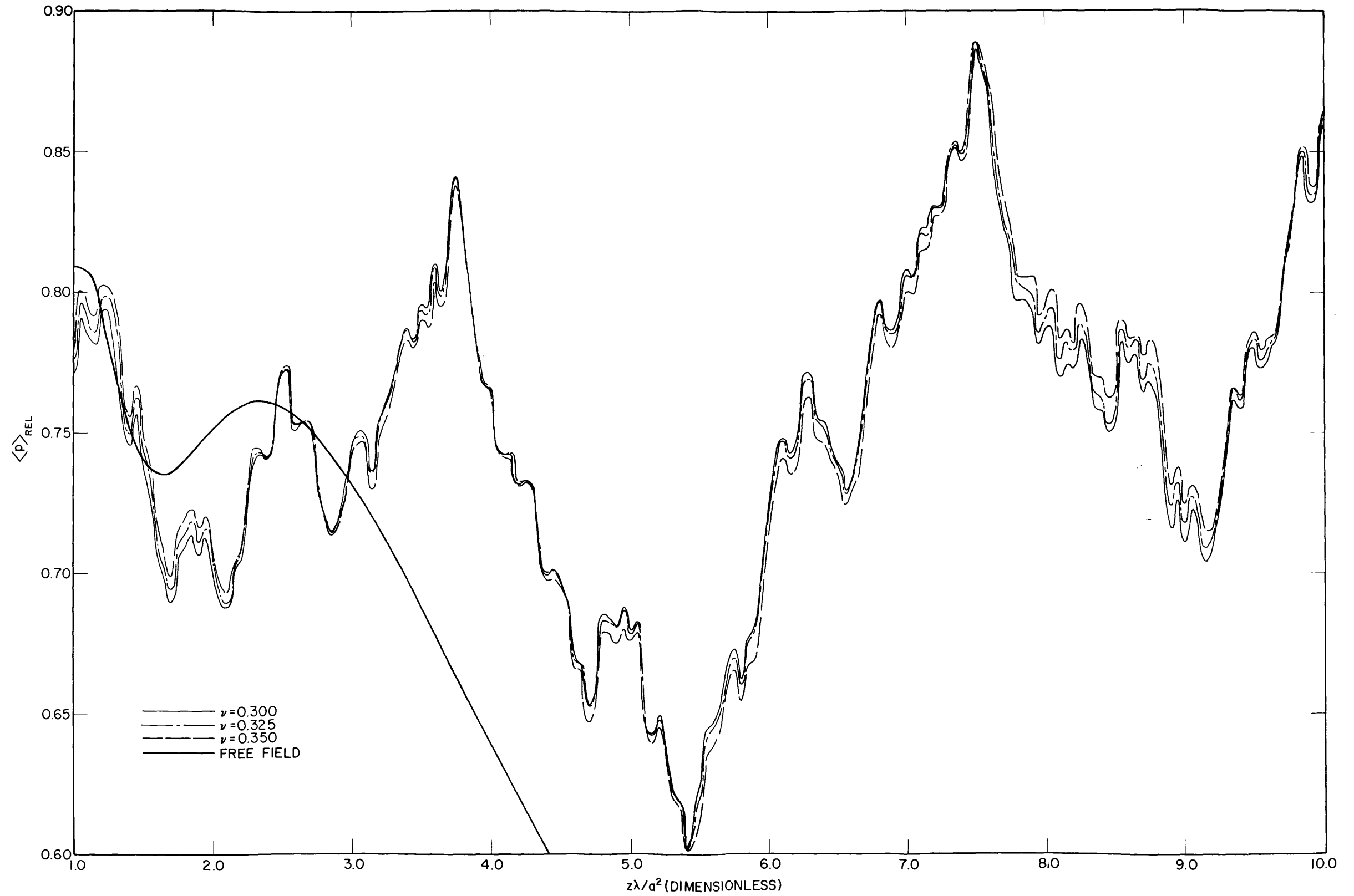


Fig. 39a - Average relative sound pressure $\langle p \rangle_{rel}$ vs $z\lambda/a^2$ for a cylindrical liquid cavity with elastic boundaries. The effect of changing the Poisson's-ratio parameter ν on the values of $\langle p \rangle_{rel}$ is shown for the elastic boundary condition. The standard parameters of Table 1 were used (except that ν is not restricted to 0.325) and $0 \leq z\lambda/a^2 \leq 1$.

Fig. 39b - Same as Fig. 39a except $1 \leq z\lambda/a^2 \leq 10$

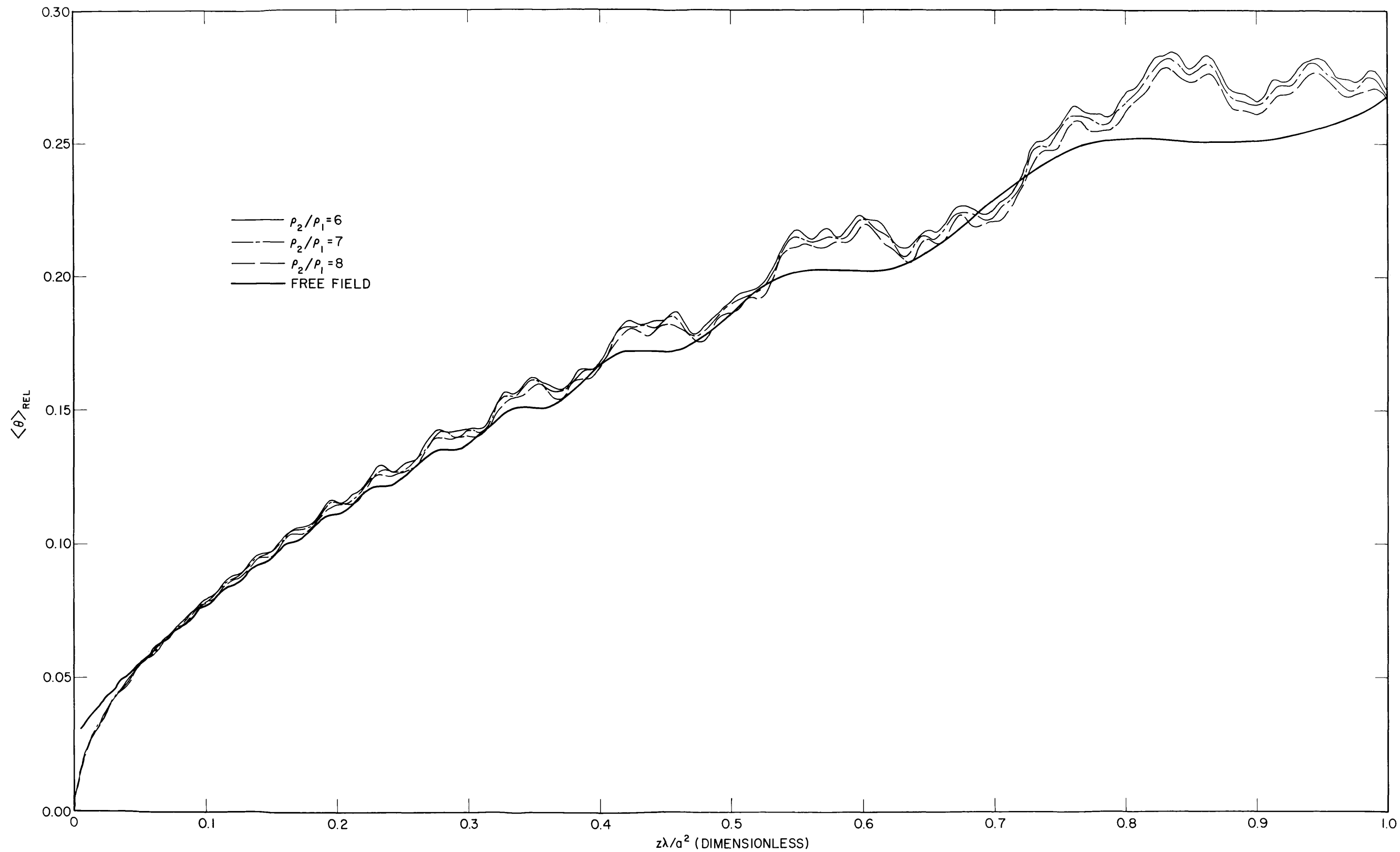
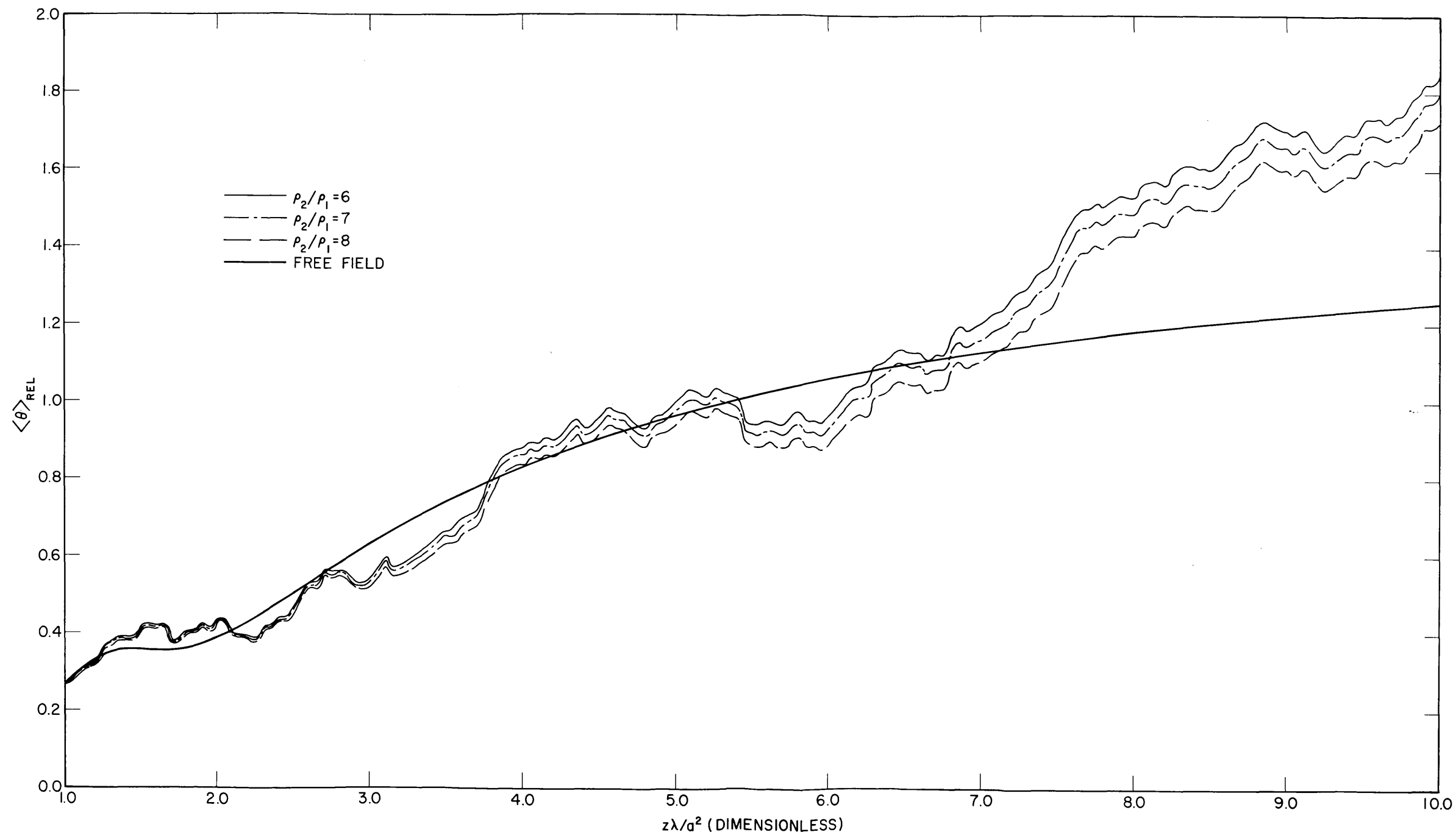


Fig. 40a — Average relative phase difference $\langle \theta \rangle_{REL}$ from plane-wave phase vs $z\lambda/a^2$ for a cylindrical liquid cavity with elastic boundaries. The effect of changing the Poisson's-ratio parameter ν on the values of $\langle \theta \rangle_{REL}$ is shown for the elastic boundary condition. The standard parameters of Table 1 were used (except that ν is not restricted to 0.325) and $0 \leq z\lambda/a^2 \leq 1$.

Fig. 40b - Same as Fig. 40a except $1 \leq z\lambda/a^2 \leq 10$

DOCUMENT CONTROL DATA - R&D		
<i>(Security classification of title, body of abstract and indexing annotation must be entered when the overall report is classified)</i>		
1. ORIGINATING ACTIVITY <i>(Corporate author)</i> U.S. NAVAL RESEARCH LABORATORY Washington, D.C. 20390		2 a. REPORT SECURITY CLASSIFICATION Unclassified
		2 b. GROUP —
3. REPORT TITLE SYSTEMATIC ERRORS IN ULTRASONIC PROPAGATION PARAMETER MEASUREMENTS Part 2—Effects of Guided Cylindrical Modes		
4. DESCRIPTIVE NOTES <i>(Type of report and inclusive dates)</i> This is an interim report on the problem; work is continuing		
5. AUTHOR(S) <i>(Last name, first name, initial)</i> Del Grosso, V. A.		
6. REPORT DATE January 29, 1965	7 a. TOTAL NO. OF PAGES 133	7 b. NO. OF REFS 48
8 a. CONTRACT OR GRANT NO. NRL Problem S01-02	9 a. ORIGINATOR'S REPORT NUMBER(S) NRL Report 6133	
b. PROJECT NO. RF 001-03-45-5251	9 b. OTHER REPORT NO(S) <i>(Any other numbers that may be assigned this report)</i> None	
c.		
d.		
10. AVAILABILITY/LIMITATION NOTICES Unlimited availability		
11. SUPPLEMENTARY NOTES	12. SPONSORING MILITARY ACTIVITY Office of Naval Research Department of the Navy	
13. ABSTRACT It was shown in Part I of this series of reports that appreciable errors in sound speed and sound absorption determinations may be attributed to a neglect in applying appropriate corrections to those situations closely approximating free-field conditions (finite size, plane-parallel source). In the present report it is shown that appreciable errors in the measurement of sound speed and sound absorption for guided mode propagation may be attributed to neglect in applying corrections that may be required because of the selection of geometric parameters or the method of measurement. This report contains graphs of pressure and phase, relative to plane-wave values and averaged over a plane-parallel receiver of size equal to the source size, for acoustic energy propagation down a right-circular liquid cylinder with lateral boundary condition appropriate to one of the following: absolutely rigid walls, infinitely flexible walls, liquid walls, or elastic solid walls. The latter boundary condition, which is considered to be that most appropriate to the situation of a liquid contained within a thick-walled metal tube, is shown to result in maximum anomalies in sound speed determinations when the transducer completely closes one end of the tube.		

Security Classification

14. KEY WORDS	LINK A		LINK B		LINK C	
	ROLE	WT	ROLE	WT	ROLE	WT
Sound Speed Sound Propagation Acoustic Boundary Conditions—Theory Liquid Cylinder—Propagation Sound Pressure (relative to plane wave) Phase Difference (from plane wave) Attenuation Coefficient Liquid Boundary Elastic Solid Boundary Infinitely Flexible Boundary Absolutely Rigid Boundary						

INSTRUCTIONS

1. **ORIGINATING ACTIVITY:** Enter the name and address of the contractor, subcontractor, grantee, Department of Defense activity or other organization (*corporate author*) issuing the report.

2a. **REPORT SECURITY CLASSIFICATION:** Enter the overall security classification of the report. Indicate whether "Restricted Data" is included. Marking is to be in accordance with appropriate security regulations.

2b. **GROUP:** Automatic downgrading is specified in DoD Directive 5200.10 and Armed Forces Industrial Manual. Enter the group number. Also, when applicable, show that optional markings have been used for Group 3 and Group 4 as authorized.

3. **REPORT TITLE:** Enter the complete report title in all capital letters. Titles in all cases should be unclassified. If a meaningful title cannot be selected without classification, show title classification in all capitals in parenthesis immediately following the title.

4. **DESCRIPTIVE NOTES:** If appropriate, enter the type of report, e.g., interim, progress, summary, annual, or final. Give the inclusive dates when a specific reporting period is covered.

5. **AUTHOR(S):** Enter the name(s) of author(s) as shown on or in the report. Enter last name, first name, middle initial. If military, show rank and branch of service. The name of the principal author is an absolute minimum requirement.

6. **REPORT DATE:** Enter the date of the report as day, month, year; or month, year. If more than one date appears on the report, use date of publication.

7a. **TOTAL NUMBER OF PAGES:** The total page count should follow normal pagination procedures, i.e., enter the number of pages containing information.

7b. **NUMBER OF REFERENCES:** Enter the total number of references cited in the report.

8a. **CONTRACT OR GRANT NUMBER:** If appropriate, enter the applicable number of the contract or grant under which the report was written.

8b, 8c, & 8d. **PROJECT NUMBER:** Enter the appropriate military department identification, such as project number, subproject number, system numbers, task number, etc.

9a. **ORIGINATOR'S REPORT NUMBER(S):** Enter the official report number by which the document will be identified and controlled by the originating activity. This number must be unique to this report.

9b. **OTHER REPORT NUMBER(S):** If the report has been assigned any other report numbers (*either by the originator or by the sponsor*), also enter this number(s).

10. **AVAILABILITY/LIMITATION NOTICES:** Enter any limitations on further dissemination of the report, other than those

imposed by security classification, using standard statements such as:

- (1) "Qualified requesters may obtain copies of this report from DDC."
- (2) "Foreign announcement and dissemination of this report by DDC is not authorized."
- (3) "U. S. Government agencies may obtain copies of this report directly from DDC. Other qualified DDC users shall request through _____."
- (4) "U. S. military agencies may obtain copies of this report directly from DDC. Other qualified users shall request through _____."
- (5) "All distribution of this report is controlled. Qualified DDC users shall request through _____."

If the report has been furnished to the Office of Technical Services, Department of Commerce, for sale to the public, indicate this fact and enter the price, if known.

11. **SUPPLEMENTARY NOTES:** Use for additional explanatory notes.

12. **SPONSORING MILITARY ACTIVITY:** Enter the name of the departmental project office or laboratory sponsoring (*paying for*) the research and development. Include address.

13. **ABSTRACT:** Enter an abstract giving a brief and factual summary of the document indicative of the report, even though it may also appear elsewhere in the body of the technical report. If additional space is required, a continuation sheet shall be attached.

It is highly desirable that the abstract of classified reports be unclassified. Each paragraph of the abstract shall end with an indication of the military security classification of the information in the paragraph, represented as (TS), (S), (C), or (U).

There is no limitation on the length of the abstract. However, the suggested length is from 150 to 225 words.

14. **KEY WORDS:** Key words are technically meaningful terms or short phrases that characterize a report and may be used as index entries for cataloging the report. Key words must be selected so that no security classification is required. Identifiers, such as equipment model designation, trade name, military project code name, geographic location, may be used as key words but will be followed by an indication of technical context. The assignment of links, roles, and weights is optional.